Attempts to analyse D/H ratios of sub-micromole quantities of hydrogen : applications in the study of ordinary chondrites

Thesis

Attempts to analyse D/H ratios of sub-micromole quantities of hydrogen: Applications in the study of ordinary chondrites.

by

Andrew David Morse B.Sc. Hons. (London, 1985)

A thesis submitted for the degree of
Doctor of Philosophy

Author's number : M7024148

Date of submission : 07.05.91

Date of award : 18.07.91

May 1991
Department of Earth Sciences
The Open University

EX12

HIGHER DEGREES OFFICE

LIBRARY AUTHORISATION FORM

STUDENT: ANDREW MORSE SERIAL NO: M7024448

DEGREE: Doctor of Philosophy

TITLE OF THESIS: Attempts to analyse D/H ratios of sub microgram quantities of hydrogen : Applications in the analysis of archaeological samples

I confirm that I am willing that my thesis be made available to readers and maybe photocopied, subject to the discretion of the Librarian.

SIGNED: A.D. Morse DATE: 7 May 91

Abstract

Semarkona is an unequilibrated ordinary chondrite which has experienced the least amount of thermal metamorphism and has the highest whole-rock D/H ratio of the ordinary chondrites. It is also unusual in that it has undergone some mild aqueous alteration, previously considered a secondary process restricted to some deuterium-rich carbonaceous chondrites. Semarkona was chosen to be the object of a more detailed study of secondary alteration and to determine whether the deuterium-rich phase was related in any way to the aqueous alteration process. A procedure was developed involving three analytical techniques (chemical/petrographic, thermoluminescence and hydrogen isotope) to study individual fragments of this meteorite.

The deuterium-rich phase was found to be concentrated in the chondrules, average δD = +3890‰, with a maximum measured δD of +7500‰ in one of the chondrules. The matrix had a moderate deuterium enrichment, of average δD = +2670‰. The isotope results in conjunction with the other techniques employed indicated that the chondrules that had experienced aqueous alteration are deuterium-rich. The water involved in the aqueous alteration was either deuterium-rich or transported deuterium-rich organics to the sites of aqueous alteration.

In order to reduce sample size requirements, it was necessary to develop an inlet and mass spectrometer system capable of the isotopic analysis of less than 0.1μmol hydrogen. Two inlet systems were developed for use with a dynamic mass spectrometer and compared with a conventional inlet system. The inlet system with greatest sensitivity, capable of analysing 0.1μmol hydrogen, was used for the isotopic study of Semarkona; however, the accuracy of this system was poor due to the presence of a memory effect. Experiments, using the conventional inlet, showed that this memory effect was due to sample water remaining on the surfaces of the inlet system. The presence of the memory effect could not be eliminated, but a correction procedure was obtained. These experiments have shown various methods in which the memory effect can be overcome by careful design of an inlet system.

Finally a static mass spectrometer system was developed, capable of analysing less than 1nmol hydrogen, in the form of methane. Initial results show that this system is capable of the isotopic analysis 0.01μmol of water with δD in the range of -500‰ to +5000‰ to an accuracy of ±20‰.

Acknowledgements

It is with pleasure I take this opportunity to thank all those people who have made this work possible. First my supervisor Colin Pillinger, who has provided guidance and ideas throughout the course of this work, Ian Wright for day-to-day supervision, interest in the experiments and considerable help with the early drafts of this thesis and Iain Gilmour who helped during the initial stages of this work. Judy Pillinger is thanked for managing to process orders and obtain equipment. The nature of this work involved people from different disciplines who were helpful with their experience and advice and with whom it was a pleasure to work. Robert Hutchison and Conel Alexander for the mineralogical and petrographic information, Kyle Guimon for the TL analyses. I would especially like to thank Derek Sears with the co-ordination of the Semarkona project, arranging for a six week lab visit (holiday) to the States and arranging the meteoritical society funding.

Thanks to all the members of the Planetary Sciences Unit for making the work enjoyable. Leon and Stuart for many happy hours at Ye Olde Swan. Paul for loan of the data point; Sara for the entertaining hair cuts; Jason, lethal paper dart designer, for transport; and Richard, proof reader, adviser and caving companion. Jim and Tim, house mates, who managed to put up with me for so long. The support from all those at 66 Towan avenue is also appreciated, for numerous cups of coffee and somewhere to crash out in an emergency (usually after nights at Ye Olde Swan).

Much needed escape from Milton Keynes was provided by the Open University Caving Club and Kings College Wargaming Group. Thanks to Tony and Steve whose experience has provided many enjoyable caving trips and managed to get me out of trouble several times. All members of the wargaming group who helped bring me back to reality, especially Baron Dredd, Tasslehof and Clint.

Most of the funding for this work was provided by the Open University. Other sources of funding were many and varied, which I gratefully acknowledge: The Barringer Mining Company *via* the Meteoritical society, for travel funding to the Fayetteville Meteoritical Society Meeting conference: Scotia Pharmaceuticals Ltd. for providing temporary employment: my parents and the players of Equinox. Thanks to my father for arranging temporary employment at Scotia Pharmaceuticals and showing that statistics can be fun.

Table of contents

Chapter 1: Introduction

List of figures

List of tables

Chapter 1
Introduction

1.1 General

Hydrogen is the most abundant element in the universe. In its simplest form it consists of a nucleus of one proton and an orbiting electron. However it is important as the starting point of nucleosynthesis, the building block of all other elements. Most hydrogen was created at the start of the universe, the amount produced by spallation, the disintegration of heavier elements, is negligible. Since hydrogen has not undergone nucleosynthetic processing its concentration, relative to other light elements and their isotopes (atomic number less than 5), has been used to place constraints on models of the early universe.

Determination of the concentration of hydrogen in stellar objects, relative to the other elements present, can give an indication of the amount of cosmogenic processing its constituents have undergone. The outer layers of relatively old stars are predominantly hydrogen, whereas those stars that formed later contain other elements formed in the cores of previous stars. Population II stars, which formed before the galaxy, have very low iron to hydrogen ratios when compared to the sun (Clayton 1988). The hydrogen concentrations can be used to place constraints on models of the early universe, however the concentration of hydrogen is very susceptible to chemical and physical processing. This severely limits the usefulness of concentration measurements in chemically processed objects. More information can be obtained by the study of the ratio of its stable isotopes, since they have similar chemical and physical properties.

The ratio of the stable isotopes of an element in an object depends primarily on formation/destruction mechanisms of the isotopes. These isotope ratios are then modified by isotopic fractionation, caused by a mixture of kinetic and equilibrium effects. Thus a study of stable isotope ratios of the solar system can provide insights as to the origin of the solar nebula (by determining the original isotope ratios and hence where they were acquired) and processes that occurred in the solar nebula which modified these isotope ratios by fractionation.

Hydrogen has two stable isotopes, protium and deuterium. The most abundant isotope is protium and is usually referred to as hydrogen. Deuterium has a nucleus of one proton and one neutron and so has approximately twice the mass of protium. On Earth it has a concentration of about 156 ppm in hydrogen. Hydrogen has one other isotope, tritium which has a nucleus of one proton and two neutrons. Tritium has a half-life of 12.26 years, decaying by beta decay to helium ($T \rightarrow {}^3He + e^- + \upsilon$). As the half-life is

so short (on the geological time scale) it has limited use in geological applications. However, since tritium is produced by spallation of heavier nuclei by cosmic ray bombardment, it can be used as an indication of the degree of recent exposure of a meteorite to cosmic rays; and has uses in atmospheric and ground water studies (Jean-Baptiste *et al.*, 1988), since it is continually produced in the upper stratosphere.

Like protium, deuterium is not produced by stellar nucleosynthesis, but owes its origin to the Big Bang. Deuterium is unusual in that nuclear processing reduces rather than increases its abundance relative to protium. Hydrogen isotopes have a larger mass ratio than other elements, so it is more easily fractionated by physical and chemical processes. Thus hydrogen isotope ratio studies provides different information about the early solar nebula and subsequent geological processing from that obtained by other elements.

The Earth has suffered from substantial differentiation and melting since its formation 4.56 Gyr ago, destroying any record of early solar nebula events. Information about the early solar nebula and processes has been gained by two different approaches.

i) Astronomical studies: The observation of star forming regions and processes that occur in interstellar space, leading to identification of possible solar system formation scenarios.

ii) Meteoritical studies: Some meteorites, known as unequilibrated ordinary chondrites (UOCs), formed early during the collapse of the solar nebula. Geological processing on the UOC parent bodies was relatively mild and ceased soon after their formation. Hence study these of meteorites can lead to information of the early solar nebula processing and place constraints on astrophysical models.

Recently, components have been found in some meteorites which are thought to pre-date the solar system due to their unusual isotopic composition and acid resistant properties (Anders *et al.*, 1989). To withstand the rigours of interstellar space and processes that occurred in the solar nebula these grains need to be very resistant and are able to withstand the chemical processing in the laboratory. Another possible pre-solar component are organic molecules, formed in dark molecular clouds, and polycyclic aromatic hydrocarbons (PAHs) detected in the interstellar medium. The solar nebula and eventual formation of the solar system may have begun with the collapse of a dark molecular cloud (Cassen and Boss, 1988); hence study of the organics may provide information on their formation region and indications of the conditions present in the early solar nebula. Being organic these molecules are not resistant to extreme chemical processing and are easily destroyed by mild geological processing. Although many organic molecules are acid insoluble, hydrogen isotopic information may be obscured by hydrogen isotope exchange during such treatment. The investigation of these components requires the study of meteorites that have undergone minimal geological

processing (secondary alteration) and quantification of the amount and effects of this small amount of processing on the original material.

1.2 Measurement of D/H ratios

1.2.1 The delta notation

With many isotope ratio analysing instruments, the measured isotopic ratio of an element may be different from the true isotopic ratio of that element. To compensate for any instrumental effects the measured isotopic ratio of a sample is compared to that of an internationally agreed reference sample and expressed as a difference, the delta notation, a concept introduced by Urey, (1948). Since changes in stable isotope ratios in terrestrial samples for most elements are usually small this difference is expressed in parts per thousand according to:

$$\delta^{H}X = \left(\frac{(^{H}X/^{L}X)_{sam}}{(^{H}X/^{L}X)_{ref}} - 1 \right) \times 1000 \text{ ‰} \qquad 1.1)$$

where $(^{H}X/^{L}X)_{sam}$ and $(^{H}X/^{L}X)_{ref}$ is the measured atomic ratio of the heavy and light isotopes of the sample and reference standard respectively. For a sample, its δ value is positive when enriched in the heavy isotope and negative when depleted in the heavy isotope, compared to the reference standard. So for hydrogen,

$$\delta D = \left(\frac{(D/H)_{sam}}{(D/H)_{ref}} - 1 \right) \times 1000 \text{ ‰} \qquad 1.2)$$

where $(D/H)_{sam}$ and $(D/H)_{ref}$ are the atomic deuterium to hydrogen ratio of sample and reference samples respectively. For hydrogen isotope analysis the international standard used is SMOW (Standard Mean Ocean Water), $D/H = 155.76 \pm 0.05 \times 10^{-6}$ (Gonfiantini, 1978). Note that a new standard V-SMOW has since replaced SMOW due to the depletion of SMOW. V-SMOW was obtained by mixing natural waters of various isotopic composition so that it would have the same oxygen and hydrogen isotopic composition as SMOW. In reality Craig (1961) has determined that the hydrogen isotope ratio of V-SMOW is 0.2‰ lower than SMOW, this amount is negligible for most D/H analyses. Due to difficulties in analysis between laboratories (probably due to memory effects and H_3^+ corrections, sections 3.3.5 and 2.4.4) Gonfiantini suggested the use of a secondary standard SLAP (Standard Light Antarctic Precipitate). The D/H ratio of SLAP is $89.02 \pm 0.05 \times 10^{-6}$ and δD is defined as -428‰. Thus

$$\delta D = \left(\frac{(D/H)_{sam}}{(D/H)_{ref}} - 1 \right) \times 1000 \times R \text{ ‰} \qquad 1.3)$$

where R is the ratio of the defined δ for SLAP (-428‰) to the measured δ value for SLAP.

1.2.2 Spectroscopic analysis of astronomical objects

Molecules are detected in astronomical objects by infrared, radio and microwave spectroscopy. Each species of molecule emits or absorbs energy at characteristic frequencies due to their vibrational and rotational energy levels. Deuterated molecules have different spectroscopic signatures due to the change of rotational and vibrational energy levels because of the increased mass. The concentration of a molecular species is estimated from the strength of the absorption and compared with laboratory measurements. Obtaining concentrations of molecules and hence D/H ratios is difficult due to the low intensity of the detected radiation and complex spectra due to the variety of molecular species present. Errors in astronomical D/H measurements are usually at least ±20% and can often only give upper limits to the D/H ratio. However astronomical spectroscopy has shown that there are a variety of organic molecules, several sources and a large range of D/H ratios.

1.2.3 Laboratory measurement of D/H ratios using mass spectrometry

Hydrogen isotope ratios of samples are usually measured by dynamic mass spectrometry. Operating on the principle of Aston's (1919) mass spectrograph, hydrogen molecules are introduced into the mass spectrometer source, ionized, accelerated and then the different mass isotopes separated by a magnetic field. Modern gas source mass spectrometers are based on the design of Nier (1947), as improved upon by McKinney *et al.* (1950). Development of gas source mass spectrometry for hydrogen isotope analysis of water samples was achieved by Alfin-Slater *et al.*, (1950). The operation of a hydrogen isotope mass spectrometer is described in more detail in chapter 2.

Hydrogen is usually extracted from samples in the form of water, by the combustion or pyrolysis of the sample. The water is cryogenically separated from other products produced during the extraction and then reduced to hydrogen. The hydrogen then flows, from a storage volume, through a capillary leak into the mass spectrometer source. The use of conventional gas source mass spectrometers requires a high pressure of gas in the inlet, at least 20 torr to ensure a viscous flow of hydrogen through the capillary leak and prevent fractionation of the gas (Halstead and Nier, 1950). This high pressure, coupled with the fact that hydrogen can not be cryogenically manipulated,

results in relatively large samples of hydrogen are required. Most gas source mass spectrometers can measure D/H ratios with good precision, better than changes of 0.2ppm of deuterium in hydrogen (±1‰). However, large samples, *ca.* 50μmol are usually required to maintain a high enough pressure in the storage volume for viscous flow.

1.2.4 Secondary ion mass spectrometry

Recently ion probes have been employed for hydrogen stable isotope analysis (Hinton *et.al.*, 1983; Zinner *et al.*,1983; and Zinner 1988). Hydrogen from the sample is ionized by bombardment of the solid sample with a primary ion beam, usually caesium. Many ion species, including hydrogen, are sputtered from the sample and form a plasma above its surface, which is then accelerated by electrostatic field. The hydrogen ion beam is then focussed and separated by use of magnetic and electrostatic fields. By focussing the primary ion beam this technique allows *in situ* analysis of areas of interest in a sample, minimum spot size 3μm (Zinner 1988). The main advantage is the very high sensitivity and hence small sample size required, around 10^{-11}g of hydrogen.

However there are disadvantages:

i) The best precision in the δD so far obtained is only ±30‰. The primary ion beam creates a cloud of ions and atoms immediately above the sample, the composition of which depend on the material being analysed. The amount of hydrogen ionised by the primary ion beam depends on the nature of the ions present, hence there is usually large isotopic fractionation, the amount of which depends on the composition of the sample. This dependence of fractionation on sample composition is termed a "matrix" effect. This can be partly compensated by analysing samples of similar composition to the sample.

ii) Two different isotopic species occupying the same place in a sample cannot be separated, both will be ionized simultaneously. For example there are many organic compounds in carbonaceous chondrites which are intimately mixed. Ion probe analysis will yield an average isotope composition. However, different compounds have different isotopic signatures which can provide clues to their origin. The separation of these compounds requires chemical techniques.

1.3 Deuterium in the universe

1.3.1 The Big Bang

The standard hot Big Bang model (Gamow, 1948; Weinberg, 1977; Close, 1983) proposes that all of the hydrogen and most of the helium currently observed in stars/galaxies/ISM was produced during the first fifteen minutes after the start of the universe. Initially the universe is assumed to be a point mass of infinite temperature and density. As it expands it rapidly cools. After 10^{-2} seconds the temperature had dropped to 10^{12}K and the only stable baryons were neutrons and protons, which are in equilibrium.

$$\upsilon + n \leftrightarrow p + e^- \qquad (1.4)$$

$$e^+ + n \leftrightarrow p + \upsilon \qquad (1.5)$$

At a temperature of 9×10^9K (*ca.* 1 second) the equilibrium is no longer maintained due to the larger mass of the neutron. The incident particles do not have enough energy for the reverse reactions to occur. The relative proportion of neutrons decreases through beta decay (1.6) or combination with a proton to form a deuteron (1.7), a deuterium nucleus.

$$n \rightarrow p + e^- + \upsilon \qquad (1.6)$$

$$\text{or} \quad n + p \rightarrow d + \gamma \qquad (1.7)$$

In reaction (1.7) the photon emitted has an energy of 2.2MeV, so the reaction is reversed by photons with energy greater than 2.2MeV. Consequently any deuterons produced almost immediately undergo photodisintegration until there are fewer high energy photons present, this occurs at a temperature of *ca.* 10^9K, 100 seconds after the big bang. Below 10^9K neutrons and protons interact to form deuterons. However most deuterons then react with protons to form ^{3}He.

$$d + p \rightarrow {}^3He + \gamma \qquad (1.8)$$

This ^{3}He is then involved in the production of other light elements, mainly ^{4}He with some ^{7}Be and ^{7}Li, according to:

$${}^3He + {}^3He \rightarrow {}^4He + 2p \qquad (1.9)$$

$${}^3He + {}^4He \rightarrow {}^7Be + \gamma \qquad (1.10)$$

$${}^7Be + e^- \rightarrow {}^7Li + \upsilon \qquad (1.11)$$

These processes continue until the temperature drops below 8×10^5K, after a period of about 1000 seconds, at which temperature protons do not have enough energy to overcome the Coulomb repulsion between deuterons and protons. Thus the concentration of deuterium formed during the early universe depends greatly upon the rate of expansion and density of the early universe. Wagonner (1973) showed that the D/H ratio is proportional to ρ^{-5}, where ρ is the mean baryon density. A D/H ratio of about 20×10^{-6} has been measured for the local universe (*ca.* 200 parsecs) by the observation of the

absorption lines of bright stars (York and Rogerson, 1976). Which gives a mean baryon density of $6x10^{-31}$g cm^{-3}. This is nearly an order of magnitude less than the density of $4.5x10^{-30}$gcm^{-3} required by cosmological models for the closure of the universe. On the basis of this the universe is open and will expand forever. A closed universe will eventually stop expanding and collapse back to a singularity (Big Crunch). For closure the initial rate of expansion needs to be slower with the result that the D/H ratio would be $\sim 2x10^{-9}$. Thus if the universe is closed then most of the deuterium is not produced during the Big Bang but by some other process. This has prompted detailed investigation and calculations of other possible mechanisms of deuterium production (section 1.3.2 to 1.3.6). It is generally concluded that most are not capable of producing the observed D/H ratio of the universe (Trimble, 1975 and Epstein *et al.*, 1976). However these other mechanisms could be a source of deuterium enrichments in the solar system.

1.3.2 Spallation

Spallation is the production of nuclei by the break up of a heavier nuclei in collisions, either by knock-on type reactions

e.g. $$p + {}^{13}C \rightarrow d + {}^{12}C \qquad (1.12)$$

or by the complete destruction of the target nuclei as in

$$p + {}^{13}C \rightarrow d + {}^{6}Li + 3p + 3n \qquad (1.13)$$

Epstein *et al.* (1976) showed that, from measured reaction rates, the observed universal abundance of deuterium cannot be produced by spallation without over production of Li, Be and B, the amount depending on the energy of the incident particle. Confirmation of this is obtained by observations of cosmic rays which are produced by spallation. Comparison of cosmic ray abundances with galactic abundances for Li, Be and B show that they are enriched by a factor of 10^5, whereas D is not greatly enriched (Meyer 1974). Spallation has been suggested as a local source of deuterium enrichment in meteorites by exposure to an energetic young sun, or cosmic rays. This should be detected by an increase in the Li, B and B abundances. The amount of D produced is usually not detectable although the Li abundances usually are (Geiss and Reeves, 1981).

1.3.3 Novae

Hoyle and Clayton (1974) have suggested that large amounts of deuterium could be produced on the surface of a white dwarf during a nova event. Protons with an energy greater than 0.63MeV, produced during the nova, react with ^{14}C nuclei thereby ejecting a neutron.

$$^{14}C + p \rightarrow {}^{14}N + n \qquad (1.14)$$

The neutrons then combine with hydrogen to form deuterium (reaction 1.7). D/H ratios as high as 10^{-2} are possible, higher concentrations produce ^{3}He. Trimble (1975)

considered this mechanism unlikely since the amount of energy required is a large fraction of the total available energy of a nova event. Also there needs to be a mechanism of removing deuterium from the surface of a white dwarf without further nuclear processing. This method could be a possible source of a local deuterium, along with ^{13}C, ^{15}N and ^{17}O enrichments which are also produced by novae (Trimble, 1975).

1.3.4 Supernovae shock waves

Colgate (1974) has suggested that during a supernova protons can be accelerated to high energies and could interact with heavier nuclei such as C,N, and O, to form deuterium by spallation. It is generally considered unlikely because such a process would produce in addition large amounts of ^{7}Li, ^{9}Be and ^{11}B (which are not observed) . A second problem is that the energy of the ions in the shock wave is probably not enough to cause spallation. A supernova energy of 10^{53} ergs is required which is not observed in most supernova events. SN1987A, a powerful type II supernova had an observed energy of 10^{51} ergs (Lattimer and Yahil 1989). Thus this mechanism is unlikely to be a main source of universal deuterium, but may provide a mechanism for a local deuterium enrichment. Any deuterium enrichment by this mechanism would be accompanied by large concentrations of ^{7}Li, ^{9}Be and ^{11}B as with spallation.

1.3.5 Hot explosions

Neutrons are stable at temperatures of 10^{9} to 10^{10}K, depending on density. If matter at these temperatures is rapidly expanded and cooled then deuterium could be formed by reaction (1.7). For the deuterium to survive, the expansion must be very rapid so that either

i) the neutrons and protons do not combine until the temperature has dropped sufficiently to prevent further nuclear reactions or

ii) there is not enough time for all of the deuterium to form helium, as in the case of the Big Bang. Epstein *et al.*, (1976) showed that this is not possible unless the region of the hot explosion is $< 10^{-7}M_{\odot}$ except for the case of the big-bang. This mass is too small for an observable astronomical event that is to provide most of the deuterium observed.

1.3.6 Disrupted neutron stars.

Neutron stars consist of mainly neutrons surrounded by a thin layer of the most stable elements, mainly iron. Lattimer and Schramm (1974) have shown that a disrupted neutron star can be a source of neutrons. Most neutrons will form clumps with the few protons to form heavy elements and so no deuterium is formed. If the expansion is very rapid then some will escape and a source of free neutrons is available. However in order to form deuterium these neutrons must interact with hydrogen before the neutrons undergo beta decay. Epstein *et al.*, (1976) considered that such a source of deuterium is possible, but unlikely since it requires the neutrons

i) to be ejected unrealistically fast
ii) to interact with a hydrogen cloud nearby, within a few life-times of the neutrons (half life *ca.* 700s) and
iii) must not interact with the outer layer of iron at the neutron star surface during the disruption event.

1.3.7 The fate of deuterium in stars

Main sequence stars generate most of their energy by hydrogen burning, *i.e.* the conversion of hydrogen to helium. The first step of this process is the formation of deuterium.

$$p + p \rightarrow D + e^{+} + \upsilon \qquad (1.15)$$

This reaction requires a temperature of around $2x10^{7}K$ to enable protons to have enough energy to overcome the electrostatic Coulombic repulsion between them. The deuterium then combines with other protons eventually to form helium.

$$D + p \rightarrow {}^{3}He + e^{+} \qquad (1.16)$$

$$^{3}He + {}^{3}He \rightarrow {}^{4}He + 2p \qquad (1.17)$$

The temperature required for deuterium burning is $8x10^{5}K$, much lower than that for deuterium production. Thus in any equilibrium environment where deuterium is produced it will be almost immediately consumed to form helium. The amount of deuterium to hydrogen at equilibrium in the core of a star is estimated to be 10^{-11}ppm or less (Rolfs *et al.*, 1987). Thus it is clear that stellar processing results in the almost complete destruction of deuterium.

1.4 Isotopic fractionation processes affecting hydrogen

The deuterium to hydrogen mass ratio of 2 is the largest among stable isotopes. Thus it is the easiest element to fractionate since both chemical and physical processes are affected by the mass difference between two isotopes of an element. The α factor is a measure of the amount of fractionation between two phases in equilibrium.

$$\alpha = \frac{[D/H]_1}{[D/H]_2}$$

where [D/H] is the deuterium to hydrogen ratio of phases, 1 and 2.

1.4.1 Physical fractionation

Physical fractionation is directly caused by the mass difference between hydrogen and deuterium. It involves processes such as diffusion, evaporation and condensation. For diffusion the rate of diffusion of a gas is proportional to $(1/\text{mass})^{1/2}$ (Graham's law). With fractionation between physical phases the heavier isotope tends to become enriched in the less volatile phase. The actual amount of fractionation depends upon the ratio of the isotopes in the two phases when in equilibrium (the α factor) and upon the amount of evaporation/condensation. In the case of evaporation the less volatile phase becomes more depleted during progressive evaporation, the amount of fractionation depending on the α factor and degree of evaporation as shown in fig 1.1. During condensation the heavier isotope condenses preferentially. Examples of physical fractionation for hydrogen on Earth are:

i) The depletion of up to 50% deuterium in Antarctic precipitate, due to the gradual depletion of deuterium in the evaporated water by precipitation as the water vapour moves towards the Antarctic.
ii) The enrichment in deuterium of up to 20% in East African lakes due to evaporation.

1.4.2 Chemical fractionation

This is caused by the differences in the bond strengths of the two isotopes in a molecule, mainly due to different vibrational energy which is caused by the mass difference. The α factor between the two phases depends on the temperature and the chemical composition of each phase. The α factor tends to increase with decreasing temperature. Examples for hydrogen are the fractionation between hydrogen and water

$$H_2O + HD \leftrightarrow HDO + H_2 \qquad (1.18)$$

and hydrogen and methane

$$CH_4 + HD \leftrightarrow CH_3D + H_2 \qquad (1.19)$$

The dependence of the α factor on temperature for hydrogen is shown in fig 1.2 (from Reeves and Bottinga, 1972). For hydrogen it can be seen that the amount of

fractionation between hydrogen molecules and the second hydrogen bearing phase is insensitive to the nature of the second phase but is very sensitive to the equilibrium temperature. With chemical fractionation the process relies upon a physical process to separate the two phases, however the separation process is controlled by the differences between the chemistry of the two phases rather than the mass.

1.4.3 Ion molecule reactions

At temperatures below 100K chemical reaction rates between neutral molecules are almost negligible due to the activation energy required. At these temperatures chemical equilibrium is attained by ion molecule reactions (Watson 1976).

$$D^+ + H_2 \leftrightarrow HD + H^+ \qquad (1.20)$$

$$CH_3^+ + HD \leftrightarrow CH_2D^+ + H_2 \qquad (1.21)$$

$$HCN^+ + HD \leftrightarrow DCN^+ + H_2 \qquad (1.22)$$

Reaction 1.20) and 1.21) have been measured in the laboratory under molecular cloud conditions and are exothermic (Smith *et al.*, 1982). This is the main cause of the deuterium enrichments observed in dark interstellar molecular clouds. Hydrogen/Deuterium ratios as high as 45 000x10^{-6} have been observed for some species of molecules in dark molecular clouds (Millar *et al.*, 1989). Enrichment by ion molecule reactions would also lead to enrichment of ^{13}C by similar ion molecule reactions.

$$^{13}C^+ + {}^{12}CO \leftrightarrow {}^{13}CO + {}^{12}C^+ \qquad (1.23)$$

However the amount of carbon in a molecular cloud is small and mostly taken up to form organic molecules so no exceptional fractionation occurs. Most of the hydrogen is in the form of hydrogen molecules and more is available from the interstellar medium. Thus the organic molecules can become exceptionally enriched in deuterium.

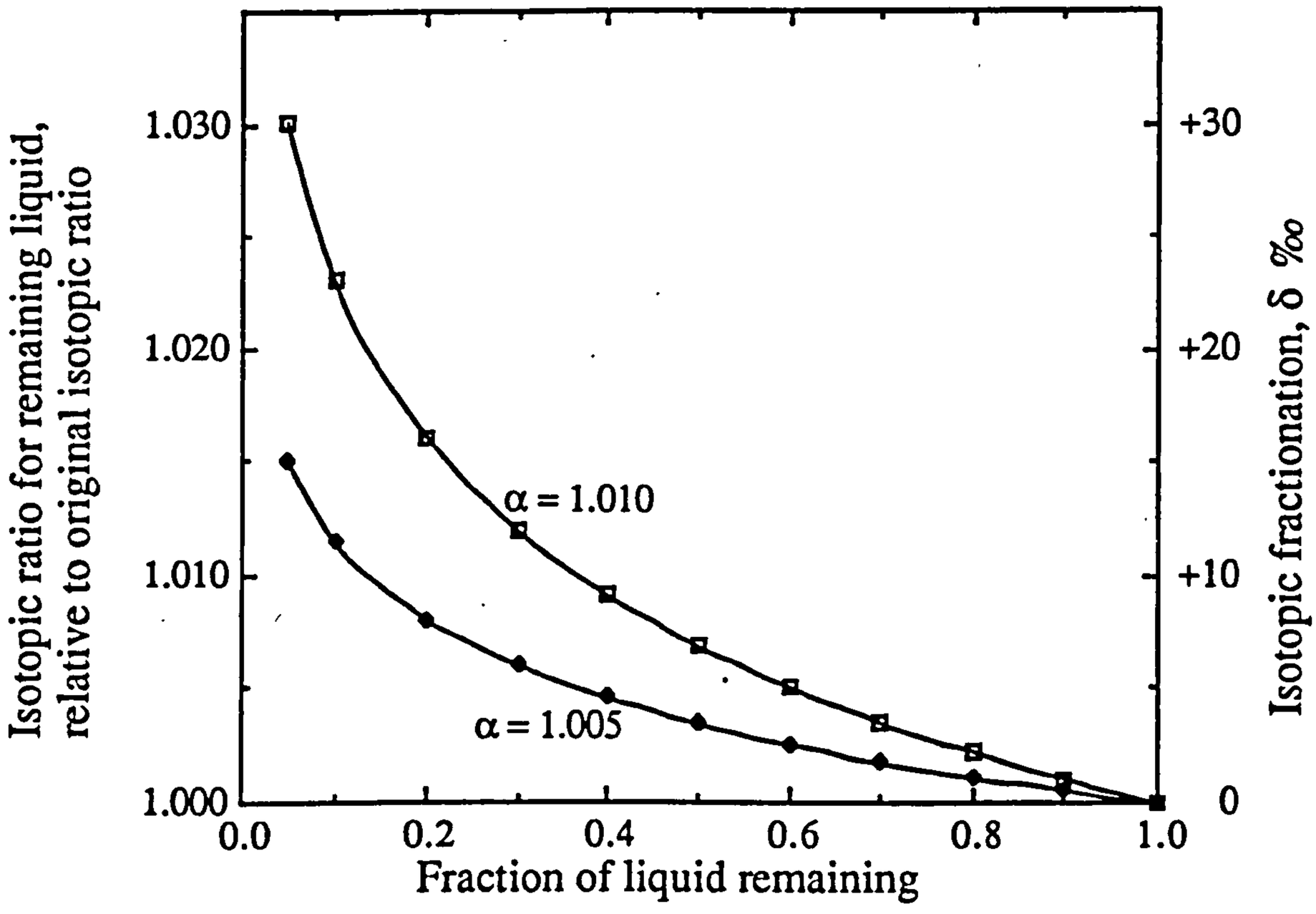

Fig 1.1 Example of physical fractionation during evaporation, Rayleigh fractionation, for two different condensates with an a factor of 1.005 and 1.010. The degree of isotopic fractionation in the condensate depends upon the α factor and the fraction of condensate remaining. The degree of fractionation was calculated from equations given in Hoefs, (1987).

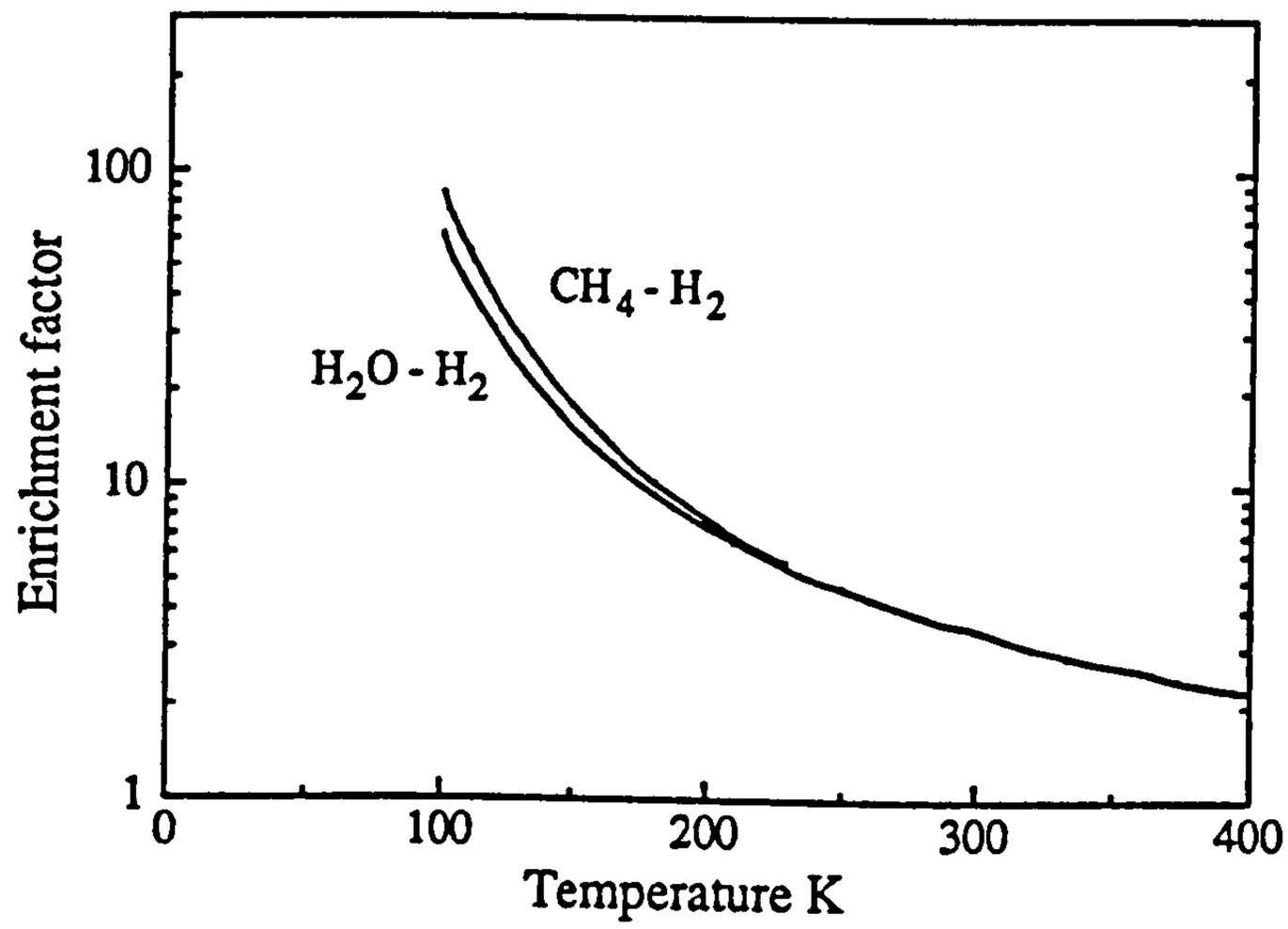

Fig 1.2 Graph showing the enrichment obtained by chemical equilibrium of hydrogen with water or methane and the effect of temperature on the deuterium enrichment obtained. Data from Reeves and Bottinga, (1972).

1.5 Hydrogen/deuterium ratios in the solar system

The solar system shows a wide range of D/H ratios ranging from practically zero in the sun to 1.5×10^{-3} in the upper atmosphere of Venus. Table 1.1 gives the range of D/H ratios for various solar system components. This wide range of D/H ratios reflect different formation processes of the planets and the ease with which hydrogen isotopes can be fractionated.

Object	D/H Ratio $\times 10^{-6}$	δD ‰	Reference
Sun	0	-1000	Rolfs *et al* . 1987
Solar wind	0	-1000	Rolfs *et al*. 1987
Earth	150	-40	Craig 1961
Moon	100	-360	Merlivat *et al*. 1972
Venus	16000	+101,000	Donahue *et al*. 1982
Mars	900	+4800	Owen *et al*. 1988
Jupiter	18	-865	Drossart *et al*. 1982
Saturn	22	-870	Gautier and Owen 1983
Titan	150	-40	Coustenis *et al*. 1989
Uranus	48	-690	Trafton and Ramsay 1980
Neptune	< 100	< -360	Smith *et al*. 1989
Comets	60 to 480	-600 to +2000	Eberhardt *et al*. 1986

Table 1.1 Deuterium to hydrogen rations for various objects in the solar system.

1.5.1 The sun and solar wind

Since the sun obtains most of its energy from hydrogen burning, temperatures are high enough that any deuterium formed will be destroyed. As such the sun is expected to have a D/H ratio of practically 0. The solar wind is a constant stream of particles emitted by the sun and so is expected to contain no deuterium (see 1.5.3 below). Solar wind fluxes and composition for some elements, mainly noble gases, have been measured by its implantation in meteorites and the Apollo Solar Wind Composition experiment (Geiss *et al*.,1970, 1971). Although the major component of the solar wind is hydrogen, analytical techniques do not yet have the ability to measure the D/H ratio of the solar wind, using hydrogen from these sources. The D/H ratio of the early solar nebula has been estimated to be $20 \pm 5 \times 10^{-6}$ from measurement of the $^3He/^4He$ ratio of the solar wind (Black, 1973; Geiss and Reeves 1972).

1.5.2 Earth

The D/H ratio for various terrestrial samples range from $80x10^{-6}$ for Antarctic precipitation to over $180x10^{-6}$ for atmospheric hydrogen. These differences in isotopic composition are well understood in terms of fractionation by physical and chemical processes. The Earth has an average D/H ratio of *ca.* $150x10^{-6}$ (Craig,1961), this is approximately ten times higher than the estimated early solar nebula D/H ratio of $15\pm5x10^{-6}$. Most of the terrestrial hydrogen is in the form of water and has been out-gassed from the Earth's mantle. Loss of hydrogen molecules from the atmosphere has led to a gradual increase in the D/H ratio of atmospheric hydrogen compared to water in old rocks but only by around 10%. So the factor of ten enrichment was present in the water during the Earth's formation. Geiss and Reeves (1981) have proposed that this enrichment is caused by chemical fractionation between gaseous hydrogen and water ice bound to silicate grains - fractionation requiring a solar nebula temperature of 200K. A second possibility is deuterium enrichment from organic matter during the Earth's accretion (Anders and Owen, 1977). These two models affect all the inner planets (inside Jupiters orbit, 5AU) by an approximately equal amount. Alternatively Robert *et al.*,(1979) suggest that the inner planets could have been subjected to large proton fluxes, leading to deuterium formation by spallation, during a T-Tauri* phase of the young sun. This would lead to Li, Be and B enrichments and greater deuterium enrichments on bodies closer to the sun. The large proton fluxes required have not been observed in primitive meteorites which would have been exposed to them (Geiss and Reeves 1981).

1.5.3 Moon

The basaltic igneous lunar rocks appear to have a D/H ratio of around $100x10^{-6}$ (Merlivat *et al.*,1972) which is similar to that of the Earth. However the lunar regolith acts as an ideal trap for solar wind particles. The moon has no atmosphere, no magnetic field of its own (although paleomagnetic data indicate that it had a magnetic field that decayed *ca.* 3Gy ago; Hutchison, 1983) and lies outside the Earth's magnetic field so the solar wind is not deflected away from the moon. Hence the lunar regolith has had a long exposure to the solar wind. The D/H ratio of hydrogen released from lunar fines is less than $13x10^{-6}$ (Merlivat *et al.*, 1972, Epstein and Taylor, 1972). This high ratio, compared with the expected solar wind D/H ratio, is attributed to lunar water and terrestrial water exchanging with the solar wind hydrogen. Epstein and Taylor (1973) have attempted to prevent this exchange enriching the hydrogen by displacing lunar water with water which is deuterium free. This assumes that the solar wind is deuterium free.

---

* Most stars are thought to undergo an energetic phase, resulting in a strong stellar wind, shortly after formation. This has been observed in recently formed stars in the Taurus molecular cloud. For a review see Bertout (1984)

Some hydrocarbons have been found in the lunar regolith (*e.g.* Abell *et al.*, 1970). These are mainly methane, up to 5ppm by weight, see review by Pillinger, (1979). Abell *et al.*, (1972) suggest the methane is formed by solar wind interaction in the lunar regolith. Direct measurement of solar wind D/H ratio could be made by measuring the D/H ratio in these organics.

1.5.4 Venus

Since Venus is of similar size and has a close orbit to Earth it might be expected to have a similar D/H ratio. However, the atmosphere of Venus has a very low concentration of H_2 and H_2O due to loss of hydrogen from the atmosphere into space. This effect is much greater than on Earth due to the higher temperatures caused by a runaway green-house effect (Watson *et al.*, 1981). Models of atmospheric escape (Watson *et al.*, 1981) show that there is no significant fractionation until the volume of hydrogen in the atmosphere is reduced to less than 2 percent by volume, because deuterium is dragged into space by the flow of escaping hydrogen. When the amount of hydrogen dropped to less than 2% then the flow rate was not high enough to drag away deuterium and the atmosphere became progressively enriched in deuterium. Mariner 5 spectroscopic experiments detected Ly α lines of hydrogen in the atmosphere which were interpreted as being due to the presence of a high D/H ratio of 15000×10^{-6} (McElroy and Hunten, 1969). However, more recent measurements of the Ly α emission have placed an upper limit on the D/H ratio of 3600 ± 1500 (Bertaux and Clarke, 1989). Supporting evidence for extremely high D/H ratios has been provided by the mass spectrometers on the Pioneer Venus probe (Donahue *et al.*, 1982) which indicate that Venus has a D/H ratio of $16000 \pm 2000 \times 10^{-6}$.

1.5.5 Mars

Estimates of the D/H ratio and water content of Mars has been provided by *in situ* atmospheric measurements (from the Viking Landers, Owen *et al.*, 1977), spectroscopic and meteoritic analysis. The SNC group of meteorites are thought to originate from Mars, ejected by meteorite impact (McSween 1984). Remote sensing of Martian surface features and analysis of the volatile content of the SNC meteorites indicate that Mars has outgassed at least a 500m layer of water (Carr, 1987). Unlike Venus most of the water has not been lost into space, but remains trapped in either the polar regions, ices underground or in hydrous minerals; estimates of the total amount of water lost into space range from 6 to 160m, (Carr, 1987). The loss of some water by reduction to hydrogen and subsequent loss of the hydrogen by hydrodynamic escape has resulted in a deuterium enrichment, giving the high deuterium ratio of $900 \pm 400 \times 10^{-6}$ measured spectroscopically by Owen *et al.*, (1988). Kerridge (1988) found that the D/H ratios for Shergotty and

Lafayette, two SNC type meteorites, were $300x10^{-6}$ and $220x10^{-6}$ respectively. Terrestrial contamination may have reduced the D/H ratio since the water concentration in the meteorites was so low.

1.5.6 The outer planets and Titan

Observation of D/H ratios of Jupiter and Saturn have been made by CH_3D/CH_4 spectroscopic analysis (Owen *et al.* 1986), corrected for chemical fractionation with hydrogen (reaction 1.19) or by direct HD/H_2 measurement (Trauger *et al.* 1973 and Drossart *et al.* 1982). These two different spectroscopic methods both give a D/H ratio of *ca.* $20x10^{-6}$ for Jupiter and Saturn. Formation models of Jupiter and Saturn predict a runaway growth of a protoplanet core consisting of dust and ice grains. When the protoplanet attains a mass of about $10M_E$ a portion of the solar nebula becomes gravitationally bound to the core to give the planets atmosphere (Hubbard and MacFarlane 1980). Thus measurement of the D/H ratio of Jupiter and Saturn provide the best estimate of the solar nebula D/H ratio.

The D/H ratio of Uranus is in the range $33x10^{-6} < D/H < 63x10^{-6}$ (Trafton and Ramsay 1980). Due to its greater distance from the centre of the solar nebula, where presumably the density was lower, the core of Uranus took longer to form and captured a smaller portion of nebula gas. The atmosphere is thought to have equilibrated with the deuterium rich core to give the higher D/H ratio (Hubbard and MacFarlane 1980).

Titan has a D/H ratio of 165^{+165}_{-80} $x10^{-6}$ (deBergh *et al.* 1988 and Coustenis *et al.* 1989), indicating that equilibrium between hydrogen and water/methane occurred at 200K. Thus it appears that most water equilibrated with hydrogen at 200K throughout most of the solar nebula to give water with a terrestrial D/H ratio.

Spectroscopic data for the D/H ratio of Neptune only give an upper limit of $100x10^{-6}$ (Smith *et al.* 1989). However the recent flyby of Voyager may provide more accurate results soon.

1.5.7 Comets

Comets are small bodies, with nuclei *ca.* 1 to 10km in diameter, which condensed from the early solar nebula and are mainly composed of water ice (Whipple, 1987). Most information about comets have been obtained from the flyby of comet Halley by the Giotto and VEGA 1&2 spacecraft. A source of accessible cometary material may be interplanetary dust particles (Bradley *et al.*, 1988). Two main types of dust particle were detected by the flyby encounters with comet Halley; silicate particles and 'CHON' (containing mainly, in decreasing abundance, hydrogen, carbon, oxygen and nitrogen) particles (Langevin *et al.*, 1987). Thus comets may contain three sources of hydrogen:

i) Trapped hydrogen gas from the solar nebula which would have the D/H ratio of the solar nebula *ca.* $20x10^{-6}$.

ii) Water which forms the bulk of the comet. If the D/H ratio of Earth and Titan were obtained by chemical equilibrium with the pre-solar hydrogen then it would have a similar terrestrial D/H ratio, *ca.* $150x10^{-6}$.

iii) Organic molecules which may be the major constituents of 'CHON' particles. If these are similar to organic molecules found in carbonaceous chondrites (see 1.6.2) then these, like their meteoritic counterparts will have high deuterium enrichments, $> 300x10^{-6}$.

The D/H ratios of 'CHON' particles have not been obtained, however ion probe analysis of interplanetary dust particles show extreme enrichments in deuterium (Zinner *et al.*, 1983; McKeegan *et al.*, 1985; McKeegan *et al.*, 1987) with a D/H ratio between $170x10^{-6}$ and $1500x10^{-6}$. D/H ratios of water were obtained by measurement of H_3O^+ and H_2DO^+ ions during the Giotto flyby of comet Halley, giving $60x10^{-6} < D/H < 480x10^{-6}$ (Eberhardt *et al.*, 1986). This is consistent with water ice having obtained chemical equilibrium with pre solar hydrogen at a temperature of *ca.* 300K, but could also include some deuterium-rich organic component. More detailed analysis of the three hydrogen sources, if present, will probably have to wait for a comet sample return mission.

1.6 D/H ratios in meteorites

Meteorites are extraterrestrial objects that have survived the passage through the Earths atmosphere. Those that are observed to fall to Earth and later collected are termed 'falls'. Most meteorites , termed 'finds', were not observed to fall, but were recognised as such and collected because of their anomalous appearance compared with local rocks. The distinction between falls and finds is important because the amount of terrestrial weathering and possible isotope exchange is better characterised for the falls. Most meteorites are thought to be fragments of asteroids, which have been fragmented and sent into Earth crossing orbit by recent collisions within the asteroid belt (Wetherill and Chapman, 1988).

Most meteorites belong to one of two main types, the stony meteorites (described below in section 1.6.1) and iron meteorites which mainly consist of two iron-nickel alloys, kamacite (< 7% nickel) and taenite (> 25% nickel). There is a third minor type, the stony-iron meteorites, which consist of approximately equal amounts of the iron-nickel alloys and silicate minerals. Most iron meteorites are finds, whereas most falls are stony meteorites. This results from iron meteorites being easier to find because they have

a greater resistance to terrestrial weathering and a more obvious difference to terrestrial rocks than the stony meteorites (Hutchison, 1983).

Most iron meteorites are thought to originate from the cores of asteroid-type bodies. The presence of excess ^{107}Ag from the extinct radionuclide ^{107}Pd (half-life $6.5x10^6$ years) indicates that the melting and differentiation of a parent body to form a metallic core occurred within a few million years of nucleosynthesis of the ^{107}Pd (Kelly and Wasserburg, 1978; Kaiser *et al.*, 1980). Most iron meteorites have a high cooling rate of 10-100°C/million years indicating that they cooled in small parent bodies approximately 50km diameter (Wood, 1979).

Few studies of hydrogen isotopes in iron meteorites have been made since the concentration of hydrogen is very low and moderate heating of iron meteorites to 450°C liberates some hydrogen which results in the fractionation of the isotopes (Friedman, 1953). In an attempt to measure the D/H ratio of hydrogen in the solar nebula Edwards, (1955) analysed the hydrogen released by 10g quantities of iron meteorite upon heating. Obvious terrestrial contamination was reduced by removing surface rust. Results indicated that the irons contained about 20ppm hydrogen with δD ranging from -99 to -189‰, with most of the hydrogen concentrated in a fine powder between the kamacite/taenite interfaces. The location and terrestrial δD values the hydrogen released, and the fact that all the irons studied were finds, indicates that most of the hydrogen was probably due to terrestrial contamination.

1.6.1 Classification of stony meteorites

Stony meteorites are split into two main groups, the achondrites and chondrites. The achondrites are meteorites that have undergone major geological processing and include the SNC's, thought to be martian meteorites (see 1.5.5 above); lunar meteorites and meteorites that originate from a differentiated parent body.

Over 90% of meteorite falls are chondrites, these meteorites generally contain millimetre sized silicate spherules called chondrules. Petrographic and experimental studies of chondrules indicate that they formed from small dust aggregates in the solar nebula by some transient heating process lasting a few seconds (reviewed in Grossman *et al.*, 1988). Many processes have been suggested for their formation regions and mechanisms, reviewed by Grossman, (1988). Most are too inefficient at producing the large abundance of chondrules observed. Grossman (1988) concluded that the most plausible methods of chondrule formation consisted of heating dust clumps in a cool solar nebula. Possible transient heat sources included lightning in a turbulent nebula, (Whipple, 1966; Cameron, 1966); energy released by reconnecting magnetic fields (Sonnett, 1979); magnetic flares, (Levy, 1988); frictional heating of dust aggregates

falling in to the nebula plane (Wood, 1983, 1984); and heating by an energetic T-Tauri phase of the sun (Herbig, 1978).

Between the chondrules there is a fine grained material, usually termed matrix, although some workers restrict the term matrix to the extremely fine grain material (<5μm) between chondrules (see Scott *et al.*, 1988). Matrix material may represent the original dust which formed chondrules, but which remained unheated (Anders, 1964; Scott *et al.*, 1988). Alternatively the matrix may consist of chondrules broken by inter-chondrule collisions in the solar nebula (Alexander *et al.*, 1989b).

There are several lines of evidence which prove that the chondrites formed very early during the solar system formation:

i) They have formation ages of *ca.* 4.55 Gy and are the oldest rocks known (Tilton 1988).

ii) They have non-volatile abundance ratios similar to the solar photosphere, indicating that the sun and chondrites formed from a similar starting material (Anders and Ebihara 1982).

iii) Many contain non-equilibrium assemblages indicating that little geological processing has occurred since their formation.

iv) Many have minor components that have unusual isotope ratios indicating that they contain relict materials formed before the solar system formed.

Hence the chondrites are generally thought to be accretion of the material present in the early solar system to form asteroid type bodies. Since their formation they have not undergone major planetary processing and have remained essentially unchanged (however, most show signs of some processing, described later).

Although the chondrites have chemical abundances similar to the solar photosphere there are small systematic chemical differences between them which have been used to divide the chondrites into three main chemical groups. These are defined by the oxidation state and concentration of non-volatile lithophile elements relative to silicon in the meteorites, usually magnesium and calcium (Ahrens *et al.*, 1968). These groups are

i) Carbonaceous chondrites. These have a Mg/Si ratio greater than 1.05 and nearly all the iron is in the oxide or sulphide form. Although this group is small it is important as many of the carbonaceous chondrite meteorites contain indigenous organic molecules and have a high water content (section 1.6.2). These molecules formed either in or before the solar nebula and the processes that formed them may have been involved in the origin of life on Earth.

ii) Ordinary chondrites. These meteorites have a Mg/Si ratios of around 0.95 and most of the iron is in the oxide or sulphide form. Most chondrites are ordinary chondrites.

iii) Enstatite chondrites. These have a Mg/Si ratio of less than 0.85 and most of the iron is in the metallic form, indicating a more reducing environment for their formation region.

Further chemical and mineralogical differences are used to divide the chondrites into a total of nine groups. Four of these groups are carbonaceous chondrites and each group is named after a meteorite that is representative of the group. The CI (Ivuna) chondrites are unusual in that they contain no chondrules and have an abundance of hydrous minerals, up to 20 wt.% water. The CM (Mighei) chondrites contain a few chondrules; are similar in mineralogical composition to the CI chondrites but contain less water, approximately 10 wt.% water. The CO (Ornans) and CV (Vigarano) chondrites contain less hydrated minerals and the two groups are more readily distinguished by petrologic features. The CO chondrites contain many small close packed chondrules, whereas the CV chondrites contain large chondrules and irregular calcium-aluminium rich inclusions.

The ordinary chondrites are divided into three chemical groups, the H, L and LL groups, based on their iron and nickel abundance (Urey and Craig 1953; Craig 1964). The H-group, high-iron, contain about 27% total iron and from 12 to 20% iron-nickel by weight. Of the three ordinary chondrite groups these have the lowest oxygen content. The L-group, low-iron, 23% total iron and from 5 to 10% iron-nickel metal and the LL-group, low-iron and low-metal, contain 20% total iron and 2% iron-nickel metal. The LL ordinary chondrite group has the highest oxygen content.

The enstatite chondrites are divided into two chemical groups, the H and L groups (Sears *et al.*,1982a). This is based on the iron content, in a similar manner to the ordinary chondrites. H group enstatite chondrites have a Fe/Mg ratio greater than 0.9 whereas the L group enstatite chondrites have a Fe/Mg ratio between 0.65 and 0.75.

Although the chondrites are thought to have escaped major processing since their formation, there are textural and petrological variations between the chondrites within each chemical group which has long been attributed to secondary processing, mainly thermal metamorphism (Sorby, 1877; Merrill, 1921). These differences are used to classify the chondrites into six petrographic types and together with the chemical differences produce a two dimensional classification scheme (Van Schmus and Wood, 1967). The textural and petrologic differences used to distinguish between the petrographic types are shown in table 1.2. A seventh petrographic type has since been added to include some meteorites which had experienced thermal metamorphism to such an extent that they have almost melted (Dodd *et al.*, 1975).

The variation from type 3 to 7 chondrites shown in table 1.2 is due to the effects of increasing temperatures of thermal metamorphism, from 400°C to 950°C (Dodd, 1981), in small parent bodies soon after their formation (reviewed by Dodd, 1969; McSween *et al.*, 1988). As the temperature of thermal metamorphism increased the distinction between chondrules and matrix became blurred, glass devitrified to feldspar,

Petrologic type	Type 1	Type 2	Type 3	Type 4	Type 5	Type 6	Type 7
Carbonaceous chondrites							
Chondrules	absent	sparse	abundant and distinct		indistinct		
Matrix	serpentine and water rich minerals abundant		fine	olivine-rich, grained	coarse and granular		
Olivine	very rare	variable composition		uniform composition			
Chemical groups	CI	CM2	CO3	CO4			
		CV2	CV3	CV4	CV5		
Ordinary chondrites							
Chondrules			sharply defined	distinct	not distinct	sparse indistinct	absent
Matrix			opaque, fine-grained	opaque, less fine-grained	granular	granular, coarse-grained	coarse-grained
Glass			clear	turbid	completely absent		
Olivine			var. comp.	uniform composition			
Pyroxene			mainly disordered	mainly ordered	pyroxene is ordered (orthorhombic) throughout		
Plagioclase			totally absent	turbid crystals	clear, well defined crystals		
Enstatite chondrites			Olivine is almost totally absent, criteria for petrologic types 4-7 of the ordinary chondrites apply				

Table 1.2 Table showing the petrographic properties used to classify the chondrites (from Hutchison, 1983)

diffusion of iron and magnesium resulted in homogenisation of olivines and pyroxenes and their enrichment in iron due to chemical exchange with the matrix. The type 3 chondrites are often termed unequilibrated (Dodd and Van Schmus, 1965) due to the lack of homogenisation of iron and magnesium in olivine and pyroxene crystals.

The petrographic type 1 and 2 chondrites contain hydrous minerals and show signs of extensive aqueous alteration. In the type 1 chondrites aqueous alteration has proceeded to such an extent that all chondrules have been destroyed. Aqueous alteration in the type 2 chondrites was not as extensive and some chondrules survived. Petrographic studies of these meteorites indicate that this alteration occurred in the meteorite parent body. The observed effects of aqueous alteration include:

i) alteration minerals bridging chondrules,

ii) hydrous minerals lining fractures and forming veins in the meteorite and

iii) the presence of carbonates and sulphates in these meteorites.

Evidence that the aqueous alteration occurred soon after the formation of the meteorite parent bodies is provided by Rb-Sr ages of carbonates in Orgueil (type CI1) which indicated that they formed within 100Myr of the formation of the meteorite parent body (Macdougall *et al.*, 1984). For the aqueous alteration to occur requires a source of water (ices accreted with the parent body or water already present in hydrous minerals?) and a heat source (short lived radionuclides, electromagnetic induction, or impact melting). These heat sources could be the same as those that caused thermal metamorphism in the type 4 to 6 chondrites, but a lower temperature being achieved. For a complete review see Zolensky and McSween (1988).

Fig.1.3 is a schematic diagram showing the relationship of the secondary alteration processes with petrographic type. Each of the chemical groups of meteorites has not suffered the complete range of aqueous alteration and thermal metamorphic effects as shown in fig.1.4. The possible causes of thermal metamorphism and aqueous alteration are discussed in chapter 4.

Other secondary processes that have occurred are shock and brecciation. Shock effects, caused by impact between meteorite parent bodies, indicate the processes by which brecciation and fragmentation occurred on the parent bodies. However the amount of shock experienced by meteorites is largely independent of chemical and petrographic types and so not generally used for classification. Meteorite breccias are indications of surface conditions on parent bodies and are produced by impact events, that occurred soon after parent body accretion. Most chondrite breccias contain fragments of only a single chemical group though often of different petrographic type, suggesting that each of the nine chemical groups of chondrite formed on a separate parent body (Bunch and Rajan, 1988).

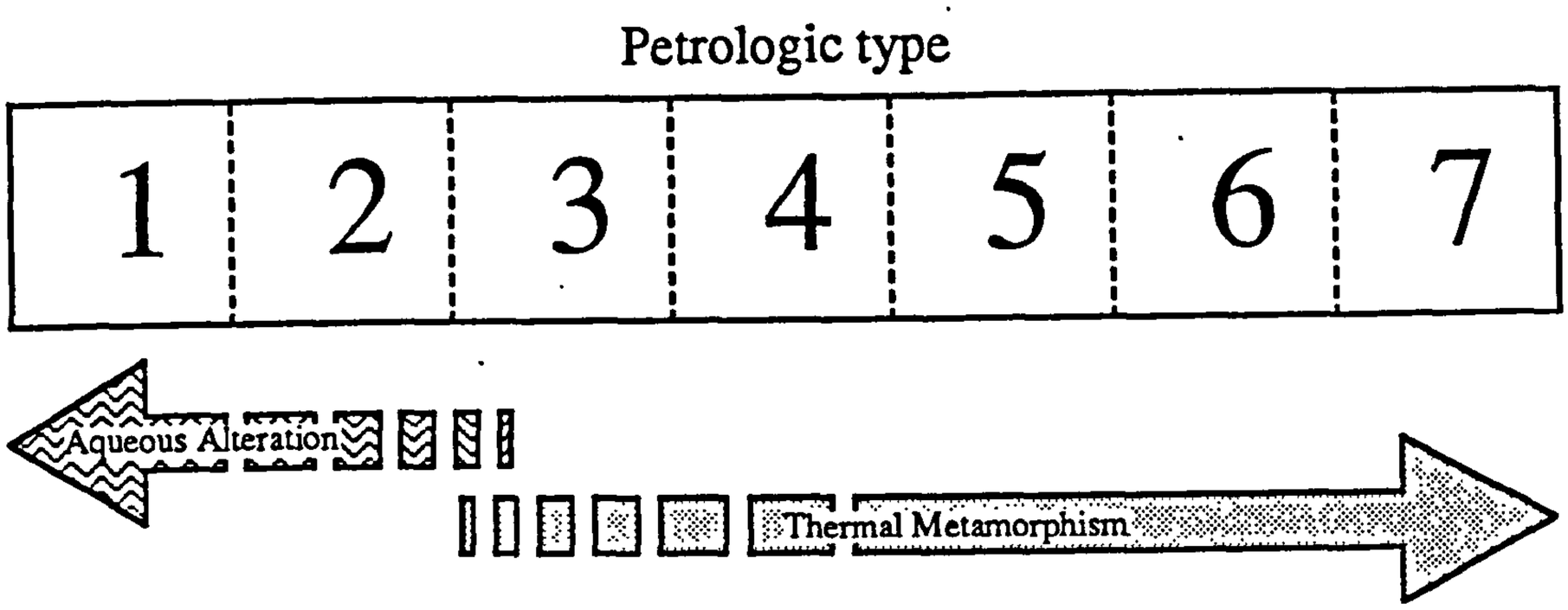

Fig 1.3 Relationship between petrologic classification and the degree and type of secondary processing experienced by chondrites

Meteorite class		Type 1	Type 2	Type 3	Type 4	Type 5	Type 6
Carbonaceous chondrites	CI	5					
	CM		33				
	CO			10			
	CV			14	1	2	
Ordinary chondrites	H			25	157	271	154
	L			22	53	105	423
	LL			14	10	20	47
Enstatite chondrites	H&L			2	8	3	11

Fig 1.4 Approximate numbers of meteorites in each chemical and petrologic group, data from Graham *et al.*, (1985).

Further evidence that each chemical group of chondrite originated on different parent bodies has been provided by oxygen isotopic analysis of the chemical groups (Clayton, 1981). Most of the chemical groups plot in distinguishable fields on a three isotope plot. Hence each of the chemical groups are thought to originate from separate parent bodies, differences between the various chemical groups of chondrites are mainly due to their formation regions and/or time of formation (Sears and Dodd, 1988). Thus the study of chondritic meteorites provides an opportunity to study the differences in various regions of the solar nebula at the time of their formation. However, all the chondrites have undergone secondary processing to some extent (usually thermal metamorphism or aqueous alteration) on their parent bodies, which has modified their primary properties. Study of these secondary processes and effects on chondrites can give insights to the conditions prevalent during the early solar nebula.

1.6.2 Carbonaceous chondrites

Carbonaceous chondrites contain about 2 wt.% carbon; however, the amount of carbon is not a good indicator of chemical classification scheme, many other classes of meteorite contain individuals with higher carbon content than some of the carbonaceous chondrites (Van Schmus and Wood, 1967). The carbon in the petrographic type 3 or higher carbonaceous chondrites is in the form of poorly graphitised or amorphous carbon. Type 1 and 2 carbonaceous chondrites contain a large concentration of water (up to 11wt.%) and contain carbon in the form of organic molecules. Because of the obvious interest in extraterrestrial organic material and the possible implications for the origins of life, hydrogen isotope studies have concentrated on analysis of type 1 to type 3 carbonaceous chondrites.

1.6.2.1 Organics in carbonaceous chondrites

Approximately 30% of the organic compounds in carbonaceous chondrites are solvent extractable, the remaining 70% consisting of a macro-molecular material, often called polymer, or kerogen-like material (Hayes, 1967). Initial studies of organic molecules in carbonaceous chondrites were hampered by the possibility of terrestrial contamination. Briggs (1963) first showed that the solvent extractable organic molecules in the carbonaceous chondrites were extra-terrestrial since they had a high δD ratio of up to +275‰.

Analysis of individual organic compounds is achieved by gas chromatography (GC) or gas chromatography-mass spectrometry (GC-MS). Considerable effort has concentrated on the detection of the amino acids because of the possible implications for the origins of life. So far 74 amino acids have been detected, including all possible types

containing 5 or fewer carbon atoms (Cronin and Pizzarello 1986). Terrestrial contamination is excluded because

i) Of the 74 amino acids detected only 19 occur naturally by biogenic synthesis (Cronin *et al.* 1988).

ii) Each type occurs in a mixture of both L and D form (Kvenvolden *et al.* 1970), biological amino acids only occur in the L form.

iii) They have unusual stable isotope ratios (Epstein *et al.* 1987).

Other solvent extractable classes of organic compounds have been detected and their properties are shown in table 1.3. Since chemical processing on primitive meteorite parent bodies halted soon after their formation it is clear that organics must have formed early in the history of the solar system; alternatively they may pre-date the solar system. Possible formation mechanisms are:

i) Fischer-Tropsch-Type reactions (FTT). Organic molecules are formed from CO, H_2O and NH_3 by catalysis on phyllosilicate grains either in the gaseous nebula or on the meteorite parent body (Hayatsu and Anders 1981).

ii) Photochemistry and radiation chemistry. A variety of organic molecules have been formed by energising an atmosphere of CH_4, H_2O and NH_3 (thought to be similar to the primitive Earth atmosphere), the energy being provided by lightning discharges (Miller, 1953; Miller and Urey, 1959). Similar organics have been produced using U-V light as an energy source in gases, (organics produced in planetary atmospheres or the solar nebula, Sagan and Khare, 1979) and in ices (organics produced in comets, Greenberg, 1982). These type of reactions could take place in the solar nebula or in the atmosphere of a planet (Miller 1953).

iii) Ion-molecule reactions in dark molecular clouds (section 1.4.3). More complex organic molecules are formed by addition of simple ions until neutralised by electrons in the molecular cloud, for example

$$CH_3^+ + H_2O \leftrightarrow CH_3OH_2^+ \qquad (1.24)$$

$$CH_3OH_2^+ + e^- \leftrightarrow CH_3OH + H \qquad (1.25)$$

Each type of reaction produces different types of organic molecules and isotopic signatures as shown in table 1.4.

The acid and solvent insoluble macro-molecular material appears to consist of aromatic and hetero-aromatic ring systems which are highly unsaturated and connected by short aliphatic chains and ether linkages (Hayatsu *et al.* 1977 and Hayatsu *et al.* 1980). The aromatic components contain 3 to 5 benzene rings referred to as polycyclic aromatic hydrocarbons (PAH). Tentative identification of PAHs have been made for the unidentified IR bands in diffuse interstellar clouds (Lepp *et al.* 1987). These PAHs can survive the UV radiation in the interstellar medium as their large size enables them to

Compound	Abundance (ppm, µg/g)
Aliphatic hydrocarbons	12 - 35
Aromatic hydrocarbons	15 - 28
Monocarboxylic acids (C_2-C_8)	330
α-hydrocarboxylic acid (C_2-C_5)	14.6
Amino acids	10 - 22
Alcohols (C1-C4)	11
Aldehydes (C2-C4)	11
Ketones (C3-C5)	16
Amines (C1-C4)	10.7
Urea	25
Basic N-heterocycles	0.05 -0.5
Pyrimidines	0.06
Purines	1.2
Acid insoluble phase (polymer type)	1450

Table 1.3 Types of organic compounds detected in the Murchison carbonaceous chondrite, from Mullie and Reisse (1987)

Compound	Fischer-Tropsch-Type (FTT)	Photochemistry and radiation chemistry	Ion molecule reactions
Alkane Chains	Straight	None?	Branched
Alkynes	Some	Common	Rare
Cyanoacetylenes	Some	Common	Rare
Aromatics	Yes	?	Rare
High D/H	No	Yes	No
C isotope fractionation	No	Yes	No
Polymer (slightly heated)	Aliph.-Arom.	Acetylenic	Aliphatic
Polymer (strongly heated)	Aromatic	Aromatic	Aromatic

Table 1.4 Types of organic compounds and isotopic signatures produced by various synthesis mechanisms, from Anders, 1986

absorb the radiation without disruption of the molecule. They have not been detected in dark molecular clouds, probably due to the lower concentration compared to other organic molecules. Recently Wdowiak *et al.* (1988) have measured the IR spectra of acid-insoluble residues of Orgueil and found therm to be similar to that of the PAH in diffuse interstellar clouds. Anders (1973) has managed to produce macro molecular type material by prolonged FTT synthesis which polymerises the organics, suggesting FTT reactions in the interstellar medium or solar nebula as a production mechanism.

1.6.2.2 D/H ratios in carbonaceous chondrites

Hydrogen isotope studies of meteorites have concentrated on carbonaceous chondrites because of their high water and organic content. Initial studies of D/H isotopes on whole-rock samples of carbonaceous chondrites showed that they contained a deuterium enrichment (Boato, 1954). Becker and Epstein (1982) measured the D/H ratios of the solvent extractable organics and obtained D/H ratios of +346‰ to +486‰. This is above the terrestrial range of D/H ratios indicating that these organics are extraterrestrial. Kolodny *et al.* (1980) measured indirectly the D/H ratio of the organics by measuring the change in D/H ratios of samples which had all the organics removed by low-temperature plasma ashing. The oxidised samples had lower D/H ratios than the unoxidised samples, down to -159‰. The calculated D/H for the organics was up to +1600‰ for Renazzo. The presence of high D/H ratios in the solvent-insoluble material has been measured directly by preparing acid residues (Smith and Rigby 1981, Robert and Epstein 1982, Yang and Epstein 1983). The acid residues exhibit a wide range of D/H ratios from -500‰ up to +2000‰ for Renazzo, possibly indicating that the acid-insoluble material originates from several sources. Calculation of the D/H ratio of the soluble material (water and solvent extractable organics) gives $\delta D = -110‰$, apart from Renazzo which had $\delta D = +920‰$. Most of the hydrogen in the acid soluble phase is in the form of water bound in phyllosilicates. Thus it appears that most of the water in the solar nebula attained chemical equilibrium with the hydrogen at a temperature of ~260K giving it a terrestrial-like D/H ratio of *ca.* -100‰, consistent with the D/H ratios of water in other solar system bodies (section 1.5). This temperature is about 100K lower than that indicated by other "cosmothermometers" of around 360K (Hayatsu and Anders 1981 and references therein), indicating that the water attained equilibrium with hydrogen in the solar nebula before incorporation into the meteorite where other "cosmothermometers" attained equilibrium.

1.6.3 D/H ratios in ordinary chondrites (OCs)

Most, approximately 80%, meteorite falls are ordinary chondrites. Ordinary chondrites range from petrographic type 3 to 7 and show signs to some degree of thermal metamorphism. Searches for pristine nebula material have concentrated on the matrix of type 3 unequilibrated ordinary chondrites (UOCs), since these have been affected least by secondary processes.

Hydrogen isotope studies of ordinary chondrites have concentrated on the unequilibrated ordinary chondrites due to their higher water content and the possibility that they may contain organic compounds similar to the carbonaceous chondrite organics. To date there have been no GC or GC-MS studies of ordinary chondrites to determine whether they contain extraterrestrial organics. However, the presence of organic compounds has been inferred by comparison of H,C and N isotopes and the similarity of pyrolysis release profiles with the carbonaceous chondrites (Robert *et al.* 1987a,b; Alexander *et al.*, 1988).

Stepped pyrolysis of Semarkona, a type LL3 ordinary chondrite, by McNaughton *et al.* (1982a,b) indicated the presence of a deuterium-rich component that pyrolysed between 600 to 850°C with $\delta D = +5740‰$. Most of the water released at lower temperatures appears to have a terrestrial D/H ratio and is probably phyllosilicate water, similar to the carbonaceous chondrites. Experiments by Yang and Epstein (1982) indicated that an acid-residue of Semarkona had a lower D/H ratio than the whole-rock. Either the deuterium-rich phase is in the silicate water, or in the acid-soluble organics. Renazzo, an unusual carbonaceous chondrite and Bishunpur, another type LL3 ordinary chondrite, also had a deuterium-rich acid-soluble phase, which Yang and Epstein (1982) suggested was due to mixing between phyllosilicate water with $\delta D = -110‰$ and a deuterium rich phase with $\delta D = +10\,000‰$.

Robert *et.al.* (1987a) have shown by high-resolution continuous pyrolysis of Chainpur (type LL3.4) that it contains several hydrogen components.

i) A component that pyrolyses below 450°C with $\delta D = -450‰$

ii) A deuterium-rich component that pyrolyses above 450°C with $\delta D > +4500‰$.

Robert (1987a) attributed the high temperature component to the organics since its release profile is similar to carbonaceous chondrite organics. This component was concentrated in the rims of the chondrules rather than in the matrix. The low temperature component is thought to be phyllosilicate water indigenous to the meteorite. Possibly indicating that the 'phyllosilicate water', calculated by Yang and Epstein (1982) to have $\delta D = -110‰$, was in fact a mixture of two components; water with $\delta D = -450‰$ and acid soluble deuterium-rich organics. Hence chemical equilibrium between water and solar nebula hydrogen may have been attained at a higher temperature of *ca.* 300K.

1.7 Research objectives

1.7.1 Project outline

The main objective of this project was to undertake a more detailed study of the deuterium-rich carrier in type 3 unequilibrated ordinary chondrites. Most effort has concentrated on Semarkona since it has been affected least by thermal metamorphism (described in more detail later, chapter 4) and it has the highest whole-rock D/H ratio, indicating that it contains the greatest concentration of the deuterium carrier. The aims of the project were to determine:

i) the source of the deuterium carrier in type 3 UOCs and how it gained such a high deuterium enrichment.

ii) whether the deuterium carrier is an organic compound and if there is any similarity with carbonaceous chondrite organics and

iii) the sequence of secondary processing events on the Semarkona parent body and to determine whether the deuterium carrier was formed by the secondary processes or merely survived them.

As Semarkona has not been metamorphosed to a great extent it is very heterogeneous and hence individual studies using different techniques cannot be correlated. Semarkona has many unusual properties, compared with other ordinary chondrites, which could all be related to either the lack of thermal metamorphism, or unobscured nebula processes, or the affects of aqueous alteration. In an attempt to overcome the heterogeneity and relate hydrogen isotope ratios with petrology and thermoluminescence (a sensitive indicator of secondary processing, Sears 1980) a combined project was undertaken. Individual chondrules and matrix samples were separated from a sample of whole-rock Semarkona. Each separate was split into three fragments for analysis by the following techniques.

i) Petrology using electron microscope and microprobe, to determine any unusual features, the amount of thermal metamorphism and type of material being analysed.

ii) TL to determine the extent of any aqueous alteration.

iii) Hydrogen isotope analysis to determine the concentration of the deuterium rich carrier, the amount of water and whether this water is due to terrestrial contamination or a parent body process.

Chapter 4 explains in detail the methods used, the results obtained and comparison with other unequilibrated ordinary chondrites and carbonaceous chondrites.

1.7.2 Analytical techniques

A prime requisite for this project was the ability to perform hydrogen isotope analysis of samples containing less than 1μg of water. Analysis by ion probe might appear suited to this project in that individual points on a polished thick section could be analysed and a precision of ±30‰ is adequate. However, hydrogen in any organic molecules is likely to be situated in the same areas as terrestrial contamination and indigenous water. Terrestrial contamination can be separated from meteorite hydrogen by pyrolysis under vacuum at around 200°C (Boato 1953). High temperatures would release first the meteorite water and then organic hydrogen allowing separation of the water from organic material. Therefore samples were analysed by a stepped pyrolysis to release water and the water analysed by mass spectrometry.

As mentioned in section 1.2.3 commercial dynamic mass spectrometers require samples of about 50μmol of hydrogen. Thus, much of this project has focussed on improving the capability of the analytical techniques. Mass spectrometer sensitivity was increased by delaying the conversion of water to hydrogen until the water entered the mass spectrometer source volume, effectively reducing the size of the storage volume of hydrogen. The techniques used and their evaluation are described in chapter 3.

Throughout this project, analytical problems were encountered with the movement within the extraction system of small water samples. The ways in which attempts were made to solve these analytical problems are described in detail in section 3.3.6. While satisfactory results were obtained for Semarkona lack of precision in δD measurements prevented continuation of the project for similar analysis of Bishunpur and Chainpur. Further work has concentrated on a different hydrogen isotope method, utilising the results learnt in the evaluation of the original technique. This work is described in Chapter 5. Initial results show that this is capable of measuring 1nmol of hydrogen with a precision in δD of ±20‰.

Chapter 2
The D/H Mass Spectrometer

2.1 Dynamic mass spectrometry

Light element (H, C, N, O and S) stable isotope ratios are usually measured by dynamic gas source mass spectrometry. Operating on the principle of Aston's mass spectrograph (Aston, 1919), gas molecules are ionized, accelerated and then the different mass isotopes separated by a magnetic field. Modern gas source mass spectrometers are based on the design of Nier (1947), as improved upon by McKinney *et al.* (1950). Fig. 2.1 shows a schematic diagram of such a mass spectrometer (often referred to as a "dynamic" instrument because there is a continuous flow of gas into the ionisation source during analysis). Sample and reference gas from storage reservoirs are leaked through capillary tubing to a change-over valve, which links either the sample or reference capillary outlet to the source where some is ionized by an electron beam and then accelerated by the electric HT voltage of the source. The ion beam is deflected by a magnet and focussed onto one or more Faraday buckets, positioned to collect the ions of interest.

The mass spectrometer is continuously evacuated by a diffusion pump to maintain a low pressure of gas in the flight tube thereby reducing the incidence of ion-neutral collisions. An important feature of a dynamic mass spectrometer is the change-over valve (Murphey, 1947) which allows introduction of either the sample or the reference gas (of known isotopic composition) into the mass spectrometer source. With this facility it is possible to obtain rapid change-over between sample and reference gas and repeated

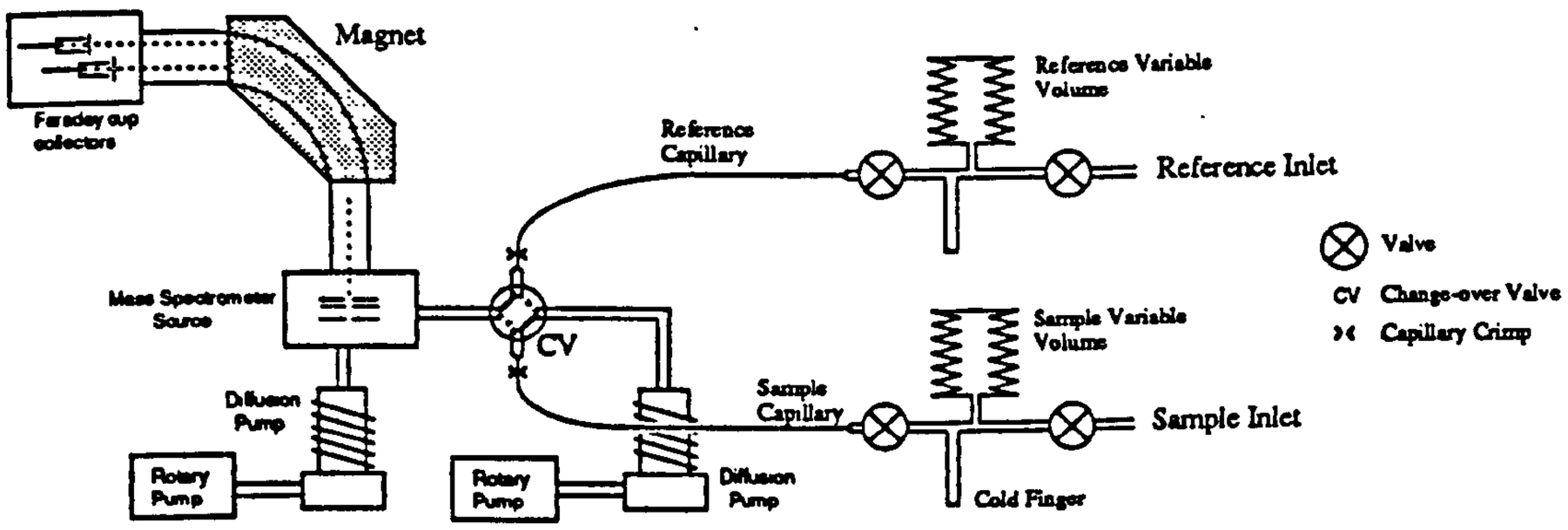

Fig.2.1. A schematic diagram of a conventional dynamic mass spectrometer. Gas from both the reference and sample inlets flows continuously, through their respective capillaries, into the change-over valve. There is a continuous flow of either reference or sample gas from the change-over valve into the mass spectrometer source, whilst the other gas is bled to waste.

comparisons, improving precision of the isotopic measurements by reducing errors caused by source fluctuations (drifting of the source accelerating and focussing voltages) during analysis.

Further precision is gained by keeping both reference and sample gas at equal pressure during analysis to eliminate source pressure effects (changes in the ionisation efficiency between the isotopes of the gas caused by the pressure of gas in the source). This is achieved by the variable volume, usually, but not always a stainless steel bellows, which allows the pressure of the reference and sample gas to changed. The variable volume for the sample gas is often omitted to keep the sample reservoir volume as small as possible.

In order to preserve viscous flow and thus prevent significant isotopic fractionation of the gases during analysis it is necessary to maintain the pressure in the capillaries to greater than 20 torr, (Halsted and Nier 1950); this is achieved by crimps, shown in fig. 2.1, which constrict the end of the capillary. The degree of constriction in the capillary can be adjusted using the crimps to control the flow rate of gas into the ionization source. Whilst one gas is analysed the other is bled to waste, *via* a similarly pumped exit, so that any isotopic fractionation arising from the capillaries is equivalent for both sample and reference gas.

The features of a dynamic mass spectrometers enable the measurement of stable isotope ratios to high precision (typically much better than ±0.1‰ for carbon and around ±1‰ for hydrogen), but has the disadvantage that a large amount of sample is required for the following reasons:-

i) Most of the sample gas in the storage reservoir does not reach the change-over valve but is merely used to provide a stable pressure to push some sample through the capillary.

ii) During analysis at least half of the sample gas that reaches the change-over valve is bled to waste.

iii) Less than 1% of the gas that enters the mass spectrometer source is ionised and detected by the collectors. Most of the gas is pumped to waste by the mass spectrometer pumps.

Problem i) poses severe constraints on D/H measurements since hydrogen can not be cryogenically manipulated using liquid nitrogen and thus the storage reservoir also includes the sample preparation and transfer volume. To some extent the minimum volume can be reduced by use of toepler pump or mercury pistons (Dumke *et al.*, 1989) In conjunction the three problems listed above limit the sensitivity of hydrogen isotope analysis to samples containing at least 10μmol of hydrogen. Obviously, if the volume of the inlet, or storage volume, can be reduced then sensitivity can be improved. It was with this aim in mind that the inlet designs discussed in chapter 3 were conceived. What

follows in the rest of the present chapter is a description of the dynamic instrument which was employed during these studies. Many of the components used were obtained from commercial companies, where appropriate the model number and manufacturer are given in the text. The addresses of these companies are listed in appendix B.

2.2 The D/H mass spectrometer

2.2.1 D/H analyser and associated hardware

A D/H mass spectrometer was designed, incorporating maximum flexibility to enable further development work. The research unit already had a D/H mass spectrometer, as part of a VG SIRA 24 (VG Isogas, now Isotech). The SIRA 24 had two analyser heads, one for D/H isotope analysis and the other for carbon and oxygen isotope analysis, arranged in a siamese twin configuration. The siamese twin arrangement, shown in fig 2.2, enabled a single gas inlet system to analyse either hydrogen or carbon and oxygen isotopes, although not simultaneously.

In theory the siamese twin arrangement made it quick and easy to switch between carbon/oxygen and hydrogen isotope analysis. However, in practice, due to the time

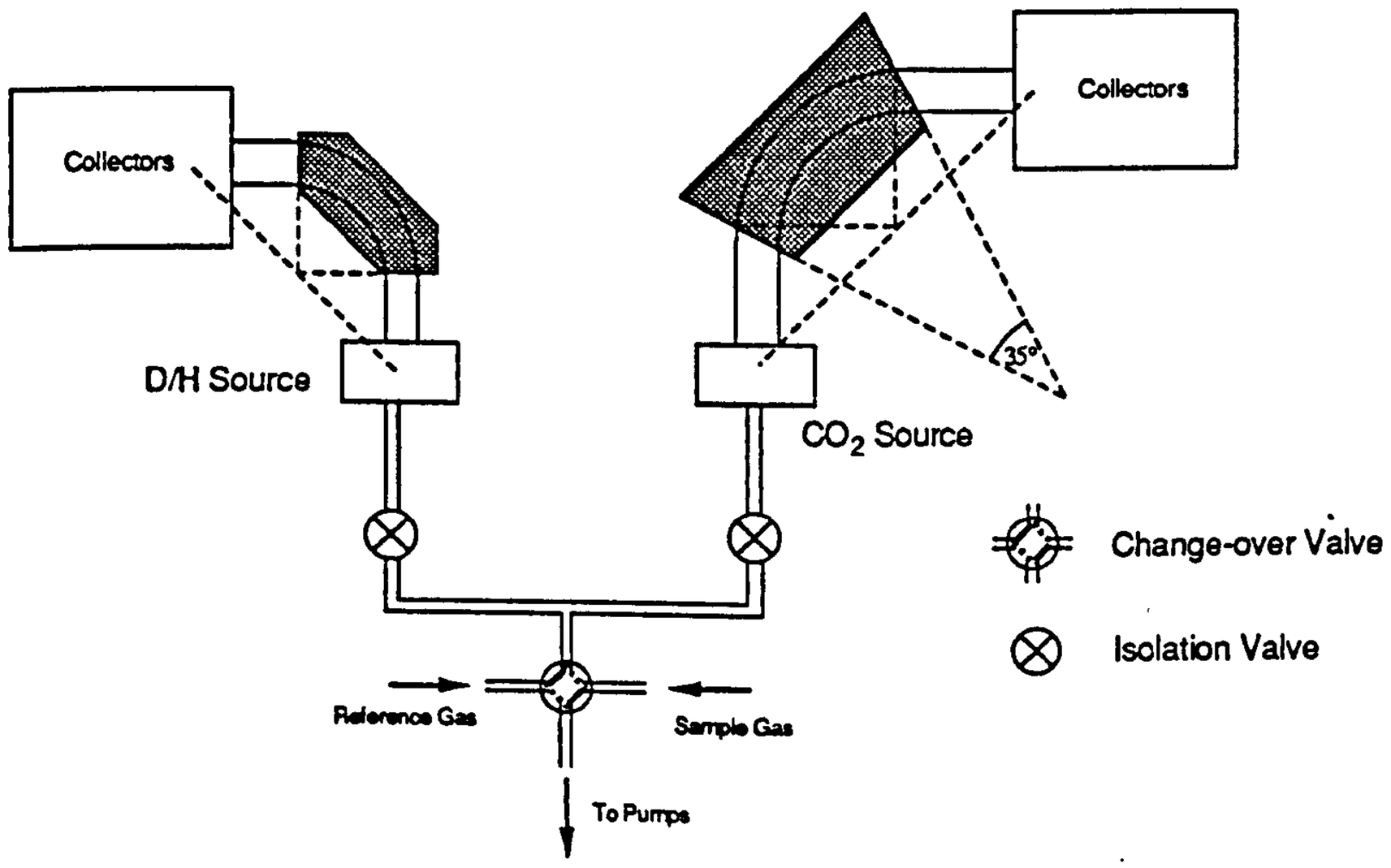

Fig. 2.2. Schematic diagram of the Siamese twin arrangement for the SIRA 24 mass spectrometer. The twin arrangement enabled a single gas inlet and electronics system to analyse either carbon/oxygen isotopes or hydrogen isotopes, although not simultaneously. The hydrogen analyser was removed for use as a stand-alone D/H analyser.

taken to switch between analysis modes and the almost continuous use of the SIRA 24 for carbon isotope analysis, the hydrogen analyser was rarely used. Also the position of the hydrogen analyser, enclosed in an oven underneath a table top and close to the carbon/oxygen analyser, was not conducive for development work. The hydrogen analyser was removed and reconfigured as a stand-alone mass spectrometer specifically for hydrogen isotope analysis. In this new configuration the D/H analyser was supported on top of a 71cm square table, height 78cm, constructed from 2" angle iron with a 1/2" thick aluminium plate on top. The analyser was positioned towards the back of the table, leaving the front portion available for construction of the reference and sample inlet systems.

The mass spectrometer components (source, flight tube, vacuum piping etc.) were assembled in-house. The stainless steel welding and manufacture of some of the components for the vacuum system was undertaken by members of the Open University workshop. Some of the electronics for control of the mass spectrometer and data collection were designed and built as part of the project.

The mass spectrometer ionisation source, magnet, collector assembly and first stage amplifiers form what is essentially a Micromass 602 type D/H analyser (VG Micromass, now Isotech). This is made of stainless steel and comprises of an 'open' Nier-type ionisation source, a flight tube (60mm radius, 90° sector), two Faraday cup collectors and two first stage amplifiers. A tungsten source filament was used, operating at a current of approximately 3.6A to give a trap current of 440μA. Under normal conditions the tungsten filament had a life time of at 12 months. The deflection magnet, with nominal field strength of 0.2 Tesla, was supported by a magnet carriage which allowed its position to be adjusted precisely. The first stage amplifiers (described in 2.2.3) were housed in a metal casing close to the collectors to reduce electrical noise and voltage drift due to ambient temperature and humidity variations.

The design of the D/H analyser incorporates some special features, due to problems associated with D/H isotopic analysis (Bridger *et al.*, 1974). First, in order to reduce the production of H_3^+ ions, the source includes a special repeller arrangement and is of a more open design. This results in the rapid removal of H_2^+ ions thus reducing the formation of H_3^+ ions by ion-molecule collisions in the source (described in section 2.4.3). The 'open' design of the Nier source also allows a high trap current to be used, of at least 440μA, leading to greater ionisation efficiency and hence greater mass spectrometer sensitivity. Secondly, since the D/H ratio of most samples (*i.e.* terrestrial samples) is only *ca.* $150x10^{-6}$, secondary ion emission at the collectors can contribute significantly to the minor ion beam signal. Usually this is reduced by supplying a suppressor voltage of -45V above the collectors. In addition to this the D/H analyser had two small moveable magnets mounted externally on the collector housing to reduce even further any

secondary ion emission (the exact positioning of the magnets required careful optimisation during initial instrument testing).

The analyser could be baked to 300°C by means of a demountable oven (dimensions 71x38 and height 45 cm) to aid degassing of atmospheric gases. The oven was heated by a 2kW electric cooking ring element (Southern Electricity Board) mounted on the mass spectrometer table, controlled by a variable transformer (Zenith Electrical).

2.2.2 Mass spectrometer vacuum system

A schematic diagram of the mass spectrometer vacuum system is shown in fig. 2.3. The pumps and vacuum components were positioned under the mass spectrometer table. The mass spectrometer source was pumped by two diffusion pumps (E02k, Edwards) filled with 75 ml polyphenyl ether oil (Santovac 5, Monsanto Company) with a nominal pumping speed of 150 ls^{-1} of air. The bleed-line from the change-over valve was pumped by a similar type of diffusion pump. The diffusion pumps were backed by a rotary pump (E2M8, Edwards) fitted with a foreline trap (FL20k, Edwards), filled with activated alumina (Edwards) which prevented back streaming of the rotary pump oil into the backing line.

The isolation valve (PV25, Edwards) prevented air entering the mass spectrometer by automatically closing in the event of a power failure to the pumps. The pumps were protected by a Pirani trip so that they switched off in the event of loss of vacuum, detected by the Pirani head (PRM10, Edwards). The diffusion pumps were further protected by thermal trips so that they were switched off before overheating in the event of the loss of the cooling water supply. The thermal trips operated if the diffusion pump casing temperature went above 70°C, detected by a thermal switch (N/C bimetallic 70°C switch, RS, Corby, England). They were designed so that once tripped off they would remain off until manually reset. The circuit diagrams for the Pirani and thermal trips are given in appendix A.

The vacuum system was constructed from 316 stainless steel tubing, 1" O.D., 16 gauge, connected by clamped couplings (KF25 flanges and KF25 'O' ring assemblies, Edwards). Where necessary flexible stainless steel sections (321-16-X-1, North London Valve & Fitting Co. Ltd.) were used to reduce stress and allow greater tolerances in the fitting of the vacuum components.

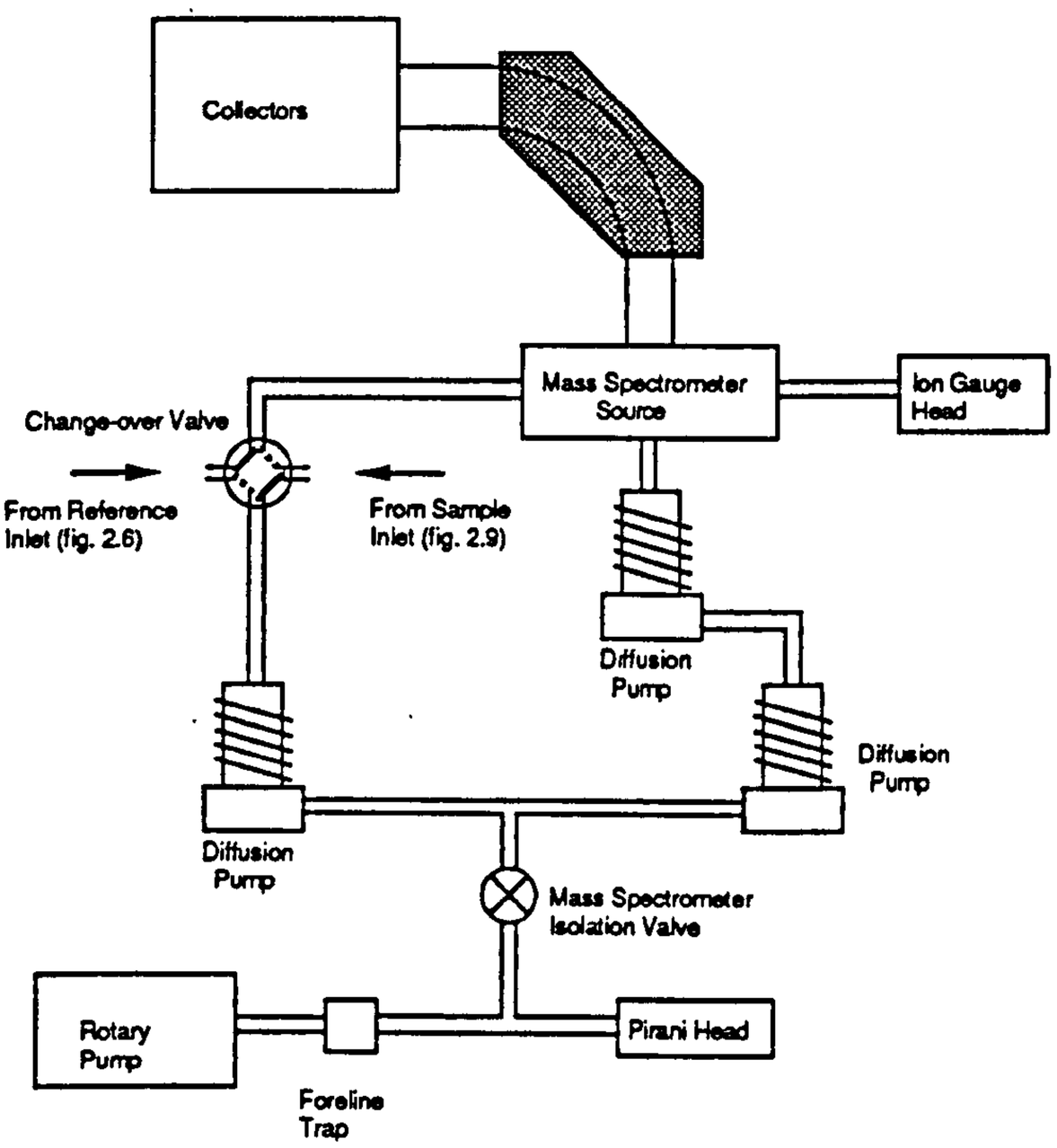

Fig. 2.3. A schematic diagram of the D/H mass spectrometer pumping system. The mass spectrometer was pumped by two oil diffusion pumps to prevent the possibility of the gas being bled to waste back streaming into the source and contaminate the gas being analysed.

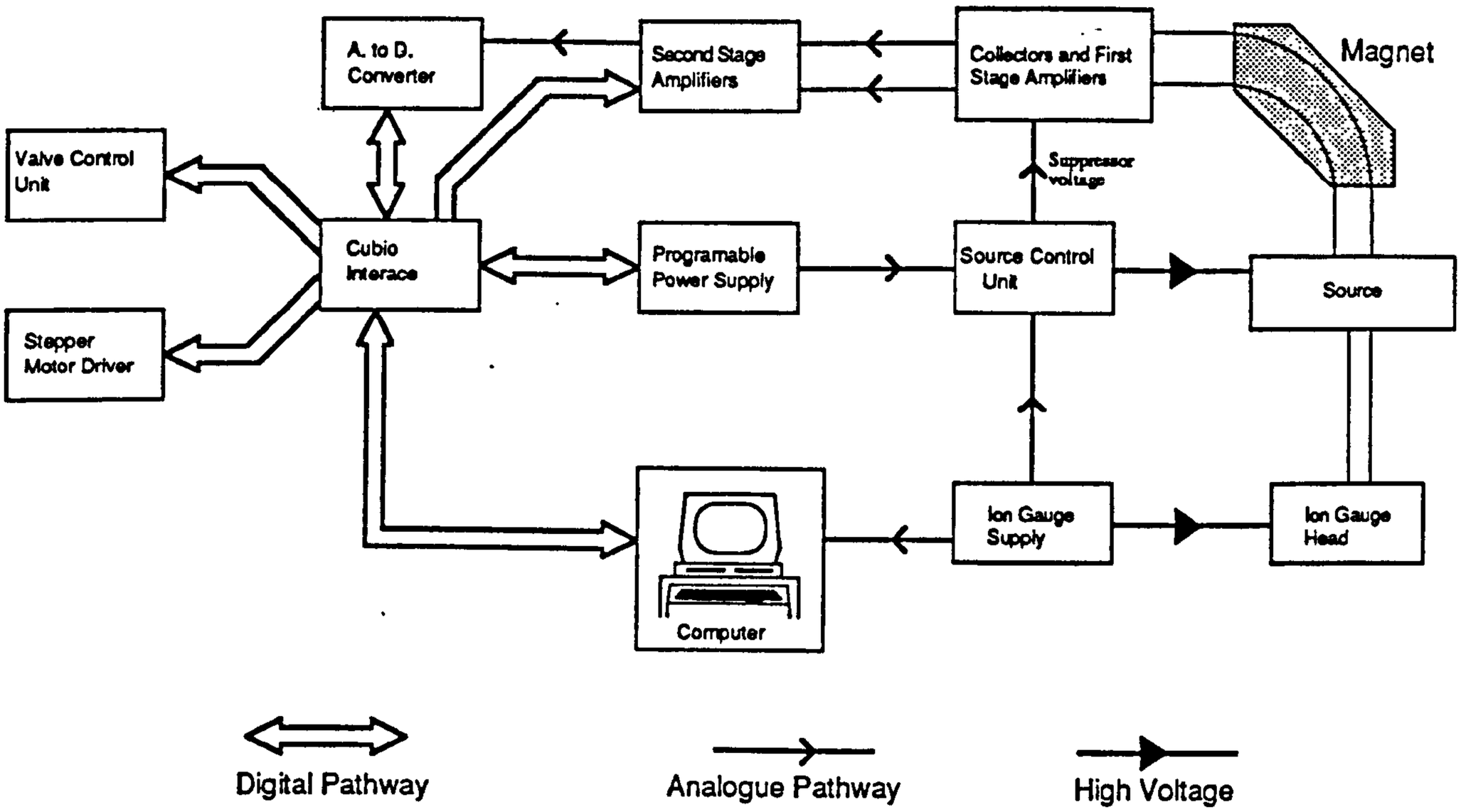

Fig. 2.4. Schematic diagram of the mass spectrometer control and data acquisition electronics. Most of the electronic units are controlled by the computer via the Cubio interface.

2.2.3 Control electronics

A schematic diagram of the electronics for the mass spectrometer control and data collection is shown in fig. 2.4. It was designed to be semi-automatic, with the possibility of full automation, if needed, at a later date. Each of the systems is briefly described below. The circuit diagrams of the units designed and constructed in-house are given in appendix A.

Control of the mass spectrometer and data acquisition was performed by a 6502, 8-bit, 1MHz micro-computer (128k BBC micro-computer, Acorn Computers Ltd.). This was interfaced to the electronics by a digital input/output adapter (Cubio, Control Universal) through a 20mHz bus output from the micro-computer. The computer also had four 12-bit Analogue-to-Digital converter (ADC) input channels which were used to read data from some of the other electronic units (for example: from the ion gauge, described below). The inputs to the computer ADC channels were protected by a buffer circuit since input voltage signals of greater magnitude than 1.8V would damage the computer. The buffer circuit had four voltage input ports, one for each computer ADC channel. Input voltage ranges available were one port with 0 to +20V, two with 0 +10V and one with 0 +5V, these were converted to a 0 to +1.8V output signal. The design of buffer circuit, shown in appendix A, ensured that the maximum output voltage was 1.8V even if the input voltage was above the accepted range.

The programmable power supply unit converted a 16-bit digital signal sent from the computer to an analogue 0 to +5V using a 16-bit Analogue-to-Digital converter (DAC709KH, Burr Brown). The output signal was used by the source control unit (880 Unit supplied by VG Isogas, now Isotech) to provide a 0 to 5kV accelerating voltage to the mass spectrometer source. This also supplied the mass spectrometer source focussing voltages, and filament current, as well as the suppressor voltage of -45V for the Faraday cups. The 880 Unit was modified slightly by moving the recessed front panel forward, adding a mains power on/off switch to the front panel and moving the suppressor voltage output from the 19 pin HT socket to a separate socket on the back panel. These adjustments were considered necessary not just for ease of operation but also to cure an internal arcing problem evident in the 880 Unit.

The ion gauge (IGC21, Vacuum Generators) measured the pressure of gas in the source. The supply unit was modified to act as a protective trip for the mass spectrometer and ion gauge filaments using the in-built trip relays. The mains power supply for the ion gauge and +5V power supply for the source control unit were each connected through one of the trip relays. If the source pressure exceeded 10^{-5} mbar then the trip relays opened, switching off the filaments in both the mass spectrometer and the ion gauge. The ion gauge relay was fitted with an over-ride switch to enable the ion gauge be switched back on after tripping off, or to measure source pressures of greater than 10^{-5} mbar.

Hydrogen gas ionized in the mass spectrometer source is accelerated and focused onto the two collectors for m/z = 2 (H_2^+, the major ion beam) and m/z = 3 (HD^+ and H_3^+, the minor ion beam). The ion current was obtained from the voltage produced across a large value resistor (Welwyn), 1GΩ for the major and 100GΩ for the minor. The voltage across each resistor was measured by the first stage amplifiers, very-low-input impedance varactor bridge amplifiers (type 310J, Analogue Devices). For the major beam an ion current of 10^{-9}A gave an output of +1V, whilst the minor beam gave an output of +1V for an input current of 10^{-11}A. The two voltage signals were amplified still further by the second stage amplifiers (AD524, RS) with variable gain of from x1 to x1000. The exact configuration and design of the second stage amplifiers are given in appendix A. Usually the major beam was not amplified any further (gain x1), whilst the minor beam was amplified with a gain of x100. The ion beam signals were then digitised so that they could be input to the computer by a 16-bit bipolar ADC (MP8037, Analogic Ltd.). The gain of the second stage amplifiers, control of the ADC and reading the digital signal were performed by the computer *via* the Cubio interface.

In order to allow automated adjustment of the source pressure of the reference gas a stepper motor was incorporated into the design of the variable volume (described in section 2.3.2). The stepper motor was operated by a computer controlled power supply.

A logic circuit (described in appendix A) was added to detect when the bellows were fully in or out and stop the motor from over-extending or over-compressing the bellows.

The valve control unit operated up to 12 solenoid valves by either computer or manual control. Ten of the solenoid valves (3 way, 48V D.C., Zoedale) regulated the compressed air supply to the automatic valves of the mass spectrometer, reference and sample inlet systems (see sections 2.3.1 and 2.4.5). The other two solenoid valves, consisting of the solenoid parts of a three way, 24V D.C. valve (Radio Spares), controlled the change-over valve. Despite the advantages of computer valve control it was necessary to operate all the valves manually, apart from the change-over valve, because of the problem of memory shortage in the computer.

Power for the DC voltages required by most of the electronics was supplied by a single power supply unit (described in appendix A). The power supply unit supplied voltages of +5V (10 Amps), ±15V (2 Amps) and +48V (6 Amps). This simplified the construction of the electronics built in-house as well as allowing the +5V supply required by the source control unit to be used as a protective trip. The power supply for the stepper motor was supplied by a separate unit (+5V, 10 Amps) as stepper motors can introduce large voltage fluctuations in the power supply during their operation.

2.2.4 The software

The mass spectrometer control and data collection programs were written in BASIC programming language. The layout consisted of a core program with a menu, operated from the keyboard by single keystroke, for various sub-programs. These sub-programs were

1. Data Acquisition: During data acquisition five comparisons were made between the D/H ratio of the reference gas and D/H ratio of the sample gas. Prior to this a preliminary comparison was used to calculate the approximate D/H ratio of each gas and initialise the variables used by the computer to give a real time plot of the data. Each comparison consisted of 200 measurements of the ratio of the digitised ion beam signals from m/z 2 and 3 of the reference gas, followed by 200 measurements of the sample gas. Each set of 200 measurements was made in blocks of 20, after which time a graphical representation was output to the VDU. The real time trace enabled the observation of any potential problems with the analysis. Fig. 2.5 shows a diagram of various computer traces obtained and their probable causes. The final δD of the sample gas, relative to the reference gas, was calculated from the average D/H ratios of the sample and reference gas over the five comparisons.

2. Zero offset: The zero offset program measured the output signal obtained from the major and minor amplifiers when no gas was being admitted to the mass spectrometer. The magnitude of the offset was automatically subtracted from the signal

strengths obtained by the computer during data acquisition to compensate for any background hydrogen in the mass spectrometer and the amplifier bias. When the sub-program was initiated both sample and reference inlets at the change-over valve were closed but the source parameters (i.e. accelerating voltage) and amplifier gain settings were left unchanged. Then 200 measurements were made of the output signal and an average signal strength calculated for each amplifier. Typically the zero voltage offset was about 0.3% of the major ion beam signal and 5% of the minor ion beam signal.

3. H_3^+ calibration: This sub-program compensates for the presence of H_3^+ ions in the minor ion beam. The cause of the H_3^+ ions and the correction method used is discussed further in section 2.2.6.

4. HT control: The HT control was used to set the source HT to a particular desired voltage. This was occasionally used to focus a particular ion beam onto one of the collectors, usually nitrogen (m/z=28) allowing the mass spectrometer to detect the presence of air, or helium (m/z = 4) when using the mass spectrometer as a leak detector.

5. Background Scan: This sub-program allowed the accelerating voltage to smoothly vary from one value to another while monitoring the output of the minor collector, thereby producing a mass scan. The limits correspond to m/z = 30 and m/z = 2. The program was useful in identifying air leaks (m/z 28) or the presence of water (m/z=18 and m/z=17), indicating incomplete conversion of sample water to hydrogen. (see section 3.2).

6. Peak Set up: This sub-program scanned the HT between two chosen voltages to aid in choosing the optimum settings of various control voltages and magnet position to gain symmetrical peak shapes.

7. Inlet Valve Control: This allowed control of the inlet valves (section 2.3.1 and 2.4.5) through the valve control unit from the computer, providing the possibility of automatic operation of the mass spectrometer inlet, but was rarely used due to lack of computer memory.

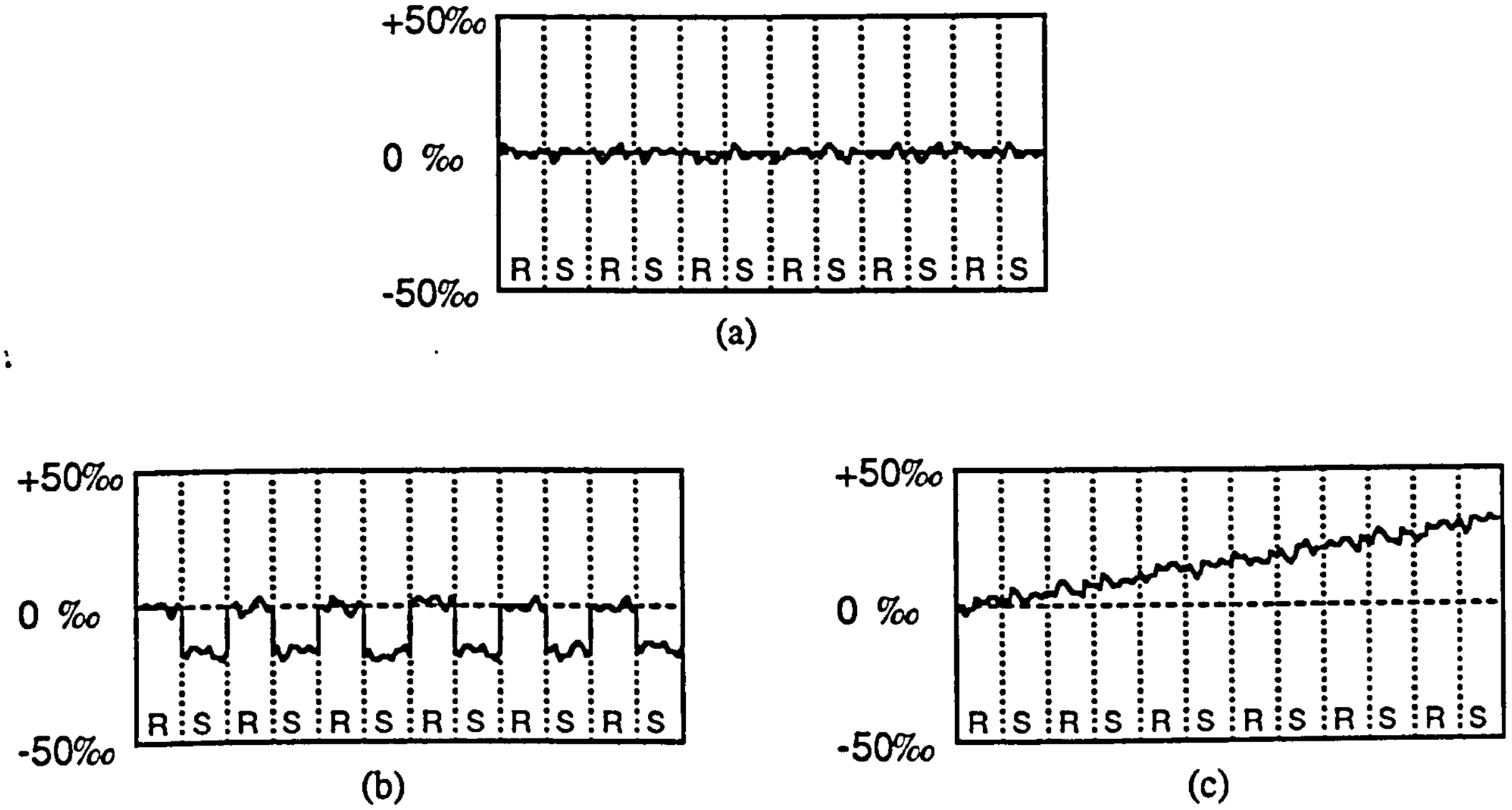

Fig. 2.5. Example of various real time traces obtained during data analysis. A total of six comparisons are made between the D/H ratio of the sample gas (S) and the reference gas (R). The initial comparison is used to initialise the variables used by the computer program during the analysis. a) desired results. b) Incorrect offset prior to data collection, this does not affect the results. c) Source fluctuations, causing a gradual drift in the D/H ratio measured. d) sample side of change-over valve not opening properly. e) Electrical (external) noise present.

2.3 Reference gas manipulation

The reference gas inlet design and operation remained the same throughout the development and evaluation of various sample inlet and preparation systems described in chapter 3. Hydrogen reference gas obtained from this inlet was used in the evaluation of the mass spectrometer characteristics and performance as described in section 2.4.

2.3.1 Reference gas inlet

A schematic diagram of the reference gas inlet and pumping system is shown in fig. 2.6. The vacuum pipework made from sections of seamless 316 stainless steel tubing (1/4" O.D., 16 gauge) connected to each other and the valves by 34mm stainless steel rotatable flanges (FC914, Vacuum Generators Ltd.). These flanges seal on a knife edge/copper gasket principle. The valves were CRD919 bakeable valves (Vacuum Generators Ltd.) which sealed by a knife edge on a copper pad and were operated by compressed air at a pressure of 5 bar.

The compressed air necessary for controlling the valves was produced by an air compressor (Bambi Air Compressors Ltd.) fitted with a regulator (model AW111, Bambi Air Compressors Ltd.) to maintain a constant air pressure and remove moisture from the air supply. The regulator required draining about twice a week. The compressed air to each CRD919 valve was controlled by the solenoid valves (Zoedale) *via* the valve control unit described in section 2.2.3.

The components for the pumping system of the reference inlet were similar to those employed in the mass spectrometer system. The reference inlet was pumped through valve RP by an oil diffusion pump (E02k, Edwards) and backed by a rotary pump (E2M8, Edwards). The foreline trap (FL20k, Edwards) was filled with activated alumina. The connecting pipes were made from 316 stainless steel tubing (1" O.D., 16 gauge) welded to KF10 flanges (Edwards).

The valves LV, HV (PV10, Edwards) and DI (PV25, Edwards) were operated by compressed air controlled by the same type of solenoid valves as above. These valves enabled the isolation of the diffusion pump so that the relatively high pressures of reference gas (*ca.* 80 mbar under normal operating conditions) could be pumped through the rotary pump without going through the diffusion pump. The solenoid valves that controlled LV and HV were operated from the valve control unit, whereas the solenoid valve that operated valve DI was operated manually.

The pressure in the vacuum line was measured by a penning gauge (CP25EK gauge head and model #505 supply, Edwards). The rotary and diffusion pumps were protected by a pirani trip (appendix A), vacuum loss being detected by a pirani head (PRM10,

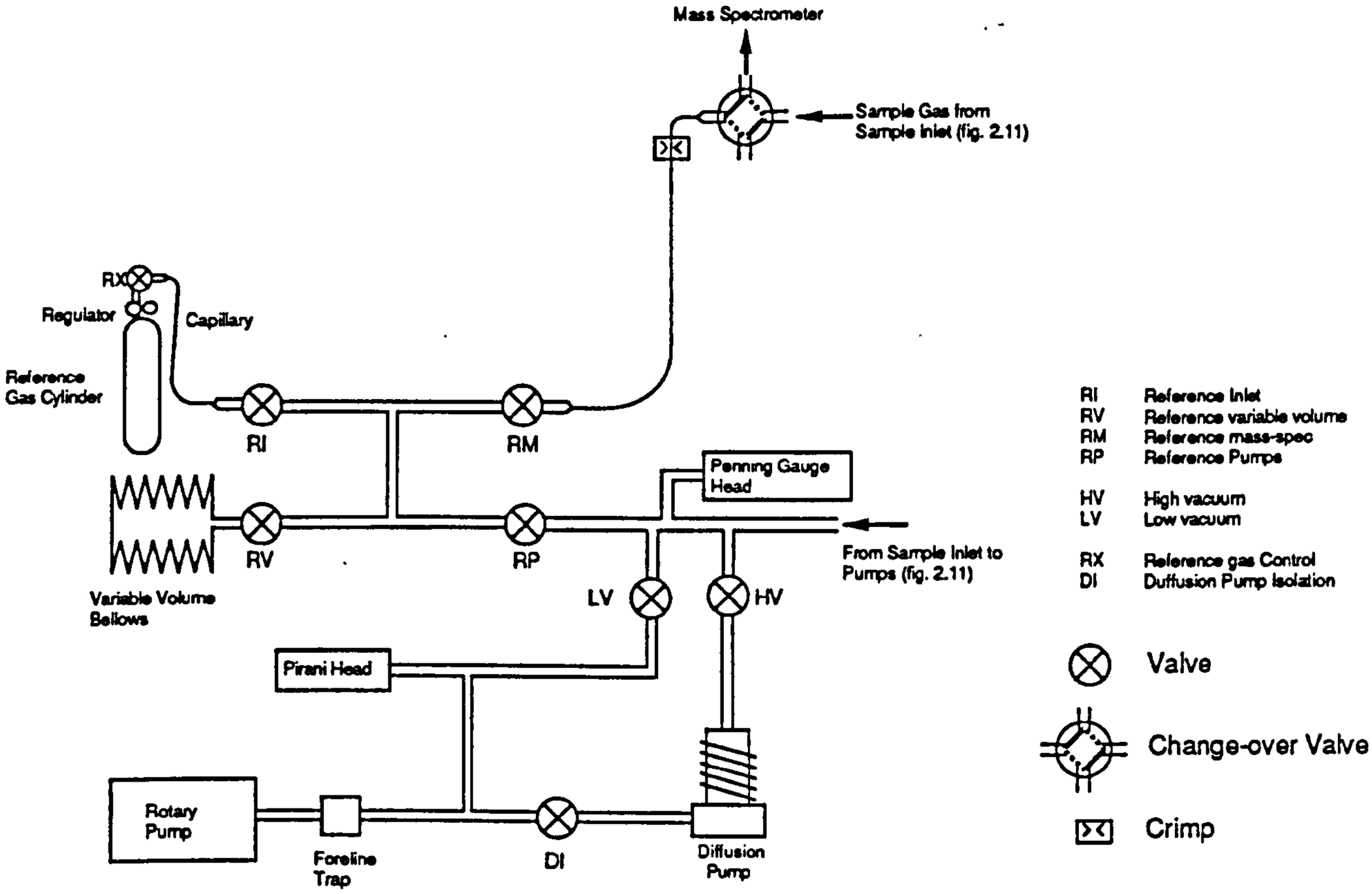

Fig. 2.6. Schematic diagram of the reference inlet and pumping system. Hydrogen reference gas was obtained from the reference gas cylinder. The variable volume bellows could be replaced by a mercury manometer to aid in adjusting the crimps (see section 2.3.3)

Edwards). The diffusion pump was protected by a thermal trip of the same design as the thermal trips for the mass spectrometer diffusion pumps (see section 2.2.2).

Hydrogen reference gas (99.98% purity) was obtained from a 25 litre cylinder (BDH chemicals Ltd., Poole). The flow of hydrogen gas from the cylinder was controlled by a diaphragm regulator fitted with a brass control valve (BDH, Atherstone). The connection from the control valve to the valve RI of fig. 2.6 consisted of a 3 cm length of stainless steel tubing (1/4" O.D., 16 gauge) silver soldered to a 60cm length of stainless steel capillary (1/16" O.D., 0.030" I.D.; Phase separation Ltd.). The capillary in turn was attached (*via* a silver soldered joint) to a FC914 flange. The capillary reduced the flow rate of hydrogen into the reference inlet, allowing more accurate control over the amount of gas admitted.

2.3.2 Variable volume design

The variable volume consisted of a bellows (250-175-2-BD, Standard Bellows Co.) which had a nominal volume of between 23 cm^3 when fully compressed and 124 cm^3 when fully extended. This was attached to the valve RV by a 3cm length of stainless steel tubing (1/4" O.D., 16 gauge) welded to a 34mm rotatable flange. The bellows was moved by a 4 phase, 400mNm torque, 1.8° stepper motor and 50:1 gear box (McLennon Servo Supplies Ltd., Camberly, England) connected to the bellows by a teflon screw. The teflon screw (2mm pitch) was manufactured by the O.U. workshop from two teflon rods, length 900mm and diameters 25mm and 12mm. These were attached to the bellows and stepper motor by metal retaining pins (3mm dia.), this required the welding of a metal ring to the end of the bellows. The whole assembly was supported by a simple metal frame.

The stepper motor was operated by the computer *via* the stepper motor driver unit (see section 2.2.3). To prevent the bellows being extended or compressed beyond its design limits a metal flag was attached to the bellows. When the flag made contact with one of two wire gate at each end of the bellows frame this was detected by the stepper motor driver unit, which would then cut the power to the stepper motor if the computer attempted to over-extend or compress to bellows.

The approximate volume of the reference inlet between valves RI, RP, RM and the bellows (see fig. 2.6) was 60 cm^3. The bellows were able to change the pressure of gas in the reference inlet by a factor of 2.5.

2.3.3 Mass spectrometer capillary

The mass spectrometer capillary consisted of a 60cm length of stainless steel capillary (1/16" O.D., 0.010" I.D.; Phase separation Ltd.). One end was attached to a 34mm blank flange, for connection to valve RI, of fig. 2.6, and the other end to the flange of the change-over valve; both of the connections were made by silver soldered joints.

The crimp close to the change-over valve (fig. 2.6) constricted the capillary, maintaining a high pressure of gas in the storage reservoir. Thus during normal operating conditions reference gas was admitted to the mass spectrometer under conditions of viscous flow which reduces isotopic fractionation to a minimum. Fractionation only occurring at the constriction and in the short length of capillary between the crimp and the change-over valve. This ensured that no significant fractionation of the reference gas occurred between sample analyses. The crimp consisted of two 1/4" diameter stainless steel rods with the capillary fed between them. The spacing between the two rods could be finely adjusted by tightening or loosening two bolts. To set the crimp to the correct tightness the variable volume assembly was replaced by a mercury manometer.

Hydrogen gas was then carefully admitted until the pressure of gas in the reference inlet was 10 cm of mercury (130mbar), read by the manometer. The crimp was the slowly tightened until the ion gauge indicated a source pressure of $3x10^{-7}$ mbar.

2.4 Mass spectrometer performance

This section describes the performance of the mass spectrometer, control supplies and electronics. Hydrogen gas was obtained from the reference inlet described above.

2.4.1 Ion source characteristics

The peaks were set up with the aid of a chart recorder output from the second stage amplifiers. The object was to obtain symmetrical flat top peaks for both the major and minor ion beams as they were scanned across the collectors by smoothly increasing the accelerating voltage. The optimum source parameters were found to be :-

Filament current	3.6A	Repeller voltage	+20V
Trap current	440μA	Electron energy	+80V
Source current	1.9mA	Half plate # 1	2.89kV
Accelerating voltage	3.40kV	Half plate # 2	2.83kV

With these source parameters the peak shapes obtained from the chart recorder are shown in fig. 2.7. During normal operation these parameters were not changed. However after a bake out, during which the magnet had to be removed, some slight re-adjustment was occasionally necessary.

A graph of major ion beam intensity against source pressure of hydrogen, measured by the ion gauge is shown in fig. 2.8. The minor ion beam intensity is not proportional to source pressure due to the presence of H_3^+ ions (see section 2.4.3). The best fit line has a slope of $14.12\pm0.32x10^{-3}$ A $mbar^{-1}$, the correlation coefficient of 0.993 indicates that the major ion beam intensity was proportional to hydrogen gas pressure over the range measured. Hence a source pressure of $2x10^{-7}$ mbar of hydrogen gave an ion beam intensity of $2.16x10^{-9}$ Amps. This is comparable to the results obtained by Halliday and Miller, (1977) for a similar VG Micromass 602C D/H analyser head.

The resolving power of the mass spectrometer was about 20. During a background scan the peaks from water, m/z=18 and m/z=17 were clearly separate whereas peaks from acetylene m/z=26 and m/z=25 (see appendix C) were not well resolved. The low resolution enabled a broad flat topped peak for the minor beam, m/z=3, so that any small source voltage fluctuations during analysis would not cause large errors in the ion beam

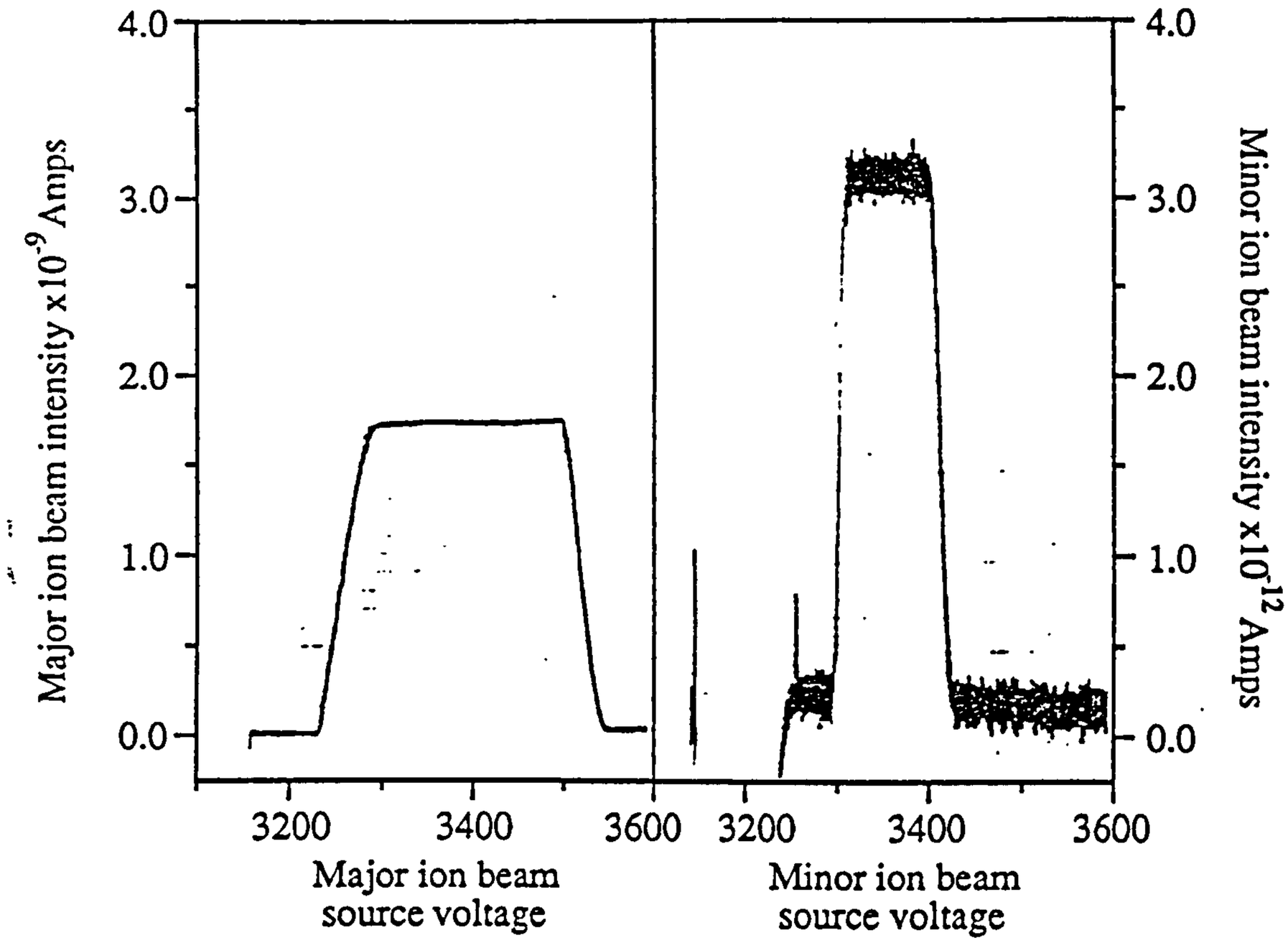

Fig. 2.7. Chart recorder output for major and minor beams scanned over their respective collectors by gradually increasing the source acceleration voltage. During data acquisition the source acceleration voltage remains at the peak centre so that small source fluctuations do no cause large errors in the major/minor ratio.

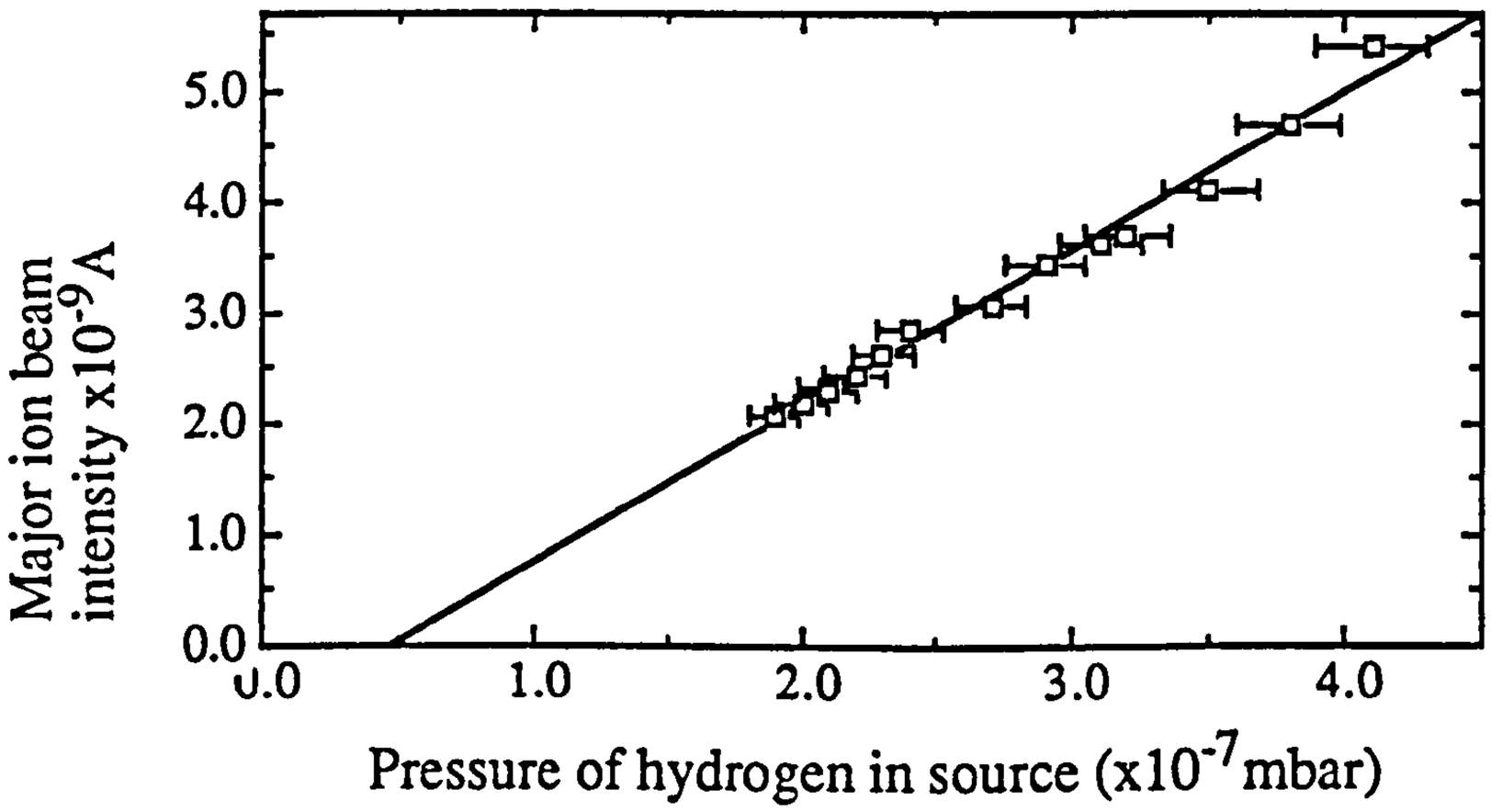

Fig 2.8. Variation of major ion beam intensity (m/z = 2) against the pressure of hydrogen gas in the mass spectrometer source, measured by the ion gauge.

intensity measurements. *i.e.* the measured D/H ratio remained constant for small changes in accelerating voltage.

2.4.2 Noise associated with ion beam amplification system

The precision of the second stage amplifiers and digital-to-analogue converter (DAC) was determined by connecting the input signal to ground and measuring the output from the DAC. The computer made 1000 measurements of the DAC output (the same number as during routine D/H determination) and the standard deviation calculated. The results for both major and minor second stage amplifiers for various amplification gains are shown in table 2.1. Digitisation of the ion beam signal is not a major source of error since an error of 1 bit from the 16-bit DAC is equivalent to 0.15mV on the input signal. Both the major and minor second stage amplifiers were of similar design except that the minor amplifier incorporated a larger smoothing filter on the output. For a typical analysis of hydrogen, the major amplifier had a gain x1 and output voltage of 1V and the minor amplifier had a gain x100 and output voltage of 3V. Thus the precision in the D/H ratio was limited by the second stage amplifiers and DAC to 0.03‰.

Table 2.2 shows the 1σ noise associated with the detection system and the noise during a typical analysis of hydrogen; this includes noise from the first stage amplifiers as well as any statistical variations in the ion beam intensities and effects due to source fluctuations. Most of the signal noise for the major ion beam is due to statistical variations in the ion beam intensity and source fluctuations, whilst for the minor beam amplifier noise also contributes to the signal noise. Usually the precision was about ±1‰, however when initially set up the precision was often much worse and varied on a day-to-day basis, up to ±10‰ on a humid day when the air conditioning was not working. This loss in precision was overcome by placing silica gel in the amplifier housing. The silica gel needed replacing about twice a week (depending on the weather).

Amplifier Gain	Major amplifier RMS noise (mV)	Minor amplifier RMS noise (mV)
x1	0.04	0.01
x10	0.2	0.1
x100	1.5	1.0
x1000	27	14

Table 2.1. The amount of noise produced on the output of a 0V input signal by the second stage amplifiers and DAC.

Amplifier Gain	Major amplifier RMS noise (mV)	Minor amplifier RMS noise (mV)
x1	0.03	0.24
x10	0.14	2.1
x100	1.7	14.4
x1000	37	381
Hydrogen	24	37

Table 2.2. Noise associated with the data acquisition electronics for different amplifier gains. When analysing hydrogen the major gain was x1 and minor gain x100.

2.4.3 Problems with 880 high voltage unit

Shortly after the mass spectrometer was assembled it was found that HT arcing in the source control unit was a major problem. This phenomenon, which could happen as frequently as once an hour, would often destroy some of the components in the second stage amplifiers. Usually HT flash-over problems are due to charge build-up in the mass spectrometer source. However this possibility was discounted since the source was cleaned several times and great care was taken to ensure that any metal parts not connected to the source control unit were properly earthed to prevent charge build-up. In order to reduce the arcing problem the magnet was positioned so that a lower source accelerating voltage of 3.4kV was required, instead of 3.6kV as when initially set up. With this setting a flash-over still occurred about once a day, even with the source turned off between analyses.

The problem was solved when some modifications were made to the 880 source control unit. A mains switch was added to the front panel (see section 2.2.3) to allow the rapid shut down of the HT if a flash-over was suspected. In addition the suppressor voltage output was moved from the original 19 pin HT socket to a separate BNC socket (RS, England) on the back panel. This modification was made since the suppressor voltage is only a low d.c. signal, whereas the other wires in the HT connector all carried HT voltages to the source. After these modifications HT flash-over events were rare and in any event non-destructive to the other electronics.

2.4.4 The H_3^+ correction

The collectors of the mass spectrometer are positioned so that for a fixed HT setting they collect ions with m/z = 2 and m/z = 3. These ions are mainly H_2^+ and HD^+ which are ionized in the source from H_2 and HD. However due to conditions in the source such as high operating temperature of the filament, the thermionic emission of electrons from the filament and relatively high gas pressure, other ions can be formed, such as

$$H_2 \leftrightarrow H + H^+ \qquad (2.1)$$

$$H \leftrightarrow H^+ \qquad (2.2)$$

Table 2.3 lists the possible ions with m/z = 2 and m/z = 3 detected by the mass spectrometer. Helium is not admitted to the mass spectrometer, being removed as a non-condensible gas during the sample preparation. As the concentration of deuterium is of the order of only 150 ppm in hydrogen the ions of m/z = 2 are nearly all H_2^+ ions. However m/z = 3 ions can be either HD^+ or H_3^+ ions. The resolving power of the mass spectrometer of 20 is not enough to separate HD^+ ions from H_3^+ ions, which requires a resolving power of 3000. So the D/H ratio needs to be corrected for the H_3^+ contribution to the minor beam.

Smythe (1931) showed that the production of H_3^+ ions is mainly by reaction 2.3., other reactions occurring at a negligible rate.

$$H_2^+ + H_2 \rightarrow H_3^+ + H \qquad (2.3)$$

Ion species with			
m/z = 1	m/z = 2	m/z = 3	m/z = 4
H^+	H_2^+	HD^+	D_2^{2+}
H_2^{2+}	D^+	H_3^+	$^4He^+$
	D_2^{2+}	$^3He^+$	
	$^4He^{2+}$		

Table 2.3. A list of hydrogen and helium ions with m/z between 1 and 4 produced in the source. To prevent errors in the D/H ratio helium must be absent from the hydrogen gas. The main contribution to the major ion beam is H_2^+. However, both HD^+ and H_3^+ contribute to the minor ion beam.

Hence the reaction is second order since the concentration of H_2^+ ions is directly proportional to the concentration of H_2 in the source region.

$$[H_3^+] = c[H_2^+]\,[H_2] = k[H_2^+]^2 \qquad (2.4)$$

where c and k are constants.

The actual ratio of the gas , R_T is given by

$$R_T = \frac{[HD]}{[H_2]} = \frac{[HD^+]}{[H_2^+]} \qquad (2.5)$$

This assumes equal ionisation rates for H_2 and HD. However the measured ratio R_M has a contribution from the H_3^+ ions and is

$$R_M = \frac{[HD\,] + [H_3^+]}{[H_2^+]} = \frac{[HD^+]}{[H_2^+]} + k\,\frac{[H_2^+]^2}{[H_2^+]} \qquad (2.6)$$

Therefore

$$R_M = R_T + k\,[H_2^+] \qquad (2.7)$$

Hence the true ratio, R_T, is given by

$$R_T = R_m - k[H_2] \qquad (2.8)$$

There are various methods of calibrating the H_3^+ correction. Bridger *et al.* (1974) used an electronic circuit to remove the H_3^+ contribution from the minor ion beam. The major ion beam signal was squared and a fixed proportion subtracted from the minor beam signal, essentially using equation (2.4). The value k in equation (2.4) was set by a potentiometer, being adjusted until the reference gas gave a constant ratio for different source pressures. Schoeller *et al.* (1983) designed a method of measuring two reference gases of known D/H ratio and then calculating the H_3^+ correction. This required a three-way change-over valve. The usual method used is by mathematical correction (Friedman *et al.*, 1953 and Fisher and Brown, 1971). This was the method adopted here since it required no special components and was simple to program. Using the H_3^+ sub-program (described in section 2.2.4), the variable volume was fully compressed and then measurements of the m/z = 2 to m/z = 3 ratio were made as the bellows volume was increased. Twelve discrete volume settings were used each time. Plotting the measured D/H ratio against the major ion beam intensity for various source pressures gives a straight line with slope k and intercept R_T, an example plotted from data obtained by the

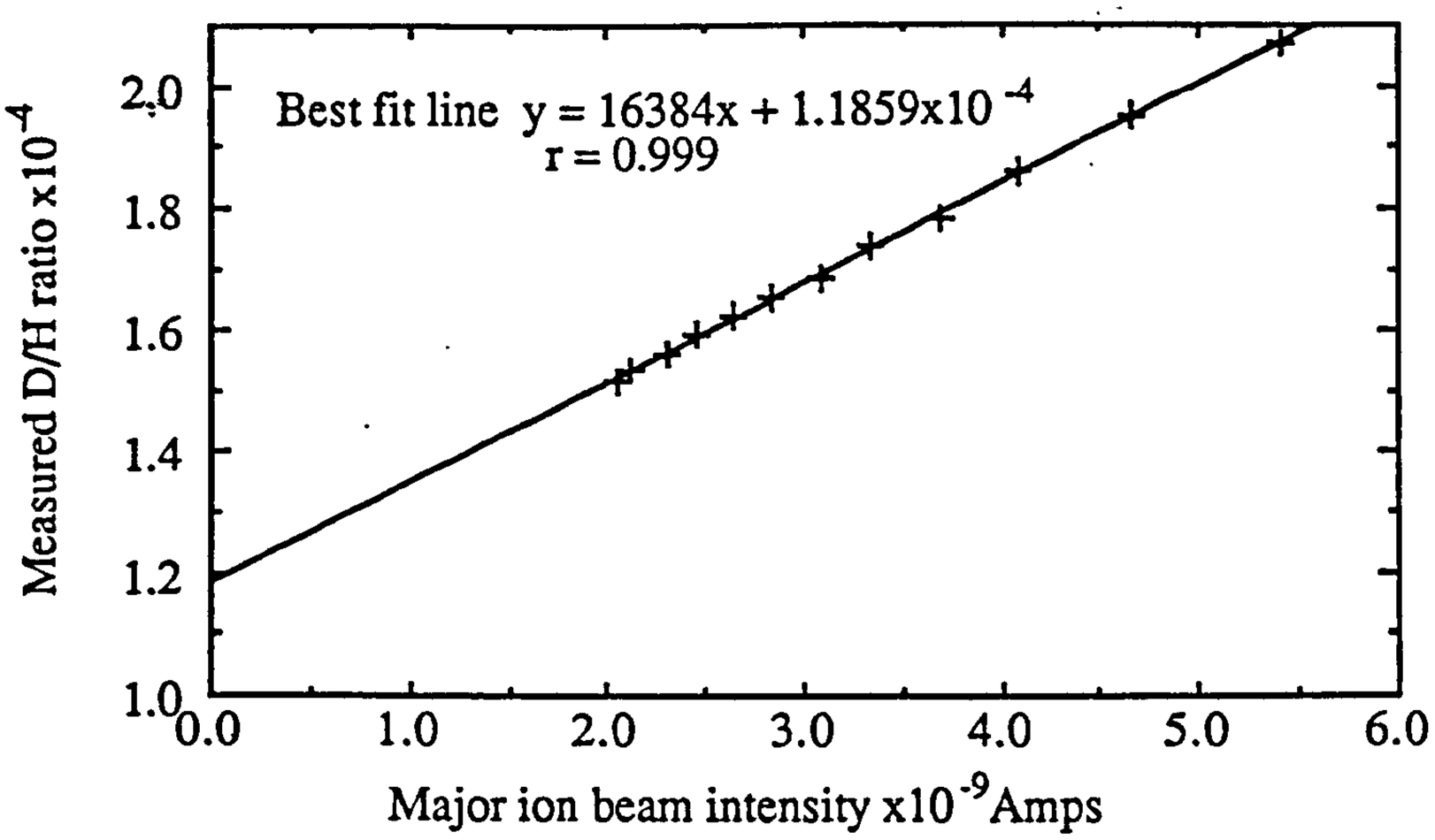

Fig. 2.9. Variation of the measured D/H ratio of hydrogen reference gas against source pressure. The best fit line has a correlation coefficient, r = 0.999. The true ratio of the reference gas is found by extrapolating back to where the best fit line cuts the y axis. i.e. the D/H ratio of the reference gas, R_T = 1.1859±0.0015 x10^{-4}.

computer is shown in fig. 2.9. The value of k and R_T for the reference gas were then calculated, by computer, using least squares method. During data collection the computer automatically corrected for the H_3^+ ions using equation (2.8).

2.4.5 Mass spectrometer operation

Prior to use of the mass spectrometer, at the start of each day, hydrogen reference gas was loaded into the inlet system. Usually enough gas was admitted to give a source pressure of 2x10^{-7} mbar (*ca.* 80mbar in the reference inlet) with the bellows fully compressed.

Before analysis of sample gas was possible, the H_3^+ correction needed to be determined (see section 2.4.3 above) and also the δD of the reference gas had to be measured since the capillary between the inlet system and gas cylinder fractionated the reference gas (see below). Generally the H_3^+ correction was made soon after the reference gas had been loaded and was not recalculated during the day unless it was noted that the D/H ratio had changed by more than 1ppm† from R_T, the true ratio obtained when the H_3^+ correction was first calculated.

---

† Sample D/H ratios were compared to V-SMOW (D/H=155.76±0.05) during analysis so a 1ppm error in the D/H ratio due to the H_3^+ correction would give a 3‰ error in the δD of the sample for every 1000‰ difference between the δD of the sample and V-SMOW. So a sample with δD of +50‰ would give a δD of 49.85‰. This is negligible compared to other sources of error.

The δD of the reference gas was measured by analysing hydrogen obtained from V-SMOW (δD defined as 0‰), by running V-SMOW as a sample (this is described in chapter 3). The δD of a sample, against V-SMOW, δD_{VSMOW}^{Sam} is given by

$$\delta D_{VSMOW}^{Sam} = \left(\frac{\delta D_{ref}^{sam} + 1000}{\delta D_{ref}^{VSMOW} + 1000} - 1 \right) x \ 1000$$

where δD_{Ref}^{VSMOW} is the measured δD value of V-SMOW against the reference gas and δD_{Ref}^{Sam} is the measured δD value of the sample against the reference gas.

The calibration of the reference gas to V-SMOW also compensated for any differential fractionation of the isotopes between the reference and sample inlet systems. This was required since, in the attempts to analyse small quantities of hydrogen (sections 3.4 and 3.5), the design of sample inlet system was very different from the reference inlet.

Table 2.4 and fig. 2.10 show the D/H ratio of the reference gas as determined by the mass spectrometer on 13 separate days over a period of 17 days. There are two possible causes of the large variations in D/H ratio between days. The first is due to isotopic fractionation of the reference gas in the capillary when loaded into the reference inlet and the second is source fluctuations. During the admission of the reference gas into the inlet system its isotopes would be fractionated to some extent by the capillary, the amount of fractionation depended upon the flow rate of the gas through the capillary. This shows the need for the reference gas to be calibrated each time it is loaded. On a single day the one sigma variation was much smaller and only due to source fluctuations during the day. A typical example of the variation of the measured D/H ratio of the reference gas on a single day is shown in table 2.5. However this would still only give an absolute precision of ±10‰ (assuming a measured D/H ratio of V-SMOW of 155.76×10^{-6}). This is compensated by running the mass spectrometer in a dynamic mode so that any drifting of the source parameters is automatically compensated, described below.

Date	No. of Analyses	HD/H_2 ratio of reference gas $x10^{-6} \pm 2\sigma$ error	D/H ratio of reference gas $x10^{-6} \pm 2\sigma$ error
23-10-88	24	112.1 ± 1.0	56.1 ±0.5
25-10-88	20	113.8 ± 1.6	56.9 ±0.8
27-10-88	17	114.8 ± 0.7	57.4 ±0.4
28-10-88	27	111.0 ± 1.4	55.5 ±0.7
29-10-88	18	109.5 ± 1.2	54.8 ±0.6
30-10-88	18	108.8 ± 1.7	54.4 ±0.9
1-11-88	30	107.0 ± 1.4	53.5 ±0.7
2-11-88	18	105.2 ± 1.8	52.6 ±0.9
3-11-88	27	101.5 ± 1.0	50.8 ±1.0
4-11-88	23	108.6 ± 1.0	54.3 ±0.5
6-11-88	21	110.0 ± 1.4	55.0 ±0.7
7-11-88	30	114.6 ± 1.6	57.3 ±0.8
8-11-88	24	114.6 ± 1.0	57.3 ±0.5

Table 2.4. D/H ratio of the hydrogen reference gas determined on different days. Most of the variation is caused by fractionation of the reference gas when admitted into the reference gas inlet. The average D/H ratio of the reference gas was 55.1±4.0 $x10^{-6}$. The variation on a single day, shown by the 2σ error and table 2.5 was much smaller.

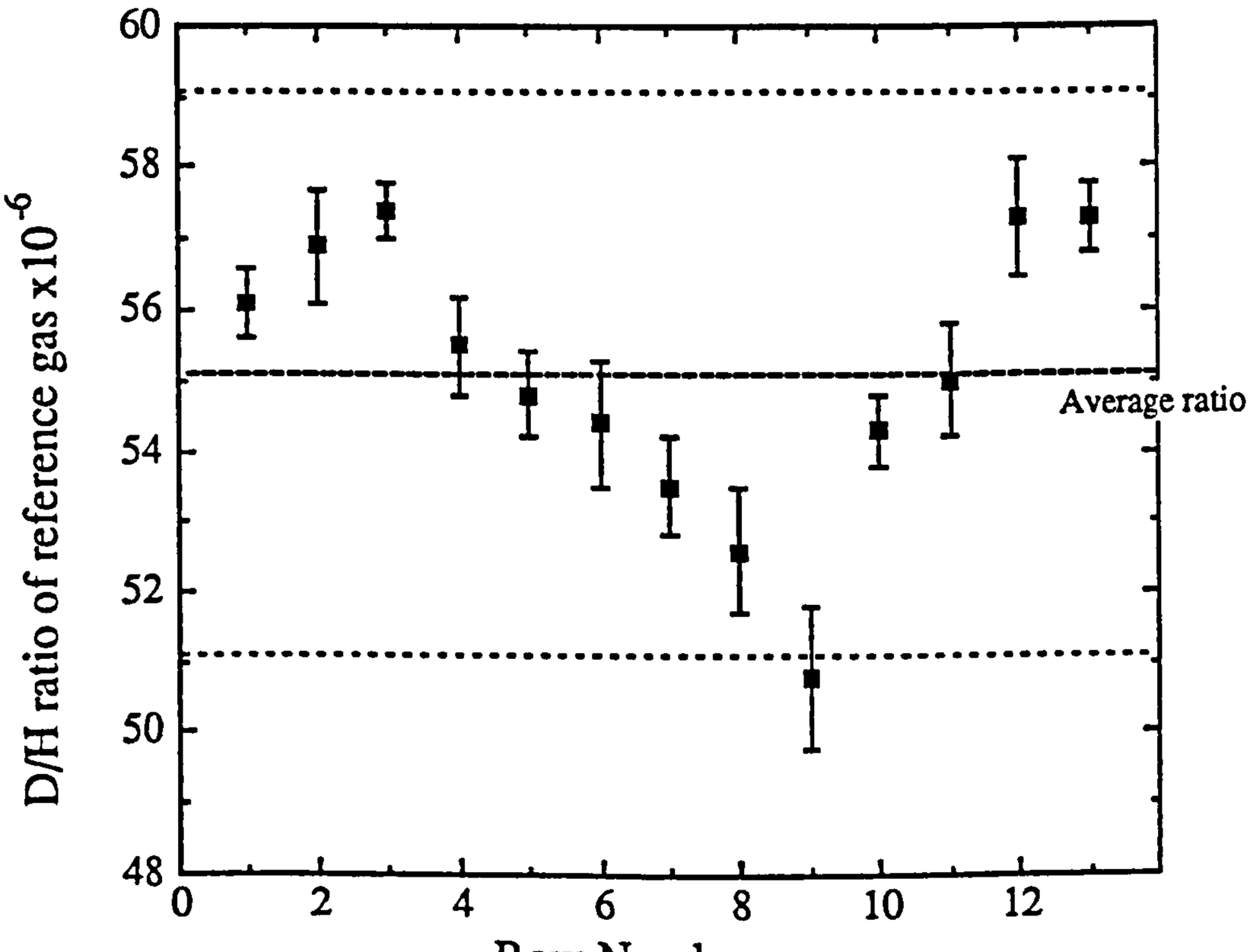

Fig.2.10 Graph of the variation of the D/H ratio of the reference gas on different days, from table 2.4. The mean of all the results along with 2σ error bars are shown by dashed lines.

Analyses No.	D/H ratio of reference gas $x10^{-6}$	Analyses No.	D/H ratio of reference gas $x10^{-6}$
1	54.3	10	54.7
2	54.4	11	55.0
3	54.7	12	54.9
4	54.3	13	54.7
5	54.5	14	55.0
6	55.0	15	55.1
7	54.4	16	55.0
8	54.7	17	55.1
9	54.9	18	55.1

Table 2.5. Variation of the D/H ratio of the reference gas measured during a single day. The average D/H ratio was 54.8±0.6, most of the error due to either statistical variations in the ion beam intensities and source fluctuations throughout the day.

2.4.6 Zero enrichment

The sample inlet that was used for the zero enrichment is shown in fig 2.11. This was made from the same components as the reference inlet (fig 2.6), mainly 316 stainless steel tube (1/4" O.D., 16 gauge) welded to 34 mm rotatable flanges and connected to CRD919 valves. There was no variable volume on the sample inlet, the end of valve SV was replaced by a blank 34mm flange. Valve SI led to a sample preparation line described in chapter 3, section 3.2. The capillary and connections from valve SM to the change-over valve were the same as for the reference inlet.

The crimp on the sample inlet was tightened in the same way as the crimp on the reference inlet (2.3.3). To exactly balance the flow rate of hydrogen through the two capillaries on either side of the change-over valve hydrogen gas from the reference gas cylinder, was admitted into both the sample and reference inlets to give a source pressure of *ca.* $2x10^{-7}$ mbar, measured from the reference side. The crimp on the sample capillary was then carefully adjusted until there was no difference in the major ion beam intensity when the change-over valve was switched between reference and sample inlet.

For the zero enrichment measurement an aliquot of hydrogen gas from the reference cylinder was admitted into both reference and sample inlets as above. After allowing several minutes for the gas to equilibrate the inlet sections were isolated from each other by closing valves RP and SP (figs. 2.6 and 2.11). The δD of the hydrogen gas in the sample inlet was then analysed compared to the hydrogen in the reference inlet, treating the reference gas in the sample inlet as an unknown sample using the data acquisition program (section 2.2.4). The results obtained for a series of three different aliquots of hydrogen gas from the cylinder are shown in table 2.6.

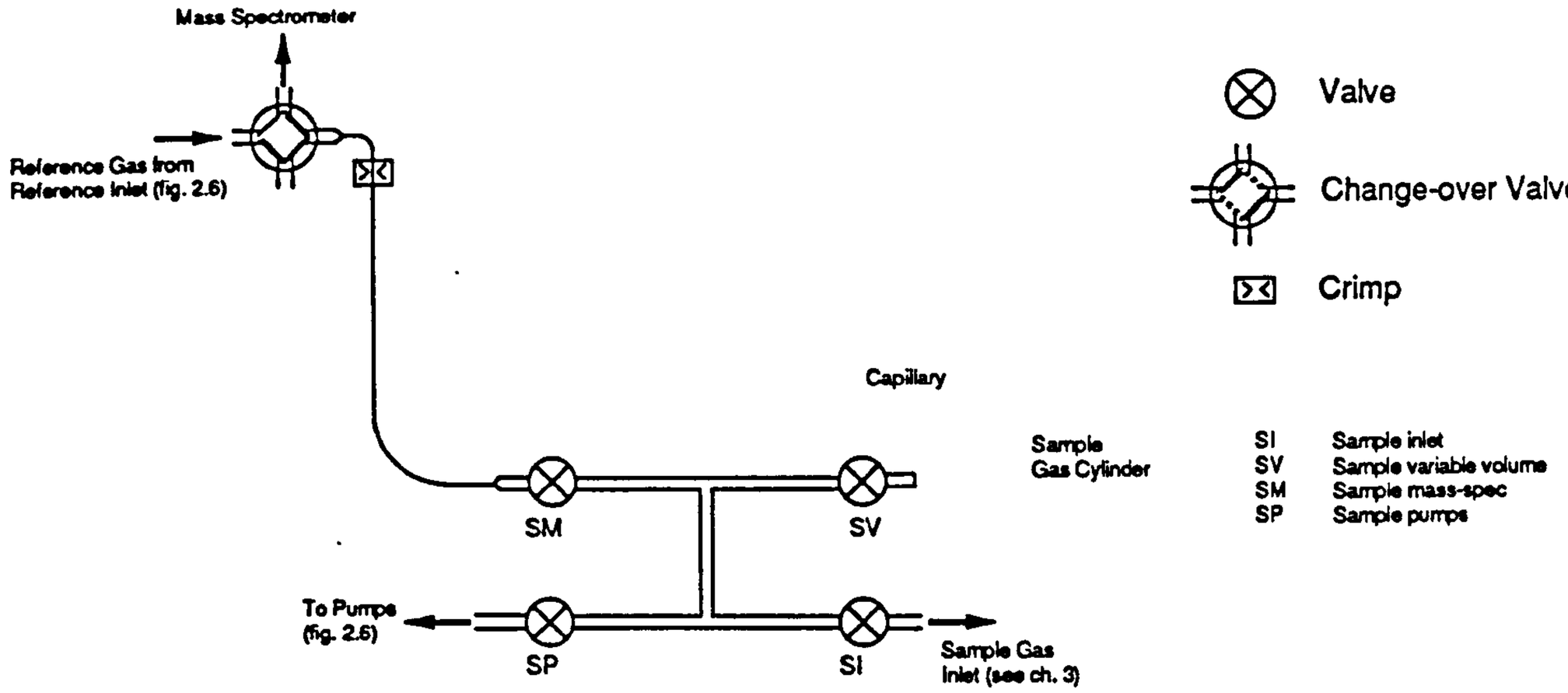

Fig. 2.11. A schematic diagram of the 'sample' inlet used during the zero enrichment procedure.

No. of Analyses	HD/H_2 ratio of reference gas $x10^{-6} \pm 2\sigma$ error	D/H ratio of sample gas $x10^{-6} \pm 2\sigma$ error	δD (sample vs ref ‰) $\pm 2\sigma$ error
15	58.59 ± 0.28	58.69 ± 0.20	+1.64 ± 2.40
5	56.85 ± 0.05	57.05 ± 0.12	+3.14 ± 0.66
8	56.31 ± 0.19	56.41 ± 0.18	+3.00 ± 1.35

Table 2.6 Zero enrichment analyses on three different aliquots of hydrogen gas from the reference gas cylinder, performed on three different days. Each separates analysis consisted of a comparison, between the gas admitted through the sample inlet and the gas measured through the reference inlet, was achieved by the exactly the same data acquisition procedure as used for an unknown sample gas (see section 2.2.4).

In the first series of measurements the average D/H of the reference gas ratio was $58.59x10^{-6}\pm0.28x10^{-6}$ and the sample was $58.69\pm0.29x10^{-6}$. This would suggest that the δD of the reference gas in the sample side would be +1.7±5.9‰ due to instrumental limitations, mainly source fluctuations. However when analysing in the dynamic mode each analysis gave the δD for the reference in the sample side measured against the reference gas under the same source conditions. Hence precision was greatly improved, the δD measured was +1.6‰ ± 2.4‰, showing the advantage of analysing samples in the dynamic mode. Over the series of three aliquots of hydrogen the δD of the gas on the sample side was 2.24‰ ± 2.06‰. This indicates that there was probably a small amount of fractionation between isotopes of the gas in the sample and reference sides. Initially when the sample inlet was constructed a zero enrichment over seven analyses gave a sample δD of +15‰ ± 1‰. This occurred because the sample inlet capillary was 1cm longer than the reference inlet capillary. The sample inlet capillary was cut down to length and rewelded to the 34mm flange. A possible 2‰ fractionation suggests that the capillary was still a little bit longer, by about 1mm. However, during operation the reference gas was calibrated against V-SMOW by analysing V-SMOW as a sample, hence this small amount of fractionation is automatically compensated.

The precision of the instrument as set up was ± 2‰ for each analysis, comparing to the reference gas. Noise from the amplifiers and data collection was not a significant source of error when the major ion beam intensity was $\sim1x10^{-9}$ Amps. For a major ion beam of less than 10^{-9} Amps the minor ion beam amplifiers contribute to the loss in precision. Most of the loss in precision was caused by variations of the major and minor ion beam strength detected by the collectors during the analysis of hydrogen gas. The performance of the mass spectrometer was similar to that of other 602 D/H analysers (e.g. Bridger *et al.*, 1974 and Halliday and Miller, 1980).

Chapter 3
Sample Inlet Development

This chapter describes three different sample inlets which were developed during the quest to analyse D/H ratios of small quantities (<0.1μmol) of hydrogen. The inlets were as follows:

1) A conventional inlet system which was built to gain experience in the operation of the mass spectrometer and to determine potential problems associated with the conversion of water to hydrogen. In common with other inlets of this type it was capable of processing samples containing *ca.* 10 μmol of hydrogen. The precision in δD was limited by the mass spectrometer, as detailed in chapter 2, to ±2‰.

2) An inlet system with a greatly reduced volume constructed from capillary tubing. In this system aliquots of hydrogen (0.3μmol) were transferred to the mass spectrometer by a flowing stream of helium. The precision in δD of this system was limited to ±15‰.

3) A system in which water was manipulated in the inlet itself. Since water is condensible, by liquid nitrogen, it could readily be transferred to a small volume situated close to the mass spectrometer. The sample water was converted to hydrogen as it was about to to enter the change-over valve. This technique was by far the most sensitive, capable of analysing less than 0.1μmol of hydrogen but suffered greatly from technical problems.

Section 3.1 gives a brief description of the various types of inlet systems that have been used in previous studies to analyse D/H ratios. The rest of the chapter describes each of these inlet systems constructed here and assesses their performance. The type and manufacturer of the various components used to build the inlets are given in the text; the addresses of the relevant companies or suppliers are listed in appendix B.

3.1 Measurement of hydrogen isotopes by mass spectrometry

Hydrogen is obtained from samples in the form of water, by heating the sample. The main sources of water are obtained from the heating (with or without oxygen) of hydrated minerals and the combustion (heating with oxygen present) of organic compounds. This water must be converted to a hydrogen containing compound suitable for admission into a gas source mass spectrometer. Usually, as in the case of the instrument described in chapter 2, the water is reduced to hydrogen, however other gases have been used such as water, methane and ethane. This section describes the various methods that have been used to convert sample water to a suitable gas for hydrogen

Mass Spec. Gas	Conversion Method	Sample Size (µmol)	Memory Effect (µmol)	Comments	Reference
Hydrogen	Zinc, *ca.*400°C	170-280	3.4	Continuous flow,	Graff and Rittenerg (1952)
Hydrogen	Zinc, 420°C	830-1400	20-72	Continuous flow, zinc supported by sand matrix	Lyon and Cox (1980)
Hydrogen	Zinc, 450°C	5-50	None	Batch method	Coleman *et al.* (1982)
Hydrogen	Zinc wire, 450-500°C	278	None	Batch method	Sudzuki (1987)
Hydrogen	Uranium 400-700°C	1400	7	Continuous flow	Bigeleisen *et al.* (1952)
Hydrogen	Uranium 800°C	280	Not reported	Continuous flow	Halliday and Miller (1977)
Hydrogen	Uranium	56-280	9% sample size	Continuous flow	Hagemann and Lohez (1978)
Hydrogen	Uranium 600°C	500	50	Continuous flow	Hartley (1980)
Hydrogen	Uranium			Continuous flow	Wong *et al.* (1984)
Hydrogen	Uranium	2	None	Helium carrier gas. Hydrogen separated by Pd	Robert *et al.* (1987a)
Hydrogen	Magnesium 550°C			Used in the reduction of tritium oxide to tritium	Kamen (1948)
Hydrogen	Tungsten 1000°C	430	Not reported	Filaments required frequent replacement	Farkas and Farkas (1934)
Hydrogen	Equil^{n} Pt at 1400°C		large	Pt filament. Poor isotopic results	Graff and Rittenerg (1952)
Hydrogen	Equil^{n} Pt at 25°C	28000	None	Pt impregnated teflon beads. Equil^{n} 2-3 hours	Horita (1988)
Methane	Aluminium Carbide	Not used to analyse samples		Low yields, interference from OH^+	Friedman and Irsa (1952)
Methane	Aluminium Carbide			Low yields	Wright and Pillinger (1983)
Methane	Methyl magnesium iodide	550-1100	Not reported	Low yields	Orchin *et at.* (1949)
Ethane	Zinc diethyl	550	Not reported		Friedman and Irsa (1952)
Water	-		Some	Memory effect reduced by using metal valves	Thomas (1950)
Water	-	1250	7.5	Interference from $H_2{}^{17}O^+$ and $H^{18}O^+$ on m/z = 19	Majzoub and Nief (1968)
Water	-		0.8% sample size	Memory effect for both D/H and $^{18}O/^{16}O$	Hageman and Lohez (1978)
Water	-	27.8	10	Memory effect for both D/H and $^{18}O/^{16}O$	Wong *et al.* (1984)

Table 3.1. A comparison of the various techniques of obtaining D/H ratios by mass spectrometry.

isotopic analysis and any problems encountered. A summary of the techniques is given in table 3.1.

One persistent problem with many of the methods given in table 3.1 and described briefly below was the occurrence of a memory effect. During the analysis of samples the memory effect, if present, would displace the measured δD for a particular sample from its true value towards the δD of the material which was previously put through the system. It appears as though the sample water is contaminated by some of the previous sample water. The occurrence of a memory effect and its magnitude was instrument specific.

3.1.1. Reduction of water to hydrogen

The use of hydrogen as the mass spectrometer analysis gas has several advantages over other hydrogen-containing gases:

i) no isobaric interferences due to isotopes of elements other than hydrogen

ii) relatively simple to obtain the complete reduction of water to hydrogen. Hence there is no fractionation of the isotopes introduced by the reaction

iii) it is in a clean part of the mass spectrum. *i.e.* peaks from possible contaminating gases are far from those produced by hydrogen.

Hydrogen does have a major disadvantage in that it is non-condensible by liquid nitrogen. Hence, once produced from water, it cannot be easily transferred to a small storage reservoir for mass spectrometric analysis. Instead the hydrogen is usually allowed to expand into a storage volume, resulting in the requirement for a relatively large amount of gas. It can be manipulated to some extent by use of a Toepler pump or mercury pistons (Dumke *et al.*, 1989).

The reduction of water to hydrogen can, in theory, be achieved by any metal which is above hydrogen in the electronegative series. However not all metals are suitable since there must be complete conversion of all the sample water to hydrogen to prevent fractionation of the hydrogen isotopes. The various metals that have been used are described below. There are two basic ways of achieving the reduction of the water:

i) A continuous flow method. The sample water is passed over the hot metal and reduced to hydrogen. Usually there is a facility for trapping any unreacted water and passing over the metal a second time.

ii) A batch method. The sample water is transferred to a reaction vessel containing the metal. The reaction vessel is then sealed and heated to the required temperature. This has the advantage that the reaction can be continued until completion. If carried out on a separate preparation line from the mass spectrometer then many samples can be prepared simultaneously.

Zinc

One of the most common methods of reducing water to hydrogen is by passing the sample water over hot zinc metal.

$$Zn + H_2O \rightarrow ZnO + H_2 \qquad 3.1)$$

Graff and Rittenberg, (1952) employed a continuous flow method, reducing 170-280μmol of sample water to hydrogen as it passed through over hot zinc granules (100 mesh). Any unreacted water could be passed through the zinc furnace a second time. The temperature of conversion was found to be initially 386°C but, after the analysis of many samples, was gradually increased to 415°C as the zinc was exhausted. If the water was not completely reduced by passing over the zinc at 415°C then the zinc granules were replaced. The furnace was capable of reducing about 200 samples before the zinc required replacement. This technique had a memory effect equivalent to contamination of the sample water by 3.4μmol of water from the previous sample. This memory effect was attributed to water becoming firmly adsorbed to the glass walls of the apparatus between the sample combustion section and the zinc furnace.

Lyon and Cox (1980) used a similar method to that of Graff and Rittenberg, (1952) for the reduction of 830-1400μmol amounts of water except that the conversion furnace consisted of granulated zinc (30 mesh) mixed 2:3 by weight with sand (40-72 mesh). The supporting sand enabled a higher conversion temperature of 420°C to be used (melting point of zinc = 419°C), allowing faster reduction of water and outgassing of the zinc. This technique had a large memory effect varying between 20-72μmol of water from the previous sample.

More recently a batch method of water reduction by zinc has been developed by Coleman *et al.* (1982) which does not suffer from a memory effect. Sample water (5-50μmol) was introduced either by a micro-syringe or condensation from a preparation line, to a reaction vessel containing 0.25g zinc shot (-30 to +60 mesh). The water was then reduced to hydrogen off-line by placing the sealed reaction vessel in a heating block at 450°C for 30 minutes. It was noted that the zinc shot did not fuse even though it was heated 30°C above its melting point, although a ring of zinc metal did sublime on the cooler glass above the furnace. The zinc above the furnace was formed by the condensation of zinc vapour, zinc having a vapour pressure of 0.4 torr at 450°C (Kubaschewski *et al.*, 1967). Coleman *et al.* (1982) suggested that the zinc oxide in the zinc supported the molten zinc during the reduction preventing it from fusing into a single drop.

Uranium

Uranium is often used in the reduction of water to hydrogen using a continuous flow technique originally used for isotopic analysis by Bigeleisen *et al.*, (1952).

$$U + 2H_2O \rightarrow UO_2 + 2H_2 \qquad 3.2)$$

The reduction of water to hydrogen has been achieved at temperatures varying from 400°C to 800°C (Bigelsein *et al.*, 1952; Halliday and Miller, 1977; Hageman and Lohez, 1978; Hartley, 1980; Wong *et al.*, 1984; Robert *et al.*, 1987). The use of uranium does pose several problems:

i) Uranium is radioactive.

ii) Regulations, imposed because of its nuclear importance, often make it difficult to obtain.

iii) Uranium is toxic, its effects being similar to lead poisoning.

iv) Uranium hydride, formed by reaction with hydrogen at room temperature, exchanges readily with hydrogen. This may lead to serious memory effects if some uranium powder escapes from the conversion furnace.

v) The uranium oxide formed as a product of the water reduction (equation 3.2) is very fine grained and so can be transported in a flowing gas stream., Thus great care must be taken to ensure that it remains in the conversion furnace.

The usual continuous techniques all have some memory effects. Robert *et al.*, (1987) avoided memory effects by using a helium carrier gas to push small amounts of hydrogen through a uranium furnace. The hydrogen sample gas was then separated from the helium by a paladium thimble before entry to the mass spectrometer. This enabled much smaller samples to be analysed (containing a total of *ca.* 2μmol of hydrogen) and apparently eliminated memory effects.

Magnesium

Magnesium metal has been used to convert tritium oxide to tritium at 550°C (Kamen, 1948). Magnesium reacts readily with steam, however to prevent the formation of magnesium hydroxide the reaction must be carried out above 400°C.

$$Mg + H_2O \rightarrow MgO + H_2 \qquad 3.3)$$

Its lack of use as a reducing metal for hydrogen isotope analysis probably results from the potential formation of magnesium hydroxide and the presence of a protective oxide layer on magnesium.

Tungsten

Tungsten, in the form of a filament at a temperature of 1000°C, was used by Farkas and Farkas, (1934) to reduce water to hydrogen. Using large filaments, length 20cm, 0.2mm dia tungsten wire, up to 1300µmol of water could be reduced to hydrogen before the filament burnt out. This technique required the frequent replacement of the tungsten filament, limiting the usefulness of this technique.

3.1.2 Equilibration of water with hydrogen

An alternative method of preparation of hydrogen gas for isotopic analysis is by water-hydrogen equilibration method (Graff and Rittenberg, 1952; Horita, 1988). The sample water is equilibrated with hydrogen of known isotopic composition using a platinum catalyst.

$$HDO + H_2 \leftrightarrow H_2O + HD \qquad 3.4)$$

If the isotopic fractionation factor of equation 3.4) is known, as well as the amount of hydrogen and sample water, then the original isotopic composition of the sample water can be calculated by measuring the isotopic composition of the hydrogen after equilibration. Graff and Rittenburg, (1952) achieved rapid equilibration between 280µmol of water and 45µmol hydrogen by using a platinum filament catalyst at a temperature of 1400°C. However, they reported large memory effects and the gradual formation of a platinum film on the reaction vessel. Isotopic exchange between the sample water and hydrogen was also catalysed by this platinum film at 25°C, hence altering the equilibrium constant by an unquantifiable amount.

Horita, (1988) used platinum impregnated teflon beads at 25°C as a catalyst. Due to the much lower temperature an equilibration time of several hours was required. There was no detectable memory effect, but this could be due to the much larger sample size used 0.28mol of water.

3.1.3 Conversion of water to hydrocarbons

Light hydrocarbon gases have been used for hydrogen isotope analysis. Isobaric interferences from ^{13}C have been overcome by either ensuring that the hydrocarbon contains only ^{12}C or by calculation, if the $^{13}C/^{12}C$ ratio of the hydrocarbon is known.

Methane has been produced by the reaction of water with aluminium carbide (Friedman and Irsa, 1952; Wright and Pillinger, 1983) or methyl magnesium iodide (Orchin *et al.*, 1949).

$$6H_2O + Al_4C_3 \rightarrow 3CH_4 + 2Al_2O_3 \qquad 3.5)$$

$$H_2O + 2CH_3MgI \rightarrow 2CH_4 + MgO.MgI_2 \qquad 3.6)$$

Both reactions were found to give low yields of methane, although this did not affect the D/H results for either aluminium carbide (Wright and Pillinger, 1983) or methyl magnesium iodide (Friedman and Irsa, 1952). Methane was also found to be unsuitable because of interference of the minor ion beam (m/z = 17) from water, which forms OH^+ (m/z=17) under electron impact in the mass spectrometer source (Orchin *et al.*, 1949).

Friedman and Irsa (1952) also assessed the use of ethane in D/H analysis. Ethane was produced by the reaction of water with zinc diethyl.

$$Zn(C_2H_5)_2 + H_2O \rightarrow ZnO + 2C_2H_6 \qquad 3.7)$$

The reaction required careful heating to ensure that all the water reacted otherwise large errors in fractionation of the D/H isotopes occurred. Although there was 100% yields the presence of ^{13}C in the ethane limited the usefulness of this technique to samples greatly enriched in deuterium.

3.1.4 Use of water as a mass spectrometer gas

Attempts have been made to measure the isotopic composition of water by direct injection into a mass spectrometer source (Majzoub and Nief, 1968; Hageman and Lohez, 1978 and Wong *et al.*, 1984). The high corrosion properties of water necessitated specially designed mass spectrometer sources made from copper to reduce corrosion. To prevent water vapour adhering to the internal surfaces of the mass spectrometer Majzoub and Nief, (1968) heated the instrument to 150°C. Interference of the minor beam (HDO^+, m/z = 19) occurs due to the presence of ^{18}O and ^{17}O ($H_2{}^{17}O^+$ and $H^{18}O^+$ both with m/z=19) hence this technique has not yielded D/H ratios for samples containing normal concentrations of deuterium. However it has been used to determine $^{18}O/^{16}O$ ratios in water samples, once the D/H ratio has been determined by reducing some of the water to hydrogen (Wong *et al.*, 1984).

3.1.5 Choice of mass spectrometer gas and preparation technique.

Hydrogen gas was chosen as the mass spectrometer gas due to its advantages listed in 3.1.1. It was envisaged that the disadvantage of being non-condensible by liquid nitrogen could be overcome by design of sample inlet system. In the following designs zinc was usually used as the reducing agent because of its less hazardous effects than uranium and its frequent use by in other hydrogen isotope analyser systems.

3.2 Standards

During development of the various inlets, several standards were used to calibrate the instrument. The standards used were three NBS (National Bureau of Standards) water standards and one NBS solid standard listed below.

V-SMOW	Vienna Standard Mean Ocean Water D/H ratio = $155.76 \times 10^{-6} \pm 0.05 \times 10^{-6}$	Defined as 0‰ (Craig, 1961)
SLAP	Standard Light Antarctic Precipitation	δD=-428‰ (Gonfiantini, 1978)
GISP	Greenland Ice Sheet Precipitation	δD=-190‰ (Gonfiantini, 1978)
NBS#30	Biotite, 3.5wt.% water	δD=-64‰

The water standards were originally contained in sealed 25 ml glass ampoules. Once these were opened the waters were transferred to 50ml Pyrex bulbs (described below) to enable routine use of the water standards. The biotite standard was sent in a glass container with a screw top lid, which was subsequently stored in a desiccator.

Four 50 ml Pyrex glass bulbs were constructed with a 10cm neck of Pyrex tube (10mm O.D., 8mm I.D.). The Pyrex bulbs were cleaned by leaving in chromic acid for 24 hours, then thoroughly washed with de-ionised water and dried in an oven at 100°C. The ampoules containing the water standards were then broken open and the water transferred into the bulbs, using a separate pipette (cleaned by the same method as the Pyrex bulbs and stored in an oven at 100°C) for each water standard. The fourth bulb was used to store 50ml of de-ionised water, which was used as a secondary standard. The necks of the bulbs were then sealed using a hydrogen/oxygen gas torch, taking care that no water from the torch formed on the inside of the necks as they were sealed by positioning the flame away from the exposed inner surface of the neck. The transfer of water was carried out as quickly as possible to avoid atmospheric contamination or exchange.

When some standard water was required the neck was broken open and two 4 ml vials (Weaton Scientific) were each filled with approximately 2 ml of water. The neck was then resealed. The standard waters were admitted to the various inlets, through an injection port (described below) by means of a 1µl syringe (Scientific Glass Engineering (UK) Ltd.). One of the vials was used to rinse out the syringe (by repeated loading of the water into the syringe and ejection onto a piece of tissue paper) and the other was used as the standard water to be injected into the various inlets. In this way any possible contamination of the standard water by water adsorbed on the syringe was reduced.

3.3 Conventional inlet and sample preparation system

3.3.1 Apparatus

A schematic diagram of the conventional inlet system is shown in fig. 3.1. Most of it was constructed from Pyrex glass tube (10mm O.D., 8mm I.D., Cambridge Glass) and greaseless valves (PSU/10/RA and POR/10/RA, J.Young). Most of the valves were backed valves, which incorporate an auxiliary pumping line to prevent leakage of atmosphere as described by McNaughton *et al.*, (1983). The backing line was connected to valve SI, of fig. 2.11 and evacuated by the pumps (fig. 2.6) to a pressure of approximately 10^{-4} mbar.

The gas preparation line was pumped by an oil-diffusion pump (E02k, Edwards) filled with 75 ml polyphenyl ether oil and backed by a rotary pump (GDN5, Genevac Ltd.). The pumps were protected by Pirani and thermal trips, the same as those described in section 2.2.2. The pressure above the diffusion pump was measured by a Penning

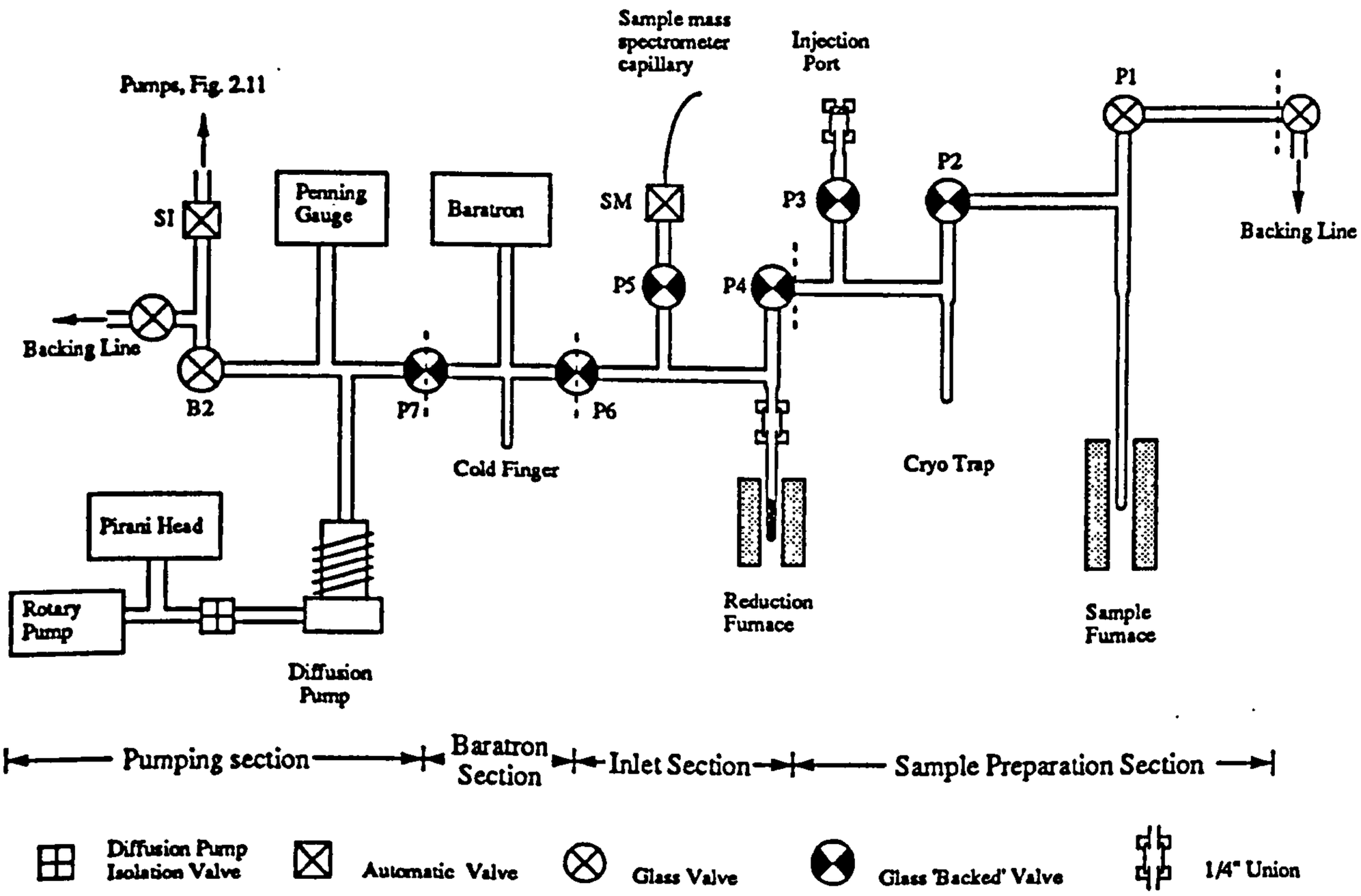

Fig. 3.1. A schematic diagram of the conventional inlet. Water is obtained either by the pyrolysis of solid samples in the sample furnace or from liquid samples injected through the injection port (expanded in fig. 3.2). The water is transferred to the reduction furnace whereupon it is reduced to hydrogen by zinc at 450°C. The hydrogen is then admitted to the mass spectrometer, described in chapter 2, through valve SM.

gauge (CP25EK gauge head and Penning 505 mbar gauge, Edwards,). An isolation valve (PV10K, Edwards) was incorporated to allow closure of the diffusion pump from the rotary pump.

The design of the mass spectrometer inlet in fig. 2.10 was modified by removing valve SM, sealing the line by a 34mm blank flange (FC2, Vacuum Generators Ltd.). Valve SM was then used as shown in fig. 3.1, one end connected to the mass spectrometer capillary and the other connected to a 34mm flange (FC914, Vacuum Generators Ltd.) incorporating a glass metal seal (G321-4-GX-2, North London Valve & Fitting Co.) which allowed connection to the inlet . The backing line of the sample preparation system was connected by a similar 34mm flange and glass metal seal to valve SI of fig. 2.10. This allowed the backing line to be evacuated by different pumps (fig. 2.5) from those used to evacuate the main sample preparation line.

To prevent sample water adhering to the surfaces of the vacuum system all of the glass was heated to 100°C by insulated electrical heating tapes (length 0.9m, Electrothermal Engineering Ltd.) wound around the glass. The current in the heater tapes were controlled by a device constructed as part of this project (circuit diagram A.8 in Appendix A). The temperature of various components in the system, described below, were measured by using cromel-alumel thermocouples, read by a 10-input microprocessor-controlled digital thermometer (Model 610R, Comark Electronics Ltd.). Most of the other components (furnaces, cryotrap and reaction vessel) were constructed in a similar way to those described by Boyd *et al.* (1988).

Two types of electric furnace were used, both described by Boyd *et al.* (1988):

i) Insulated furnaces, capable of attaining temperatures of 1300°C. These had stable temperature characteristics but were relatively slow to reach the desired temperature.

ii) Non-insulated furnaces, capable of reaching temperatures of 1000°C. These were capable of rapid temperature changes but were only controlled to within ± 20°C.

Both types of furnace were controlled manually by variable transformers (Zenith Electrical). The power input for the insulated furnaces were stepped down form mains voltage (240V AC) to 60V by fixed transformers (60V, 8A enclosed transformers; Morite Windings).

The reaction vessel consisted of a quartz tube (6mm O.D., 4mm I.D.; Cambridge Glass), joined to the Pyrex glass by a quartz/Pyrex graded seal (Jencons). Samples loaded into the reaction vessel (see 3.3.2) were heated by an insulated furnace.

Liquid samples could be injected using a 1µl syringe (Scientific Glass Engineering (UK) Ltd.) through an injection port. The injection port, shown in fig. 3.2, consisted of a 0.25" Ultra-Torr union (SS-4-UT-6, North London Valve & Fitting Co. Ltd.) with one end sealed by a 10mm septum (Scientific Glass Engineering (UK) Ltd.). The syringe

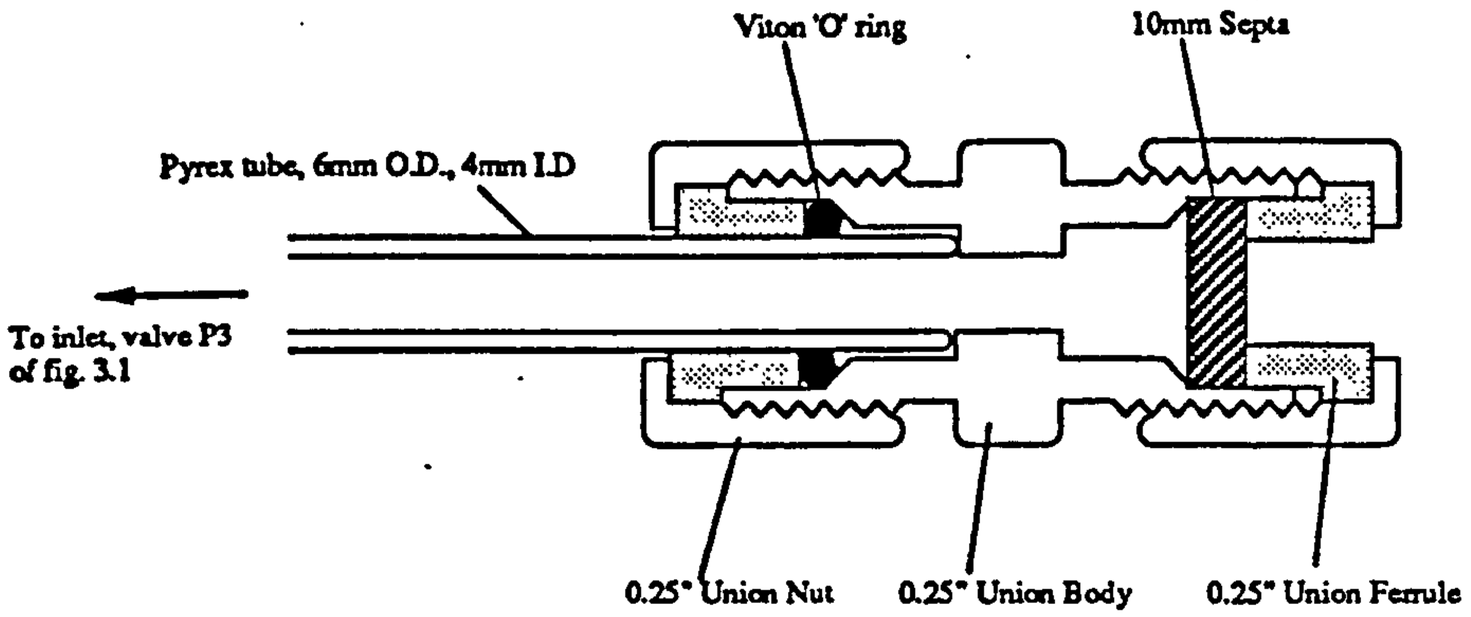

Fig. 3.2. Diagram of the design of the injection port used to inject water samples directly into the conventional inlet, (fig. 3.1), using a 1μL syringe. The 0.25" stainless steel union connected the septa, through which the water was injected, to the vacuum line.

had 20 nl graticules which enabled water sample to be injected with an accuracy of about ±10 nl. The minimum amount of water that could be injected accurately was limited to about 60 nl (about 3 μmol of water). Below 60 nl the relatively small movement of the syringe plunger and the comparatively large error of ±10 nl contributed to poor reproducibility in the amount injected.

The variable temperature cryotrap consisted of a Pyrex tube (6mm O.D., 4mm I.D.), in contact with a thermocouple for temperature measurement, surrounded by a coil of insulated resistance wire. The whole assembly was enclosed by a Pyrex sheath. When immersed in liquid nitrogen the temperature of the cryotrap could by varied from -196°C to about -50°C by passing an electric current through the resistance wire, controlled by a Variable Cryotrap Controller (circuit diagram A.9, Appendix A). When the cryotrap was not immersed in liquid nitrogen, a current was passed through the resistance wire to maintain a temperature of +100°C, in order to prevent water remaining in the trap.

The reduction furnace consisted of a quartz tube (6mm O.D., 4mm I.D.) containing 300 to 500mg zinc and connected to the Pyrex system by a 0.25" Ultra-Torr union. (Uranium was not used due to associated problems, described in section 3.1.1). Usually the reduction of water to hydrogen was carried out by 8-30 mesh zinc shot, 99.9% purity (BDH Chemicals Ltd., Poole). The zinc was prepared by cleaning in concentrated HNO_3 (sp. gr. 1.42) for a few seconds to remove surface zinc oxide, rinsed in de-ionised water and then dried in an oven at 100°C. The zinc was stored in a glass bottle with a screw top lid and kept in a desiccator to prevent excessive oxidation by atmospheric water. Before

use, the zinc was degassed by heating to 450°C, whilst under vacuum, for at least an hour.

The pressure of gas in the inlet was measured by the baratron, a capacitance manometer (sensor head type 315HS-10 and indicator type 170M6C, Chell Instruments Ltd.) capable of measuring gas pressure from 0 to 10 torr to an accuracy of *ca.* $5x10^{-3}$ torr (or to an accuracy of 0.1%, limited by the four figure indicator at pressures > 0.1 torr). The sensor head was enclosed in an oven at 100°C to enable the baratron to measure the pressure of water in the inlet before reduction to hydrogen.

3.3.2 Operational procedure

Solid samples

All processing of materials for D/H analysis was carried out in a clean room. Before use, all tools that came in contact with the sample were cleaned by washing in acetone for 15 minutes, using an ultra sonic bath, then dried in an oven at 100°C. Solid samples (0.1 to 10mg) were placed in a 'boat' (approx. 5x5x1 mm) made of aluminium foil and weighed using a Sartorius balance (4504 MP8-1, Göttingen) which had an accuracy of ±0.1µg. The sample was then loaded into a quartz bucket (a 1cm length of quartz tubing, 3mm O.D., 2mm I.D., sealed at one end) so that the sample could be transferred to the extraction line. Prior to use, the quartz bucket was baked to remove atmospheric water and organic contamination; this was carried out overnight in a muffle furnace at 1200°C.

The quartz bucket containing the sample (enclosed in aluminium foil to prevent dust entering the quartz bucket) was then transferred from the clean room and into the lab housing the mass spectrometer and extraction line. The sample was loaded into the preparation system by closing valves B1, P2, removing the body of valve P1 (see fig. 3.1) and dropping the bucket through valve P1 into the pyrolysis vessel. The valve body, P1, was then replaced and the pyrolysis vessel slowly evacuated by carefully opening valve B1. It was imperative to proceed cautiously to ensure that trapped air between grains in the sample was removed at a rate that did not cause sample loss. Following evacuation to better than 10^{-5} mbar, the sample was then heated by an insulated resistance furnace. During the pyrolysis of the sample any water released, and other condensible gases, such as CO_2 and SO_2, were collected into the cryotrap by liquid nitrogen, *i.e.* operated at -196°C. After 30 minutes any non-condensible gases, which include hydrogen and methane, were removed through valve P4. The cryotrap temperature was increased to -110°C and any CO_2 and SO_2 pumped away, the water remaining frozen in the cryotrap (Burgess, 1987). The water was then transferred

through valve P4 to the reduction furnace by immersing the the reduction furnace in liquid nitrogen and heating the cryotrap to +100°C.

Once the water had been transferred to the reduction furnace the liquid nitrogen was removed and the zinc heated to 450°C by a small non-insulated furnace. To ensure a complete reaction the water was reacted with the zinc at 450°C for 15 minutes (see section 3.3.3). The valve P5 was then opened to admit hydrogen into the mass spectrometer system through valve SM. During the isotopic analysis the reduction furnace remained at a temperature of 450°C.

Isotopic analysis of the hydrogen consisted of three measurements of the D/H ratio of the sample each separated by four minutes. This allowed sufficient time to balance the major ion beam intensity between the sample and reference gas (between each analysis) and perform the data acquisition (section 2.2.4). Usually the δD was taken as the average of the three measurements. However if one reading was greatly different (more than twice the 2 sigma variation given during data acquisition) from the other two or if it was noted that the real-time trace during data acquisition was poor then it was discarded.

After analysis the inlet section was evacuated, to a pressure of better than 10^{-5} mbar for at least 10 minutes before the next water sample was transferred to the zinc reduction furnace.

Water samples

Liquid water samples were admitted through the injection port (see figs. 3.1 and 3.2) using the 1μL syringe. To reduce any potential contamination of the sample water, the syringe was flushed several times with the sample water before being loaded into the syringe and injected through the injection port. After use the syringe was thoroughly rinsed in acetone and then stored in an air-tight container along with some silica gel to prevent contamination from atmospheric water.

Following the admission of water, through the injection port, it was then frozen into the cryotrap at -110°C whereupon any non-condensible gases (mainly atmospheric nitrogen and oxygen) were removed by pumping. It was then transferred to the reduction furnace and the D/H ratio of the resultant hydrogen analysed as described above.

3.3.3 Inlet characteristics

This section describes the characteristics and performance of the conventional inlet system in terms of the accuracy in determining the hydrogen concentration and δD of samples.

The reduction of water to hydrogen by zinc is fairly rapid, as indicated by the use of zinc in a continuous flow method (Bigeleisen *et al.*, 1952; Lyon and Cox 1980). However in this inlet system there was no way of detecting whether the reaction had gone

to completion before admission of the gas to the mass spectrometer. Incomplete reduction of water was easily detectable, once admitted to the mass spectrometer, since the major ion beam intensity would rapidly decrease with time (half-life approximately 30 seconds) as water entered the mass spectrometer capillary and source. Once water had entered the mass spectrometer capillary it took at least an hour to remove. With a new charge of zinc in the reduction furnace the reaction was found to take less than two minutes, but longer after the analysis of several samples. To ensure that water did not enter the mass spectrometer, 15 minutes was allowed for the reduction of water to hydrogen. The zinc in the reduction furnace was replaced at the end of each working day to allow the zinc to degas overnight.

As already described in chapter 2, the best precision in δD that could be obtained was limited by the mass spectrometer to ±2‰. Fig. 3.3 shows how the precision in δD varied when analysing different quantities of V-SMOW. It can be seen that precision in δD varied from ±4‰ for 10μmuol of hydrogen to ±2‰ (i.e. limited by the mass spectrometer) for greater than > 20μmol hydrogen. The precision decreased rapidly for <10μmol of hydrogen since the condition for viscous flow in the capillary was no longer satisfied (see section 2.1). This limited the smallest amount of hydrogen that could be analysed routinely by the conventional inlet was restricted to 10μmol of hydrogen.

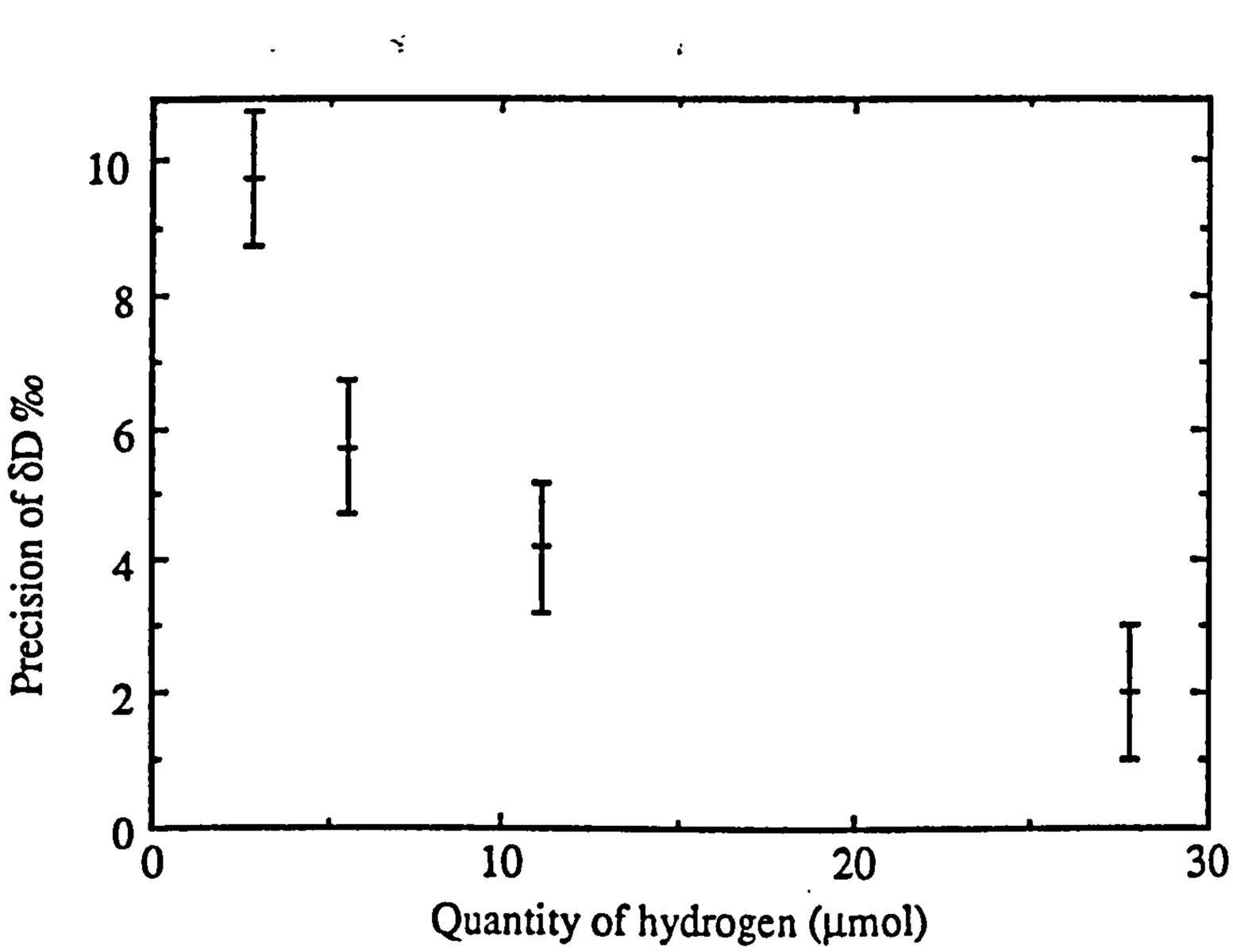

Fig. 3.3. Plot of the precision obtained for various quantities of hydrogen. For samples containing more than 20μmol of hydrogen the precision is limited by the mass spectrometer to ±2‰.

Although the quantity of hydrogen in a sample could be measured by the capacitance manometer to an accuracy of ±0.1%, this was rarely used since the volume of this section of the extraction line (about 1.5 times the volume of the inlet section) increased the smallest sample size that could be analysed from about 10 to 25 μmol of hydrogen.

Alternatively, sample water could be transferred to the cold finger between P6 and P7 (see fig. 3.1) after the water had been separated from other gases by the cryotrap. Valves P6 and P7 were then closed and the cold finger heated to +100°C. The pressure of water vapour was then measured by the capacitance manometer. After measuring the pressure of water in the manometer the water was transferred back to the reduction furnace where it was converted to hydrogen for D/H analysis. It was found that the capacitance manometer was inadequate for measuring the quantity of water, even though the sensor head and all of the associated glass line were heated to at least 100°C. As water evaporated from the cold finger it was found that some of it was rapidly removed by condensation. This resulted in the pressure of gas, as indicated by the reading from the capacitance manometer, quickly rising to a peak and then slowly to decreasing. Fig. 3.4 shows the pressure of water vapour against time for two different amounts of water (2.2 and 4.4μmol).

In order to circumvent the problem of a changing pressure reading, measurements were made by waiting five minutes for the pressure reading to stabilise. Results obtained for pressure reading against quantity of water are shown in fig. 3.5. Clearly in the case of water, the pressure is not proportional to the amount of water. The results for carbon dioxide, also shown in fig. 3.5, confirmed that the capacitance manometer voltage output was proportional to gas pressure (Loriot and Moran, 1975) and that the non-linear response for water was due to some of the water not remaining in the vapour phase. An equation for the calibration curve can be obtained, assuming that the condensation of water vapour on the surface follows the Langmuir adsorption isotherm (Bond, 1987); the fractional amount of surface covered, Θ, is given by:

$$\Theta = \frac{bP}{1 + bP} \qquad 3.8)$$

where P is the pressure and b is the adsorption coefficient.

At low pressure $\Theta \rightarrow bP$ and at high pressures $\Theta \rightarrow 1$ *i.e.* the available surface becomes saturated by a layer of water. Since the capacitance manometer reading is proportional to pressure and the conditions in the baratron section are constant in temperature, volume, surface area and materials, then the relationship between quantity of gas, n, in the baratron section and capacitance manometer reading, R, is given by:

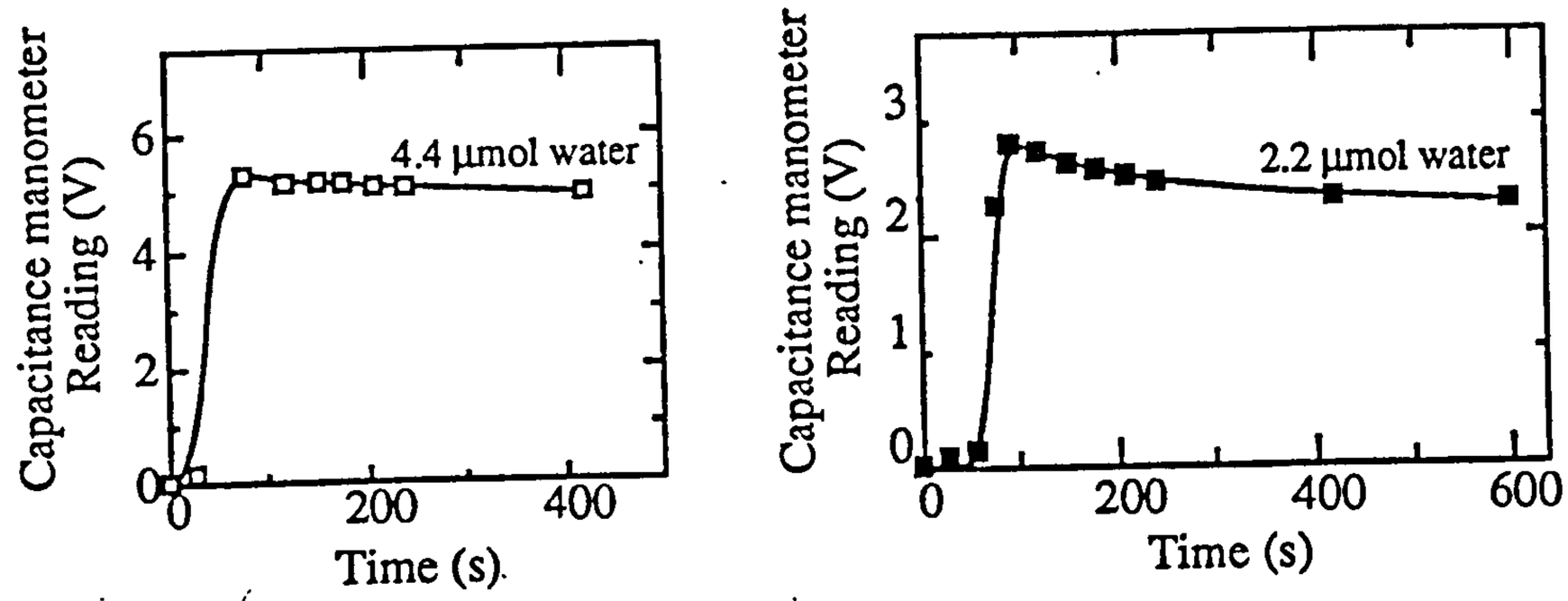

Fig.3.4. Variation of the pressure, as indicated by the capacitance manometer, against time for two different quantities of water. The pressure of water rapidly rises to a maximum and then slowly decreases as the water condenses on the inner surfaces of the manometer volume.

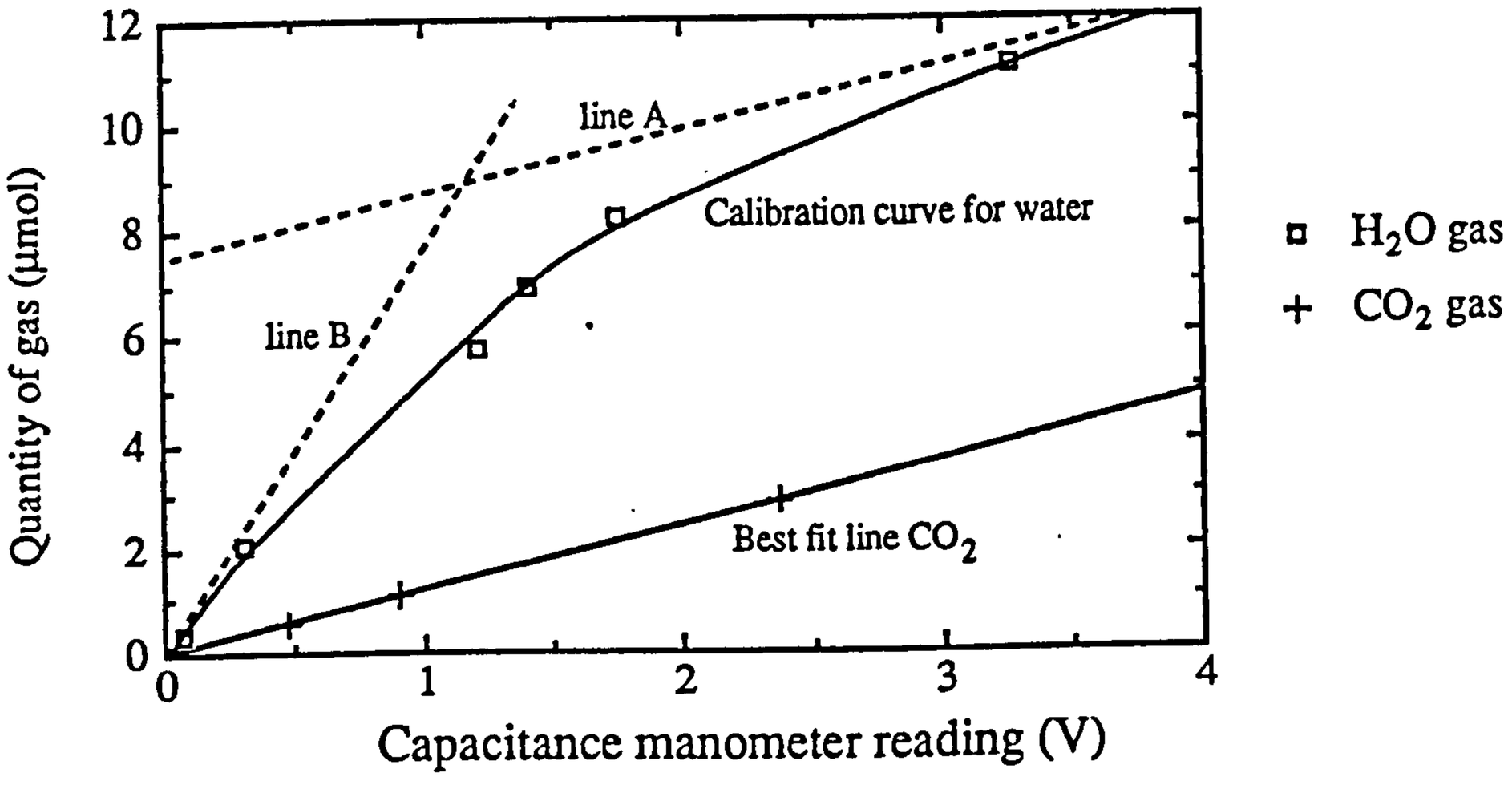

Fig.3.5. Variation of the pressure reading as indicated by the capacitance manometer for different quantities of water. Clearly the relationship between quantity of water and pressure is not linear. Whereas for carbon dioxide the best fit line has slope $1.22\mu molV^{-1}$ and passes through the origin. The calibration curve estimated from the intercept of line A and slope of line B, described in equation 3.10), below.

$$n = k_1R + k_2\Theta \qquad 3.9)$$

where k_1 and k_2 are constants. At high pressure the pressure approaches line A, which has the same slope as the best fit line for CO_2, $1.22\mu molV^{-1} = k_1$, but has an intercept, $k_2\Theta$, of $7.4\mu mol$. At low pressure:

$$n = k_1R + k_2bP = k_1R + k_3R = k_4R \qquad 3.10)$$

where k_3 and k_4 are constants, shown as line B in fig. 3.5. The slope of line B, is given by the constant,k4.; The results of fig. 3.5 were used to estimate the parameters, k_2 and b for calibration curve,

$$n = k_1R + k_2\left(\frac{bR}{1 + bR}\right) \qquad 3.11)$$

where $k_1 = 1.22\mu molV^{-1}$, $k_2 = 7.4\mu molV^{-1}$ and $b = 5.2\mu molV^{-1}$.

If required greater accuracy in these parameters could be obtained using computer curve fitting algorithm (see section 3.5.4); however it can be seen from fig.3.5 that use of the calibration curve would only give an accuracy of approximately ±5%.

Instead of using the capacitance manometer, the quantity of hydrogen in the sample was assessed from the major ion beam intensity. Fig. 3.6 shows that over the range of interest the major ion beam intensity was proportional to the amount of hydrogen in a sample. The hydrogen was obtained from various amounts of water injected with the 1µl syringe. The results indicate that the amount of hydrogen in a sample could be determined to within ±5%. Although the D/H ratio could not be accurately determined for less than 10µmol of hydrogen, fig. 3.6 shows that the major ion beam intensity was proportional to the amount of hydrogen from less than 2µmol up to 50µmol hydrogen.

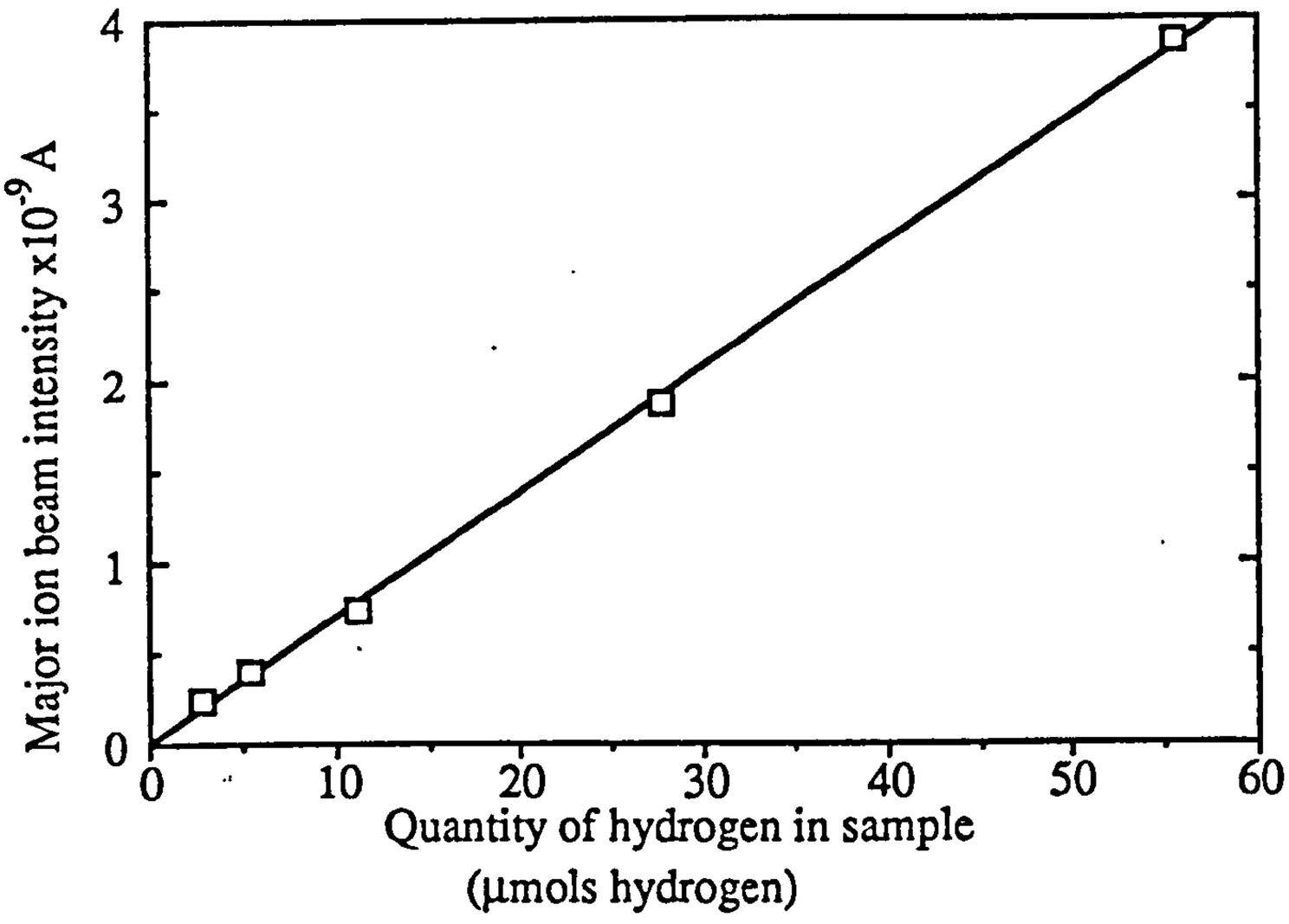

Fig. 3.6 Variation of major ion beam intensity against quantity of hydrogen in sample. The best fit line has a slope of 6.9×10^{-9} Aμmol^{-1}, passes through the origin and has a correlation coefficient of 1.000.

3.3.4 The blank

The hydrogen blank is defined as the amount of gas measured by the mass spectrometer when the analysis procedure was carried out with no sample in the quartz bucket. Obviously for the analysis of small samples it is desirable to have the blank as small as possible. Three sources of blank were identified:

(i) Adsorption of atmospheric water in the reaction vessel when it was opened to allow admission of the sample.

(ii) Water, or hydrogen, adsorbed on the quartz bucket.

(iii) Hydrogen released from the zinc furnace.

The blank from (i) was minimized by evacuating the reaction vessel as quickly as possible once the sample was loaded. The sample was left open to the diffusion pump, at a pressure less than 10^{-5} mbar, for at least half an hour before analysis to remove as much adsorbed water and hydrogen as possible. The blank from (ii) was kept low by baking the quartz bucket at 1200°C in a muffle furnace before use (described in section 3.3.2). By analysis of an empty quartz bucket the combined blank from (i) and (ii) sources was found to be less than 0.05 μmol of hydrogen.

The blank from the zinc furnace was determined (by using the operating procedure for water samples described above, but without injecting any sample) to be between 0.10 to 0.15 μmol of hydrogen. With such small amounts of gas the isotopic measurement

could not be accurately determined since the reference gas and sample gas pressures could not be equalised, pressures of gas in the mass spectrometer capillaries were too low for viscous flow and instrumental noise was a major source of error.

For small samples, where the blank can contribute a significant error in precision then a blank correction can be applied (described in more detail in section 3.5.3 and derived in Appendix C). However, since the size of the blank was less than 1% of the normal sample size and its δD unknown then no blank correction was made.

3.3.5 The memory effect

As for many other D/H isotope analysing systems (see section 3.1) the inlet system described above exhibited a memory effect. The memory effect was manifest when the δD value measured for a particular sample was displaced, from its true value, towards the δD of the material which was previously admitted through the system. This effect was not observed when consecutive replicate analyses of the same hydrogen bearing sample were performed since the δD of the memory was the same as that of the current specimen. Obviously the memory effect was most pronounced when two consecutive gases were analysed which were substantially different in δD (for instance in the case of SLAP analysed after V-SMOW). The results obtained when analysing three consecutive aliquots of SLAP (27.8μmol) after several analyses of V-SMOW are shown in fig. 3.7. The first sample of SLAP gave a measured δD of -418±2‰ instead of -428‰. The high δD value obtained was not due to contamination of the standard water, since the second and third aliquots gave, within experimental error, the correct δD value (*i.e.* δD = -429±2‰ and -427 ±2‰). When analysing V-SMOW (27.8μmol), after the third SLAP sample, the first V-SMOW sample was light, δD = -23±2‰ instead of 0‰. Clearly the contamination was occurring in the inlet system and/or injection procedure and in this example was equivalent to contamination of the sample of between 0.7 and 1.5μmol of hydrogen from the previous sample.

Two different types of hydrogen memory problem and their effects on the design of inlet for sub-μmol quantities of hydrogen were considered:

(i) A fixed percentage of the previously analysed gas remains in the inlet system to contaminate the next sample.

(ii) A fixed quantity of sample remains to contaminate the next sample. The amount of sample remaining is independent of the previous sample size.

If the memory effect is of type (i) then from the results of fig. 3.7 it can be deduced that approximately 3.7±1.6% of the sample gas remained in the inlet following analysis. If this percentage remains constant in all cases then a memory correction can be applied to the results by applying what is essentially a blank correction (using the equations in

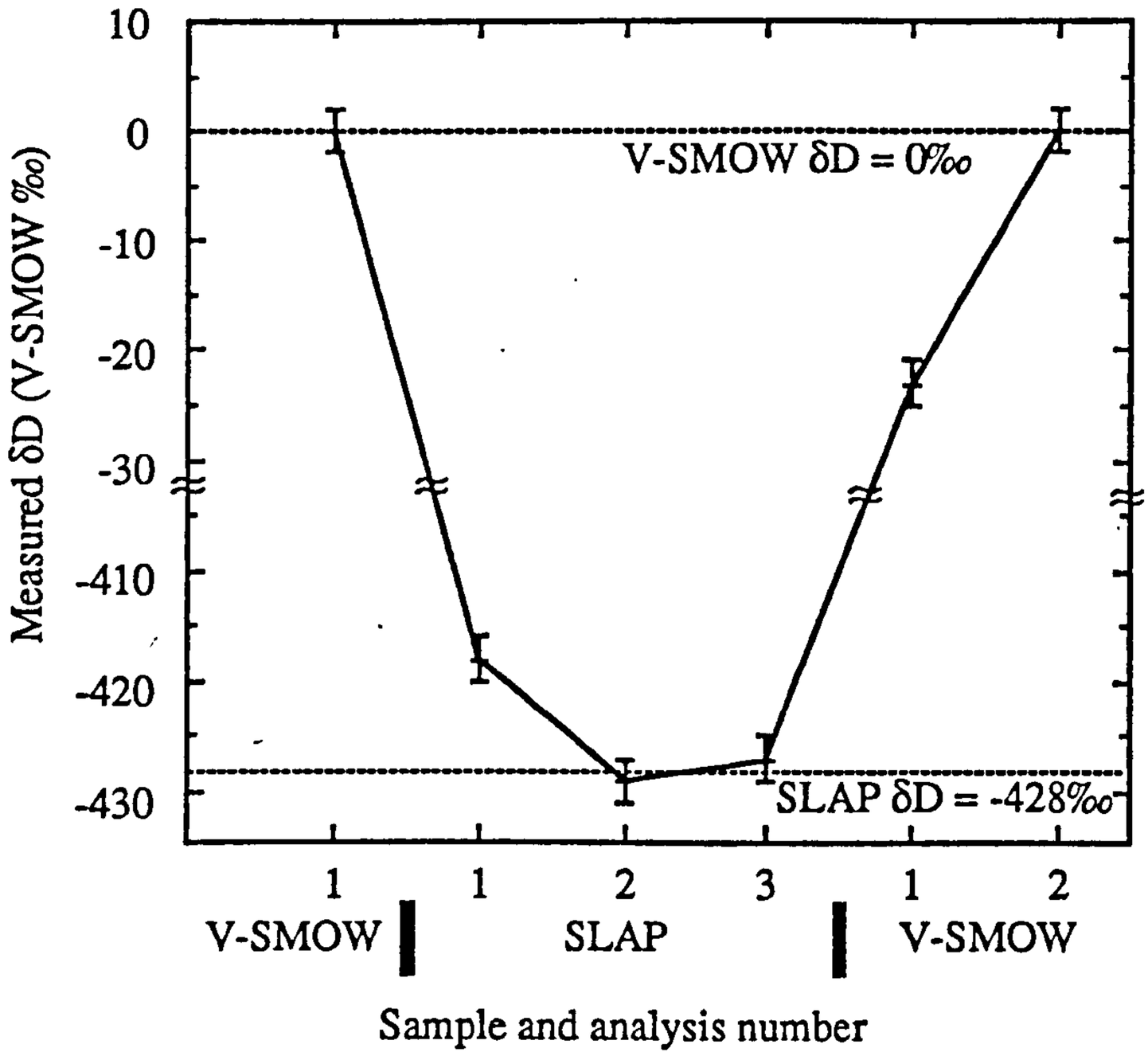

Fig. 3.7. Graph showing the memory effect on the measured δD values of 27.8 μmol quantities of V-SMOW and SLAP. Measured δD values are displaced towards the δD of the previously analysed sample. The size of the displacement is equal to 3.7±1.6% of the difference between the δD of the sample and the previous sample, equivalent to contamination of the sample by 1.1±0.4μmol of hydrogen from the previous sample.

section 3.3.6), assuming the blank has a δD of the previous sample and is between 2.1 to 5.4% of the previous sample size. This type of memory effect poses no problems for the analysis of sub-μmol quantities of hydrogen since the amount of gas remaining in the inlet, to contaminate the following sample, is directly proportional to the amount of the previous sample gas analysed, hence the relative size of the correction will remain constant, independent of sample size.

Alternatively, for a memory effect of type (ii) then the results of fig. 3.7 indicate that approximately 1.1±0.4μmol of hydrogen remained in the inlet to contaminate the next sample. As for a type i) memory effect, a blank correction can be applied, with a blank of 1.1±0.4μmol (regardless of previous sample size) and having δD equal to that measured for the previous sample. This type of memory effect is a much greater problem than the type i) for analysis of smaller samples, since the amount of the memory effect is independent of sample size, hence the correction becomes relatively larger for smaller samples.

3.3.6 Experimental investigation of the memory effect

Clearly the accuracy of δD values obtained for unknown samples is impaired because of the uncertainty in the magnitude of the memory correction. This section describes experiments performed to determine the type of memory effect, its cause and methods of reducing or eliminating it. The many possible causes of the memory effect are listed below:

(i) Incomplete removal of excess sample, water or hydrogen, between analyses.

(ii) Contamination due to the injection procedure. Some sample water might remain in the syringe or the injection port between analyses, thus contaminating the next sample.

(iii) Some of the sample water may be retained by the zinc furnace (possibly as a hydroxide) which then isotopically exchanges with the water from the next sample.

(iv) Hydrogen may be adsorbed by the zinc which is then able to exchange with the hydrogen from the next sample. Florkowski, (1985) reported that hydrogen adsorbed by the zinc reduced the accuracy of the isotope results obtained if a large excess of zinc was used. He also suggested that no more than ten times the stochiometric amount of zinc should be used for the reduction of water. The stochiometric amount of zinc required for the reduction of 25μmol of water is 1.6mg, considerably less than that used in this technique.

(v) There may be incomplete conversion of water to hydrogen by the zinc. Tanweer *et al.*, (1988) found that at least three times the stochiometric amount of zinc was required to obtain the complete reduction of water to hydrogen and obtain accurate isotopic results. However this was considered unlikely for this inlet system since a large excess of zinc was used and the incomplete conversion of the sample water could be detected by performing a background scan (section 2.2.4).

(vi) Hydrogen may be adsorbed by the hot walls of the conversion furnace. Hartley, (1980), concluded that this was the origin of the memory effect in a system where water was injected and reduced to hydrogen by a uranium furnace. The magnitude of this effect was probably lower when zinc instead of uranium was used to reduce the water since lower temperatures were employed, so the rate of diffusion of hydrogen into glass is slower.

(vii) Hydrogen adsorbed by the teflon valve barrels of the greaseless valves in the preparation line. Valley (pers.comm.) found that the memory effect was reduced by using a more dense form of teflon. Alternatively glass barreled valves could be used (these still have a teflon sealing ring, but the amount of adsorbing teflon would be considerably reduced).

(viii) Water adhering to the barrel of the teflon valves. As for (vii) above the use of glass barrel valves would reduce the memory effect.

(ix) Water adhering to the glass and/or metal walls of the inlet.

(x) Hydrogen adhering to the glass and/or metal walls of the inlet.

The series of experiments performed to determine the cause of the memory effect are described below.

Memory experiment 1 - Blank

To demonstrate that the memory effect did not result from incomplete evacuation of the sample gas between analyses, a series of blanks were measured, after the analysis of different quantities of water. Each blank was determined using the normal analysis procedure for liquid samples, except no sample was injected. The results obtained, shown in table 3.2, indicate that the size of blank was independent of the previous sample size (within experimental error) and much less than the amount of contamination, 1.1±0.4μmol, due to the memory effect . Hence the memory effect was not due to incomplete evacuation of the sample gas between analysis (cause (i) above).

Memory experiment 2 - Injection procedure

There are two possible sources of memory effect associated with the injection procedure: water either remains in the syringe or in the injection port between analyses, although in the later case it is not clear where it could reside. The thorough cleaning of the syringe in acetone after each analysis, and conditioning of the syringe with water of similar δD to the sample, should remove all traces of the previous sample water. Two experiments were performed to check that the neither of these two causes were the reason for the memory effect.

A second identical injection port was added adjacent to the first injection port. Using a single syringe one injection port was used when injecting V-SMOW and the

Quantity of water injected (μmol)	Blank (μmol hydrogen)
55.6	0.15
27.8	0.14
12.5	0.08
4.9	0.08
0.2	0.10

Table 3.2. Amount of hydrogen in blank after the analysis of samples containing different quantities of hydrogen. The size of the blank less than the amount of hydrogen causing the memory effect. Hence the memory effect is not due to incomplete removal of the sample between analyses.

other for SLAP. The injection port not in use was valved off to prevent any possible cross contamination. No detectable difference to the results shown in fig. 3.7 were observed. In a second experiment two separate 1µl syringes were used, one for V-SMOW and the other for SLAP. As in the first experiment there was no detectable difference between the results obtained and those for fig. 3.7. To ensure that neither the injection procedure or injection port were the cause of the memory effect the experiment was repeated using both injection ports and syringes. As above there was noticeable change in the magnitude of the memory effect. These experiments showed that effect related to the sample injection procedure or the injection port did not noticeably contaminate the sample.

Memory experiment 3 - Type of memory effect

Experiments were performed to determine the type of memory effect, its magnitude and dependence on sample size. The memory effect was determined for different quantities of sample water by analysing SLAP , after the zinc furnace had been conditioned by analysing V-SMOW. Sample water was injected through the injection port, reduced to hydrogen and its D/H ratio determined as described in section 3.3.2. The results of the measured δD against SLAP analysis number are shown in fig.3.8. The results obtained for different quantities of SLAP and calculation of the percentage and absolute amount of contamination by the previous sample are shown in table 3.3. The results of table 3.3 show that the memory effect was equivalent (within experimental error) to contamination of the sample water by 1.1±0.4µmol of hydrogen from the previous sample, regardless of sample size.

It is concluded that amount of hydrogen (in an unknown form) which remained in the inlet to contaminate the next sample was approximately constant. This fixed reservoir

Amount of water injected (µmol)	Amount of hydrogen contaminating sample (µmol)	% contamination
55.56	1.56±0.38	2.81±0.50
27.78	0.87±0.11	3.13±0.40
27.78	1.42±0.14	5.11±0.51
11.11	1.14±0.15	10.26±1.35

Table 3.3. Results showing the size of the memory effect when different quantities amounts of hydrogen were analysed. The amount of contamination is independent of original sample size.

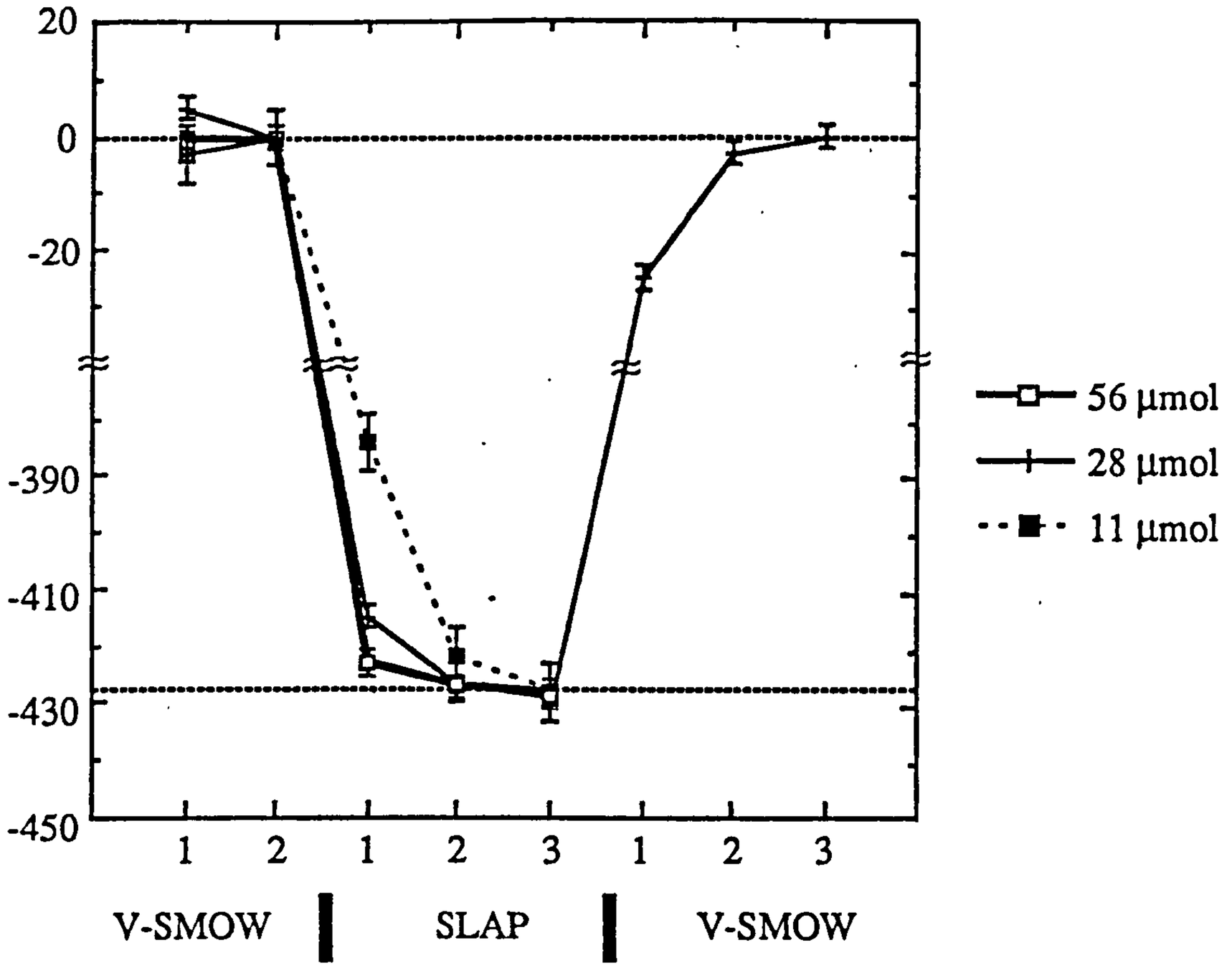

Fig 3.8. Results of δD for analysis of different quantities of V-SMOW and SLAP, showing the the memory effect is larger for samples containing less hydrogen.

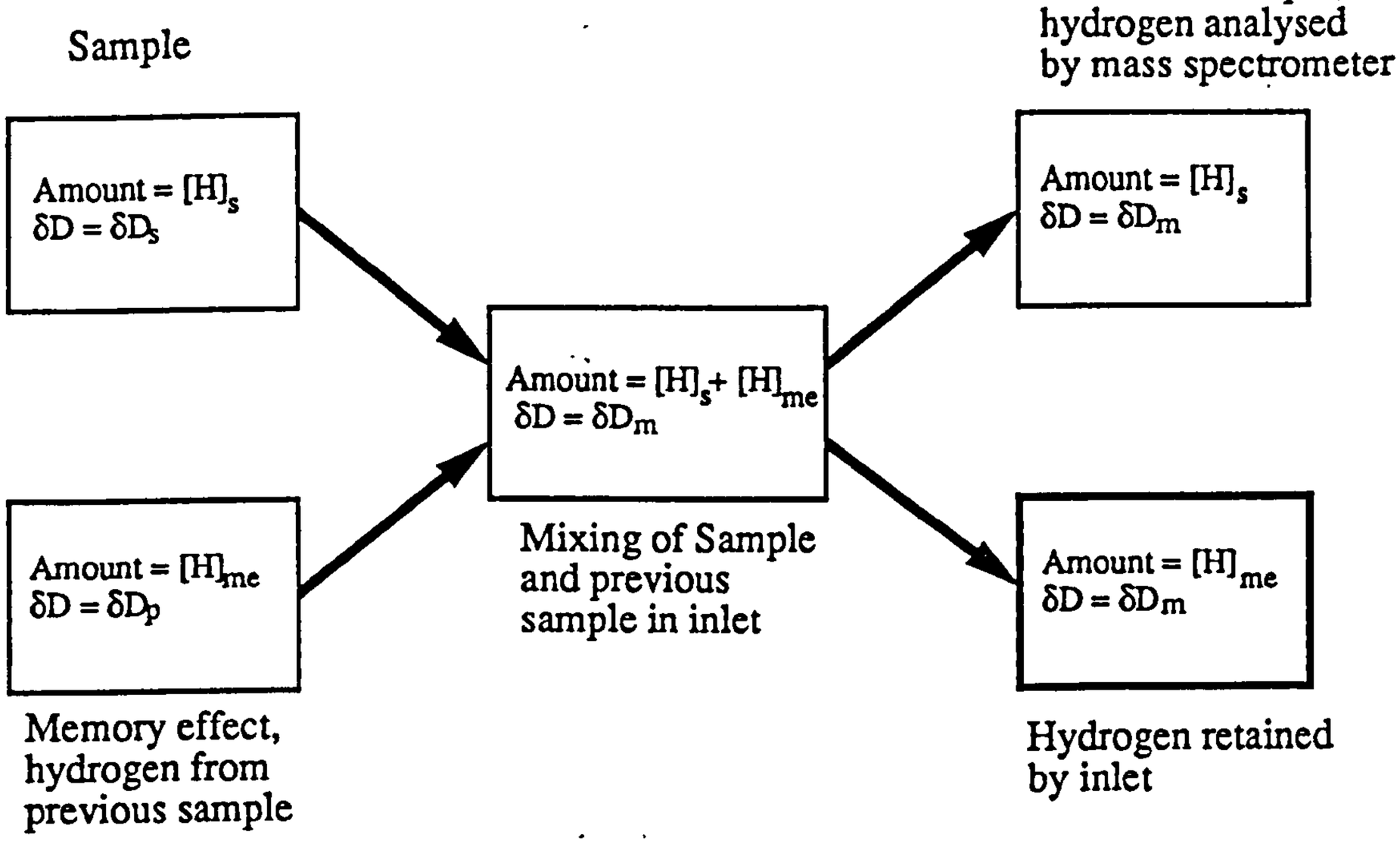

Fig.3.9. A schematic diagram of the memory effect. Hydrogen from the sample mixes with some hydrogen from the previous sample which had remained in the inlet. Most of the contaminated sample is then analysed by the mass spectrometer as hydrogen gas, then pumped away. Some remains in the inlet to contaminate the next sample.

of hydrogen in the inlet system was available for isotopic exchange with the sample hydrogen. Fig. 3.9 shows a schematic diagram of the operation of the memory effect and its effect on the measured δD of the sample. The hydrogen bearing species that causes the memory effect, either water or hydrogen gas, has not been determined. Hence the correct δD of a sample can be calculated by applying a mass balance equation. The correct δD of the sample, δD_s is given by :

$$\delta D_s = \frac{\delta D_m ([H]_s + [H]_{me})}{[H]_s} - \frac{\delta D_p [H]_{me}}{[H]_s} \qquad (3.12)$$

Where δD_m is the measured δD for the sample,

$[H]_s$ is the amount hydrogen in the of sample,

δD_p is the measured δD of the previous sample

$[H]_{me}$ is the amount of hydrogen causing the memory effect.

All the terms in equation (3.12), apart from the amount of hydrogen causing the memory effect ($[H]_{me}$), are determined during the sample analysis or are derived from measurements of the previous sample. From the results in table 3.3, $[H]_{me}$ = 1.1±0.4μmol of hydrogen.

As the amount of sample that remains to contaminate the next sample is independent of sample size then the magnitude of the memory correction becomes more significant for smaller samples.

Memory experiment 4 - Memory caused by reduction furnace

The inlet system described here operated in a sequence mode, similar to the technique used by Coleman *et al.* (1982) in the analysis of rock samples, *i.e.* water was transferred to the zinc furnace and then reacted with the zinc until completely reduced; the next sample was then considered. However batch methods described by others (Coleman *et al.*, 1982; Kendall *et al.*, 1985; Florkowski, 1985; Tanweer *et al.*, 1988) apparently do not have a memory effect (with the size of samples analysed). This inlet system was different from the batch methods in that the same zinc furnace was used for the reduction of many water samples, instead of a new reduction furnace used for each sample. Experiments by Hartley (1980) indicated that memory effects are caused by hydrogen diffusing into the hot glass walls of the reduction furnace. Thus in the batch methods there may be a small loss of hydrogen from each conversion but as a new reaction vessel is used for each reduction, a memory effect is not produced. Kendall *et al.*, (1985) suggested that the zinc shot may contain a hydrogen compound (produced during manufacture when molten zinc is quenched in water to produce the zinc shot) which could isotopically exchange with the sample hydrogen.

To investigate the possibility that the memory effect being caused by the reduction furnace (from isotopic exchange with hydrogen compounds in either the glass walls of the reduction furnace or the zinc shot) the memory effect was measured with the zinc furnace replaced between each analysis. Several 10cm long quartz tubes (6mm O.D., 4mm I.D.) were filled with 300mg of zinc shot and degassed by heating at 450°C under vacuum for at least an hour. These furnaces were then stored under vacuum until required. The experiment outlined in section 3.3.5 was then repeated using 27.8µmol amounts of SLAP, except that between each analysis the reduction furnace was replaced by a new furnace. The results were similar to those of fig. 3.7 and indicated that the memory effect was caused by 1.23±0.13µmol of contamination from the previous sample. There was no significant difference between the results obtained using only one furnace for many samples and those obtained using a new furnace for each sample, thus indicating that if the main cause of the memory effect was not due to hydrogen retained by the reduction furnace (causes (iii) to (vi) above).

Memory experiment 5 - Memory effect from water on inlet surfaces.

Bigeleisen *et al.* (1952) suggested that the memory effect associated with water reduction was caused by sample water adhering to the glass walls of their inlet system. To determine whether this was the cause of the memory in the system described here, the analytical procedure was modified, described below, to prevent water adhering to the glass walls of the inlet or teflon valves. The reduction furnace was removed and 27.8µmol of water injected on the inner glass wall of the furnace. The furnace was then re-attached to the extraction line with the 0.25" union and immersed in liquid nitrogen to condense the water sample. After two minutes the air in the furnace was pumped away, the water remaining frozen in the furnace. The reduction of the water to hydrogen and the analysis of its D/H ratio was then carried out as described in section 3.3.2. The same zinc furnace was used for all analyses. The results obtained, shown in fig. 3.10., are noticeably different from those in fig. 3.7. The first δD value obtained for SLAP was -380±2‰ and the second was -377±2‰. When the SLAP analyses were followed by analysing V-SMOW the result obtained was -1±2‰, the correct value within experimental error. There was a large blank of *ca.* 3.5µmol of water δD = -50±10‰, from atmospheric moisture. This blank resulted in increased yields as measured by the H_2^+ and the reduction in the measured δD of SLAP from -428‰ to -380‰. From this experiment it was concluded that there was no memory effect. The absence of a memory effect indicated that the memory effect exhibited by the conventional inlet was not caused by:

a) Hydrogen gas remaining in the inlet, this eliminates causes (vii) and (x).
b) Water contamination due to the injection procedure.

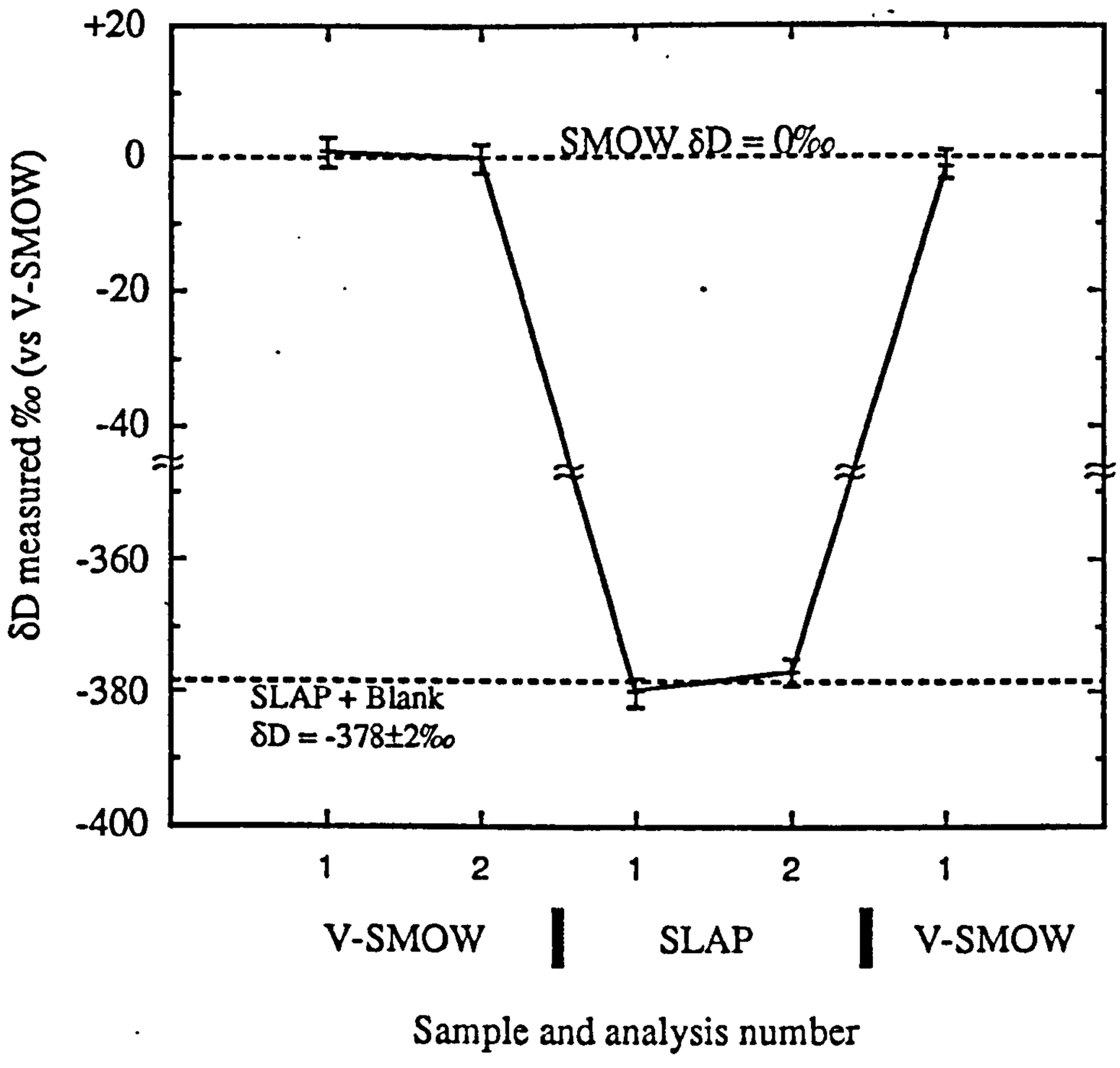

Fig.3.10. Graph showing results obtained for analysis of 27.8mmol quantities of V-SMOW and SLAP when the water injected directly into the reduction furnace. There was no indication of any memory effect since the first and second analyses of SLAP gave the same result and the analysis of V-SMOW after SLAP gave δD = 0‰. The high value for SLAP was caused by atmospheric contamination.

c) Hydrogen or water remaining in the reduction furnace.

The explanation could only be that water adheres to the surfaces of the glass and/or teflon valves of the inlet, (*i.e.* causes (viii) and/or (ix) above). The difference between this inlet system and other batch methods that caused the memory effect was the method in which the water was transferred to the reduction furnace.

3.3.6 Summary

The mass spectrometer and inlet described above had on overall reproducibility of ±2‰ for repeat samples containing at least 10μmol of hydrogen. Blanks were negligible, compared to sample size. For a sample which is isotopically different to its predecessor a loss in precision was caused by the memory effect due to its lack of accurate constraint. A memory effect correction could be applied, the main inaccuracy in this correction was caused by the lack of constraint in determining the amount of hydrogen causing the

memory effect, estimated to be 1.1±0.4μmol of hydrogen. For samples containing 25μmol of hydrogen the memory correction amounted to a loss in precision of 3% of the difference in the δD of the sample compared to the previous sample. *i.e.* for a 25μmol sample of hydrogen 200‰ different its predecessor , then there would be a reduction in precision of 6‰ due to lack of constraint of $[H]_{me}$ in equation 3.8). For most samples analysed on this inlet (>20 μmol of hydrogen with δD between -200‰ and 0‰) the correction was small, less than 10‰ and the overall precision ca. ±5‰.

3.4 Pusher technique

3.4.1 Concept

Most of the hydrogen in the conventional inlet was wasted in the analysis of its D/H ratio, since its presence is required only to maintain a pressure sufficiently high to sustain viscous flow in the capillary and to produce an almost constant flow of hydrogen through the ion source. In a typical analysis, during which the δD was measured three times in 20 minutes (section 3.3.2), the gas pressure in the sample reservoir decreased by approximately 8%. Thus the amount of hydrogen sample gas that flowed through the mass spectrometer capillary was approximately 0.4% of the original amount present per minute. The actual period for which the D/H ratio data was collected, was *ca.* 3 minutes, the remainder of the time was taken for balancing sample and reference gas pressures and acquiring equivalent data for the reference gas D/H ratio. In absolute terms this means that for 10μmol of hydrogen only 0.12μmol (0.4% x 3) produced useful information.

Halas and Krouse (1983) developed an inlet system to analyse carbon, oxygen and sulphur isotopes using a dynamic flow technique to overcome this problem. Sample gas was transferred to a capillary micro-container by liquid nitrogen, then forced through the capillary and into the mass spectrometer by a "pusher gas". The isotope ratios obtained were of a similar precision to the conventional technique but the absolute sample requirement was decreased since the majority of the sample gas was employed in the isotope measurements.

It was decided to evaluate the technique of Halas and Krouse for the analysis of hydrogen isotope ratios. Since hydrogen is not condensible by liquid nitrogen, two micro-containers were employed. Samples of water were transferred, using liquid nitrogen, to a micro-container (volume 0.115cm^3) containing zinc, which was then heated to 450°C to reduce the water to hydrogen. Aliquots of hydrogen were then allowed to expand into a second micro-container (volume 0.01cm^3). The aliquot of hydrogen was then pushed into the mass spectrometer source by a pusher gas, either hydrogen or helium and analysed in a similar fashion to flow-injection analysis (Ruzicka, 1982).

The advantages envisaged were:

i) the volume occupied by hydrogen was extremely low and so sample size requirement was reduced,

ii) several analyses could be made on each sample,

iii) the reduced surface area of the inlet may reduce the memory effect and

iv) the flow of pusher gas through the second micro-container between analyses would purge the micro-container of any remaining hydrogen and so may reduce the memory effect further.

3.4.2 Design

A schematic diagram of the pusher inlet is shown in fig. 3.11. The conventional inlet was used so that water could be transferred to the pusher inlet, the zinc furnace of the conventional inlet being replaced with a blank tube. The semi-automatic vacuum system (valves SP, SI, SV and SM, shown in fig. 2.11 and described in section 2.4.6), was used to manipulate helium pusher gas and connect the pusher inlet system to the vacuum pumps. Modification to the semi-automatic system involved the addition of a pusher reservoir after valve SM. The pusher gas reservoir consisted of a 7.5 cm length of 316 stainless steel tube (1.5" O.D., 16 gauge) welded to 70mm flanges (FC38, Vacuum Generators Ltd.). This was connected to valve SM by a 34 mm flange welded to a 316 stainless steel tube (0.25" O.D., 16 gauge) welded through a 70 mm blank flange (FC2, Vacuum Generators Ltd.). The total volume of the pusher gas reservoir was approximately 80cm^3. The capillary from the pusher gas reservoir was connected to the reservoir by silver welding through a 70 mm blank flange. The pusher gas was either hydrogen or helium, both gases obtained from 25 l cylinders of the respective gas, (99.98% purity; BDH Chemicals Ltd., Poole).

The capillaries (Phase Separations Ltd.) were stainless steel, generally 0.0625" O.D. and mostly 0.010" I.D., except for the zinc furnace and pump-out line (between the glass-line, valve A and valve SI) which were 0.030" I.D. to allow a faster transfer of gas through these sections. Manipulation of the sample gas was accomplished by needle valves N1, N2 (MOV/50, Science Glass Engineering (U.K.) Limited) and microport valves (Valve A, 3 port, port I.D. 0.010" and B 6 port, port I.D. 0.010"; Phase Separations Ltd.). Seals of the capillaries to the microport valves A and B were by 0.0625" metal one piece ferrules (Phase Separations Ltd.). The seals of other components were accomplished by 0.0625" graphite ferrules (Phase Separations Ltd.) to allow easy replacement of some capillary sections, especially the zinc furnace capillary. The "T" connections used had low dead-volumes to reduce the overall volume of the system as much as possible (T1 was type SSUT/16 and T2 type SSUT/4/16/16, Science Glass Engineering (U.K.) Limited).

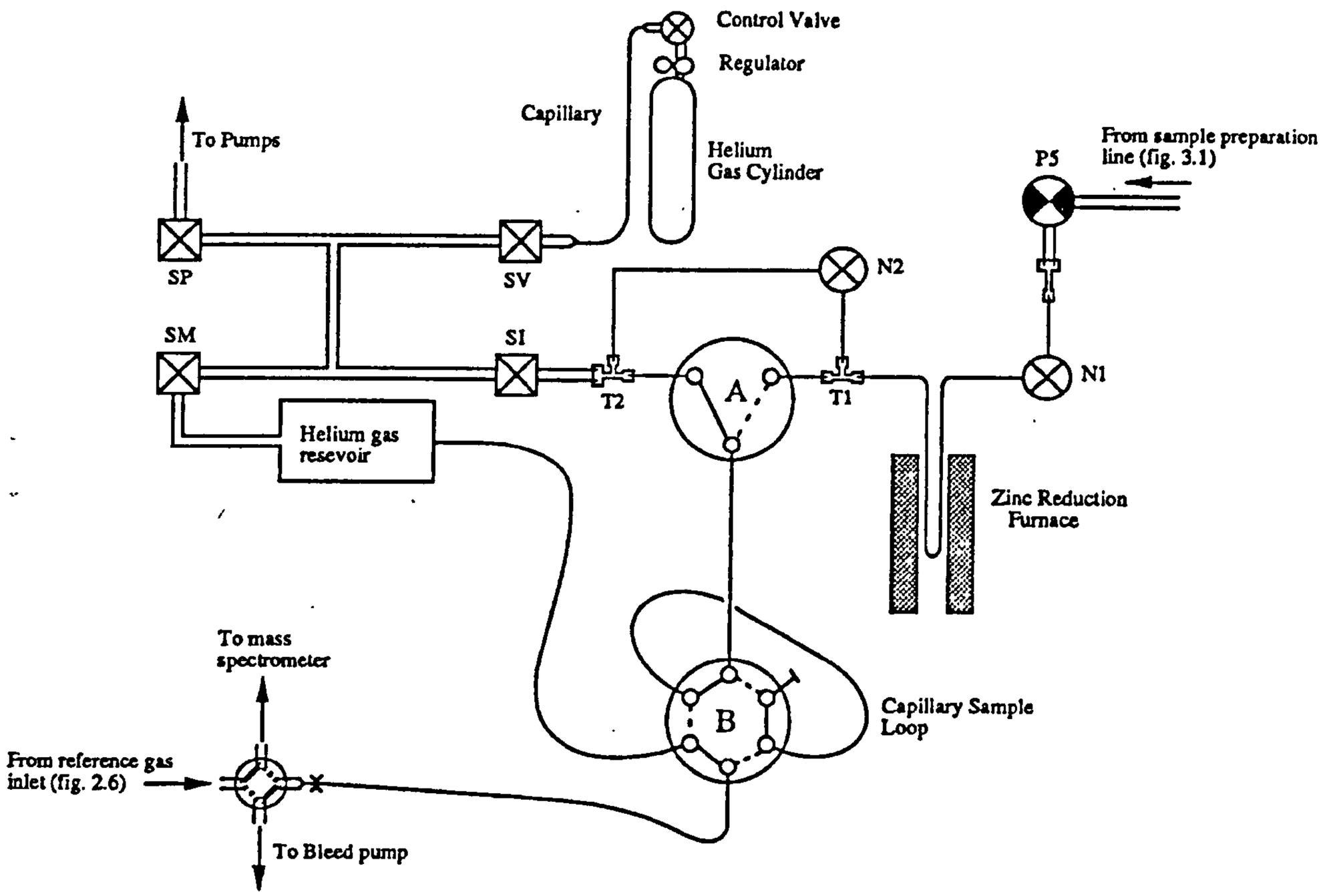

Fig.3.11. Schematic diagram of the pusher inlet. Water from the preparation line is condensed into the reduction furnace and then reduced to hydrogen by zinc powder. An aliquot of the hydrogen is then expanded into the sample loop, which is then pushed into the mass spectrometer source by a flow of helium by switching the 6 port valve B.

The zinc furnace consisted of a 24cm length of 0.030" I.D. capillary with the central 10cm packed with *ca.* 100mg of 100 mesh zinc powder (Johnson Matthey, Materials Technology U.K.) and bent into a U shape to enable immersion in liquid nitrogen. This was heated to 450°C by a small non-insulated furnace.

Capillary sections that came into contact with sample water (from the glass-line to valves A and N2) were heated to 100°C by wrapping with insulated resistance wire. The current through the resistance wire was controlled by the cryotrap controller (circuit A.9 Appendix A).

The capillary between valve B and the change-over valve of the mass spectrometer had a length of 35cm. This length was constrained by the fact that valve B had to be outside the mass spectrometer bake-out oven. (Ideally this length should be as short as possible to prevent extensive mixing between sample and pusher gas, see below). The length of capillary from the pusher gas reservoir to valve B was 24cm so that the total length of capillary from the pusher gas reservoir to the change-over valve (*i.e.* 59cm) was

the same length as on the reference side. The crimp on the capillary between valve B and the change-over valve was balanced to the reference capillary by the procedure described in section 2.4.5.

3.4.3 Operational procedure

During periods when the mass spectrometer was not used, inlet valves A and B were left in the positions shown in fig. 3.11; all the other valves were left open. Before sample analysis, the pusher gas reservoir was filled with the pusher gas, either hydrogen or helium (see section 3.4.4), to give a source pressure of 2×10^{-7} mbar (approximately 300µmol of the pusher gas). Valves SM and SV (in fig. 3.11) were then closed and valves SI and SP were opened to pump out any gas from the capillary inlet.

With valve N1 open and N2 closed the zinc furnace was immersed in liquid nitrogen thus allowing water to be transferred from the sample preparation line (section 3.2.). Due to the small diameter of the zinc furnace, ten minutes was allowed to ensure complete transfer. The zinc furnace was then heated to 450°C to reduce the water to hydrogen. The time taken to reduce the water to hydrogen was about five minutes, although ten minutes was allowed to ensure complete reduction.

Once the reduction of the sample water to hydrogen was completed, an aliquot of the hydrogen was allowed to expand into the sample loop by switching valve A. After two minutes, which allowed enough time for the hydrogen gas to equilibrate in the sample loop, valve B was rotated 60° so that the pusher gas flowed through the sample loop, pushing the aliquot of hydrogen into the mass spectrometer source. During the analysis of the hydrogen aliquot, valve A was switched back to its usual position (shown in fig. 3.11) to pump away the small amount of hydrogen between valves A and B. Following analysis of the hydrogen aliquot, valve B was switched back to pump away the pusher gas from the sample loop, after which valves A and B were switched and another aliquot of sample gas admitted. In this way several replicate analyses of the sample gas were possible, each about 10% smaller than the previous one. After the complete analysis of the sample gas any hydrogen remaining in the zinc furnace was pumped out, for 20 minutes, through valve N2.

3.4.4 Inlet evaluation using hydrogen sample gas

Hydrogen pusher gas

To evaluate the inlet system the zinc furnace (at a temperature of 100°C) was filled with hydrogen from the reference gas cylinder at a pressure of *ca.* 80mbar. Valve N2 was then closed and the hydrogen gas between valves N2, A and SP was pumped away. The pusher gas was then loaded into the storage reservoir. Aliquots of hydrogen from the zinc furnace were then analysed as described above.

One attractive possibility of the technique, suggested by Halas and Krouse, was the use of the reference gas as the pusher gas. This would allow the isotopic measurement of the sample gas followed by immediate comparison against the reference gas without switching any valves. The hydrogen cylinder had a D/H ratio of 104.8±1.4 x10^{-6}, δD = -327±9‰ (determined using the inlet shown in fig. 2.10).

Fig. 3.12 shows the variation with time of the major ion beam intensity and the measured minor/major ratio (without the H_3^+ correction on the minor beam) during admission of the sample gas into the mass spectrometer The sample gas had a D/H ratio of 54.6±4.0 x10^{-6} (see section 2.4.5). The m/z=2:m/z=3 ratio never reached a stable plateau or the correct value of the sample gas, indicating that the gas entering the mass spectrometer source always contained some reference gas. Clearly, there was appreciable

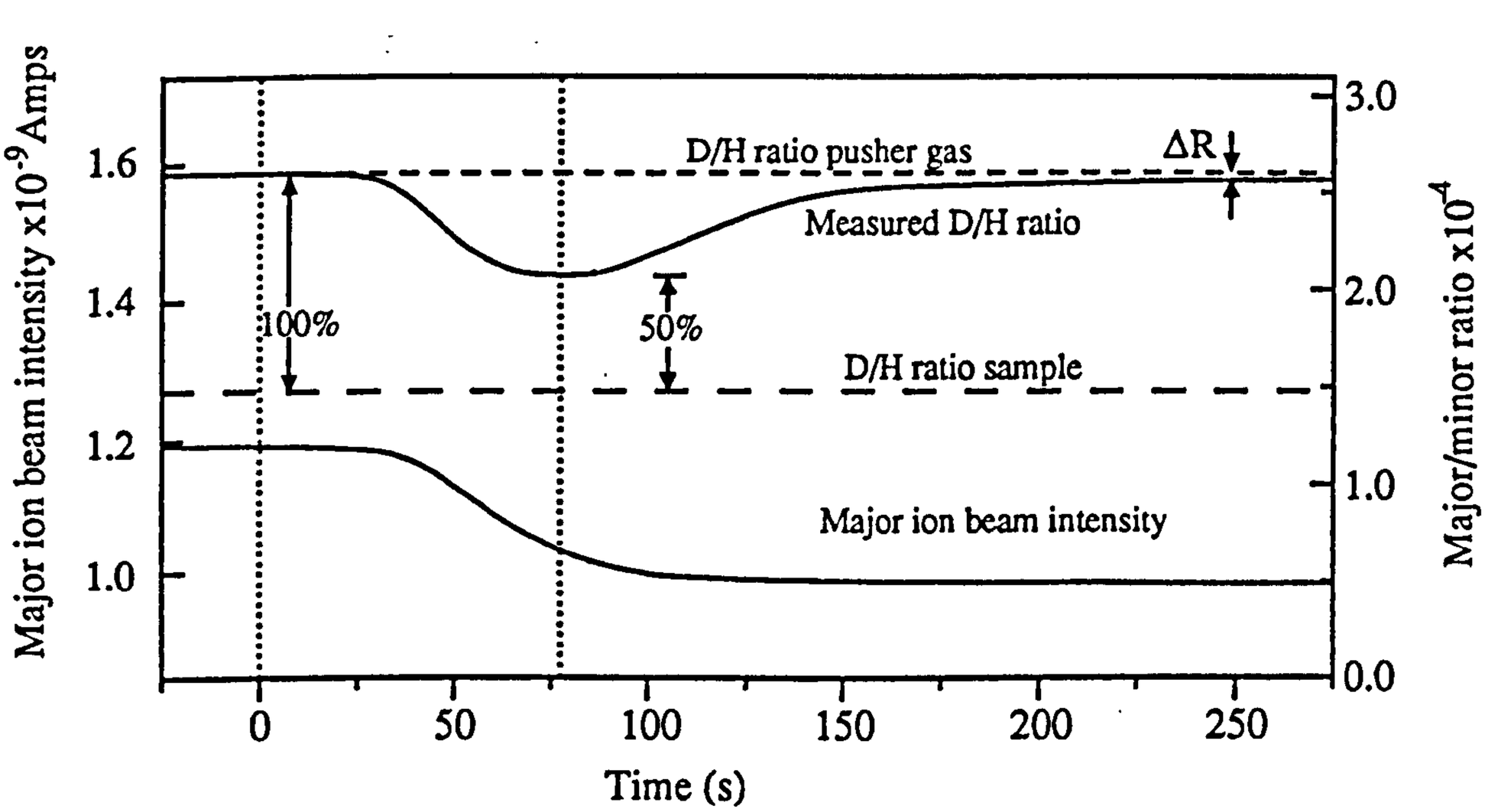

Fig.3.12 Variation of the hydrogen major ion beam intensity and D/H ratio against time as the sample gas is pushed by hydrogen gas through the sample loop and into the mass spectrometer. The microport valve was switched over at time = 0s. The measured D/H ratio reaches a minimum of 2.0x10-4, not the correct value of 1.5x10^{-4}, due to mixing between sample and reference gas.

mixing between the reference gas and the sample gas as the sample gas was pushed along the 35cm length of capillary into the mass spectrometer source. During the admission of the sample gas there was a gradual change in source pressure, as indicated by the change in major ion beam intensity, caused by the change of total capillary length between the pusher gas reservoir and mass spectrometer source when valve B was switched. This caused the shift in measured D/H ratio of the reference gas (ΔR in fig. 3.12), of *ca.* 2%, before and after the analysis of the sample gas because no H_3^+ correction was made. The change in pressure during the analysis could be rectified by modifying the inlet design. Replacement of valve B by an 8 port valve and the addition of a loop of capillary tubing similar to the sample loop would ensure that the total length of capillary tubing remained the same before and after the valve was rotated. However, as the sample gas was always contaminated by some of the hydrogen pusher gas, the use of hydrogen as the pusher gas was considered unsuitable.

Helium pusher gas

Since hydrogen was unsuitable as a pusher gas, the use of helium was evaluated as an alternative. Fig. 3.13 shows the variation with time of the H_2^+ ion beam intensity and the measured D/H ratio when helium was used to admit the sample hydrogen into the mass spectrometer. The minor ion beam intensity was automatically compensated for the H_3^+ ions by subtracting a portion of the major ion beam intensity during data collection (see section 2.4.4). Almost as soon as the valve B is switched over, hydrogen sample gas began to enter the source, reaching a maximum after about 50 seconds. There was appreciable mixing between the hydrogen aliquot and helium pusher gas which is due to the long length of capillary from valve B to the change-over valve and also because of the fast diffusion rates of hydrogen and helium. Note that as the HD molecules have a higher mass than that of H_2 they are transported more slowly in the capillary and so the maximum HD signal occurred after 70 seconds (cf. 50s for m/z=2). Approximately 95% of the hydrogen was forced into the mass spectrometer after 250 seconds.

The nature of the ion beam variation against time required a different data acquisition program to be used than that described in section 2.2.4. The data acquisition program was started as the same time as valve B was switched. The major and minor ion beam intensity was continuously measured until the major ion beam intensity dropped below 0.05×10^{-9}A. The average H_2^+ and HD^+ ion beam intensity was calculated to give an average D/H ratio over the data acquisition period. The change-over valve was then switched to the reference side and the D/H ratio of the reference gas measured for the same length of time as for the sample gas.

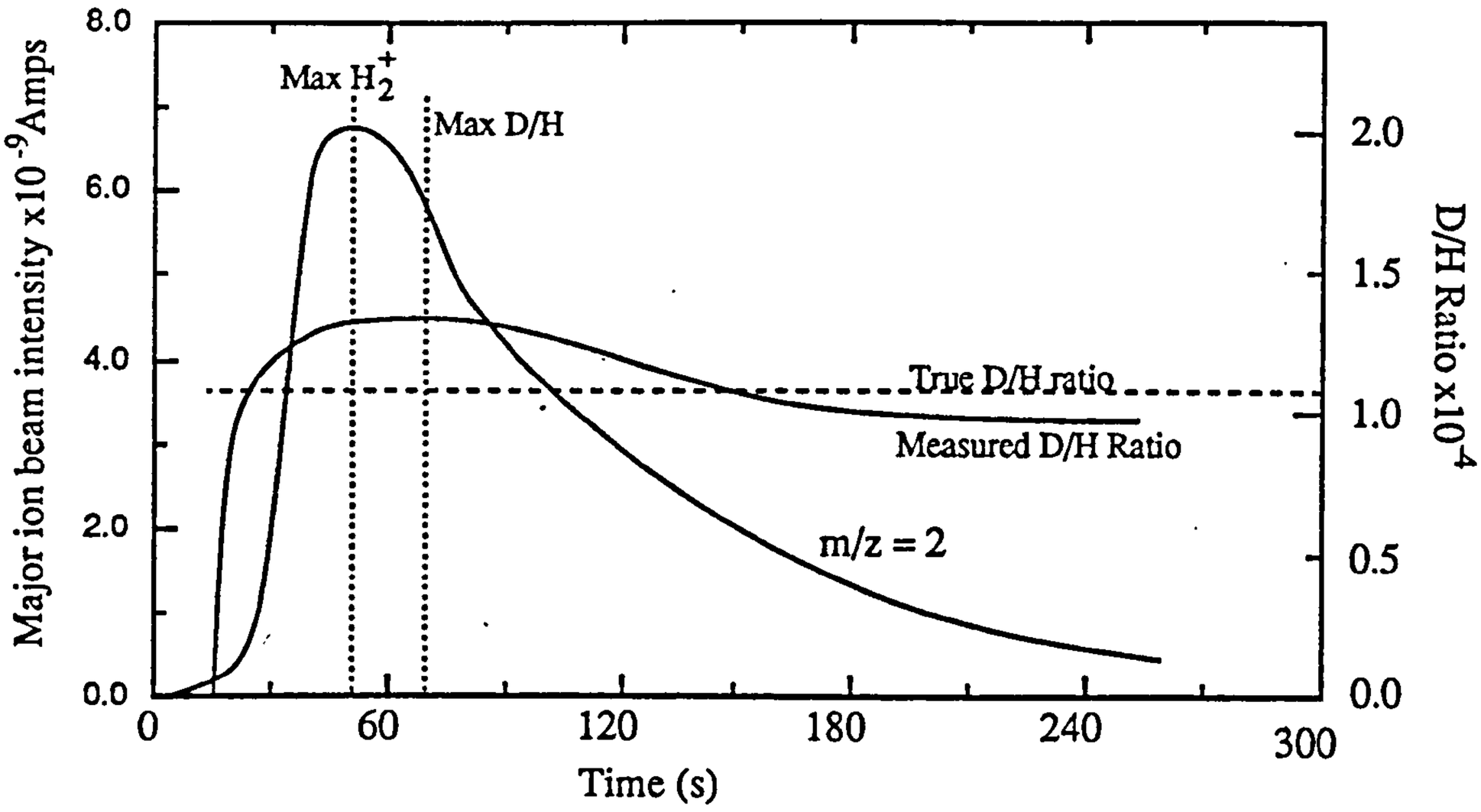

Fig.3.13. Variation of the major ion beam intensity and D/H ratio against time as the hydrogen sample gas is pushed into the mass spectrometer by helium gas. The hydrogen ions (m/z=2) begin entering the source almost immediately, reaching a maximum ion beam intensity after about 50 seconds. Due to the larger mass of the HD^+ ions, the maximum D/H ratio occurs after about 70 seconds. The D/H ratio and ion beam intensity do not reach plateau, indicating mixing between the helium and hydrogen gas.

The disadvantage with using helium as a pusher gas was the possibility of isobaric interferences of the major ion beam, m/z=2, from $^4He^{2+}$ and minor beam, m/z=3 from $^3He^+$. The effect of $^4He^{2+}$ on the major ion beam was found to be insignificant, however, the effect of $^3He^+$, which has a concentration of 1.3ppm in natural helium was detectable. To compensate for this the $^3He^+$ion intensity was measured while helium was flowing into the mass spectrometer, prior to switching valve A. This contribution was then subtracted from the minor ion beam intensity during measurement of the sample gas. Unfortunately this procedure was not entirely successful since during analysis some helium is displaced by the hydrogen sample and the helium pressure decreased due to the addition of the sample loop to the total capillary length, hence the $^3He^+$was always too large. However, this over-compensation is a systematic effect and is automatically corrected by calibrating the reference gas by analysing a standard as an unknown sample.

Zero enrichment

The pusher gas technique was assessed by performing a zero enrichment, using helium as the pusher gas. Reference gas was allowed to expand, from the reference gas inlet, into the zinc furnace at a pressure of 80mbar. Valves N1 and N2 which isolate the zinc furnace were then closed and reference gas between valves N2 and A was removed by pumping through valve SP. Helium pusher gas from the storage reservoir was then used to admit three aliquots of the hydrogen gas to the mass spectrometer and analysed as described above. Results obtained from zero enrichment analyses, between the reference gas measured by the reference inlet (section 2.3.1) and pusher inlet was $\delta D = -27‰ \pm 15‰$. This was probably due to the over-estimation of the $^3He^+$contribution to the minor beam during analysis.

Sensitivity

The volume of the zinc furnace and capillary between valves N1, N2 and A was $0.115 \pm 0.010 cm^3$. Therefore the amount of hydrogen in the zinc furnace during the zero enrichment at a pressure of 80mbar and temperature of 100°C was 0.3µmol. The sample loop had a volume of $0.010 cm^3$, about 10% of the zinc furnace volume. During a complete analysis of a sample of 0.3µmol of hydrogen, three aliquots were pushed into the mass spectrometer, hence a total of 0.1µmol was analysed by the mass spectrometer and the precision was ±15‰. The loss in precision compared to the conventional inlet in section 3.2 is due to the smaller sample size analysed, variation in $^3He^+$, and not making frequent comparisons with the reference gas during analysis.

3.4.5 Evaluation of pusher technique using water standards

For the evaluation of pusher technique in sample analysis mode the 1µl syringe was used to inject 3.3µmol quantities of standard water (containing 3.3µmol of hydrogen) which was then transferred to the zinc furnace and analysed as described above. During the analyses of several consecutive water samples the zinc furnace rapidly became exhausted, being able to reduce a maximum of 5 samples (*ca.* 17µmol of water) before hydrogen yields began to diminish, as shown in fig. 3.14. Thus it was necessary to replace the zinc furnace frequently, taking at least an hour to pump out and degas the zinc powder.

The magnitude of the memory effect was found to be much greater for this system compared to the conventional inlet (see section 3.3.5). Results obtained for D/H measurements of consecutive analyses of SLAP after analysing V-SMOW are shown in fig. 3.15. The contamination was equivalent to 2.0±0.5µmol of hydrogen from the previous sample (compared to 1.1±0.4µmuol for the conventional inlet). Assuming that

Fig.3.14. Graph of the maximum major ion beam intensity when analysing consecutive samples of water containing 3.3µmol hydrogen. In this example there is only a 80% yield for the fifth analysis of water, indicating that the zinc furnace requires replacement. The sixth analysis contains hardly any hydrogen, most of the water had not been reduced by the zinc.

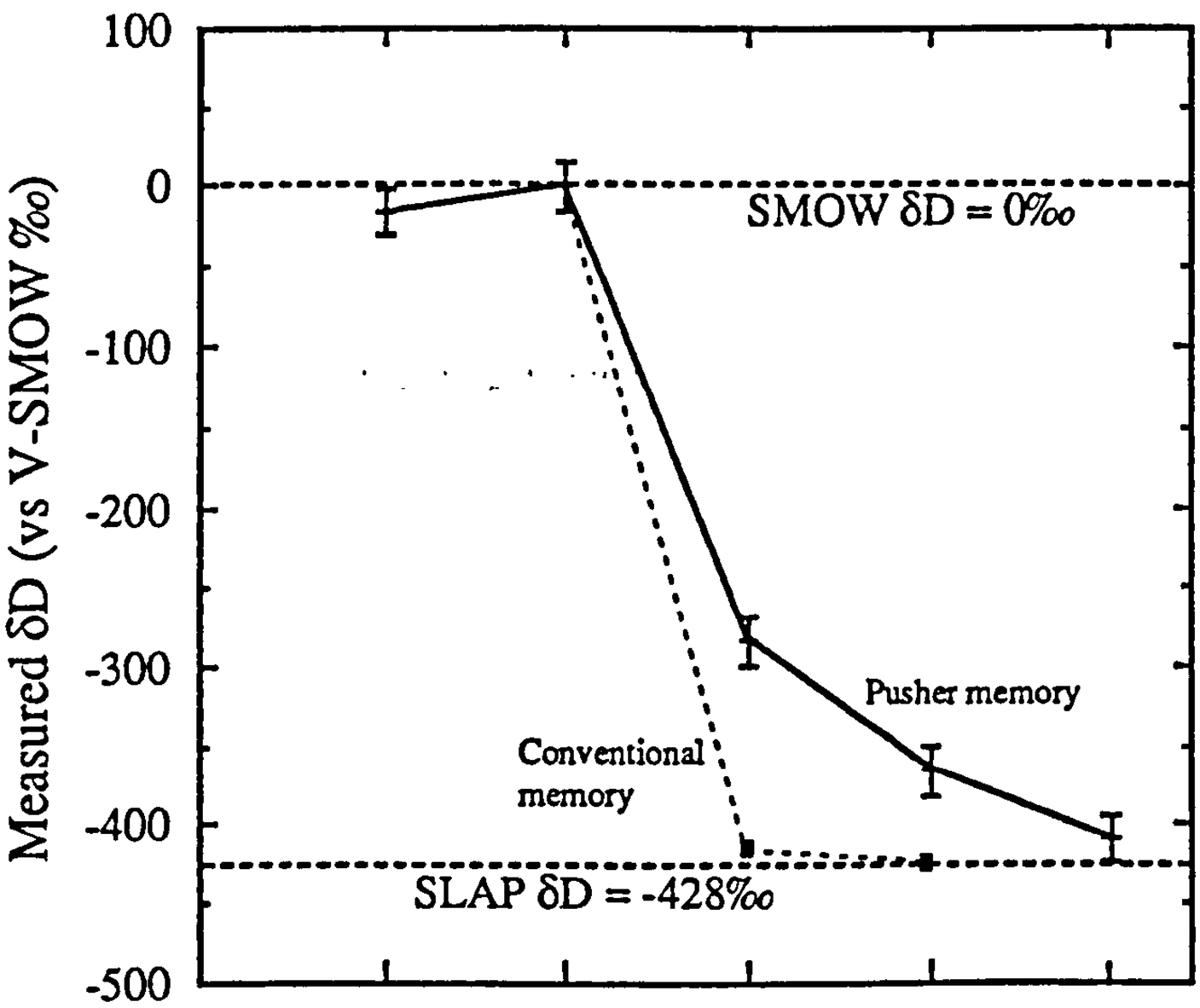

Fig.3.15. Results showing the memory effect for the pusher inlet, obtained when analysing consecutive quantities of SLAP containing 3.3 µmol of hydrogen, after V-SMOW. The third analysis almost gives the correct value within experimental error. A forth result could not be obtained as the zinc furnace required replacement. The memory effect for the conventional inlet (for a sample size of 27.7mmol of hydrogen) is shown for comparison.

the cause of the memory effect was the same as for the conventional inlet, then the quantity of water remaining in the inlet to contaminate the next sample was not much greater than the conventional inlet. The increased size of the memory effect , between the pusher technique and conventional technique, was probably due to the increased distance the sample water travelled through the preparation line before conversion to hydrogen. The third 3.3µmol sample of SLAP analysed had $\delta D = -408 \pm 15‰$, almost the correct value for SLAP within experimental error. Hence one solution to the memory effect could be to analyse 4 consecutive 3.3µmol quantities of sample water, but the short lifetime of the zinc furnace prevented this. A fourth analysis of SLAP, performed after the results shown in fig. 3.15 were obtained, only gave a 50% yield and had $\delta D = -512 \pm 20‰$. Therefore sample data were corrected by a protocol similar to that used for the conventional inlet (equation 3.12).

3.4.6 Summary of pusher gas inlet

In conclusion, this system presents a large increase in sensitivity, by a factor of 30, with a corresponding loss in precision to ±15‰. Some of the loss in precision probably results from the choice of helium as the pusher gas and mixing between the sample and pusher gases between valve B and the mass spectrometer source. This might have been remedied by the use of a pusher gas with a higher atomic mass (such as argon) and reducing the length of capillary between valve B and the mass spectrometer source. However the sensitivity gain was not large enough to the achieve the desired goal of analysing samples containing 0.05µmol of hydrogen. In consequence this technique was not investigated further; no analysis of unknown samples were undertaken with this configuration of inlet system.

A large increase in sensitivity can be gained for the isotopic analysis of condensible gases, such as carbon dioxide and sulphur dioxide, by concentrating the sample gas directly into the sample loop using liquid nitrogen. The reduction furnace would not be necessary, hence the smaller volume of the sample loop would increase the sensitivity by a factor of 10, allowing isotopic analysis of .03µmol of gas.

3.5 Hydrogen reduction by flow-thru technique

The basic principle behind the flow-thru system was to design an inlet system to give maximum sensitivity by manipulating water as the sample gas as near to the mass spectrometer as possible. Since water is condensible by liquid nitrogen it could be transferred to a small container from where a small leak flowed towards the change-over valve. The conversion of water to hydrogen was delayed until just before entry of the mass spectrometer change-over valve.

3.5.1 Flow-thru inlet

The design of the flow-thru inlet is shown in fig. 3.16. This was the same system as used for the zero enrichment (fig. 2.11 described in section 2.4.6), but with the mass spectrometer capillary being replaced by a 'U' trap and reduction furnace, as described below. Water was introduced through valve SI in the same way as for the pusher inlet (section 3.3). The entire flow-thru inlet was maintained at 100°C by an oven to prevent water vapour adhering to the metal walls of the inlet.

The 'U' trap consisted of a 20cm length of stainless steel capillary (0.0625" O.D., 0.030" I.D.; Phase Separations Ltd.) connected to valve SM by silver welding to a 34mm flange (FC2, Vacuum Generators Ltd.). Transfer of sample water from the preparation line to the capillary 'U' trap was accomplished by immersion of the 'U' trap in liquid nitrogen. The other end was silver welded to a 0.25" Ultra-torr adaptor (SS-4-UT-A-4, North London Valve and Fitting Co. Ltd.) for connection to the flow-thru conversion furnace. The crimp between the 'U' trap and conversion furnace restricted the flow of sample water from the 'U' trap into the conversion furnace. The crimp was tightened so

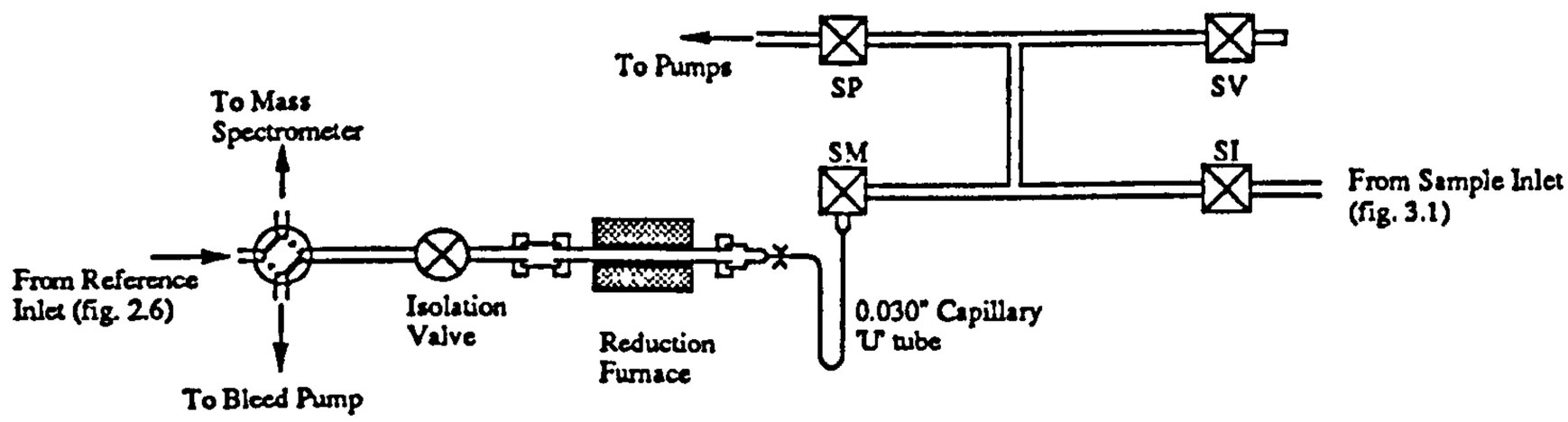

Fig.3.16. A schematic diagram of the flow-thru inlet. Water from the preparation line (fig.3.1) was transferred to a U capillary. The water the flowed passed through a constriction and, into the reduction furnace, shown in fig. 3.17 where it was reduced on-line to hydrogen. The hydrogen then flowed directly to the change-over valve and into the mass spectrometer.

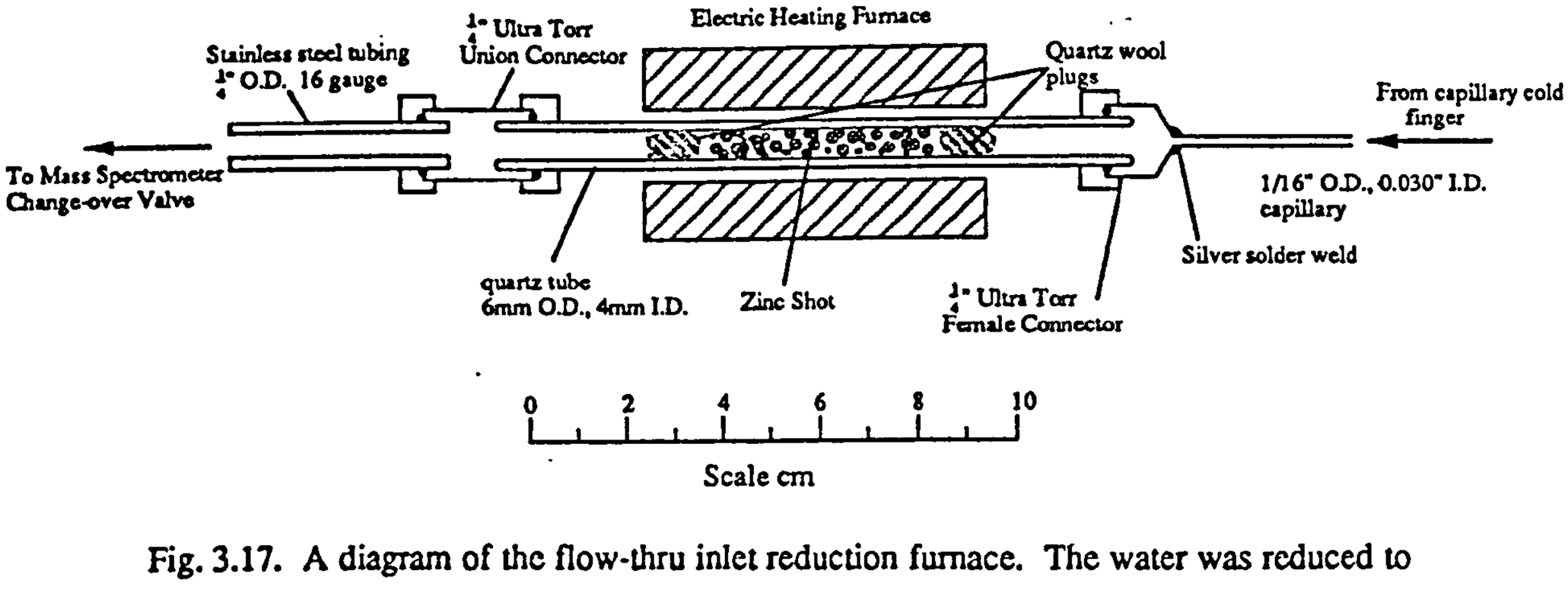

Fig. 3.17. A diagram of the flow-thru inlet reduction furnace. The water was reduced to hydrogen by zinc shot, retained by quartz wool plugs and heated to 350°C by a small electric furnace.

that a hydrogen pressure of 3cm of mercury behind the crimp gave a source pressure of $3x10^{-7}$ mbar. This was found to give an adequate flow rate of hydrogen into the mass spectrometer to allow isotopic measurement, without rapid depletion of water of the sample water in the 'U' trap.

A diagram of the conversion furnace is shown in fig. 3.17. This consisted of a 10cm length of quartz tubing (6mm O.D., 4mm I.D.; Cambridge Glass) mounted horizontally, with the central portion filled with 300-500mg 8-30 mesh zinc shot held in place by quartz wool plugs (cleaned by the same procedure used for glass, as described in section 3.2). The zinc shot used was the same as that used for the conversion furnace of the conventional inlet and was prepared in the same way (see section 3.3.1). This was heated by a small insulated furnace. The furnace was connected to the mass spectrometer change-over valve *via* a 0.25" Ultra-torr union (SS-4-UT-6, North London Valve and Fitting Co. Ltd.) and a length of 316 stainless steel tubing (0.25" I.D., 16 gauge). A subsequent modification incorporated a flexible metal section (321-4-X-2, North London Valve and Fitting Co. Ltd.) and a manual Nupro bellows valve (SS-4H-TH3, North London Valves & Fitting Co. Ltd.) to enable isolation of the mass spectrometer from the conversion furnace during replacement.

3.5.2 Operational procedure

Water samples

Water was injected into the sample preparation line using a 1µL syringe (section 3.3.2); from here it was transferred to the capillary 'U' trap using liquid nitrogen. This process required ten minutes to ensure complete transfer of the sample water because of the narrow bore of the capillary. Valve SM was then closed and the liquid nitrogen removed to allow the water to enter the gas phase. The volume between valve SM and the crimp (0.090 cm^3) was essentially the sample gas storage reservoir. Thus for 1µmol of water a sample gas pressure of 260 mbar was attained. This high gas pressure in the capillary forced a flow of water vapour past the crimp and into the conversion furnace whereupon it was reduced to hydrogen. The hydrogen was then able to enter the mass spectrometer *via* the change-over valve at a source pressure of *ca.* 10^{-7} mbar.

It was deduced after some experimentation that the optimum temperature of the zinc reduction furnace was 350°C. At lower temperatures the complete reduction of water to hydrogen was not achieved, as detected by monitoring the m/z=17 (OH^+) and m/z=18 (H_2O^+) peaks during sample analysis. At temperatures higher than 350°C the zinc vapourised and rapidly moved away from the hot centre of the furnace to the cooler ends where it recondensed. Even at 350°C the zinc metal, and also zinc oxide powder produced during reduction of water, tended to be displaced towards the mass spectrometer side of the furnace, presumably due to the flow of water/hydrogen gas over the furnace. It was important to prevent zinc or zinc oxide powder reaching the bellows and change-over valves since it could cause sealing problems. Zinc reaching the mass spectrometer source is likely to cause source instability or even flash-over problems by coating ceramic spacers and other insulating components. The zinc/zinc oxide was prevented from entering the mass spectrometer source by the quartz wool plugs (see fig. 3.17). Nevertheless the zinc in the furnace required replacing about once a week to replenish the zinc and remove zinc oxide powder. The replenished furnace was degassed at 350°C for at least 12 hours before use.

Analysis of the D/H ratio of the hydrogen produced was accomplished using the data acquisition program described in section 2.2.4., essentially analysing the gas produced in a dynamic mode.

Solid samples

The handling, water extraction and purification procedure for solid samples was achieved by the same method as for the conventional inlet (section 3.3.2). Once the sample water had been released from the specimen and purified, it was transferred to the 'U' trap and the D/H ratio analysed as described above.

3.5.3 Flow-thru inlet characteristics

The flow-thru inlet was evaluated using 3.3μmol quantities of water. Fig. 3.18 shows the typical variation of major ion beam intensity and D/H ratio against time when analysing 3.3μmol of water. Hydrogen began to enter the mass spectrometer ion source about 20 seconds after the liquid nitrogen was removed from the 'U' trap, reaching a maximum pressure after six minutes. The major ion beam intensity then slowly decreased, with a half-life of approximately 40 minutes, as water from the capillary cold finger became depleted. The measured D/H ratio (for an analysis of V-SMOW) shows that there was some isotopic variation with time. During the analysis of samples this change in measured δD was compensated by employing a strict timing protocol. Measurement of the D/H ratio of the sample was performed at 10, 16 and 22 minutes after the liquid nitrogen was removed from the capillary 'U' trap. Having the first analysis at 10 minutes allowed adequate time for the sample water to evaporate and to balance the reference and sample gas pressures, using the variable volume bellows section (2.3.2). The δD of the sample gas was taken as the average of all three measurements. Table 3.4 shows the results obtained when analysing consecutive 3.3μmol quantities of V-SMOW. The overall precision in δD was ±10‰ for samples containing 3.3μmol of hydrogen.

The blank

Two sources of blank were identified for the flow-thru inlet. The first was due to hydrogen being continuously evolved from the zinc furnace and entering the mass spectrometer source at a rate of between 10 to 20pmols^{-1}. This was equivalent to analysing a sample containing between 0.025 and 0.050μmol of hydrogen. The second source of blank was from hydrogen, or water, introduced to the inlet during the loading procedure; this was kept to a minimum by using the sample preparation and loading procedures described in section 3.3.2. The blank introduced during sample loading was found to be 0.02±0.01μmol of hydrogen.

For small samples (containing <0.1μmol of hydrogen) the blank contributed a significant error in the accuracy of the δD and so a blank correction was applied. The δD and amount of sample being calculated from the known amounts and δD of the blank and gas measured. The δD of the sample, δD_s is given by

$$\delta Ds = \frac{[H]_m \, \delta D_m}{[H]_m - [H]_b} - \frac{[H]_b \, \delta D_b}{[H]_m - [H]_b} \qquad (3.13)$$

Where δD_m is the measured δD for the sample, $[H]_m$ is the amount of sample measured, δD_b is the δD of the blank and $[H]_b$ is the amount of blank.

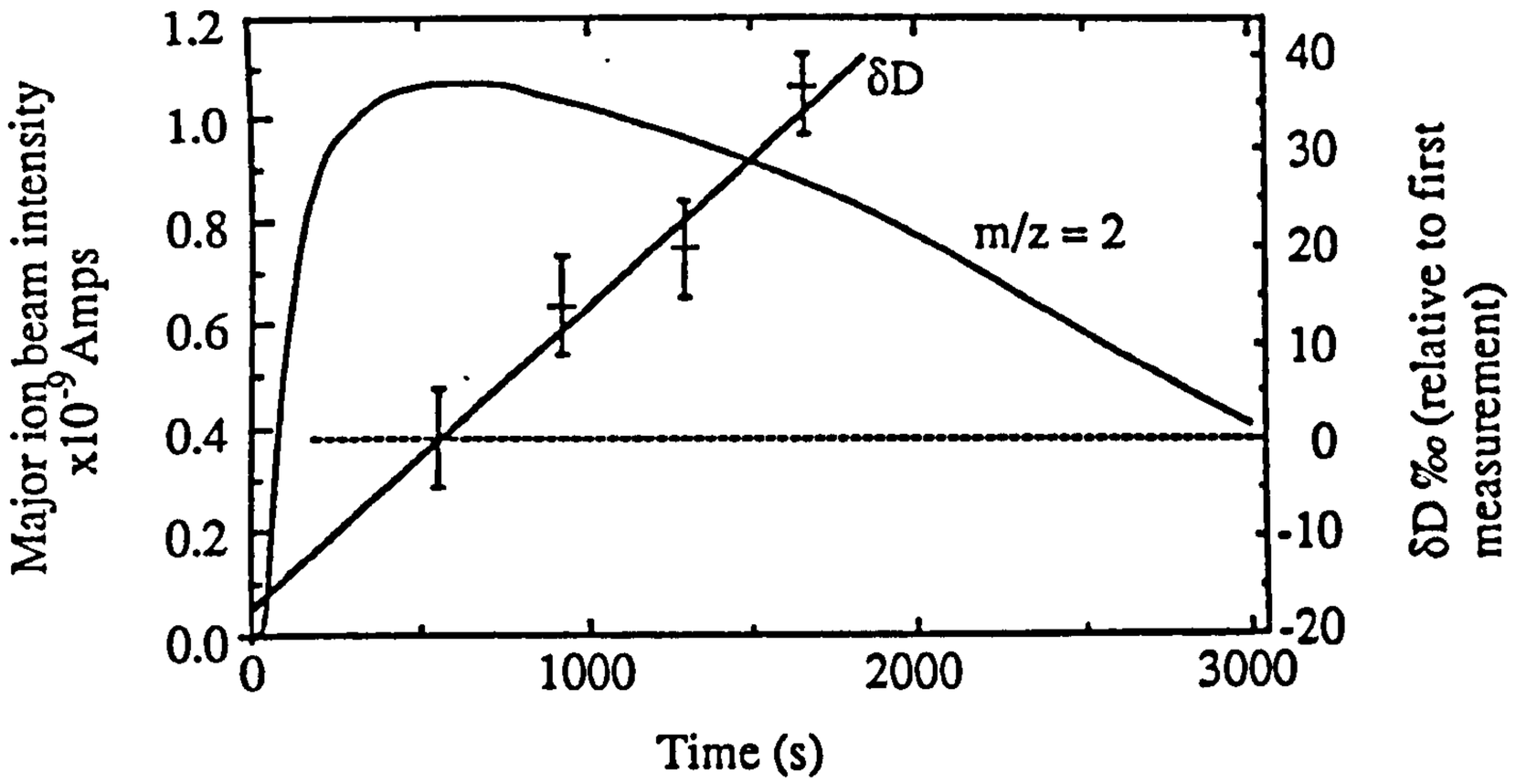

Fig.3.18. Variation of the major ion beam intensity and δD of hydrogen sample gas against time. The liquid nitrogen used to transfer sample water to the U trap was removed at time = 0s. To compensate for the isotopic fractionation vs time a strict timing protocol was used, see text, and the average of three results used for the δD.

Analysis No.	Reference gas D/H ratio $x10^{-4}$	Sample gas D/H ratio $x10^{-4}$	$\delta D_{(Ref)}$ ‰	$\delta D_{(SMOW)}$ ‰
1	1.148	3.315	+1888	-2
2	1.146	3.337	+1912	+6
3	1.163	3.339	+1871	-8
4	1.143	3.324	+1908	+4

Table 3.4. Analyses of consecutive 3.3μmol quantities of V-SMOW. The $\delta D_{(SMOW)}$ was calculated using the equation in section 2.4.4, assuming an average value for SMOW against the reference gas, $\delta D_{(Ref)} = +1895‰$.

The amount of hydrogen in the sample, $[H]_s$ is given by

$$[H]_s = [H]_m - [H]_b \qquad (3.14)$$

The total blank was determined by analysing the δD and amount of hydrogen yielded by an empty quartz bucket as an unknown sample. The total blank was found to be equivalent to the analysis of 0.055±0.017μmol of hydrogen having δD = -200‰ ± 50‰.

Memory effect

The memory effect for the dynamic conversion inlet was found to be considerably larger than for the other two types of inlet. Fig. 3.19 shows the results obtained when analysing 3.3μmol quantities of SLAP after analysing V-SMOW (c.f. Figs. 3.7 and 3.15). The first result obtained for SLAP was -147‰ ± 5‰ and the final result after 5 aliquots of SLAP (16.5μmol of water and over 9 hours analysing time) was only -300‰ ± 5‰ and still had not reached a level value. The final result for SLAP would be around -310‰, not the correct δD value of -428‰. Wong *et al.* (1984) noted similar effects for the Aqua SIRA in which water was reduced just before admission to the mass spectrometer source, *i.e.* a large memory effect and after many analyses the final result being displaced from the correct value which was termed an isotope dilution effect. Their solution to these problems was to analyse many aliquots of the sample water (approximately 7) until consecutive analyses gave the same δD value (thus eliminating the memory effect) and then multiply this δD value by a correction factor to gain the correct result. The correction factor was calibrated by analysing SLAP and fixing the result to be -428‰ as suggested by Gonfianti (1970). For the flow-thru inlet the correction factor, R, was

$$R = \frac{-428}{-310} = 1.38 \pm 0.02 \qquad 3.15)$$

When the first result for SLAP in fig. 3.19 is multiplied by 1.38 a value of -200‰ ± 7‰ is obtained, equivalent to contamination of the SLAP water by 3.8±0.1μmol of hydrogen from the previous sample.

When analysing 3.3μmol amounts of GISP after conditioning the conversion furnace by analysing several aliquots of V-SMOW the initial result was δD = -65±5‰, instead of -190‰. Multiplying the result by the correction factor R (R = 1.38) and then applying the memory correction (given in equation 3.12, section 3.3.6) assuming the

memory effect is equivalent to contamination by 3.8±0.1μmol of hydrogen gives a corrected value of δD GISP = -193‰ ± 10‰, the correct value within experimental error.

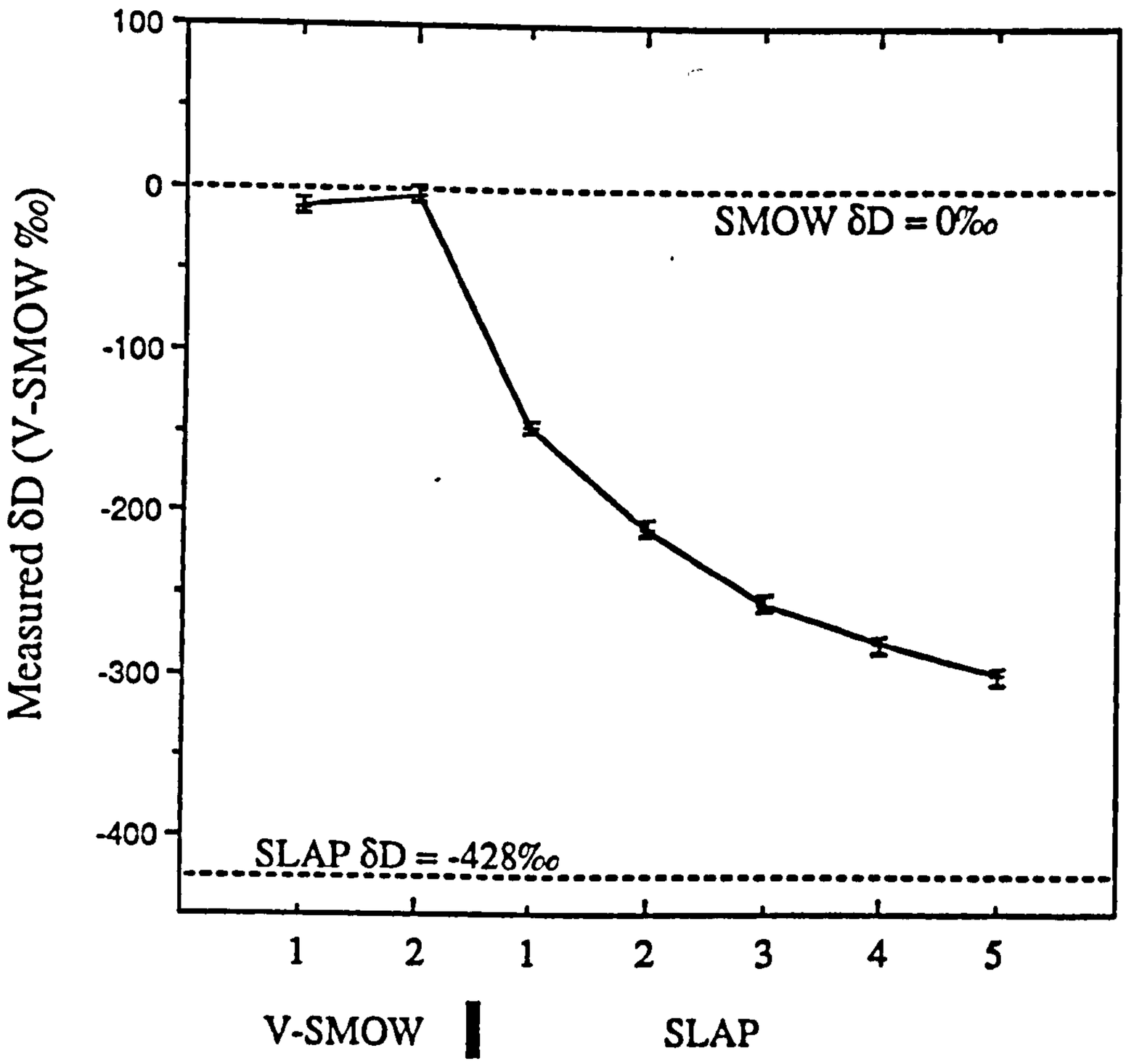

Fig.3.19. Graph showing the memory effect for the flow-thru inlet when analysing consecutive quantities of SLAP (3.3μmol) after V-SMOW. The final value does not approach the correct value for SLAP, δD = -428‰, but to δD = -300‰. The size of the memory, equivalent to contamination by 3.8±0.1μmol of the previous sample is much larger than for both the conventional or pusher inlets.

Experimental calibration curve

Results from experiments performed on the conventional inlet (section 3.3.6) indicated that the absolute amount of contamination from previous samples was independent of sample size. However, for samples of less than 1μmol of hydrogen the absolute of the memory effect was reduced, although its relative contribution increased. Thus to calculate the memory effect correction for different amounts of sample hydrogen an experimental calibration curve was adopted.

The calibration curve was intended for use with the meteorite project described in chapter 4. These samples, approx. 1mg from the Semarkona meteorite, were expected to give small amounts of water (*ca.* 0.1μmol), known from previous studies to contain large deuterium enrichments (at least +5470‰, McNaughton *et al.*, 1982b). The aim of the project was to investigate variations in δD and water concentration in various characterised fragments separated from the bulk meteorite. The calibration curve was obtained by the analysis, described below, of approx. 1mg quantities of powdered whole-rock Semarkona meteorite and the results compared with literature values (McNaughton *et al.*, 1982b; Yang and Epstein, 1983).

Approximately 1 mg, from 200mg powdered sample of whole-rock Semarkona, was weighed and loaded into the preparation line as described in section 3.3.2. The sample was kept under vacuum in the preparation line whilst the inlet and furnace were 'conditioned' by analysing 3.3μmol quantities of V-SMOW, by the procedure described in section 3.4.2, until consecutive analyses gave the same result within experimental error. Hence the δD of the memory effect was 0‰. Once the inlet was conditioned, the sample was then heated in two temperature steps, each step lasting 80 minutes. The first heating step was from room temperature to 200°C, this was an attempt to remove loosely bound water, thought to be mainly terrestrial contamination. The second heating step was from 200°C to 1100°C. The water collected after each temperature step was collected and analysed as described in section 3.4.2.

The results for the Semarkona samples and comparison with the literature values are shown in table 3.5. The calibration curve obtained is shown in fig. 3.20. For comparison, fig. 3.20 also shows the calibration line obtained for analysis of 3.3μmol quantities of V-SMOW, GISP and SLAP.

Due to the sample heterogeneity δD results obtained using the flow-thru inlet and calibration curve only approximate the V-SMOW - SLAP scale. However results obtained can be used to make comparisons of the relative deuterium enrichments between different samples analysed using this technique. It was considered that this would be adequate for the project described in chapter 4.

Analysis	δD up to 200°C (‰)	δD above 200°C (‰)	δD Total (‰)
0.8994mg	+181±106	+571±87	+376±137
0.7003mg	+262±408	+357±50	+337±160
0.8103mg	+259±128	+499±97	+407±110
Yang & Epstein (1983)			+1826
McNaughton et al (1981)		+2904	

Table 3.5. Comparison of results obtained by the flow-thru inlet when analysing whole-rock Semarkona against those obtained by others. In this work the analysis was carried out in two temperature steps (room temp.- 200°C and 200°C - 1100°C). McNaughton et al. (1981) did not analyse water released below 200°C.

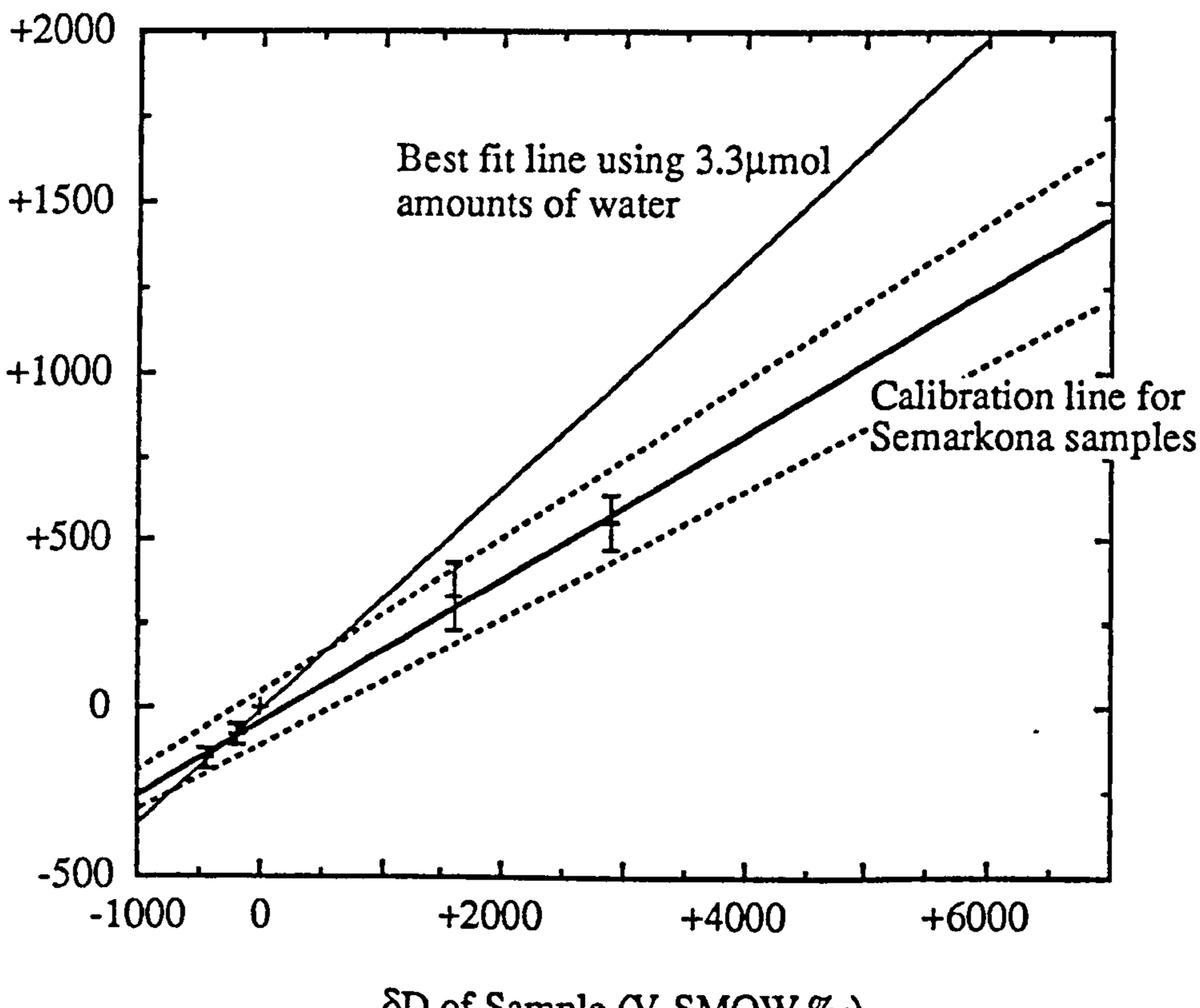

Fig.3.20. Calibration curve, obtained from the results shown in table 3.5, used to correct for the memory effect when analysing samples containing less than 1µmol hydrogen.

3.5.4 Further investigation of the memory effect

Theory

A more accurate estimate of the size of the memory effect and correction factor R can be obtained by fitting a best fit curve to the results of fig. 3.19 using a least squares regression approach. In Appendix C the theoretical equation of the curve in fig. 3.19 is derived as

$$y = A(1 - B^{x}) \quad ‰ \qquad 3.16)$$

where y is the measured δD of the sample,
x is the number of consecutive analyses of the sample,
A is the final δD, after many analyses
and B the decay rate.
The term B is an indication to the size of the memory effect,

$$B = \frac{[H]_{me}}{[H]_s + [H]_{me}} \qquad 3.17)$$

where $[H]_s$ is the amount hydrogen in the sample and
$[H]_{me}$ is the amount of hydrogen that remains in the inlet.

If there is no memory effect then B = 0 and for a very large memory effect, compared to sample size, then B approaches 1.

The correction factor R (in equation 3.15) can then be calculated from the measured final δD of the sample, A and the actual δD of the sample, δD_s by

$$R = \frac{\delta Ds}{A} \qquad 3.18)$$

In the following section, consecutive measurements of SLAP where made using different experimental procedures to attempt to reduce the memory effect. The size of the memory effect was calculated by fitting a best fit curve of equation 3.16. The terms A and B were found using an algorithm developed by Marquardt (1963) on a commercial statistical package (Statgrahics, STSC Inc.) run on a personal computer (IBM XT, IBM United Kingdom). Using the computer algorithm, the best fit curve to fig. 3.19 was found to have parameters A = -301±10 and B = 0.556 ± 0.058 (all errors quoted are 2σ). Hence the correction factor R = 1.42±0.05 and the size of the memory effect was equivalent to contamination of the sample by 4.0±0.9μmol of hydrogen. Table 3.6

Date	Measured δD SLAP ‰	Value of B eq^{n} 3.16	Size of memory effect µmol water
5-05-87	-150	0.52±0.03	3.6±0.4
6-05-87	-153	0.51±0.03	3.4±0.4
7-05-87	-160	0.48±0.03	3.1±0.4
25-05-87	-133	0.57±0.03	4.4±0.5
26-06-87	-143	0.54±0.03	3.9±0.5
4-07-87	-133	0.57±0.03	4.4±0.5
30-07-87	-145	0.53±0.02	3.8±0.4
13-10-87	-110	0.65±0.03	6.0±0.8
7-11-87	-141	0.51±0.03	3.4±0.4
Average	-141±15	0.54±0.05	4.0±0.9

Table 3.6. Results obtained when analysing 3.3µmol quantities of SLAP after the reduction furnace had been conditioned by analysing V-SMOW. The size of the memory effect was varied greatly, having an average value of 4.0±0.9µmol

shows the results, obtained over a period of several months, of the analysis 3.3µmol amounts of SLAP, after the furnace had analysed V-SMOW. The overall average amount of hydrogen causing the memory was 4.0±0.9µmol.

Experimental

Clearly to improve precision, the memory effect needed to be reduced. This was especially important for the samples containing less hydrogen than that analysed above (*i.e.* < 1µmol). The amount of hydrogen causing the memory effect, 4.0±0.9µmol, was significant larger than that exhibited by the conventional or pusher techniques (1.1±0.4 and 2.0±0.5µmol hydrogen respectively). The main difference between the flow-thru technique and the other two techniques was the design and operation of the zinc reduction furnace. In the flow-thru technique, sample water was reduced as it flowed over zinc at a temperature of 350°C. In the conventional and pusher techniques the sample water was reduced to hydrogen by zinc, at 450°C, in a sealed volume, similar, in operation to that of Coleman *et al.* (1982).

There were two differences in the design and operation of the zinc furnace for the flow-thru technique; both were a consequence of the problem of zinc migrating, in the vapour phase, out of the furnace and into the change-over valve. The modifications to prevent this were:

i) the addition of quartz wool plugs and

ii) an operation temperature of only 350°C, instead of 450°C, the vapour pressure of zinc at 350°C is only 0.14 torr compared to 0.4 torr at 450°C (Kubaschewski *et al.*, 1967).

The increased memory effect in the flow-thru technique could be caused by the quartz wool plugs as these may reduce the flow of water and/or hydrogen through the zinc furnace. Experiments by Tanweer *et al.*, (1988) indicated that if the reduction was carried out at a temperature of less than 450°C then the isotopic results obtained were poor, this was attributed to a memory effect caused by the presence of water adsorbed in zinc shot. To determine if either of these two differences were the cause of the increased memory effect the design of the dynamic conversion furnace was modified by making the horizontal furnace into a vertical 'U' tube furnace, as shown in fig. 3.21. By using a 'U' shape reduction furnace the quartz wool plugs were not required and the temperature of zinc could be increased to 450°C. The results obtained for the modified furnace were the same, within error, as the original design. Since there was no detectable difference in the memory effect the original design of furnace was used in further experiments.

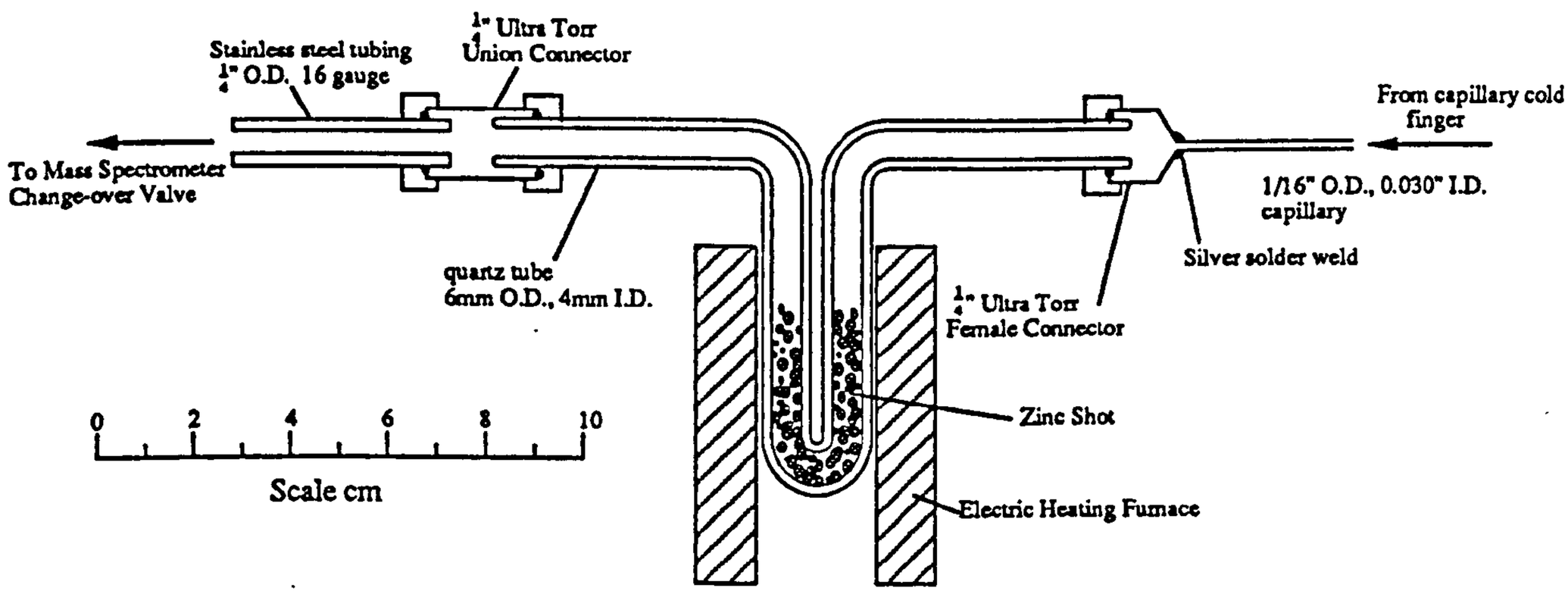

Fig.3.21. Diagram of the modified reduction furnace. By using a U configuration the quartz wool plugs were not required and the zinc furnace could be heated to 450°C.

Type of zinc

Coleman *et al.* (1982) found that the accuracy of the results obtained was affected by the type of zinc. The reduction of water to hydrogen was only found to go to completion when BDH (AnalaR) zinc shot was used. Kendall and Coplen, (1985) found that even this type of zinc did not always give good isotopic results, the quality of the isotopic results varying with different batches of BDH (AnalaR) zinc shot. They found that the zinc which gave good results contained a lead impurity (up to 36ppm). Kendall *et al.* (1985) concluded that the lead impurity may prevent the formation of a protective oxide layer. Alternatively, Sudzuki (1987) suggested that the immiscible lead impurity may force the zinc to be corroded electrochemically, to give the complete reduction of water. Several other types of zinc were used to determine whether this was the cause of the larger memory effect.

i) Zinc shot similar to that used by Coleman *et al.* (1982), *i.e.* BDH AnalaR grade. This was the type of zinc usually used. The zinc shot was prepared for use as described in section 3.2.1.

ii) Zinc granules (BDH Chemicals Ltd., Poole). The zinc granules had a thin oxide layer, but much less than the zinc shot. They were not cleaned by nitric acid, but degassed under vacuum at 350°C for at least an hour before use.

iii) Zinc powder, 100 mesh, (Johnson Matthey, Materials Technology U.K.). This was prepared for use in the same way as the zinc granules, above.

iv) Zinc wire, 0.27mm dia, 99.99% purity (Goodfellow Metals Ltd.). This was prepared in the same way as the zinc granules, above.

v) Zinc turnings produced specifically for D/H isotope analysis containing some unidentified impurity (type unknown due to intention to patent the zinc). The turnings were provided by Prof. J.M.Hayes (Indiana University) sent under vacuum and were prepared for use in the same way as the zinc granules.

The zinc wire required heating to 400°C for several minutes before any reduction of water to hydrogen was possible. After this procedure had been carried out the zinc wire was as efficient as zinc shot at water reduction. The induction period was probably necessary to remove a protective layer of zinc oxide on the wire. None of the forms of zinc showed any improvement over the AnalaR zinc shot normally used in terms of memory effect. Whether the specially prepared zinc turnings or other forms of zinc gave improved isotopic results could not be determined due to the lack of precision of the flow-thru inlet.

Type of reducing agent

Other reducing agents were also used to determine whether the zinc metal was the cause of the memory effect. The following reducing agents were explored:-

i) Uranium, first used for D/H isotope analysis by Bigelsein et al., (1952). As described in section 3.1, this is the usual alternative to zinc shot. The zinc shot was replaced by depleted uranium turnings (British Nuclear Fuels) which had been cleaned in conc. nitric acid (sp.gr.1.42) to remove the uranium oxide layer.

ii) Magnesium, as used by Kamen (1948) to reduce tritium oxide to tritium. Magnesium reacts readily with steam, however to prevent magnesium hydroxide forming the reaction required a temperature of at least 400°C. Magnesium ribbon (Harrington Brothers Ltd.) was used, most of the oxide layer being removed by reaction with conc. hydrochloric acid.

iii) Zinc shot at 350°C. Between analyses the furnace was purged with a flow Argon, in an attempt to remove any water or hydrogen remaining in the furnace between analyses, similar to the use of helium by Robert *et al.* (1987a).

iv) No reducing agent, the m/z = 18 and m/z = 19 peaks were measured using a lower mass spectrometer source accelerating voltage of *ca.*800V. The data acquisition program (section 2.2.4) needed modification since the m/z = 18 and m/z = 19 peaks could not be focussed onto the major and minor collector simultaneously.

The results obtained using the various reducing agents are shown in table 3.7. The reduction by uranium was carried at 600°C and 800°C. The results obtained for uranium, at both temperatures, were similar for those obtained for zinc.

The D/H results that were obtained when magnesium was used were very poor. No results were obtained below 550°C, probably due to a protective oxide layer, despite the treatment with HCl before use. Above 550°C the water was reduced to hydrogen, however the magnesium reacted with the quartz glass and the furnace needed replacement after each analysis.

The results from table 3.7 show that when argon was used to purge the furnace between analyses there was no significant difference in size of the memory effect. However, the final δD result obtained was different, -268±8‰ instead of -301±10‰ for the zinc furnace. This was probably due to the presence of some water in the argon. However the size of the memory effect was the same as for the normal technique.

The results obtained, of the decay rate B, for water when not using any reducing agent were the same as for uranium and zinc, indicating that the furnace was not the main cause of the memory effect. Since no hydrogen has been formed then the memory effect was not due to hydrogen contamination from the previous sample, but is caused by water remaining in the system.

Reduction Material	Equation 3.12) A	B	Size of memory effect µmol water
Zinc 450°C	-301±20	0.53±0.06	3.7±1.0
Uranium 800°C	-291±12	0.56±0.03	4.2±0.5
Uranium 620°C	-299±20	0.44±0.06	2.6±0.7
Zinc, Argon flush	-268±16	0.51±0.06	3.4±0.9
Water	-61±10	0.50±0.10	3.3±1.7

Table 3.7. Results showing the size of the memory effect when using different reducing agents in the reduction furnace. There is no significant difference between the different types of reducing agent on the size of the memory effect (including no reducing agent), indicating that the reducing agent was not causing the memory effect.

3.6. Summary

3.6.1 Implications of the memory effect on D/H isotope analysis

From the results of experiments with the various inlet designs the memory effect was caused by water adhering to the inner surfaces of the inlet (sections 3.3.6 and 3.5.4). Teflon is hydrophobic and so it appears unlikely that water will be retained between analyses by sticking to the valve barrels. Teflon may absorb hydrogen and it was suggested as a possible cause of the memory effect. However no detectable memory effect was observed when water was placed directly into the zinc furnace, indicating that the memory effect was caused by retention of water between analyses and not hydrogen.

Todd (1955) showed that water evolved from glass during bake-out originated from two sources. The main source was from surface water bound to the glass. This was only completely de-gassed at a temperature of 400°C. The amount of surface water was found to depend on the condition of the glass varying from 0.006µmol cm^{-2} for fresh glass to 0.038µmol cm^{-2} for two year old glass stored in a humid atmosphere. Heating the glass to 100°C only removed approximately 25% of the surface water. The second source was from water diffusing out of the glass at temperatures above 400°C.

The surface area of the conventional inlet system was approximately 50cm^2. Since the inner surface of the inlet is under humid conditions (100°C with a lot of sample water vapour present) then approximately 1.4µmol of surface water was adsorbed on the inlet system (0.038x50x0.75). Experiments by Graff and Rittenberg (1952) showed that this surface water is strongly bound (low vapour pressure and does not exchange with hydrogen gas) but easily exchanges with water to produce memory effects.

This suggests that a solution to the memory effect could be the use of another material for parts of the inlet system that come into contact with sample water, or heating the inlet to about 400°C. Heating the inlet to 400°C was not practical since the glass valves of the inlet have a maximum operating temperature of 150°C, at higher temperatures the teflon valve barrels and seals soften. Clearly metal is no better than glass since the memory effect was larger when water was allowed to come into contact with the extra metal of the flow-thru inlet (section 3.5). Another possibility would be to constructing the inlet with teflon tubing instead of glass, but adsorption of hydrogen may cause its own problems.

Current solutions involve the following options :

i) Using large samples, so that the size of memory effect compared with sample size is negligible.

ii) Reducing the amount of inlet surfaces that come into contact with the sample water to a minimum

iii) Applying a correction to compensate for the memory effect.

Using larger samples was not compatible with the aims of this thesis as set out in chapter 1. During the construction of the conventional inlet (section 3.2) the surface area of the inlet was reduced as much as possible to keep the volume small and allow smaller samples to be analysed. To obtain a memory effect of 0.1μmol of water would only be possible if the amount of glass at 100°C was ~3cm^2. Since the inner surface area of each glass valve used in the system was about 5cm^2 this reduction in surface area is not possible. The final option of applying the memory correction was used for the work in chapter 4, however this led to δD values of relatively poor precision (±1000‰) when analysing samples containing less than 3μmol of hydrogen.

3.6.2 Comparison of inlet systems

The aims of the work described in this chapter was to design and construct an inlet system capable of measuring the D/H ratios of extra-terrestrial samples containing less than 0.1μmol of water. The conventional inlet (section 3.3) was used to compare the performance of the pusher and flow-thru inlets, as well as determine the cause of the memory effect. It was capable of analysing samples containing 20μmol of hydrogen to a precision of ±2‰, minimum sample size was 10μmol of hydrogen. Blanks were negligible compared to sample size. The inlet had a small memory effect of 1.5±0.4μmol of water which necessitated a memory effect correction, though this was usually less than 10‰ and for most samples reduced the accuracy in δD by less than ±5‰. The conventional system has been used in the isotopic analysis of water in terrestrial rocks but due to the sample size requirement of at least 10μmol of hydrogen has not been used for the analysis of extra-terrestrial samples.

The pusher inlet had a greatly increased sensitivity, capable of analysing 0.3μmol water, but with a corresponding loss of precision in δD to ±15‰. The memory effect of the pusher inlet was 2.0±0.5μmol of water, slightly larger than for the conventional inlet. There were some modifications that could be made to improve the accuracy of the isotopic results obtained. However, the minimum sample size that could be analysed was 0.3μmol hydrogen which was considered too large for the samples envisaged.

The chosen design of the flow-thru inlet, was capable of analysing samples containing less than 0.1μmol of water. However due to the memory effect and blank problems the precision in δD was very poor (the actual amount depending on sample size and δD). An experimental calibration curve was used to obtain the δD of extra-terrestrial samples analysed, but due to the method of obtaining the calibration curve this was only useful for samples containing approximately 0.1μmol water and having large variations in δD. The flow-thru inlet was used in the analysis of extra-terrestrial samples, described in chapter 4, but due to the poor precision its use was limited.

Chapter 4
Aqueous Alteration in Semarkona

4.1 Introduction

4.1.1 Project aims

The Semarkona meteorite is classified as a type 3 unequilibrated ordinary chondrite, which type comprises of a group of *ca.* 50 meteorites (Graham *et al.*, 1985). The type 3 unequilibrated ordinary chondrites are often termed primitive due to the lack of extensive secondary processing, such as thermal metamorphism or aqueous alteration, that has affected the material after formation and incorporation into the parent body. Hence these meteorites are thought to represent the composition of material, in the formation region of the ordinary chondrites, that condensed from the early solar nebula. Investigations into the original nebula composition and processes that occurred there before accretion have focussed upon the primitive ordinary chondrites for the following reasons:

i) Chondrules, formed in the solar nebula have probably maintained a record of their formation process since little secondary processing has occurred since their accretion into the host meteorite.

ii) The matrix may be material that did not form the chondrules, hence representing the composition of the original solar nebula condensate. Alternatively the matrix may consist predominantly of chondrule fragments (broken by chondrule collisions), indicating a turbulent nebula.

Van Schmus and Wood (1967) recognised that meteorites assigned to a particular group, in their classification scheme, did not all experience exactly the same conditions and amount of secondary processing. In particular Dodd *et al.*, (1967) showed that the type 3 chondrites contained members exhibiting a range of properties consistent with wide variations in the conditions of thermal metamorphism and that Semarkona had experienced the least degree of thermal metamorphism. Several classification schemes have been used to divide the type 3 ordinary chondrites and so determine the ones that are most primitive (Wood 1967; Huss *et al.*, 1978; Afiattalab and Wasson, 1980; Sears *et al.*, 1980; Anders and Zadnik, 1985). One of the more common classification schemes used is that based on the thermoluminescence (TL) sensitivities (Sears *et al.*, 1980; described further in section 4.1.4). In this classification scheme the type 3 chondrites are divided into 10 sub-groups ranging from type 3.0 having lowest TL sensitivity (least metamorphosed) to 3.9 having highest TL sensitivity (almost type 4). The meteorites that have suffered least from thermal metamorphism (types 3.0 to 3.2) have unusual

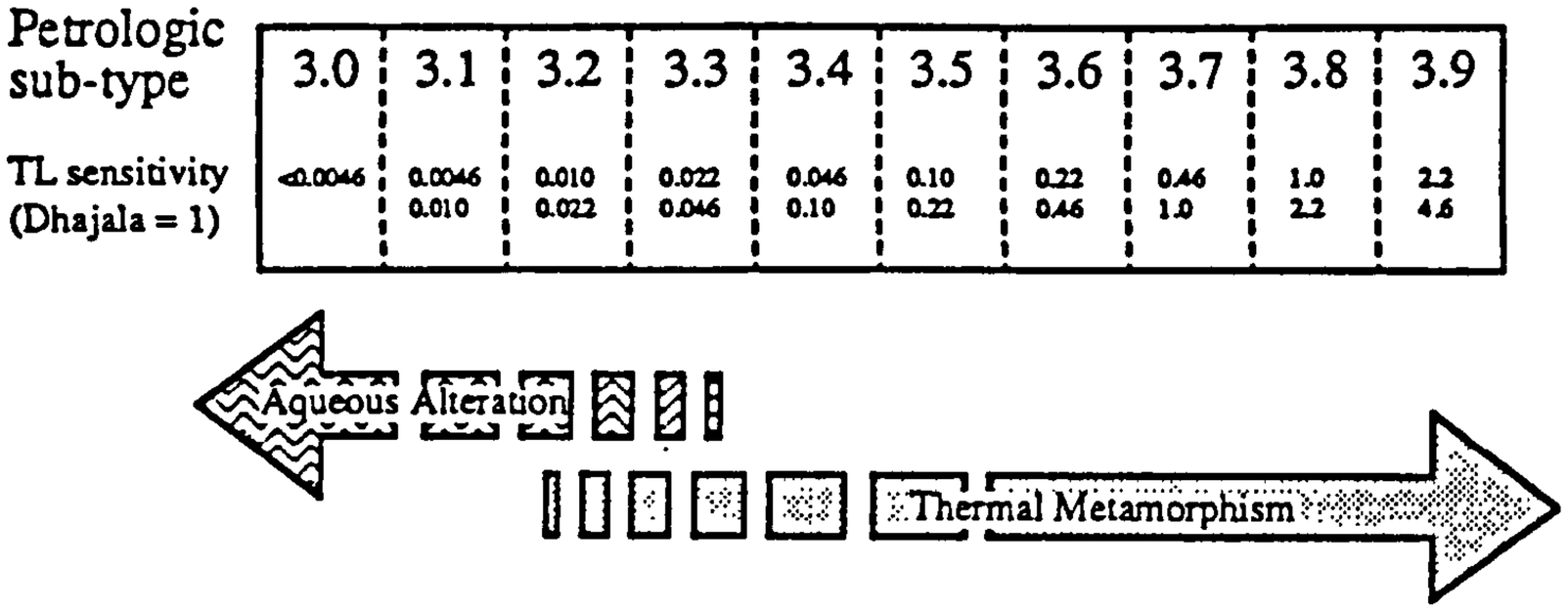

Fig. 4.1 A diagram showing the relationship between the petrologic sub-type, determined by TL, and the degree of secondary alteration experienced for type 3 ordinary chondrites. Evidence of aqueous alteration has been observed in type 3.0 and 3.1 ordinary chondrites, although the to what extent higher petrologic types have been affected by aqueous alteration and whether there is any overlap with thermal metamorphism has not been determined.

properties, such as a component with a high deuterium enrichment ($\delta D > +5740‰$; McNaughton *et al.*, 1982b), high carbon content and unusual isotopic composition (Grady *et al.*, 1982) and TL properties that do not follow trends exhibited by higher types (Sears *et al.*, 1982b). These unusual properties could be due to nebula processes which have not subsequently been destroyed by thermal metamorphism. However more detailed investigation of the TL properties of the type 3 ordinary chondrites and hydrothermal annealing experiments have shown that TL sensitivity can be reduced by aqueous alteration. Hence the low TL sensitivity and unusual properties of the low type 3 ordinary chondrites could be due to aqueous alteration rather than a lack of thermal metamorphism.

Hutchison *et al.*, (1987) found petrologic evidence for *in situ* aqueous alteration in Semarkona (LL3.0) and Bishunpur (LL3.1). Both of these meteorites were recovered shortly after their fall and so the aqueous alteration is unlikely to be the result of terrestrial weathering. Hence the wide variations between different meteorites of the type 3 ordinary chondrites could be determined by the degree of both aqueous alteration and thermal metamorphism. The type of secondary processing experienced by the type 3 ordinary chondrites and relation to petrologic sub-type are shown in fig. 4.1, (from Sears and Dodd, 1988).

D/H analyses of whole-rock samples of unequilibrated chondrites show a correlation with TL sensitivity (McNaughton *et al.*, 1982b), shown in fig.4.2. The least equilibrated chondrites (lowest petrologic sub-type) have the highest D/H ratios (except for Krymka). The link between TL sensitivity and D/H ratio tends to suggest that those meteorites which have been affected to some extent by aqueous alteration have an

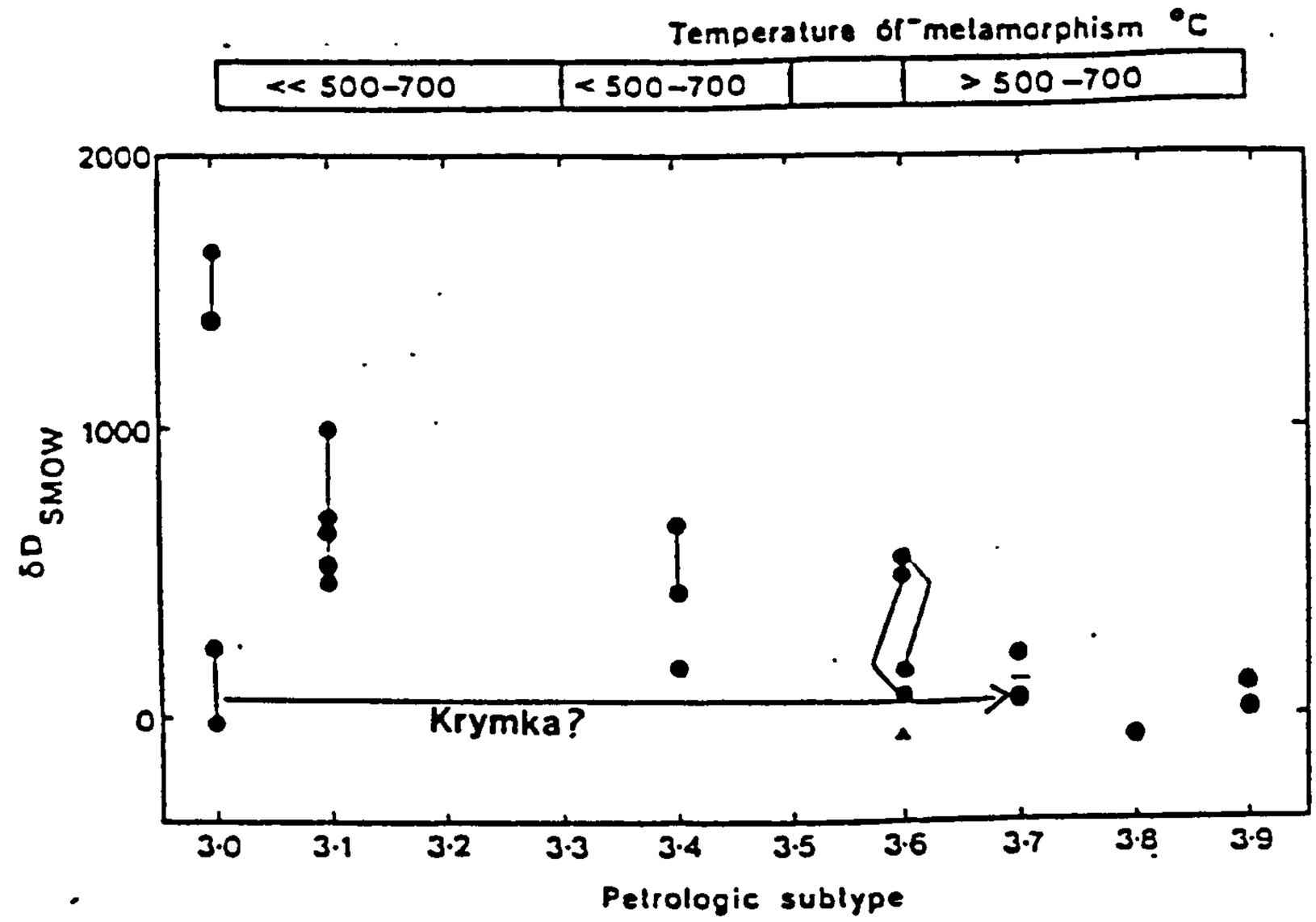

Fig. 4.2 Graph of whole-rock δD versus petrologic sub-type for the type 3 ordinary chondrites (from McNaughton *et al.*, 1982b). Points joined by tie lines are replicate analyses of a single meteorite. The estimated temperatures of thermal metamorphism from Sears *et al.*, (1982). Chondrites of lower petrologic sub-type tend to have higher δD values, although Krymka does not fit this trend.

enriched D/H ratio, analogous to the type C1 and C2 carbonaceous chondrites which show clear evidence of aqueous alteration (Kerridge and Bunch, 1979; Bunch and Chang, 1980; Tomeoka and Buseck, 1985; Zolensky and McSween, 1988) and contain deuterium-rich organic material (see section 1.5.1). Alternatively thermal metamorphism may have acted to destroy the deuterium-rich carrier. Krymka (LL3.0) does not fit this trend having a whole-rock δD of -38‰ compared to whole-rock Semarkona (LL3.0) with δD = +1650‰. However there is a suggestion that high D/H ratios have been measured in Krymka by Russian workers (see references in Pillinger, 1984), indicating that as with all unequilibrated ordinary chondrites this meteorite is very heterogeneous. Alternatively Krymka could have a reduced TL sensitivity due to terrestrial weathering. Later analyses indicate that it is type 3.1 (Sears 1987). Anders and Zadnik (1985) has suggested that it is a type 3.7 on the basis of the concentrations of its volatiles.

The aim of this study was to undertake a deeper investigation into the D/H, TL and petrographic properties of the most unequilibrated ordinary chondrite, Semarkona, and attempt to determine:

i) if the aqueous alteration observed by petrography was caused by terrestrial weathering or by water on the Semarkona parent body;

ii) the D/H ratio of the water that caused the aqueous alteration and reduced the TL sensitivity;
iii) the extent of any thermal metamorphism and,
iv) whether the other unusual properties of Semarkona are due to the effects of aqueous alteration or the lack of extensive secondary processing.

4.1.2 Models of secondary alteration in meteorites

Most meteorites are thought to originate from the asteroid belt, apart from the SNC (martian) and lunar meteorites (Wetherhill and Chapman, 1988). A schematic diagram of the sequence of events of the formation of ordinary chondrites and their eventual arrival to Earth is shown in fig. 4.3. Evidence of the existence of extinct short lived radionuclides in meteorites indicates that secondary processing must have occurred within about 200Myr after the accretion of the parent bodies (MacDougall *et al.*, 1984). This section describes the various mechanisms by which secondary processing could occur in the early solar system.

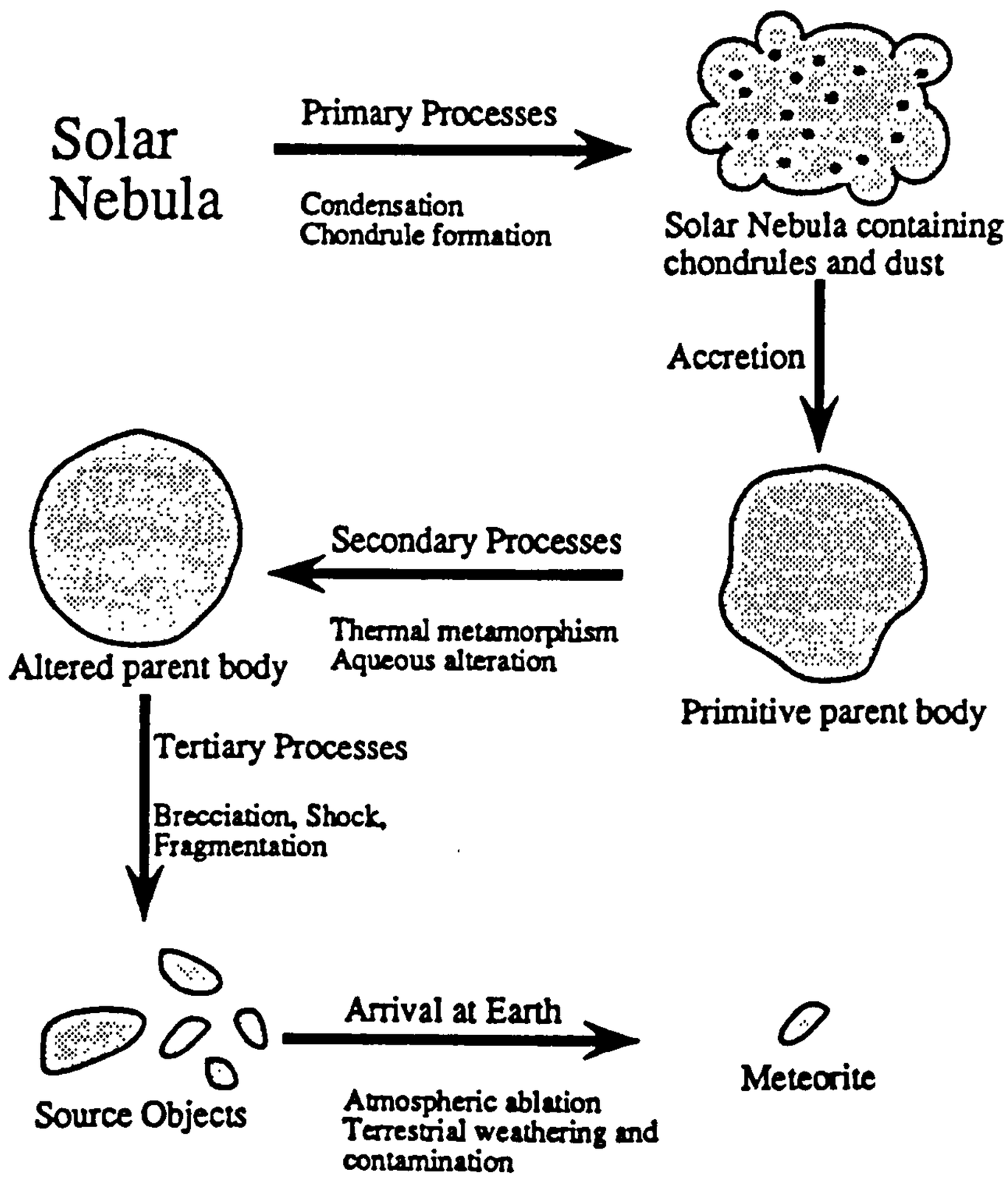

Fig. 4.3 A schematic diagram the sequence of events experienced by chondritic meteorites from their formation from the solar nebula, ca. 4.55 Gy, to their arrival at Earth.

4.1.2.1 Thermal metamorphism

Temperatures of thermal metamorphism estimated by Dodd, (1981) range from 400°C for type 3 ordinary chondrites to a maximum of 950°C for type 6 chondrites. Unlike most terrestrial metamorphic rocks there was no large scale movement of elements during metamorphism, as indicated by the fact that chondrules can still be distinguished in type 6 chondrites (Dodd, 1969). This results from the virtual lack of metamorphic fluids, mainly H_2O and CO_2, during metamorphism (McSween *et al.*, 1988). Even the carbonaceous chondrites that have experienced thermal metamorphism consist of anhydrous minerals indicating that water was driven off before metamorphic temperatures were experienced (Scott and Taylor, 1985).

The pressure under which thermal metamorphism occurred was low, about 1kbar or less, determined by mineralogy and lack of chondrule deformation caused by stress (Heyse, 1978; Dodd, 1965). Hence metamorphism occurred on small asteroid type bodies, which is confirmed by high cooling rates for the ordinary chondrites of between 0.1 and 10°K Myr^{-1} (Wood 1979).

The usual model for thermal metamorphism is the 'onion shell' model, an example shown in fig. 4.4a, where internal heating produces layers of different petrographic types of meteorite. Heat sources could be from the decay of short lived radionuclides, such as ^{26}Al (Lee *et al.*, 1976), or from electromagnetic induction heating during a T-Tauri phase of the sun (Sonett *et al.*, 1970). This model was preferred by Heyse, (1978) to explain the probable correlation between pressure of thermal metamorphism and petrographic type. The 'onion shell' model naturally explains the relative abundance of different petrographic types of chondrites. The higher petrographic types of each chemical group (apart from carbonaceous chondrites, are more abundant. This is reflected in fig. 4.4a by the amount of material in each layer corresponding to the abundance of each petrographic type (Miyamota *et al.*, 1981).

An alternative is to have external heating, from the sun during a superluminous Hayashi stage (Hayashi, 1966) which would result in the higher petrographic types being on the surface, shown in fig. 4.4b. However, calculations indicate that this would only heat the outer few metres (Sonett and Reynolds, 1979). There is the possibility that all meteorites irrespective of type come mainly from the outer layers of their respective parent body.

Larimer and Anders (1967) suggested that accretion onto a hot but cooling body would also produce a similar type of 'onion shell' body, heat being acquired from the energy of accretion. This model explains why volatile trace elements are less abundant in the more metamorphosed meteorites. Dreibus and Wanke, (1981) suggested that in an 'onion shell' parent body volatile trace elements (and CO_2 and H_2O) would be driven from the interior and deposited in the cooler outer layers.

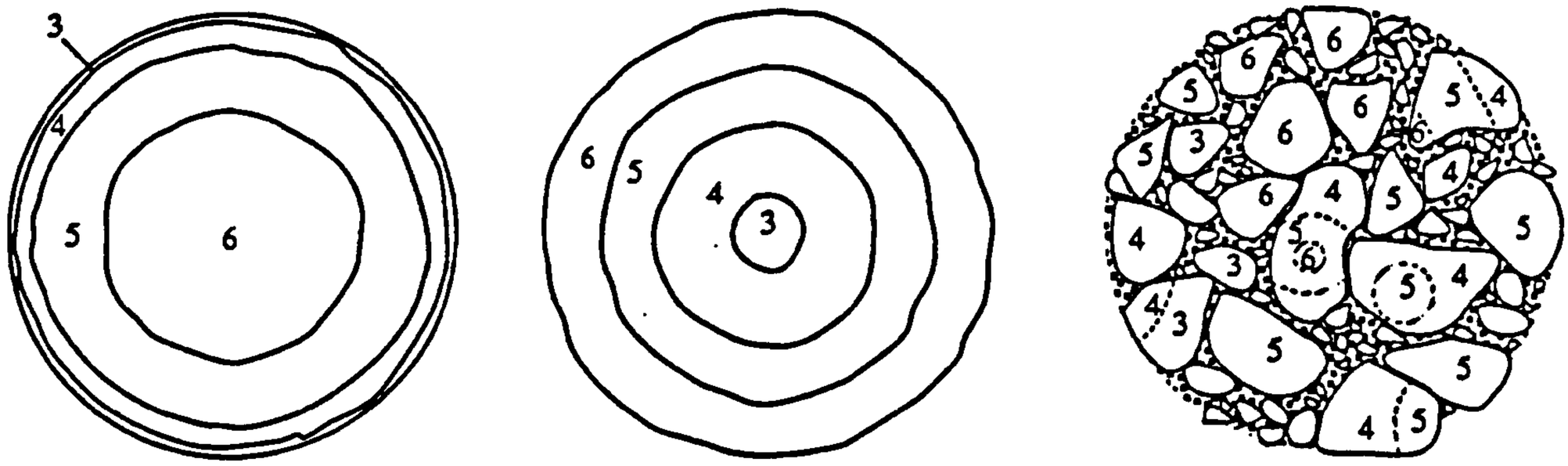

(a) (b) (c)

Fig 4.4 Models of thermal metamorphism for chondrite parent bodies: (a) an onion shell model, where internal heating results in concentric layers of petrologic types; (b) an external heating model resulting in layers with higher petrologic types nearer the surface; (c) rubble pile model, accounting for the lack of correlation between cooling rate and petrologic type.

The cooling rates for the ordinary chondrites have been used in an attempt to place constraints on the various models of thermal metamorphism, however different methods have produced conflicting results. Cooling rates determined by the retention of fission tracks by various minerals indicate that the more equilibrated chondrites have a lower cooling rate, indicating greater burial depth in the parent body (Pellas and Storzer, 1979). However, cooling rates determined by diffusion of nickel, in kamacite and taenite grains, show that the ordinary chondrites cooled from high temperature at rates between 0.1 and 10K Myr^{-1}. There is no correlation between petrologic type and cooling rate, except that unequilibrated chondrites tend to have a lower cooling rate than the equilibrated ordinary chondrites (petrographic types 4-6). Scott and Rajan (1981) suggested that meteorite parent bodies could consist of small planetesimals (approximately 100m sized bodies), the 'rubble pile' model shown in fig. 4.4c. Internal heating of small planetesimals results in their layering, similar to the 'onion shell' model. These then accreted into a larger 'rubble pile' parent body where burial depth and hence cooling rate is independent of petrographic type. Internal heating sources are the same as for the 'onion shell' model. They could also be heated externally, by a Hayashi phase of the sun, since the planetesimals are much smaller a greater amount could be heated externally. Grimm (1985) suggested an alternative where thermal metamorphism occurs in a similar fashion to the 'onion shell' model. Collision between two such bodies causes fragmentation and then gravitational attraction forms a 'rubble pile' from the fragments.

4.1.2.2 Aqueous alteration

Aqueous alteration on the ordinary chondrite parent bodies probably occurred in a similar fashion to that of the type 1-3 carbonaceous chondrites in which water was originally accreted into the meteorite parent body as ice (Bunch and Chang, 1980; Grimm and McSween 1989). Several possible models for the method in which aqueous processes on carbonaceous chondrites occurred have been proposed, listed below:

i) Direct action between ice and adjacent silicates by a layer of 'unfrozen water' (Gooding 1984; Rietmeijer 1985).

ii) Melting of ice by impact events (Lange *et al.*, 1985). The water would have been vaporised and distributed through the regolith by the impact events and then recondensed.

iii) Ice melted by internal heat generated by the parent body from the decay of short lived radio-nuclides (DuFresne and Anders, 1962), or by electromagnetic induction heating during a T-Tauri stage of the sun (Sonett and Reynolds, 1979). A zone of liquid water would form between the hot centre of the parent body and a surface layer of ice, the ice layer preventing rapid loss of water, hence enabling adequate time for aqueous alteration to occur (Bunch and Chang, 1980).

Oxygen isotope studies (Clayton and Mayeda, 1984) indicate that in CM carbonaceous chondrites the temperature of aqueous alteration was from 0 to 20°C and required a water to rock ratio of at least 1:1. The CI chondrite Orgueil required even greater amounts of water and a higher temperatures of 100-150°C. The high temperatures and large volume of water required imply that methods (i) and (ii) were probably not the cause of aqueous alteration in Orgueil and unlikely that they were the cause of aqueous alteration in the CM chondrites (Zolensky and McSween, 1988). Hutchison *et al.*, (1987) suggested aqueous alteration occurred in Semarkona as an open system. *i.e.* there was a flow of fluid, both CO_2 and H_2O, through the meteorite, driven by thermal metamorphism. These results tend to indicate that secondary alteration on an 'onion shell' type parent body, where internal heating drives CO_2 and H_2O from the centre to the outer layers in which aqueous alteration took place.

4.1.3 Secondary processing as revealed by thermoluminescence (TL)

The thermoluminescence technique measures the amount of light emitted by a sample as it is heated. This can be used to give information on the mineralogy and/or radiation history of the sample. During irradiation of a sample, by energetic particles, electrons are often excited into higher energy states. Usually these electrons drop back down to the ground state, emitting a photon in the process, however some electrons become trapped in a higher energy state, these 'traps' are often caused by defects in the crystal structure of minerals (Medlin, 1968). When a sample is gradually heated, the excited electrons will remain in their 'traps' until given enough thermal energy to escape,

whereupon they return to the ground state, emitting a photon. The amount of light emitted by TL, the TL sensitivity, depends upon:

i) the total number of electron 'traps', dependent on the sample composition and,

ii) the radiation history of the sample, *i.e.* the proportion of traps filled with electrons.

The amount of thermal energy an electron requires to escape depends on the nature of the 'trap'. Thus each mineral exhibits a characteristic 'glow' curve as the temperature is raised, which can be quantitatively described in terms the of temperature at which the maximum amount of TL is emitted and the width of the peak. An example of a 'glow' curve and parameters measured is shown in fig. 4.5. The type of apparatus used to measure the TL of a sample is described by Mills *et al.*, (1977).

There are two types of TL that can be analysed:

i) The natural TL sensitivity measures the TL properties gained by the sample due to its radiation history, before collection.

ii) The induced TL sensitivity measures the properties gained by a fixed dose of radiation. The natural TL is first removed by heating (usually by measuring the natural TL), then the sample is placed next to a radiation source for a known length of time, following which the induced TL is measured.

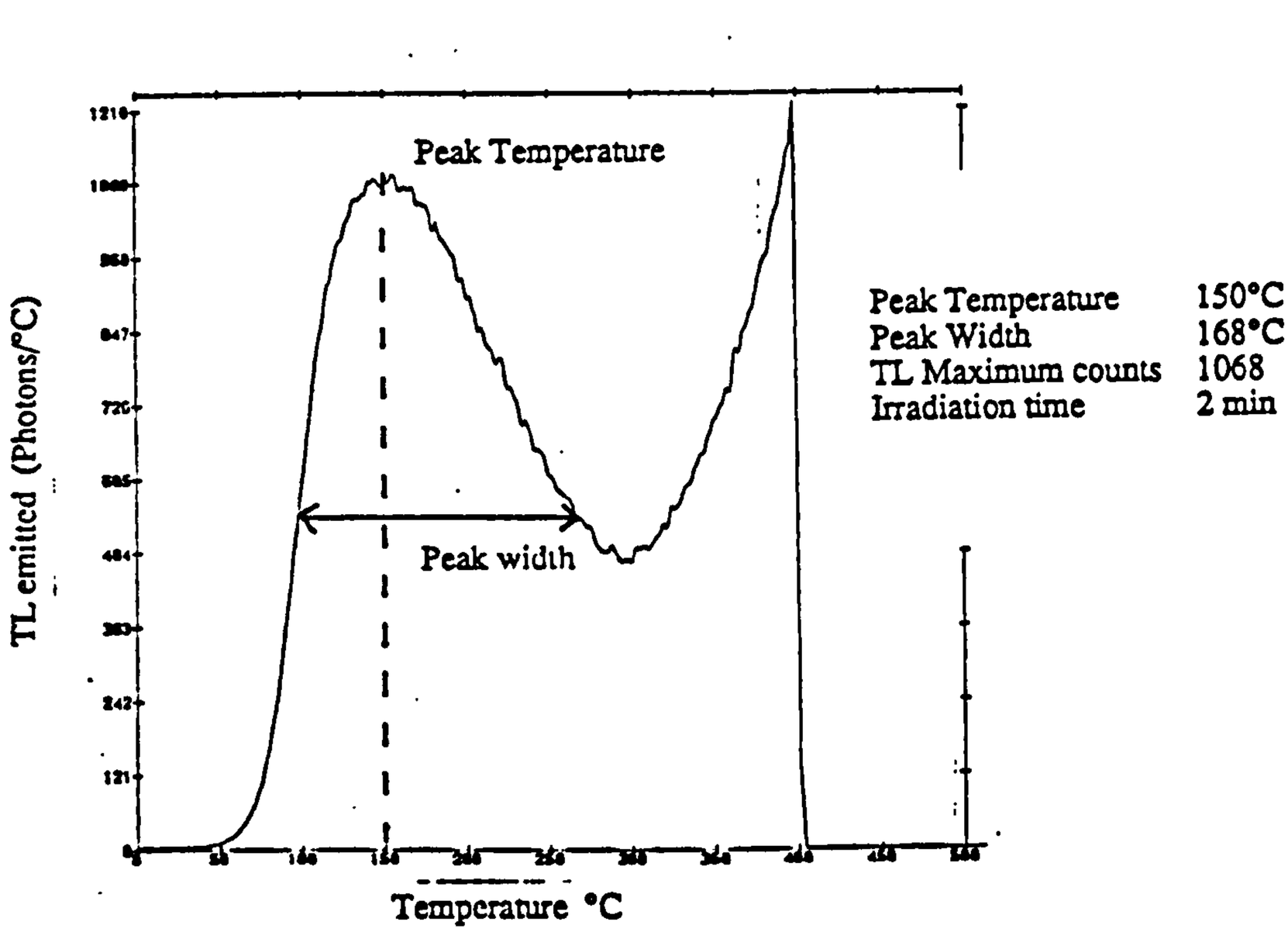

Fig. 4.5 'Glow' curve, plot of TL emitted against temperature, for an irradiated sample of Dhajala meteorite. The peak is quantified in terms of its maximum TL sensitivity, peak width (width of peak at half its maximum intensity) and temperature of maximum intensity. The increase in TL sensitivity above 350°C is due to black body radiation.

The radiation history of a sample is determined by measuring the natural TL sensitivity and comparing this with the induced TL sensitivity, hence determining the proportion of filled electron 'traps'. Mineralogical information is gained by analysis of the 'glow' curve parameters obtained by measuring the induced TL sensitivity.

Spatial information of the TL phosphor can be obtained using cathodo-luminescence (CL), in which the sample electrons are excited by an electron beam and the light emitted is photographed. Mineralogical information can then be obtained by comparing the CL pictures with scanning electron microscope (SEM) pictures; chemical information by spot analyses made using an electron microprobe (Dehart *et al.*,1987).

Sears *et al.*, (1980) noted that the greater the degree of metamorphism for the type 4 to 6 ordinary chondrites then the higher the induced TL sensitivity. The type 3 ordinary chondrites have a very large range in TL sensitivity, indicating that TL is very sensitive to low temperature thermal metamorphism. This enabled the type 3 ordinary chondrites to be split into 10 sub-groups ranging from type 3.0, lowest TL sensitivity, to 3.9, highest TL sensitivity. The effect of thermal metamorphism has been to increase the TL sensitivity, peak temperature and peak width (Sears *et al.*, 1982b). However the type 3.0-3.2 chondrites do not follow the peak temperature and width trends.

The dominant phosphor (TL sensitive) in the ordinary chondrites is feldspar (Dehart *et al.*, 1987). Thermal metamorphism enables the feldspar to crystalise to a high temperature, disordered form, which has a high TL sensitivity. Annealing studies of chondrules (Guimon *et al.*, 1985; Keck *et al.*, 1986) indicated that thermal metamorphism increases the peak temperature and peak width of the glow curve, however it also resulted in the reduction by about 50% of the TL sensitivity. Longer annealing times (that the type 3.3 to 6 chondrites have experienced), may allow time for the TL sensitivity to increase. Alternatively the presence of water may catalyse the transition of feldspar to the disordered form (Sears and Hasan, 1987) and so increase the TL sensitivity.

Guimon *et al.*, (1987) have shown that TL sensitivity can be reduced by hydrothermal annealing. The aqueous annealing below 550°C tended to increase the peak temperature but reduce the peak width and TL sensitivity. Short-term hydrothermal annealing at >550°C caused a decrease in the TL sensitivity. However after 900 hours the TL sensitivity increased. Hence it is not possible from the TL properties alone to determine whether the low TL sensitivity of the most unequilibrated ordinary chondrites, results from a total lack of secondary processing (thermal metamorphism and aqueous alteration) or from aqueous alteration causing a reduction in the TL sensitivity.

4.1.4 The Semarkona meteorite

Semarkona was observed to fall in India on the 26th October 1940. Two pieces were recovered, with no obvious signs of terrestrial weathering, having masses of 423g and 268g (Graham *et al.*, 1985). The main masses are located at Calcutta, Museum Geol. Surv. India (386g); Washington, U.S. National Museum (245g) and New York, American Museum Natural History (27g), (Graham *et al.*, 1985). Interest has focussed on Semarkona (LL3.0; Sears *et al.*, 1980) because it has the lowest TL sensitivity of any meteorite and so may represent the most primitive material, unaffected by secondary processing.

Semarkona consists of chondrules, ranging from 10μm to several mm in diameter, and rock clasts, all set in a fine-grained matrix. Nagahara (1984) observed that the matrix contained disequilibrium assemblages, indicating that little thermal metamorphism had occurred and that the matrix is not formed from chondrule fragments. Most of the matrix is silicate and consists of Fe and Mg rich fluffy particles which range from less than 1μm to several μm in diameter. These particles often lie in layers along the rims of chondrules suggesting that the matrix was compacted during chondrule accretion. The matrix also contains strings of magnetite crystals, often associated with carbides, metal and sulphides (Taylor *et al.*, 1981).

Most of the chondrules are porphyritic olivine and pyroxene; barred olivine and cryptocrystalline chondrules are rare. The porphyritic chondrules contain mineral grains of olivine, pyroxene and some patches of mesostasis consisting of clear isotropic glass. Some chondrules and clasts have opaque rims whilst the centres contain clear isotropic glass, indicating that devitrification of the glass started from the outside and worked its way inwards (Matsunani, 1984).

Hutchison *et al.*, (1987) found evidence for aqueous alteration in Semarkona, listed below:

i) Some of the mesostases of chondrules, especially near the rims, consist of brown devitrified glass which had low sums, attributed to the presence of water, on electron microprobe analysis. The presence of the devitrified mesostasis in the outer zones of the chondrules, but not in the centre, indicated that the devitrification process worked its way inwards into the chondrules.

ii) The occurrence of trains of calcite crystals in the matrix, indicating the passage of aqueous fluids.

iii) The presence of hydrous minerals in the matrix such as smectite and maghaemite. In one case they observed the occurrence of smectite surrounding a pyroxene fragment with eroded edges, indicating the alteration of the pyroxene fragment to smectite.

The presence of organic material in Semarkona, similar to carbonaceous chondrite organics, has been inferred from hydrogen and carbon isotopic studies (Yang and

Epstein, 1982; Robert *et al.*, 1987a). McNaughton *et al.*, (1982b) found that the deuterium rich component pyrolysed between 600°C and 800°C with δD of +5470‰. The actual δD was obscured by water having a terrestrial D/H ratio mainly released below 200°C, but still present at higher temperatures. Hydrogen isotopic analysis of Semarkona acid residues (Yang and Epstein, 1982) indicated that this enriched D/H component was soluble in acid and had δD of approximately +10 000‰.

4.2 Experimental techniques

Due to the heterogeneity in the Semarkona meteorite it is difficult to correlate the properties of Semarkona by different analytical methods. In an attempt to overcome this problem it was decided to perform a combined study of Semarkona using petrological, isotopic and TL techniques on separated components of the meteorite. A schematic diagram of the procedure used to separate fragments and their subsequent analysis is shown in fig. 4.6.

4.2.1 Physical separation of chondrules and matrix material

Separation of components from Semarkona was carried out in a clean room at the Open University. All of the tools and implements used for this procedure were thoroughly cleaned (described below), prior to usage, to minimise terrestrial contamination. Both the D/H isotope and TL techniques require that terrestrial contamination must be reduced to a minimum. The effect of terrestrial contamination for D/H isotopic analysis is to dilute any deuterium-enriched component. In the case of TL measurements dust and flakes of skin have a very high TL sensitivity (Sears pers. comm., 1987), hence terrestrial contamination will mask the TL properties of the Semarkona fragments which have a low TL sensitivity. Glass was cleaned by immersion in chromic acid (made by adding 2.5l AnalaR grade sulphuric acid to 300g of AnalaR grade sodium dichromate dissolved in 300ml de-ionised water) for at least 24 hours, followed by thorough washing in tap water and treatment in an ultrasound bath containing de-ionised water, for 15 minutes. Finally, the glass was dried by placing in an oven at 100°C. Stainless steel tools were cleaned by placing in the ultrasound bath containing AnalaR grade acetone for 15 minutes and then dried in the oven at 100°C. Other materials, such as the container plastic screw-top lids, were cleaned by ultrasound in a 1:1 mixture of AnalaR grade methanol and toluene. All acids and solvents were obtained from (BDH Chemicals Ltd., Poole).

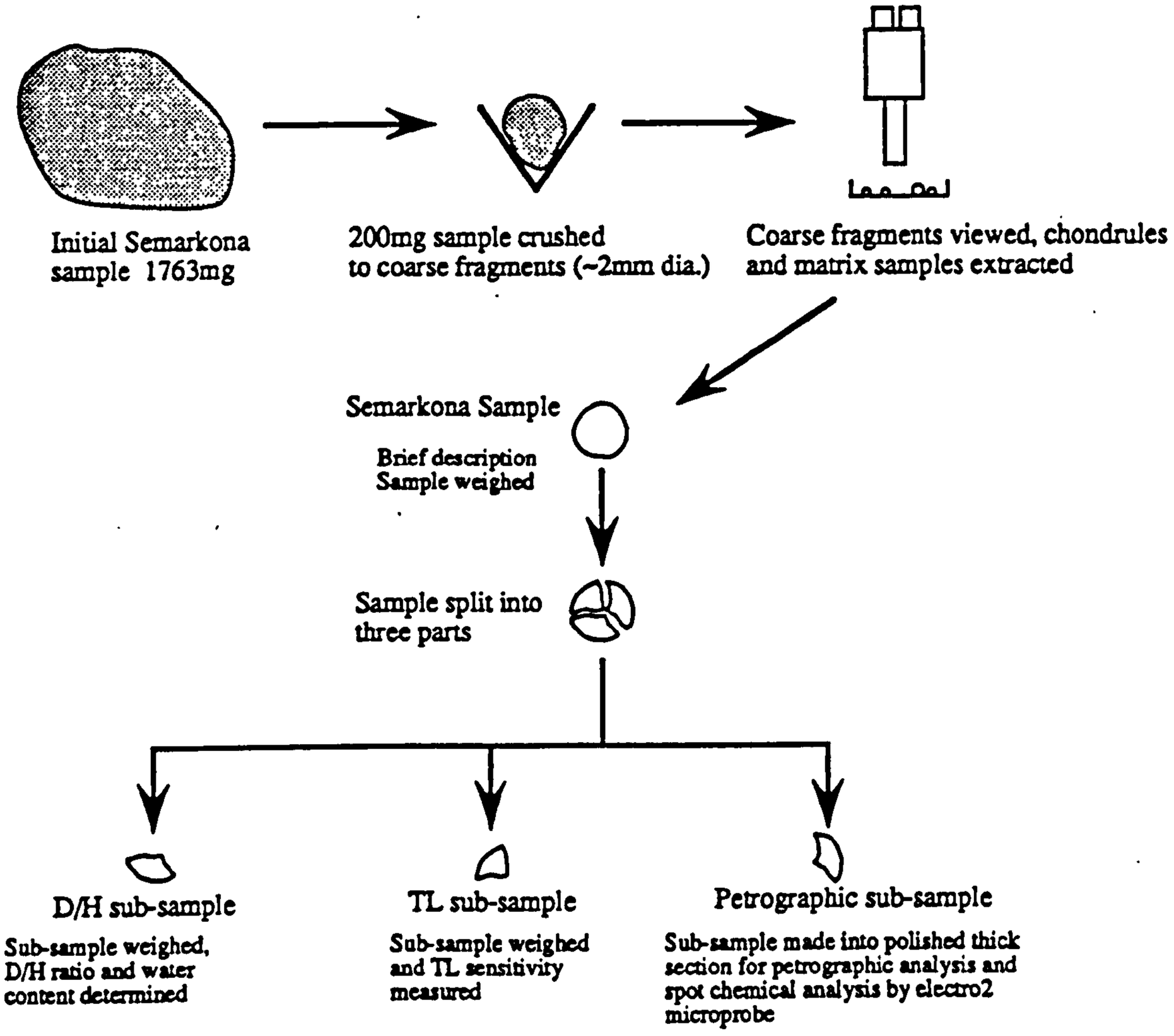

Fig. 4.6 A schematic diagram of the procedure used to separate Semarkona fragments with a binocular microscope. Each fragment was then split into three sub-samples, one for each of the analytical techniques, isotopic, thermoluminescence and petrographic.

The sample of Semarkona used herein was provided by R. Hutchison, Natural History Museum. A fragment of about 200mg, from a total mass of 1763mg, was placed in a 'V' shaped stainless steel plate (fabricated from a 5cm by 4cm, 1mm thick stainless steel plate bent into a 'V' shape) and then slowly crushed to coarse fragments, *ca.* 2mm in size, using a vice. The fragments were then transferred to an aluminium 'boat' (approx. 2cmx2cm and 0.5cm deep) made from aluminium foil (0.075mm thickness) and viewed under a low-power binocular microscope (Olympus Tokyo, objective x40). Chondrules and matrix samples were picked out using stainless steel dental tools. Matrix was operationally defined as the black fine-grained material between chondrules which contained no obvious chondrule fragments or clasts. As each sample, chondrules and matrix was extracted a brief description was made of its appearance and any unusual features. An attempt was made at this stage to scrape away any matrix adhering to the surface of the chondrule samples, using the dental tools.

All samples were then weighed using a 7 figure electronic balance (Sartorius, 4504 MP8-1,) which had a precision of ±0.1μg. Sample weights for the Semarkona fragments ranged from 0.0796mg to 6.0502mg. Each sample was then split into three sub-samples by enclosing it in thick aluminium foil and hitting it with a stainless steel mallet. The sub-sample with the best cross section through the sample was used to make a thick section for petrographic analysis (see below). The sub-sample chosen usually included any edge of the sample as well as interior material. Of the remaining sample the largest sub-sample was removed for hydrogen isotope analysis and the rest used for TL analysis. Some chondrules fragmented into many pieces; in such cases the largest fragment(s) were extracted for petrographic analysis and the remaining sample divided equally for D/H and TL analysis. The TL and isotope sub-samples were then weighed, using the Sartorius balance. Each sub-sample was stored in a 2ml glass vial (Camlab Ltd.). To facilitate manipulation of the smaller samples, these were first loaded into Pyrex tubes (2mm O.D. and 1mm I.D.) sealed at one end, which was then placed in the glass vial as shown in fig. 4.7.

4.2.2 Chemical and petrographic analysis

The sub-samples assigned for petrographic analysis were made into thick sections, as shown in fig.4.7, by drilling angled holes into a plexiglass slide, filling each hole with a drop of araldite and then placing one sub-sample into each hole. Usually 6 sub-samples were mounted per slide. The slides were then gently ground and polished, final polishing with a 1μm diamond lap. Spot chemical analysis of each sub-sample was accomplished by wavelength dispersive electron microprobe (Microscan Mark 9, Cambridge Scientific Instruments Ltd.), with 20kV accelerating voltage and 2.5×10^{-8} Amp current, at the British Museum (Natural History) and the Open University. Standards used were the same as used by Hutchison *et al.* (1987), i.e. wollastonite (for the elements Si, Ca), rutile (Ti), jadeite (Al, Na), olivine (Fe, Mg), sylvite (K), pyrite (S) and pure metal for Mn, Cr and Ni. Usually 6 mesostasis points (the glassy material between mineral grains) and 6 to 10 mineral grains were analysed for each sub-sample. Petrographic analysis, performed by R.Hutchison, was accomplished using backscattered electron images of each sub-sample obtained from the electron microprobe. A brief description of each sub-sample was then made, noting any unusual features and any evidence of aqueous alteration.

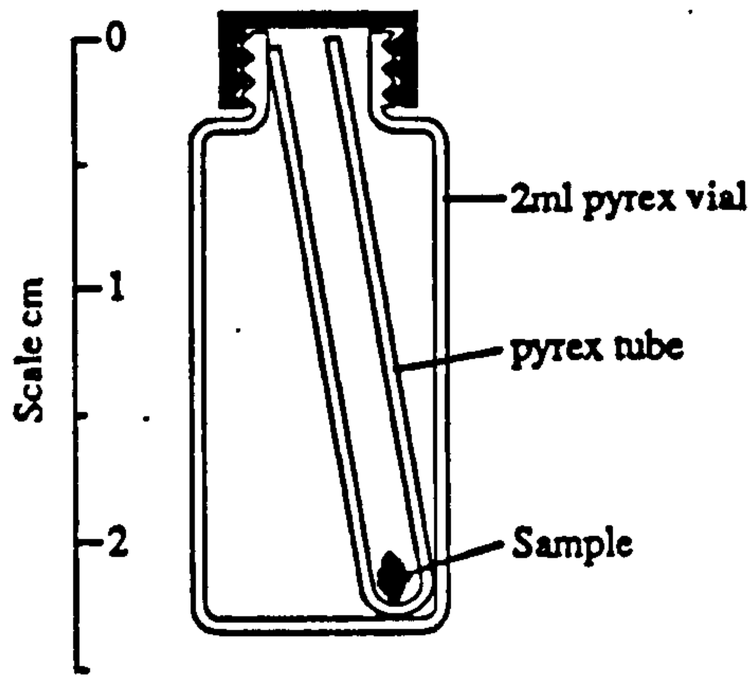

Fig. 4.7 Storage procedure for the smaller Semarkona sub-samples, *ca.* 200µm.. The sample was first loaded in a Pyrex tube which was then placed in the glass vial. This aided location of the sample for analysis.

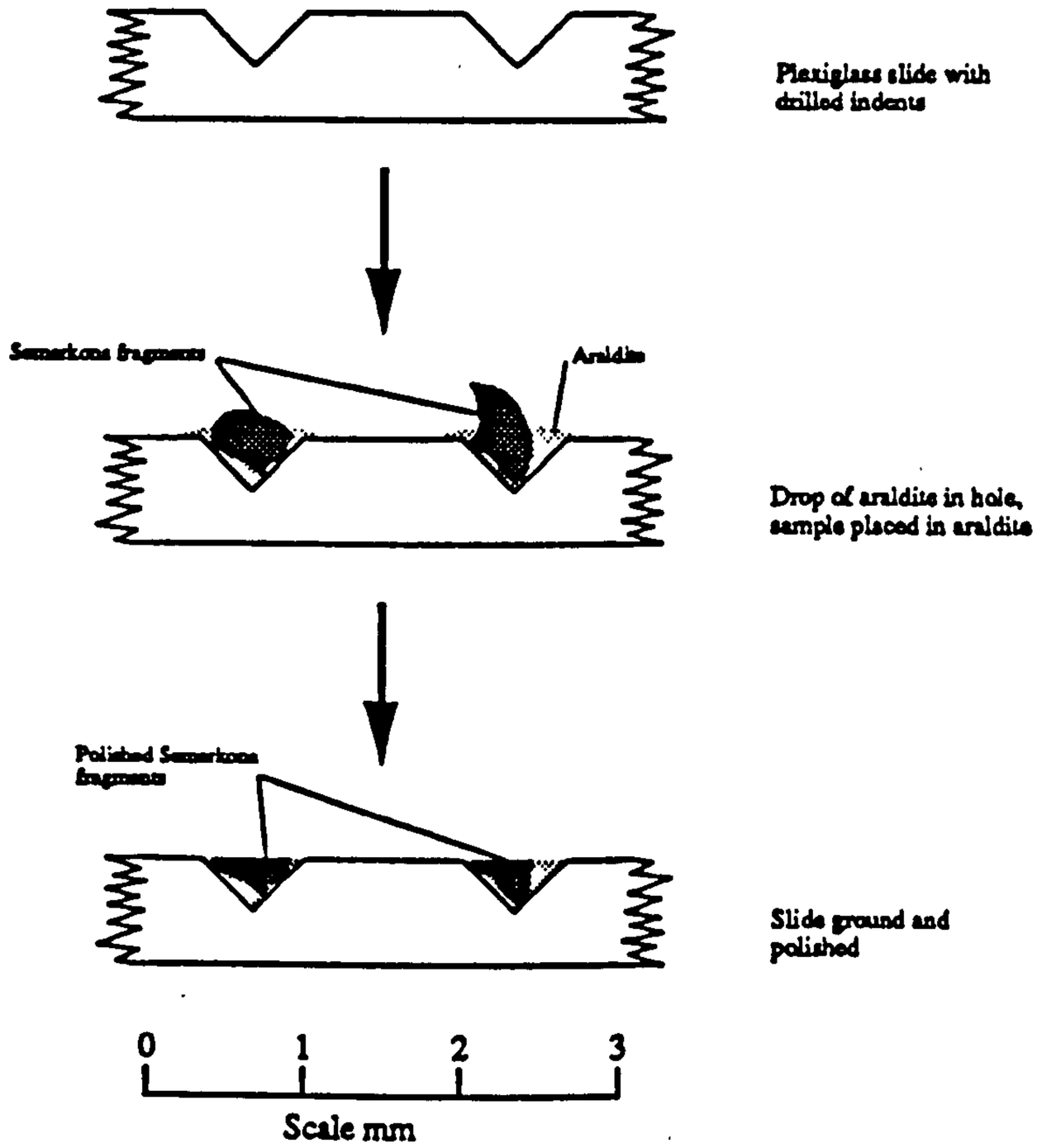

Fig. 4.8 Diagram showing the procedure used to prepare polished sections of the Semarkona sub-samples for petrographic and electron microprobe analysis. Each sample was placed in a angled hole filled with araldite on the plexiglass slide. The slide was the gently ground and polished

4.2.3 D/H analysis

D/H isotope analysis was performed using the mass spectrometer described in chapter 2 and inlet described in section 3.5 (*i.e.* the 'flow-thru' inlet, since this was the only device capable of analysing small samples). The D/H sub-sample was first loaded into a quartz 'bucket' and then admitted to the preparation line by the procedure described in section 3.3.2. The sample was then stored under vacuum whilst samples of V-SMOW (3.3μmol) were analysed until consecutive analyses gave, within experimental error, the same result (according to the protocol used to obtain the calibration curve, described in section 3.5.3). Once the mass spectrometer and reduction furnace were deemed to be working satisfactorily the sample analysis would begin.

The sample was pyrolysed in two steps and the water released at each step quantified and analysed for δD by the procedure described in section 3.4.2. The first step, which was from room temperature to 200°C, was an attempt to remove loosely bound water, mostly thought to be terrestrial contamination. The second step was from 200°C to 1100°C and water released considered to be indigenous water. However, other sources of water could be from combustion of organics (either indigenous extra-terrestrial material or terrestrial contamination), obtaining oxygen from silicate minerals or indeed from organics. The δD results, for both steps, corrected for the memory effect using the calibration curve obtained in section 3.5.3, are shown in fig. 3.20.

4.2.4 Thermoluminescence analysis

The thermoluminescence (TL) analyses were carried out at the Cosmochemistry Department of the University of Arkansas, USA, using the apparatus described by Sears and Weeks (1983), a schematic diagram of which is shown in fig. 4.9. Each sub-sample was placed in a copper pan (5mm dia., 2mm deep) which was then placed on the sample heating stage of the TL apparatus. Following evacuation of the sample chamber of the TL apparatus a flow of oxygen-free nitrogen was passed over the sample in order to prevent combustion during the analysis since this would emit radiation (Aitken *et al.*, 1968), thereby producing erroneous results. TL was measured by heating the sample stage to 500°C at 30°C s^{-1}. Photons emitted from the sample were detected by a photomultiplier tube and recorded in real time on a personal computer.

Before analysis each sample had its natural TL measured, this was to prevent interference of the induced TL from the natural TL. Following the draining of natural TL, the sample was removed from the TL apparatus and irradiated for 12 minutes by exposure to a 250mCi strength ^{90}Sr beta source. The induced TL was then measured, as described above. The TL sensitivity was then compared to that from 4mg of powdered (100 mesh) Dhajala meteorite (type H3.8). Dhajala has been used as a working standard for many years (Sears *et al.*, 1980), allows comparison with TL results obtained from other

meteorites and has also been used in a similar chondrule study (Keck *et al.*, 1986). A typical display of the results obtained and measurements made during an analysis of a Semarkona sample is shown in fig. 4.10.

The optimum sample size for TL measurements is about 4mg; once crushed this covers the whole of the copper pan. However for this study the each sample was too small to manipulate when crushed or cover the copper pan. Instead several TL measurements were made for each sample and an average value determined. Since the sample did not cover the whole of the copper pan, some of the copper was exposed to the photomultiplier tube. Copper oxide, on the surface of the copper pan, was found to have a high TL sensitivity compared with some of the Semarkona fragments (equivalent to radiation emitted by a 1mg chondrule with a TL sensitivity of 0.001). Care was taken to ensure that any copper oxide on the surface of the copper pan was removed by using emery paper and then washing in dilute HCl. The average TL value for each sample was then mass corrected for the surface exposed to the photomultiplier tube (Sears *et al.*, 1983). Hence the thermoluminescence sensitivity of each sample was given by the equation

$$\text{TL/mass} = \left(\frac{\text{TL}}{\text{mass}}\right)_{\text{sample}} / \left(\frac{\text{TL}}{\text{mass}}\right)_{\text{Dhajala}}$$

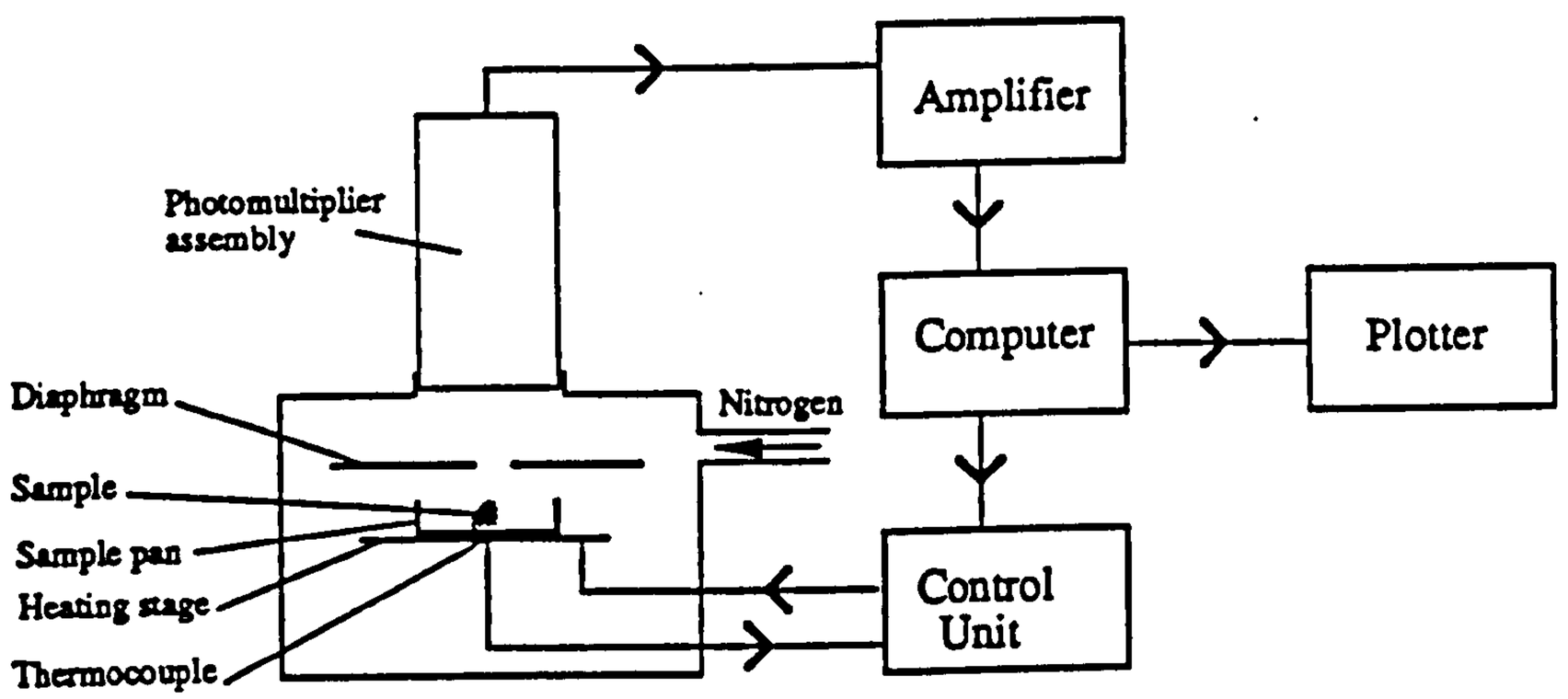

Fig. 4.9 A schematic diagram of the TL apparatus. The sample is placed in a copper pan on the heating stage and purged with oxygen free nitrogen. The heating stage is heated by the control unit, the temperature measured by a thermocouple. TL from the sample is detected by the photomultiplier, amplified and recorded by the computer. The diaphragm above the sample cuts out background TL and black body radiation from the sample pan and heating stage. A hard copy of the TL against temperature can be obtained from the computer, as well as the 'glow' curve parameters.

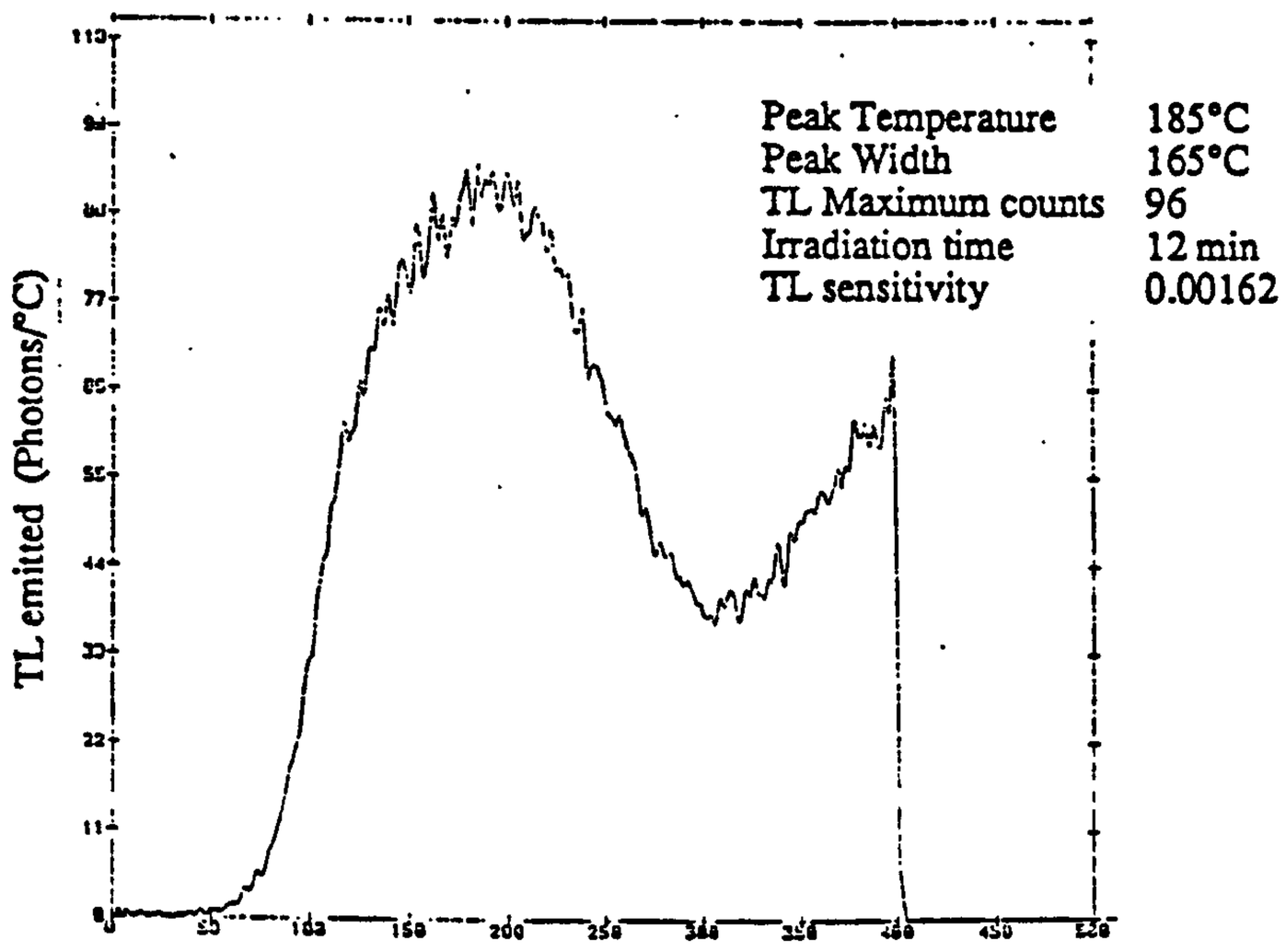

Fig. 4.10 Typical results obtained for the TL sensitivity against temperature for a Semarkona chondrule sub-sample.

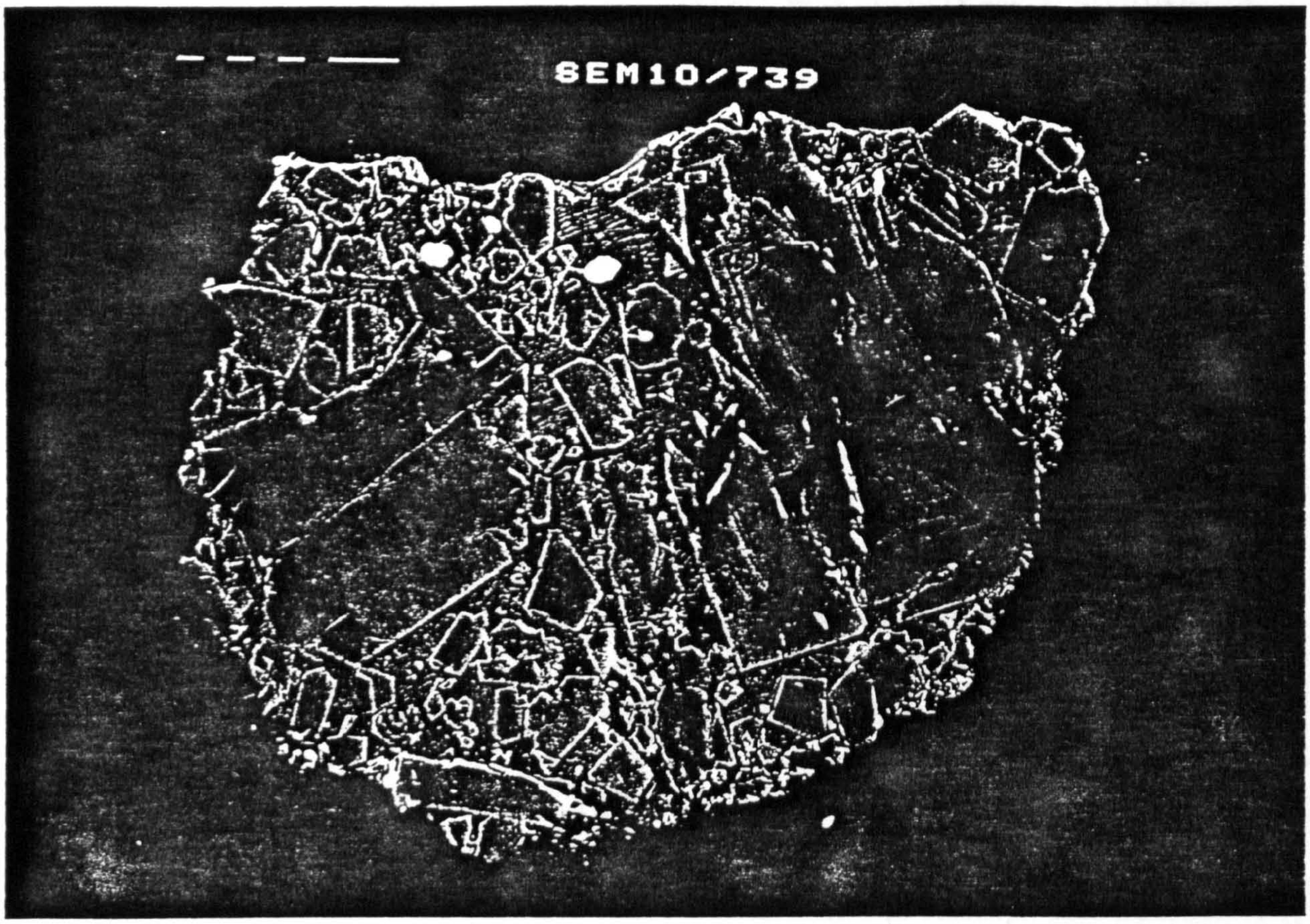

(a)

Fig.4.11 Backscattered electron photographs of some of the fragments extracted from Semarkona. The scale is shown by the scale bars in the top left of each photograph; for a) and b) the right scale bar represents 100μm and in c) and d) represents 10μm.
a) Example of a chondrule fragment, SC-01, showing grains of mainly olivine. The mesostasis is the material between the mineral grains. b) Example of a chondrule, SC-59, with adhering chondrule rim and/or matrix. c) An example of a mis-identified fragment, SC-67. Although extracted as a chondrule it appears to consist of chondrule rim or matrix, but also contains course angular fragments from broken chondrules. This was the only chondrule fragment in which smectite was observed. d) An example of a matrix fragment, SM38. This example is unusual in that it consists of pure matrix, not containing any small chondrules or chondrule fragments.

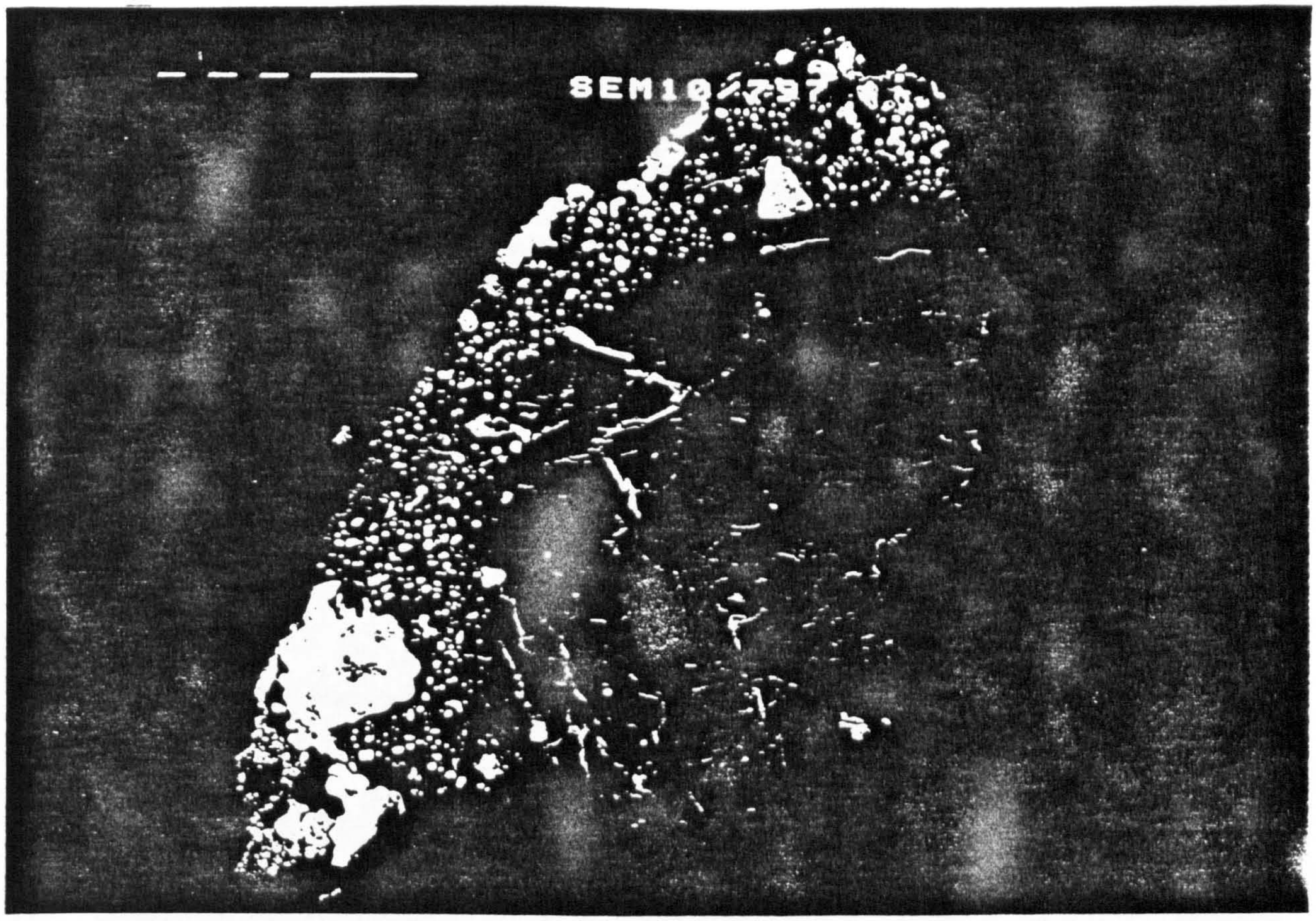

(b)

(c)

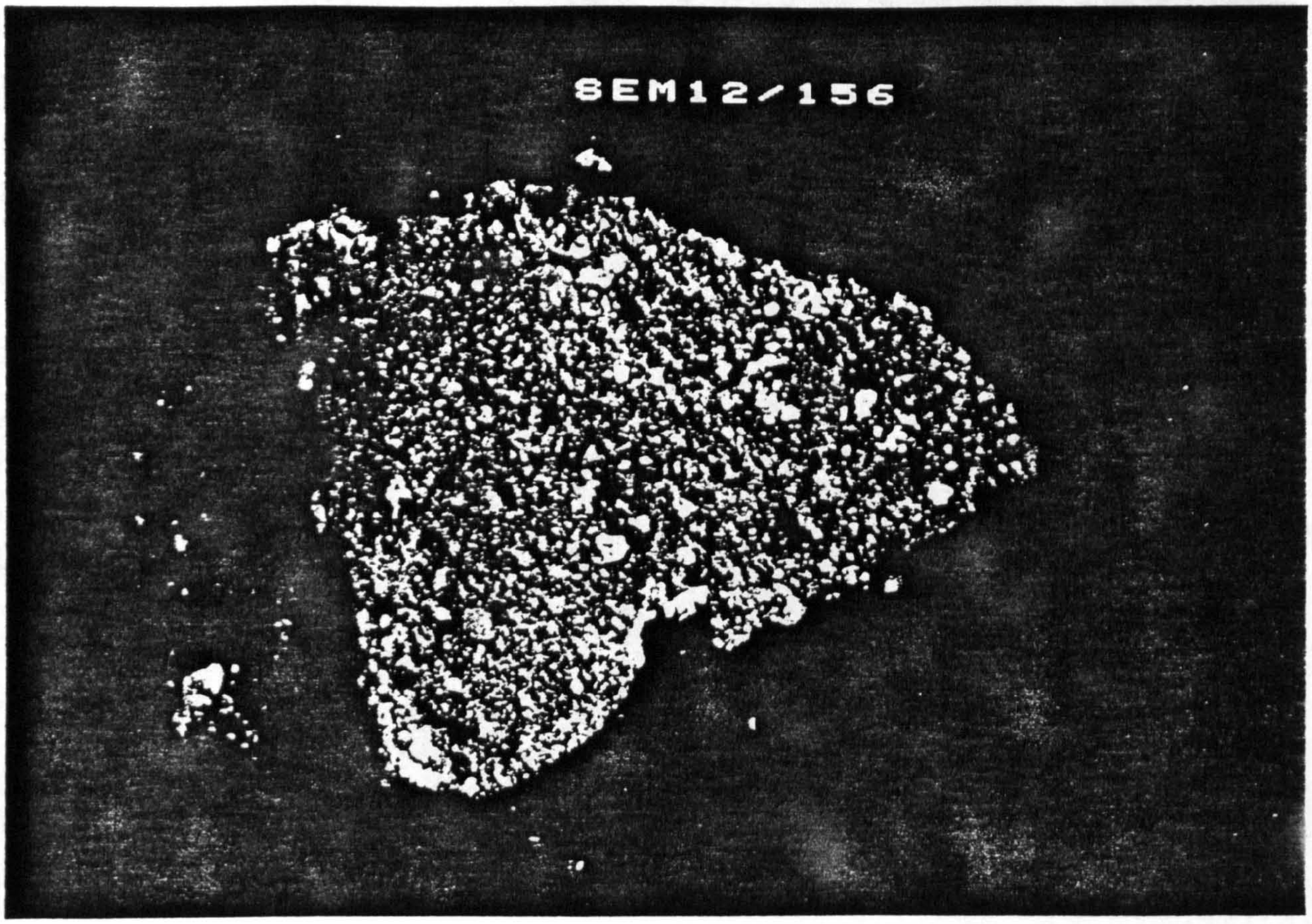

(d)

4.3 Results

Numbers were assigned to each fragment as they were extracted, prefixed by SC for chondrule fragments and SM for matrix fragments. The notes written about each fragment during extraction are shown in appendix D, table D.1. Often samples were not analysed by all three analytical techniques (isotopic, TL and petrographic). The analytical techniques applied to each sample are also indicated in table D.1. The results obtained by each individual analytical technique are described below (sections 4.3.1 to 4.3.3).

4.3.1 Petrographic results

Typical backscattered electron photographs (from the electron microprobe) of the 'chondrule' and 'matrix' thick sections are shown in fig. 4.11. Analysis by electron microprobe was useful since it gave a valuable insight into the constitution of each sample. As can be seen from fig.4.11 many of the samples were not pure chondrule or matrix separates, but often a mixture of both. Chondrule samples were often found to have matrix materials attached to the outer rim (e.g. see fig. 4.11b). Furthermore, what were from a preliminary optical investigation, thought to be pure matrix fragments were often found to contain many small chondrules (see fig. 4.11c). As noted during the separation procedure (section 4.2.1), chondrule fragments that were observed to have rim and/or adhering matrix material were usually assigned to petrographic analysis. Hence, most of the chondrule sub-samples for D/H and TL analysis were probably free of matrix material. However, the matrix fragments were thought to be essentially pure when extracted and so matrix fragments assigned to TL and isotopic analysis are more likely a mixture of matrix and small chondrules, as indicated by the backscattered electron photographs (*e.g.* fig. 4.11c).

Electron microprobe analysis of iron content in the olivine grains shows a wide variation in concentration, from 0.86 to 22.29%, with mean iron content 10.93% and a standard deviation of 6.73%. The ratio of the standard deviation to the mean iron content of >0.6 confirms that Semarkona is extremely unequilibrated, as determined by Dodd *et al.*, (1967). Electron microprobe examination found no chondrule fragments with zones of altered minerals. Furthermore the average compositions of the mesostasis of most chondrules, determined by electron microprobe analysis (appendix D table D.2) had sums between 98-102% (100% within the experimental error of ±2%). The mesostasis is more susceptible to secondary processing than the chondrule mineral grains. In contrast Hutchison *et al.* (1987) determined *in situ* sums as low as 85% for the mesostasis of some Semarkona chondrules, indicating the presence of up to 15% water. Herein only one chondrule, SC64, and a single mesostasis analysis for chondrule SC67 had a sum which was less than 95%. The mesostasis point for chondrule SC67, shown separately

from the average of other mesostasis points in table D.2, was tentatively identified as smectite. Petrographic examination of some chondrules did show some evidence of aqueous alteration.

It is important to try and understand the apparent difference in the results obtained herein and the study of Hutchison *et al.*, (1987) in which some chondrules were found to contain up to 15wt.% water in the same meteorite. It is unlikely that this is an analytical problem since in some cases the same instrument and standards were used to make the analyses for both studies. The main difference was the method in which samples from Semarkona were selected for analysis. Hutchison *et al.* (1987) were actively looking for the effects of aqueous alteration in Semarkona and as such three polished thin sections (total area about $3cm^2$) were available for analysis. Furthermore, effort was concentrated on those areas that tended to show observational signs of aqueous alteration. Whereas for this study chondrule fragments were first extracted from the meteorite and then mounted (total area viewed *ca.* $0.05cm^3$); during this physical process attempts to pick out friable fragments often resulted in their complete disintegration. It is considered possible that it was these more friable chondrules that represent the highest degrees of aqueous alteration, thus the most altered chondrules were probably not selected during this study.

4.3.2 D/H isotope results

Any water present in the chondrule and matrix sub-samples of Semarkona assigned to D/H isotope analysis was extracted by heating as described in 4.2.3. In order to establish an optimum heating schedule a stepped pyrolysis was performed on approximately 20mg of whole-rock Semarkona, the results of water content and δD against temperature are shown in fig. 4.12. The water released during the low temperature step (room temperature to 200°C) had a δD of +60‰, approximately the same as terrestrial water (overall terrestrial range is $-500‰ < \delta D < +150‰$, de-ionised tap water, at the lab, has a δD value of -50±10‰). A deuterium-rich component was released between 600°C to 1000°C which had a δD of at least +4500±1000‰. The variation in δD versus temperature (from room temperature to 1000°C) can be explained by the presence of at least two different components. One component containing most of the water was mainly released below 400°C and had a δD of *ca.* 0‰. Since this first component is indistinguishable from terrestrial water it is not possible to determine whether this component is extra-terrestrial in origin, or due completely due to terrestrial contamination. The second component, released between 600°C to 1000°C, had a high deuterium enrichment with $\delta D > +4500‰$. It was not possible to define the temperature step at which the two components are separated, some of the deuterium-rich component is

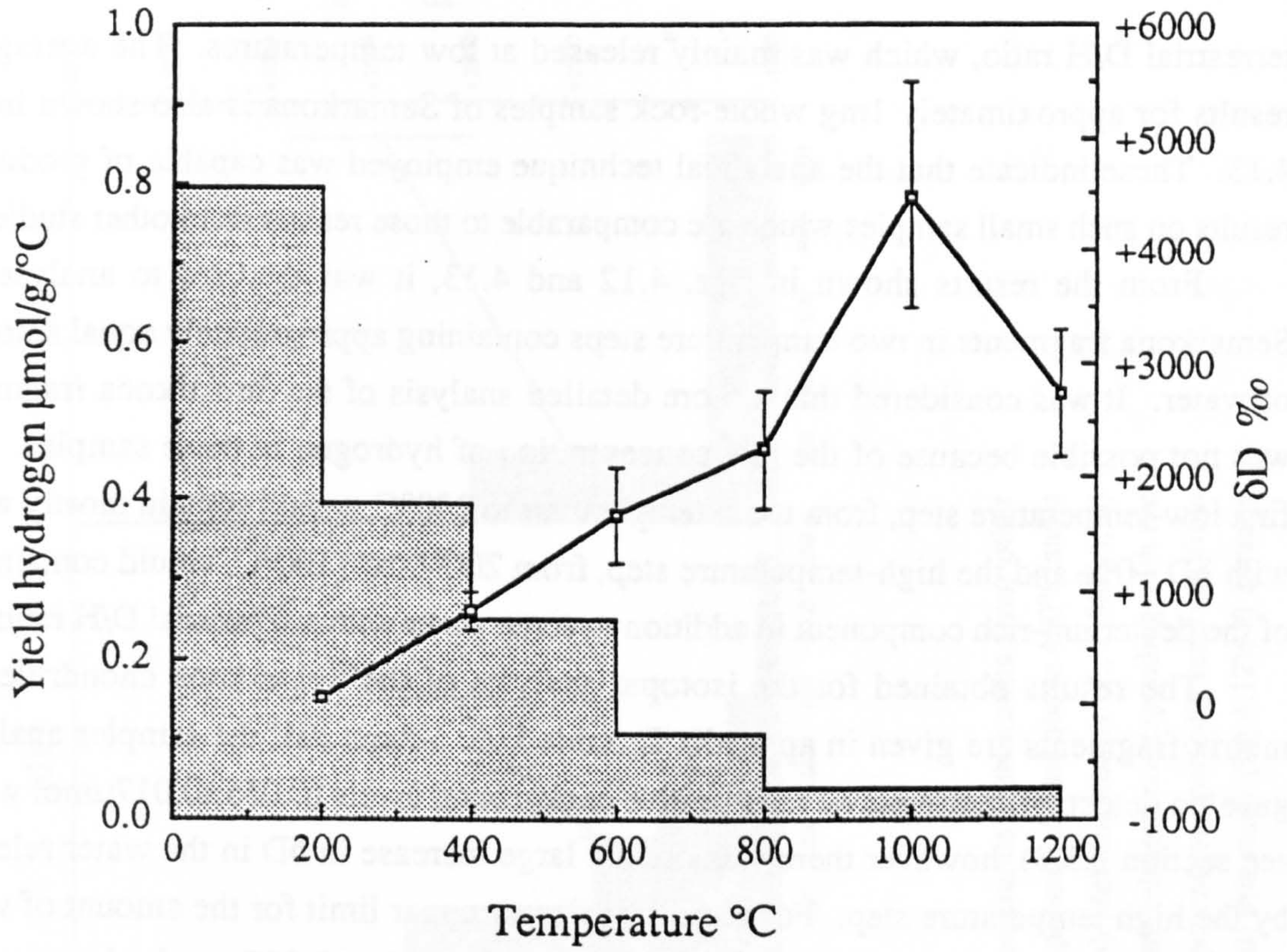

Fig. 4.12 A graph showing the release of water and its D/H isotopic composition upon stepped pyrolysis of whole-rock Semarkona. The amount of water released per temperature increment is shown in the shaded histogram and the δD of the water by joined points. The deuterium-rich phase is released above 400°C and has a dD > + 4500‰, however this is diluted by the water with δD ~0‰ mainly released at lower temperatures.

released between 200°C and 400°C the temperature over which most of the water with δD ~0‰ is released. Water released above 1000°C had a δD value which is lower than the deuterium-rich component and so it is possible that a third component with low δD is present. Alternatively most of the deuterium-rich component is released by 1000°C whereas the more abundant component still liberates water at temperatures > 1000°C. Since water with δD ~0‰ is released along with the deuterium-rich component, then the measured δD of +4500‰ represents a lower limit to the true value.

A comparison of the results obtained from Semarkona with data from other studies is shown in fig. 4.13. All the results show similarities; most of the water is released below 400°C with an approximately terrestrial D/H ratio and a deuterium-rich component is released at higher temperatures. The differences between the various analyses probably result from heterogeneity in the Semarkona meteorite and differing heating regimes. There was a small increase in the yield corresponding with the maximum δD in the more detailed stepped pyrolysis in fig 4.13b (McNaughton *et al.*, 1982b). However this peak in the yield was not detected in the other analyses due to the tailing of the water with

terrestrial D/H ratio, which was mainly released at low temperatures. The average of results for approximately 1mg whole-rock samples of Semarkona is also shown in fig. 4.13. These indicate that the analytical technique employed was capable of producing results on such small samples which are comparable to those results from other studies.

From the results shown in figs. 4.12 and 4.13, it was decided to analyse the Semarkona fragments in two temperature steps containing approximately equal amounts of water. It was considered that a more detailed analysis of the Semarkona fragments was not possible because of the low concentration of hydrogen in these samples. The first low-temperature step, from room temperature to 200°C, would contain mostly water with δD ~0‰ and the high-temperature step, from 200°C to 1100°C, would contain any of the deuterium-rich component in addition to some water with a terrestrial D/H ratio.

The results obtained for the isotopic analysis of the Semarkona chondrule and matrix fragments are given in appendix D, table D.3. About half the samples analysed gave no detectable amounts of water above background levels (0.055±0.017μmol water, see section 3.5.3), however there was often a large increase in δD in the water released by the high temperature step. For these samples an upper limit for the amount of water and a lower limit for the δD was obtained assuming that 0.017μmol of water (the uncertainty in the blank) was the smallest amount measurable.

Fig. 4.14 shows the results of the water concentration against δD value for the high-temperature steps of the chondrules. Most of the chondrules contained 0.2 wt.% water, or less, and had a range of δD values from 0 to +7500‰. The amounts of water released from the chondrules during the low-temperature steps were also low, < 0.2wt.% and were not as deuterium-rich, δD ranged from -500‰ to +3500‰. Most of the water released from the chondrules during the low-temperature extraction, plot in the shaded region of fig. 4.13. Four of the chondrules (SC-09, SC-19, SC-49 and SC-71), which released less than 0.017μmol of water during the high temperature step, also showed no sign of any deuterium enrichment. Since the fragments of these chondrules assigned for D/H analysis all had a low mass, the low water content has resulted in these chondrules appearing to have a high percentage of water (the upper limit of 0.017μmol of water was used to calculate the percentage of water released). The analytical technique was not able to determine whether these chondrules released any deuterium rich water. The average amount of water released by the chondrules during the high temperature step was 0.12±0.02wt.% with δD of +3890±500‰.

The results for other fragments of Semarkona are shown in fig. 4.15. Three of the four matrix fragments contained a much higher percentage of high-temperature water than most of the chondrules, from 0.3 to 2.5wt.%. The δD value for the high temperature

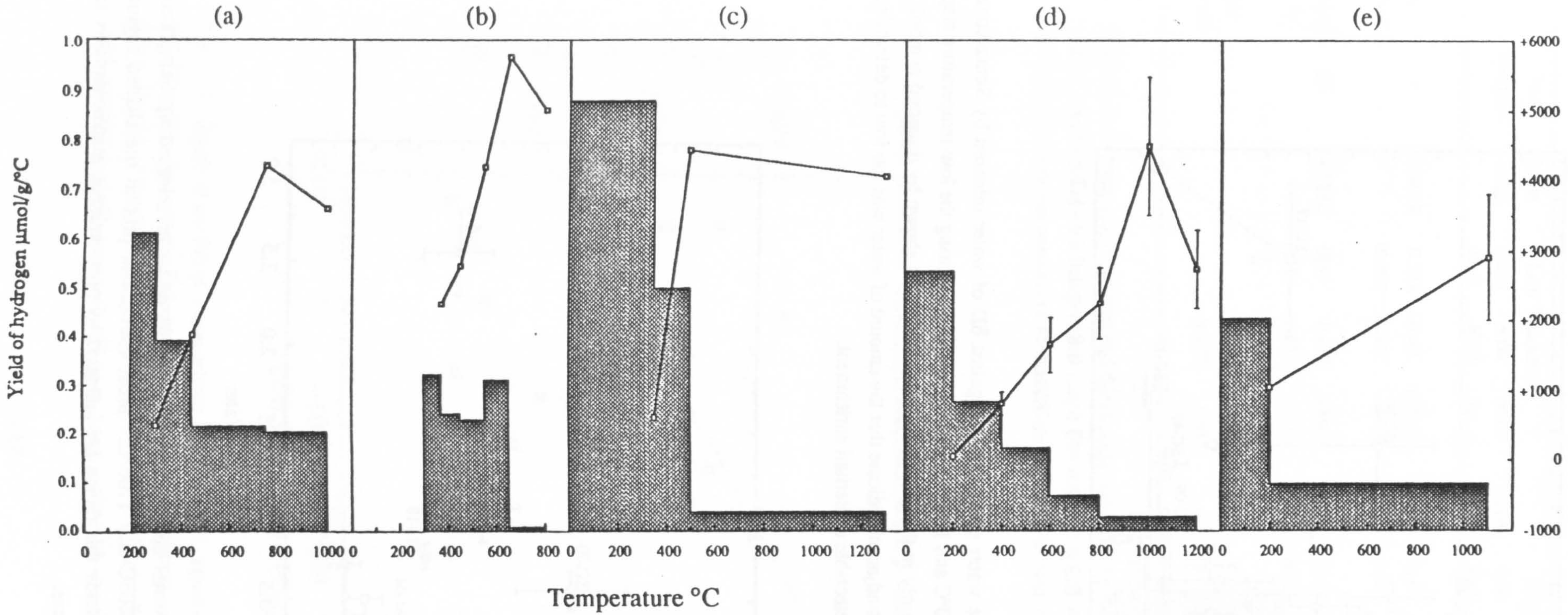

Fig. 4.13 Comparison of results of the stepped pyrolysis of Semarkona with results from other studies. All the results show similarities, with a deuterium-rich component released above 400°C and a component mainly released below 400°C with a terrestrial δD. a) McNaughton *et al.*, (1982b); b) McNaughton et al., (1982b), there is an increase in the yield of water released corresponding with the maximum δD, of +5740‰, showing that the deuterium-rich component was partially resolved from the component with terrestrial δD; c) Yang and Epstein, (1983); d) this study (fig 4.12); e) average results from three 1mg samples of whole-rock Semarkona.

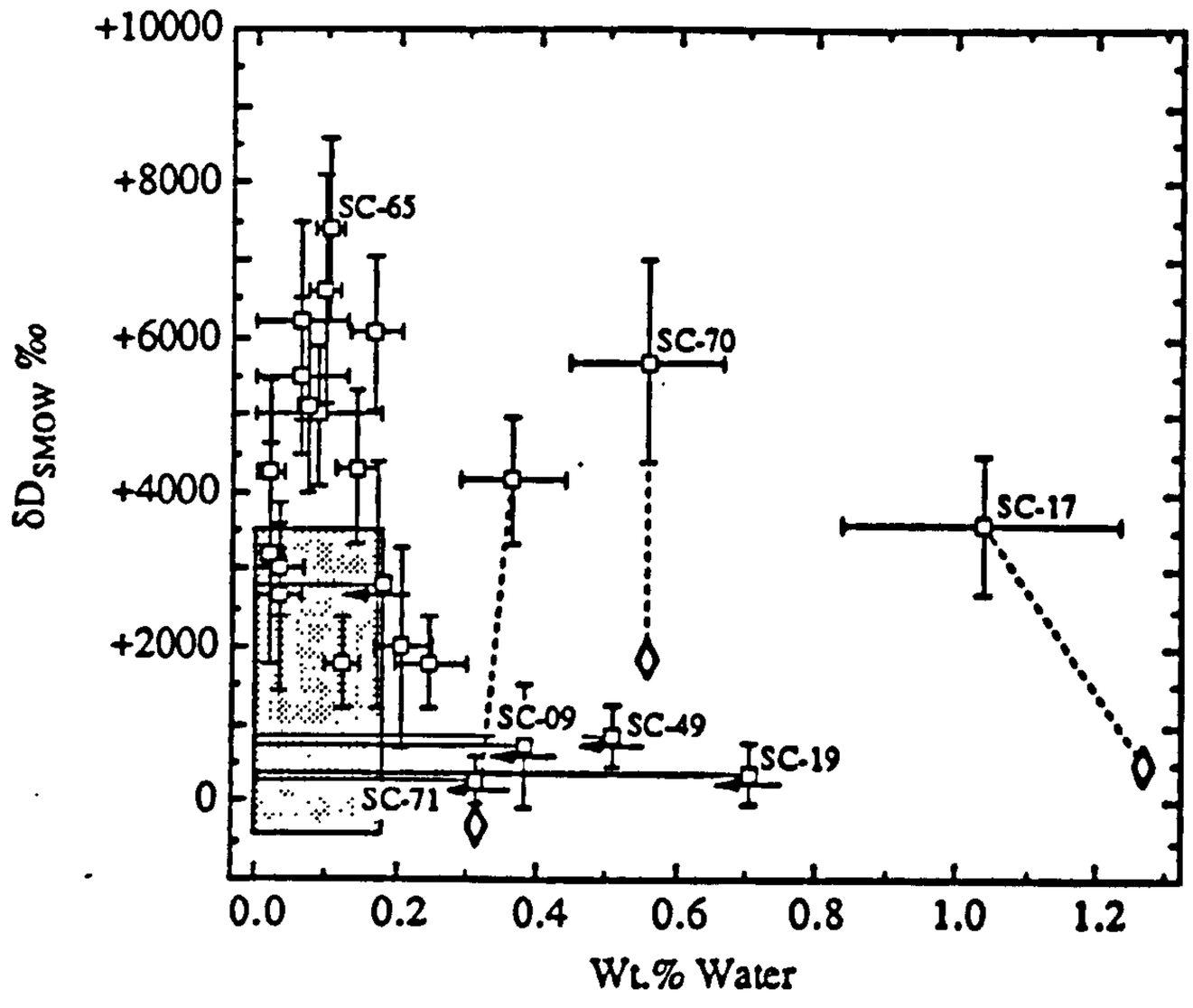

Fig. 4.14 Graph of the water concentration against δD of water released by Semarkona chondrules between 200°C and 1100°C. The water released during the low-temperature step (up to 200°C) plots mainly in the shaded regions, exceptions shown by diamond symbols. Chondrules with arrows adjacent indicate that the amount of water was too low to determine and that there was no detectable deuterium enrichment.

Fig. 4.15 Graph of water concentration against δD of water released by Semarkona fragments between 200°C and 1100°C. Most chondrules plot in the shaded region, chondrules that lie outside this region are indicated by open squares; matrix samples are indicated by filled squares.

	No. Samples	Mass (mg)	Low Temperture µmol H_2O	wt% H_2O	δD ‰	High Temperature µmol H_2O	wt% H_2O	δD ‰	Total µmol H_2O	wt% H_2O	δD ‰
Matrix	4	1.3678	0.328	0.43	+1010	0.517	0.68	+2670	0.845	1.11	+2030
(2σ error)			(0.065)	(0.08)	(160)	(0.103)	(0.14)	(520)	(0.169)	(0.22)	(320)
Chondrules	23	14.5286	0.67	0.083	+840	0.98	0.121	+3890	1.65	0.200	+2650
(2σ error)			(0.13)	(0.017)	(130)	(0.19)	(0.024)	(500)	(0.33)	(0.010)	(600)
Average				0.135	+920		0.205	+3280		0.340	+2350
(2σ error)				(0.027)	(140)		(0.012)	(430)		(0.068)	(540)

Table 4.1 Average concentration and δD of water released by the Semarkona chondrule and matrix fragments at each temperature step. The average whole-rock values were calculated assuming Semarkona consists of 85% chondrules and 15% matrix.

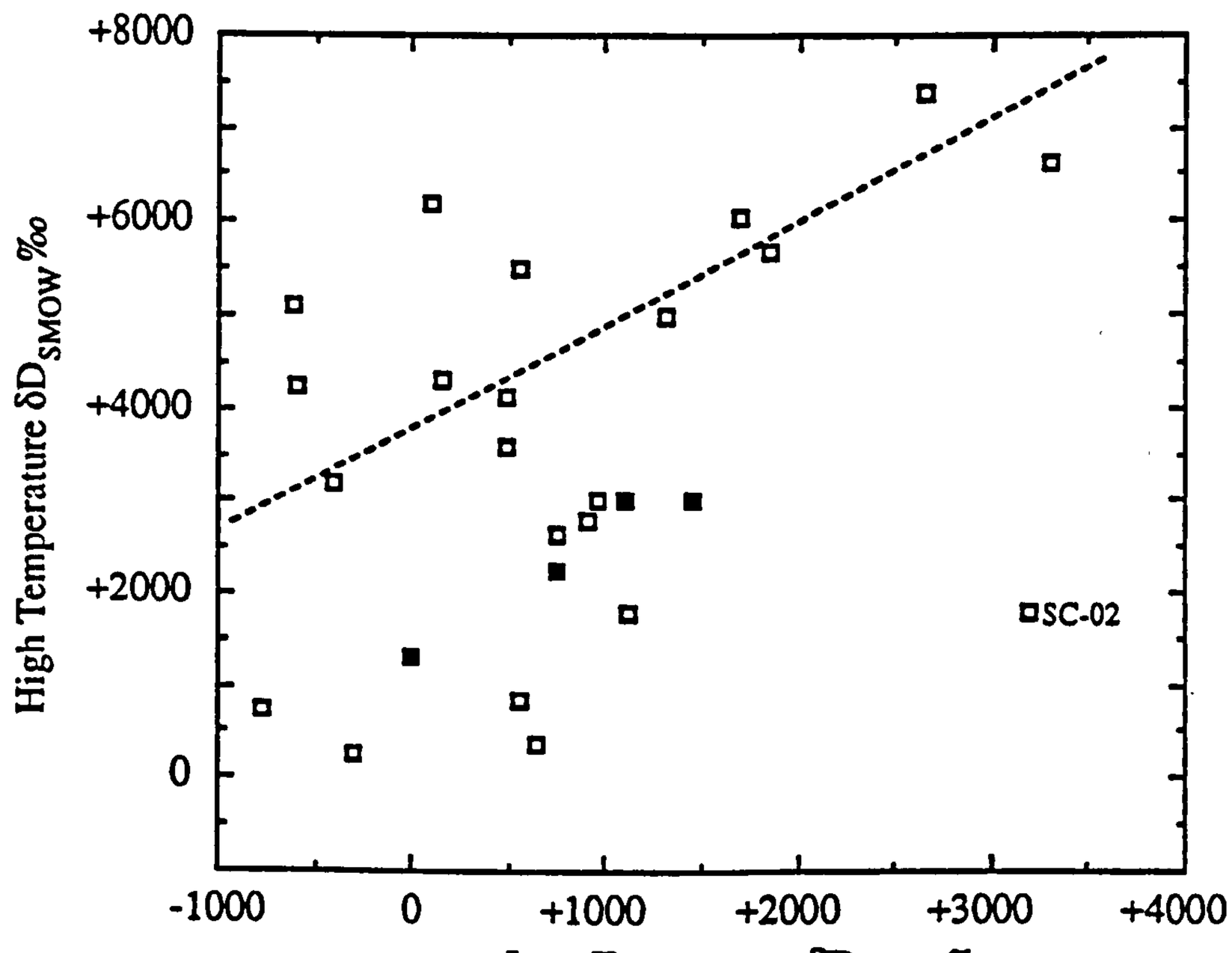

Fig. 4.16 Graph of the δD of water released above 200°C against the water released below 200°C for the Semarkona fragments. Chondrules are shown as open symbols, matrix as filled symbols. The best fit line for the chondrules, excluding SC-02 is y = 2820 + 1.03x, with correlation coefficient, r =0.498 (significant at the 95% level).

step of the matrix fragments had a moderate deuterium enrichment (compared with the chondrules), of up to +3000‰. As the matrix only had a moderate deuterium-enrichment, matrix contamination cannot be used to explain the high D/H ratios of some of the chondrules. However matrix contamination could be the cause of the very high water concentration of chondrules SC17 and SC70 (fig. 4.15). Whole-rock samples of Semarkona had small amounts of water released during the high-temperature step, *ca.* 0.2wt.%, but only a modest deuterium enrichment, $\delta D = +1000‰$ to +3000‰. The large variation of D/H ratios of the whole-rock samples is probably a reflection of sample heterogeneity, again indicating that the deuterium-rich phase is a small component of the total meteorite.

Table 4.1 shows the average water concentration and D/H results for the various components of Semarkona. Assuming that Semarkona consists of 85% chondrules and 15% matrix (Huss *et al.*, 1981), then a whole-rock sample would contain 0.34wt.% water and δD of +2350‰, released during the high-temperature step, comparable to whole-rock analyses by this study.

A plot of the δD of the water released by Semarkona fragments above 200°C against the δD of water released below 200°C is shown in fig. 4.16. The chondrules which had a moderate deuterium enrichment ($\delta D > +1000‰$) during the low temperature step usually gave the greatest deuterium enrichments (δD from +5000‰ to +7500‰) during the high temperature step, except for chondrule SC-02. Those with no deuterium enrichment in the low-temperature step had δD values ranging from 0 to +6000‰ in the high-temperature step. For these chondrules it is clear that little of the deuterium-rich component was released during the low-temperature step, hence the two components were fairly well separated. However there was probably some of the water with a terrestrial δD released during the high-temperature step leading to the wide range of δD between these chondrules. For the chondrules with $\delta D > +3500‰$ in the high-temperature step the points in fig. 4.16 tend to lie on a straight line which reinforces the suggestion of two-component mixing as indicated in fig. 4.12; some of the deuterium-rich component was released during the low-temperature step and some of the water with terrestrial δD was released during the high-temperature step. The amount of water released by SC-02 was well above the blank level and so the low δD in the high-temperature step was not due to the blank. Clearly for this chondrule the deuterium-rich component was completely released during the low temperature step of the pyrolysis. In the following section the δD of +3200‰ is used for the high temperature step of SC-02.

It is interesting to note that a graph of δD against chondrule number, shown in fig. 4.17 indicates that there is some systematic variation between the order in which chondrules were extracted and the δD measured. This was not a result of the analytical technique, chondrules were analysed in no particular order, but probably reflects

experience gained as chondrules were extracted. It is evident from the notes made during chondrule extraction, table D.1, that as experience was gained fewer chondrules were lost. Hence it is probable that chondrules which would have been too friable to separate at the beginning were separated later. Another possible effect was that as the obvious chondrules were extracted first, this left the remaining material containing the more friable deuterium-rich chondrules.

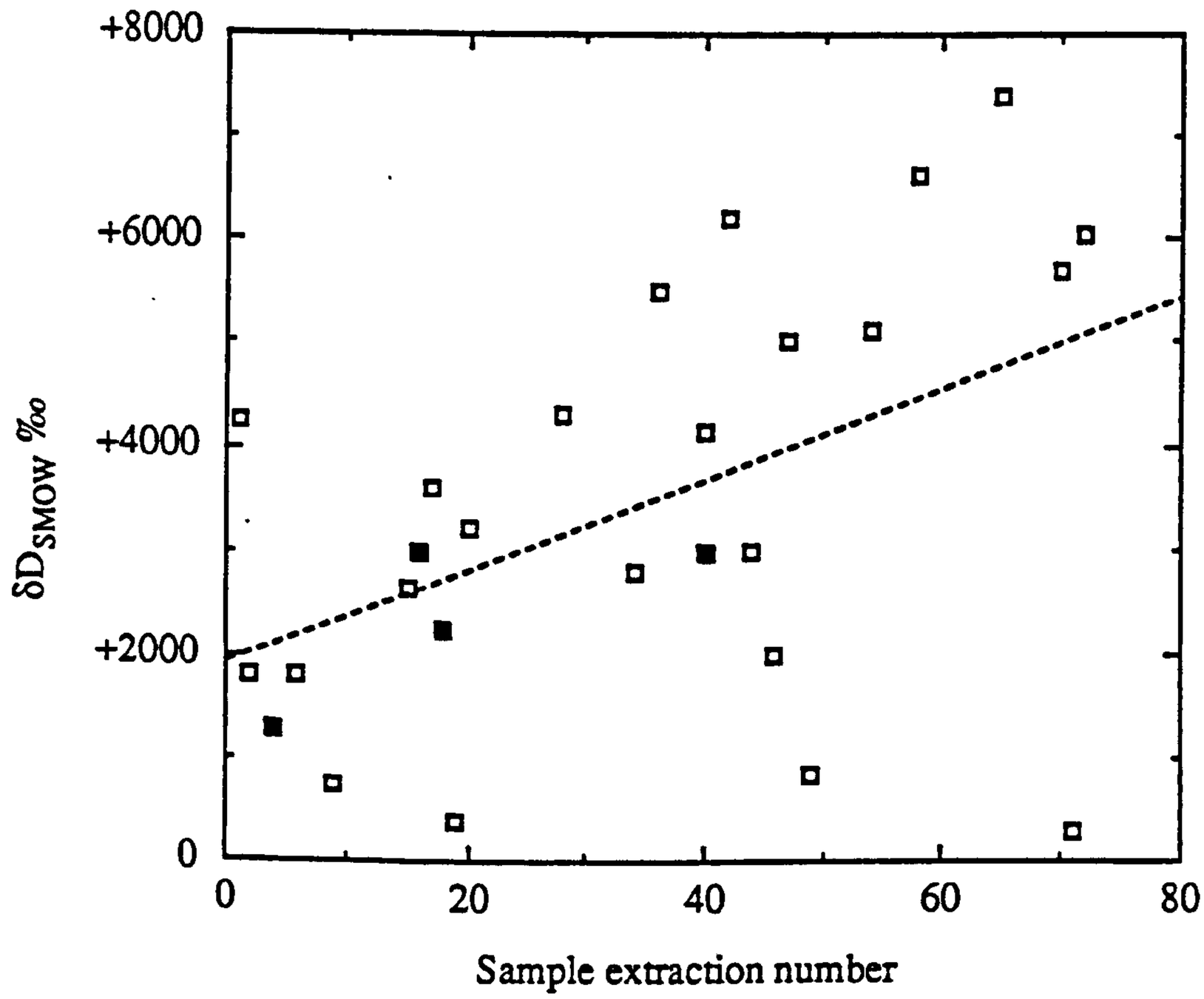

Fig. 4.17 A graph of δD of water released by the Semarkona fragments against extraction number, chondrules are shown as open symbols, matrix as filled symbols. The best fit line has equation y = 1940 + 44x, with correlation coefficient, r = 0.488 which is significant at the 95% level.

4.3.3 Thermoluminescence results

The TL data for the Semarkona chondrule and matrix fragments are shown in appendix D, table D.4. The TL sensitivity of the Semarkona chondrules had a range of five orders of magnitude, from $1.0x10^{0}$ to $1.3x10^{-5}$ (Dhajala = 1), compared with a range of $1x10^{1}$ to $1x10^{-2}$ for Dhajala chondrules, (Keck *et al.*, 1986). Fig. 4.18 shows the TL sensitivity plotted against peak temperature and the peak width. Clearly there is no correlation between TL sensitivity and the peak temperature parameters. In contrast chondrules from more equilibrated chondrites, such as Dhajala, show a correlation between TL sensitivity and the other peak parameters; chondrules with higher TL sensitivity tend to have a higher peak temperature and peak width (Sears *et al.*, 1984). The correlation for Dhajala chondrules is due to the effect of thermal metamorphism on feldspar; the high temperature disordered form of feldspar has a higher peak temperature and peak width, as well as higher TL sensitivity. The lack of correlation between TL sensitivity and the peak temperature parameters, of bulk Semarkona and the large range in TL sensitivity of individual chondrules indicates that the Semarkona meteorite has experienced little thermal metamorphism, as already determined by petrography.

Fig. 4.19 shows the peak width versus temperature relationship for the chondrule 'glow' curves. For comparison the fields in which the individual Dhajala chondrules plot are also indicated (Keck *et al.*, 1986). The Dhajala chondrules split into two groups, those with a TL sensitivity > 0.05 plotting in region A and those with a lower TL sensitivity plotting in region B. The Dhajala chondrules that fall in region B show a clear correlation between peak width and peak temperature. Clearly the Semarkona chondrules exhibit a much larger scatter, compared to the Dhajala chondrules with TL sensitivity < 0.05. Furthermore the data for Semarkona chondrules plot do not fall into the two groups shown in fig. 4.19. Chainpur chondrules tend to plot in region B (Sears *et al.* 1991, in prep.), indicating that the low-grade thermal metamorphism experienced by Chainpur (LL3.4) tends to reduce the scatter of the 'glow' curve parameters. The wide range of TL properties for individual chondrules probably reflects the range of chondrule compositions and processes that affected the individual chondrules before accretion, which have then not been heated to high enough temperatures to cause any systematic shift in the original parameters.

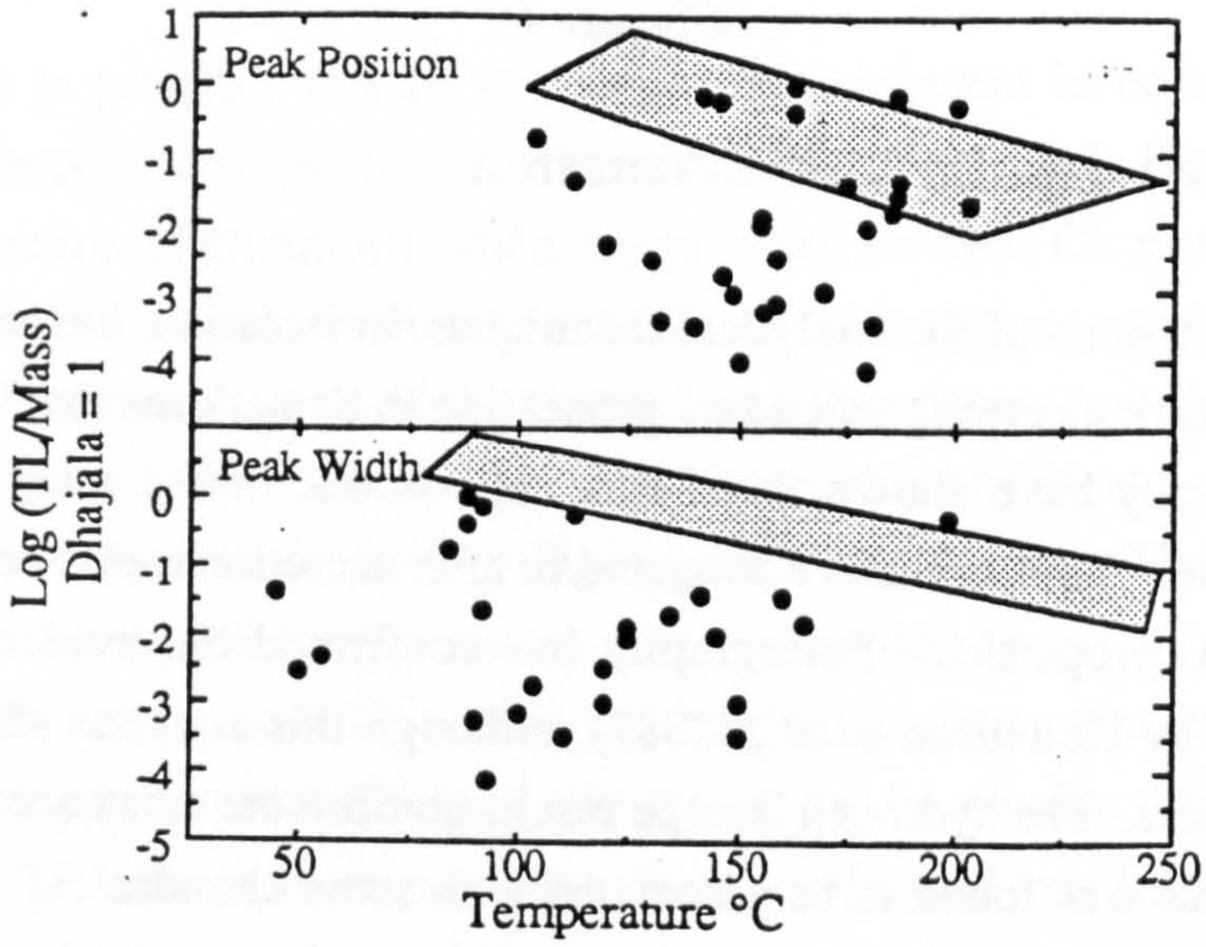

Fig. 4.18 Plot of temperature peak width and temperature of maximum TL sensitivity against TL sensitivity for the Semarkona chondrules. There is no correlation between TL sensitivity and the 'glow' curve parameters indicating that there has not been enough thermal metamorphism to affect the TL of Semarkona. The shaded fields indicate the areas in which the Dhajala chondrules plot.

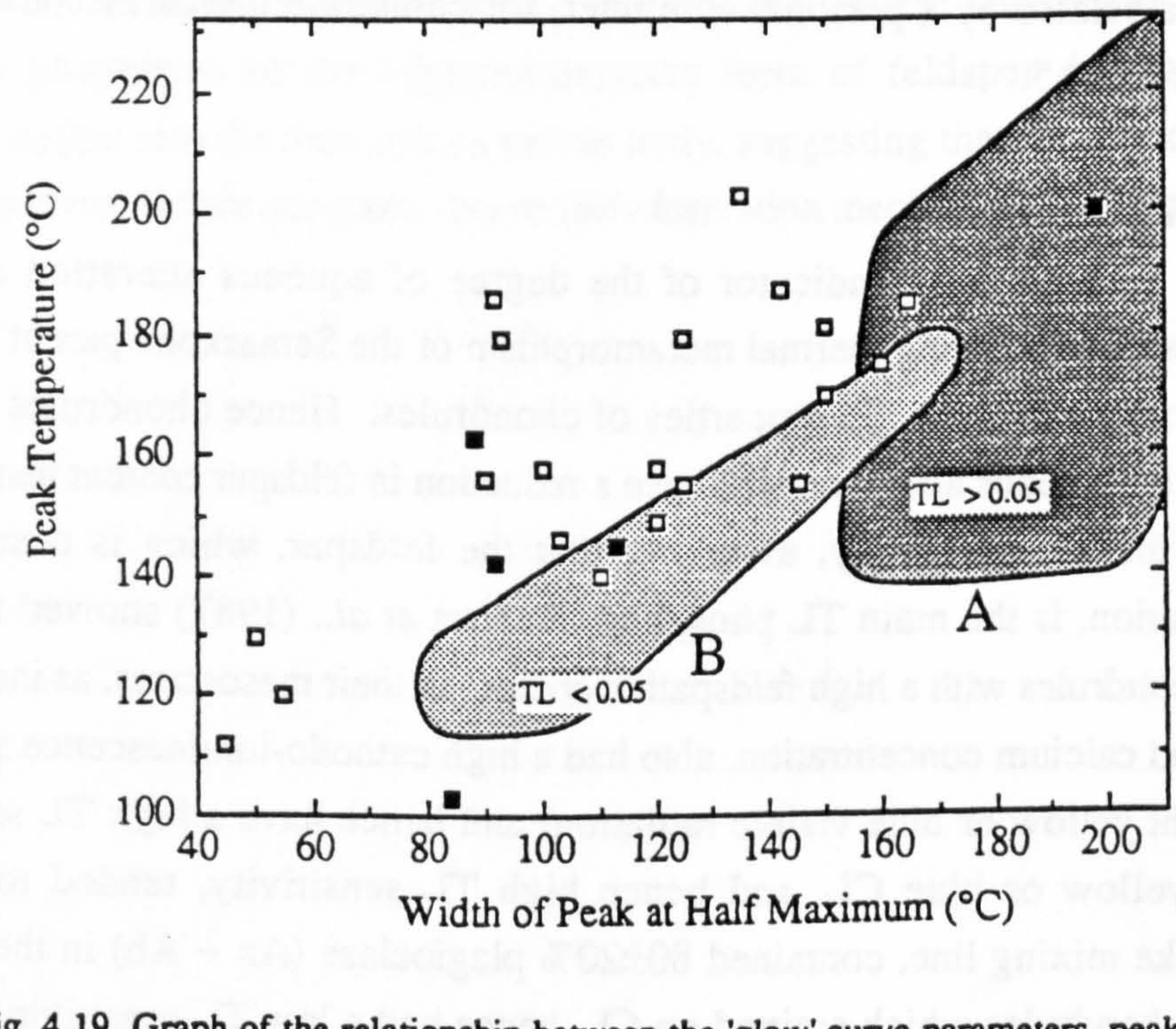

Fig. 4.19 Graph of the relationship between the 'glow' curve parameters, peak temperature against peak width, for the Semarkona chondrules. Semarkona chondrules with TL sensitivity > 0.05 are represented by filled symbols. The shaded fields indicate the regions in which Dhajala chondrules plot; chondrules with TL sensitivity > 0.05 plot in region A and those with TL sensitivity < 0.05 plot in region B. Unlike the Dhajala chondrules there is no relationship between TL sensitivity and the 'glow' curve parameters for Semarkona chondrules

4.4 Combined results and discussion

Results from each of the analytical techniques, in isolation, has not revealed any further information concerning secondary processing in Semarkona than already known. TL and petrography have shown that Semarkona is one of the most unequilibrated ordinary chondrites. Temperatures during and/or after accretion were not high enough to alter primary TL properties. Petrography has confirmed the evidence of aqueous alteration found by Hutchison *et al.*, (1987), although this aqueous alteration did not affect all chondrules. The hydrogen isotope results confirm the existence of a deuterium-rich phase and this was found to be associated with some chondrules. The high water content of the matrix probably means that the matrix contains a second component which was less deuterium enriched. This section discusses various models which could account for these properties in the Semarkona meteorite. When comparing chemical data of chondrules with D/H and TL results, a CIPW normative calculation (described in Cox *et al.*, 1979) on the mesostases of individual chondrules was found to give an insight into possible processes occurring (see below). The results of the CIPW normative calculation, calculated by a personal computer, for chondrule mesostases are given in appendix D, table D.5.

4.4.1 The TL phosphor

TL can be used as an indicator of the degree of aqueous alteration since any temperatures achieved during thermal metamorphism of the Semarkona parent body was too low to greatly affect the TL properties of chondrules. Hence chondrules that have been affected by aqueous alteration will have a reduction in feldspar content resulting in a reduction of the TL sensitivity, assuming that the feldspar, which is destroyed by aqueous alteration, is the main TL phosphor. DeHart *et al.*, (1987) showed that those Semarkona chondrules with a high feldspathic content in their mesostases, as indicated by the sodium and calcium concentration, also had a high cathodo-luminescence sensitivity (emitted bright yellow or blue visible radiation) and hence have a high TL sensitivity. Those with yellow or blue CL, and hence high TL sensitivity, tended to lie on a plagioclase-like mixing line, contained 80±20% plagioclase (An + Ab) in their norms. Whereas the chondrules which emitted no CL, hence had a low TL sensitivity, had low concentrations of sodium and calcium. A graph of CaO against Na_2O for the mesostasis of Semarkona chondrules extracted in this study is shown in fig. 4.20, along with the fields indicating CL properties as determined by DeHart *et al.* (1987). In fig. 4.20 very few chondrules lie in the plagioclase normative field, 8 out of 29 compared with 15 out of 22 for DeHart *et al.*, (1987).In this study most chondrules plot in the dark field and there are many that lie between these two fields. The difference in the numbers of chondrules

in each field is probably due to selection effects inherent in both studies. Possible selection effects in this study were discussed in section 4.3.1. Dehart *et al.*, (1987) choose a selection of chondrules for analysis based on their CL properties (Sears pers. comm.), hence chondrules which were not CL sensitive were not analysed.

Fig. 4.21 shows the sum of the plagioclase components (Anorthite + Albite) versus TL sensitivity and, for comparison also shows the bright and dark CL fields as determined by DeHart et al., (1987). If plagioclase was the main TL phosphor then most of the chondrules would be expected to plot in the shaded region, *i.e.* there would be a positive correlation between TL sensitivity and plagioclase content. Although half of the chondrules do plot in shaded region, the remainder lie outside this field. This is not because the TL and element analyses being performed on different parts of each chondrule since in this case some chondrules would be expected to have low TL sensitivity and high plagioclase content in their CIPW norm, which is not observed. Instead this could indicate that these chondrules contain some other TL phosphor instead of feldspar. Other minerals which have a high TL sensitivity include quartz and orthoclase. However, it was not possible to determine the composition of this other TL phosphor (graphs of other normative components and element concentrations against TL sensitivity revealed no correlations). Alternatively these chondrules could contain a greater proportion of the high-temperature form of feldspar due to heating before incorporation into the Semarkona parent body, suggesting that all chondrules had a high TL sensitivity before accretion due to their formation mechanism (*i.e.* a primary process).

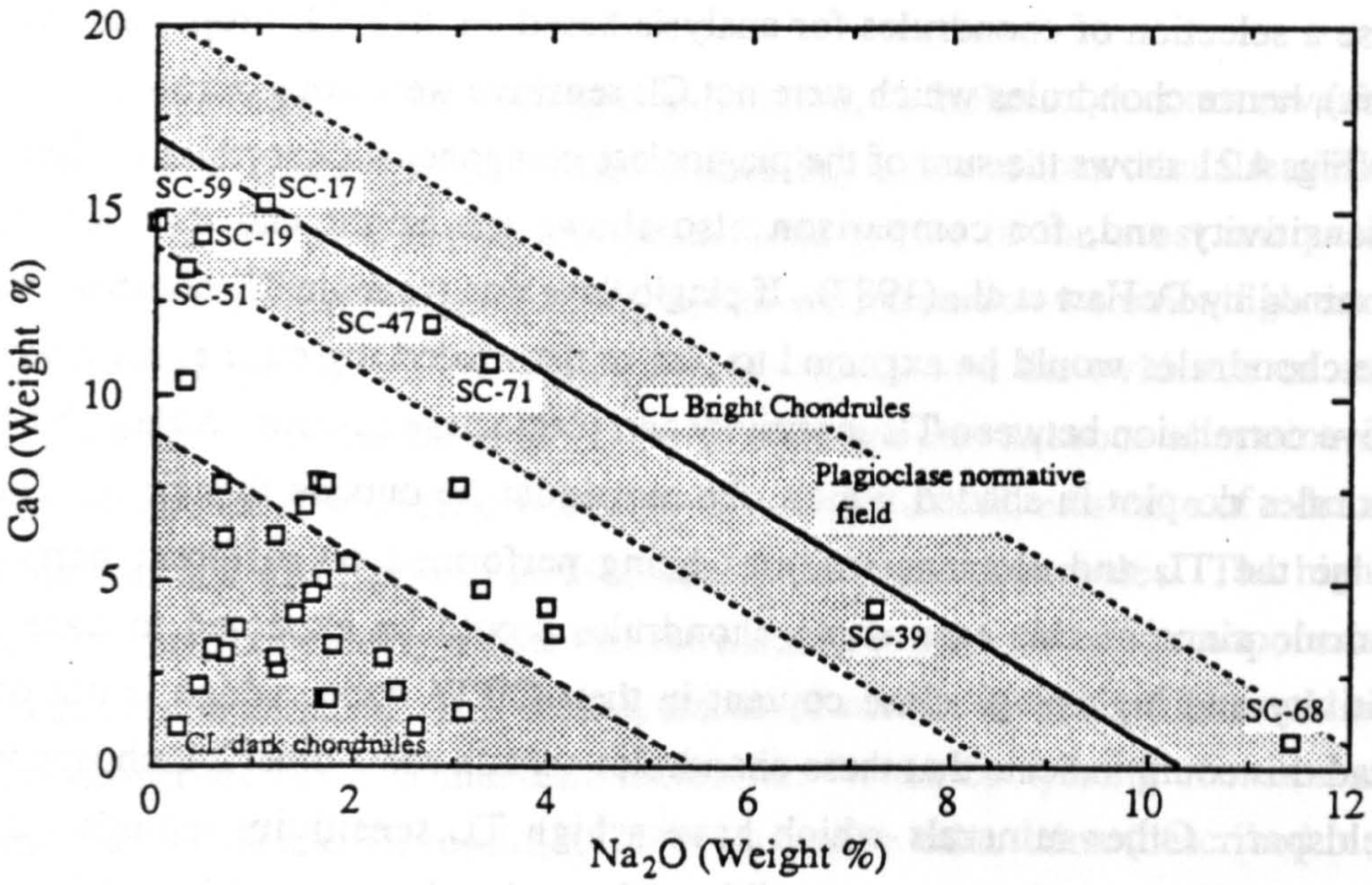

Fig. 4.20 Plot of calcium against sodium content for the mesostasis of the Semarkona chondrules. DeHart et al., (1987) found that chondrules which lie in the plagioclase normative region have high CL and TL properties whereas other chondrules have no CL properties and low TL sensitivity, indicating that feldspar is the dominant phosphor in Semarkona chondrules.

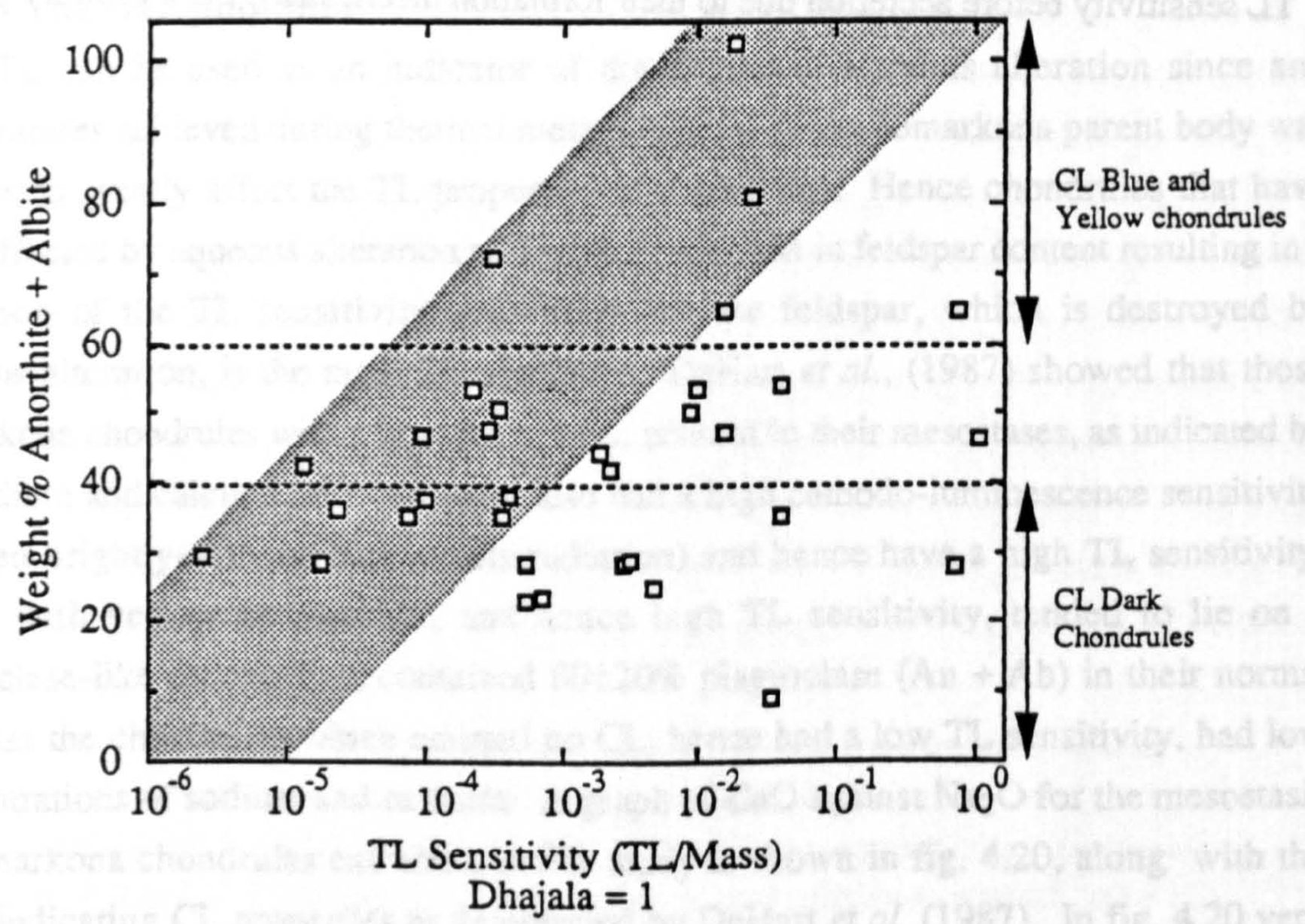

Fig. 4.21 Graph of plagioclase content against TL sensitivity. The shaded region indicates the expected field for the Semarkona chondrules if feldspar was the dominant phosphor. Many chondrules are outside this field indicating the possibility of some other TL phosphor.

4.4.2 Origin of the deuterium-rich component

The D/H isotope results from the various Semarkona fragments indicate that Semarkona contains a deuterium-rich component that pyrolyses between 200-1100°C, confirming the results from previous studies (McNaughton *et al.*, 1982a,b; Yang and Epstein, 1983). Although the experimental technique only collected water released upon pyrolysis, the deuterium-rich component may not necessarily be water in the Semarkona meteorite. Three possibilities exist:-

i) Water is released from the hydrous minerals, the product of aqueous alteration on the meteorite parent body (Hutchison *et al.*, 1987).

ii) Water is released from organic molecules due to pyrolysis/thermal degradation and/or combustion, oxygen being obtained from silicates during the high temperature step, or possibly some from the organic material itself.

iii) Deuterium is present within organic molecules but the water released originates from hydrous minerals, isotopic exchange between the organic material and the water could result in a deuterium enrichment of the water. Although this is unlikely since any water released was rapidly removed from the vicinity of the sample by cryogenic trapping during analysis.

The first option implies that water from the episode of aqueous alteration was deuterium-rich. Hence the water was of extra-terrestrial origin and aqueous alteration was not caused by terrestrial weathering. The other two possibilities indicate that organic materials are the source of the deuterium enrichment in the meteorite but involve different methods by which the deuterium-rich water released during analysis can be obtained from the organics. The occurrence of deuterium enrichments in organic material in carbonaceous chondrites has been well documented (*e.g.* Briggs 1963; Smith and Rigby 1981; Becker and Epstein 1982). The presence of organic material in unequilibrated type 3 ordinary chondrites has been inferred by comparison of the hydrogen isotope composition with carbonaceous chondrites (Yang and Epstein 1982; Robert *et al.*, 1987a,b). Further evidence has been provided by comparison between carbon and nitrogen release profiles and isotopic composition of carbonaceous and ordinary chondrites (Alexander *et al.*, 1988; Alexander *et al.*, 1989a). The observation that the deuterium-rich component is released over a range of temperatures (see 4.3.2), which varied between chondrules, tends to indicate that it is not a simple single component but a heterogeneous mixture of components. Hence the results from section 4.3.2 tend to agree with other workers that the deuterium-rich component is organic.

This section describes possible models for the origin of deuterium-rich material in Semarkona and other unequilibrated ordinary chondrites. Section 4.4.3 describes models by which the deuterium enrichment became associated with chondrules.

Irradiation of the early solar system

Robert *et al.*, (1979) considered the possibility that the deuterium enrichment in whole-rock Chainpur could be a result of production of deuterium by spallation. Indeed this model would readily explain the deuterium enrichment associated with the chondrules. Some of the mechanisms of chondrule formation (discussed in section 1.6.1) involve an energetic T-Tauri phase for the sun, hence the possibility of high irradiation of chondrules during their formation. It is assumed that matrix material, was not involved in the chondrule forming regions and so would not have been irradiated to such an extent. However if matrix material was precursor chondrule material that survived the chondrule formation or was produced by chondrule fragmentation then matrix material would show similar deuterium enrichments. Also Geiss and Reeves (1981) showed that spallation would lead to an excess of the rare light element isotopes ^{7}Li, ^{9}Be and ^{11}B (discussed in section 1.2.4), which has not been observed. By consideration of spallation products Geiss and Reeves (1981) also showed that the deuterium enrichment could not even be formed, as a result of spallation, on grains before incorporation into the solar system and subsequently meteorites.

Mass fractionation of hydrogen during chondrule formation

Robert *et al.*, (1987a) suggested that since chondrules were heated to high temperatures for only a few seconds during their formation then a large fraction of hydrogen in the chondrule precursor material would be vaporised resulting in large mass fractionation and hence deuterium enrichment of hydrogen in the chondrules. As for the irradiation model above, this would readily explain the reason why the deuterium enrichment is associated with chondrules. However, Robert *et al.*, (1987a) reasoned that other volatile elements, such as carbon and nitrogen, should show similar isotopic enrichments which was not observed.

Chemical equilibrium of water with hydrogen in the solar nebula

Chemical fractionation between hydrogen and water results in a deuterium enrichment in the water, the amount of the enrichment depends on the temperature of equilibration (discussed in section 1.3.2). A similar enrichment occurs between hydrogen and other hydrogen containing molecules. To obtain water (or organic molecules), with a D/H ratio 100 times greater than the D/H ratio of cosmic hydrogen requires the water to equilibrate with the hydrogen at a temperature of 100K. However, as described in chapter 1, the δD value of water throughout the solar system shortly after formation was probably about -100‰. The water attained its deuterium enrichment, relative to cosmic hydrogen (δD ca. -900‰), by chemical equilibrium between hydrogen and water at a temperature of about 260K (Richet *et al.*, 1977). The water could attain an

even larger enrichment by chemical equilibrium between water and hydrogen at lower temperatures, however Hayatsu and Anders (1981) concluded that the temperature of the solar nebula, as indicated by other 'cosmothermometers', was probably about 360K, leading to a δD value of *ca.* -600‰.

Deuterium enrichment by ion-molecule reactions

Geiss and Reeves, (1981) concluded that isotopic enrichment of organic molecules by ion molecule reactions, in giant molecular clouds, at low temperature was the most likely method of producing the deuterium enrichments observed in carbonaceous and ordinary chondrites (see section 1.3.3). Astronomical studies of giant molecular clouds have detected organic molecules with D/H ratios as high as 0.045, δD = +290 000‰ (Millar *et al.*, 1989 and references therein).

If the deuterium-rich component is interstellar organic material then it has survived solar nebula processing and subsequent secondary processing. This component would then be another pre-solar component, along with the interstellar diamonds and silicon carbide grains (Anders *et al.*, 1989; Ash, 1990). However, this and other studies have not measured the extremely high D/H ratios detected in interstellar molecules. Either the deuterium ratio has been diluted by solar nebula and secondary processes or this component is poorly resolved from another phase with a lower D/H ratio.

4.4.3 Association of the deuterium-rich component with chondrules

The hydrogen isotope results showed that many chondrules released water enriched in deuterium (δD up to +7500‰). Robert *et al.*, (1987a) obtained similar results for hydrogen isotopes in separates of Chainpur (LL3.4). The deuterium rich component (δD *ca.* +5500‰ pyrolysed between 800 - 1000°C), thought to be organic, was found to be associated with the Chainpur chondrules rather than the matrix, although the matrix did contain some of the deuterium-rich component. By analysis of different chondrule fractions this deuterium-rich component was found to be concentrated in the chondrule rims compared to the chondrules themselves. Further investigation (Robert *et al.*, 1987b) revealed that this component is common to all unequilibrated ordinary chondrites studied and the existence of a deuterium-depleted component (δD *ca.* -400‰ released between 400°C to 600°C), as well as the deuterium-rich component, in the matrix. Robert *et al.*, (1987b) were not able to identify the nature of this deuterium-depleted component but it was thought that some carbonaceous phase was the most likely source. The hydrogen isotope results from this study show that Semarkona also has a deuterium rich component associated with the chondrules. Although no evidence of a deuterium-depleted component was found in the matrix this could be due to contamination of the deuterium-depleted component by the deuterium-rich component (either the presence of small deuterium-rich chondrules or the temperature step size used in this study were too large). The advantage with this study was that petrological, chemical and TL properties were also determined for chondrules analysed, which can help constrain various models (discussed below) of how the deuterium-rich component became associated with chondrules.

Deuterium-rich component acquired before accretion

Clearly if the deuterium-rich component was acquired by the chondrules before accretion then they would be enriched in deuterium relative to the matrix. There are two methods by which this may occur:

i) aqueous alteration of chondrules in the solar nebula, by deuterium-rich water,

ii) chondrules becoming coated by deuterium-rich organics.

Both of these options assume that matrix material and chondrules originated from different parts of the solar nebula. The presence of a deuterium depleted component present in Chainpur matrix as well as the deuterium-rich component requires the separation of organic components in the solar nebula upon their D/H ratio so that only the deuterium-rich organics coated the chondrules, this was considered unlikely by Robert *et al.*, (1987a; 1987b). Also, a petrographic study of type 3 ordinary chondrite matrix by Alexander *et al.*, (1989b) indicated that at least 97% of the matrix is fragmented chondrule material. Hutchison *et al.*, (1987) deduced that petrographic evidence for aqueous

alteration showed that this had occurred on the Semarkona meteorite parent body rather than in the solar nebula.

Deuterium-rich component acquired by accretion

Robert *et al.*, (1987 a) postulated that both the deuterium-rich and deuterium-depleted organic components were present in the matrix material of unequilibrated ordinary chondrites. During accretion, impact of chondrules caused local vaporisation of the deuterium-depleted component, which has a lower release temperature than the deuterium-rich component. Hence material on the surface of chondrules became deuterium rich. Isotope results from this study show that some chondrules were not enriched in deuterium relative to the matrix, however the amount of enrichment varied between chondrules. The size of the deuterium enrichment associated with each chondrule will depend on several factors:-

i) Mass and velocity at which each chondrule accreted onto the meteorite parent body. Chondrules with higher mass and those which accreted at higher velocity would produce a greater amount of heating during their impact onto the parent body. Higher temperatures would vaporise more of the deuterium-depleted component, however, if the temperature is too high then the deuterium-rich component would also be vaporised.

ii) The material in which each chondrule impacted. Chondrules that impacted onto matrix would acquire the deuterium-rich coating, those that impacted onto other chondrules would acquire no coating at all.

Clearly these factors would be independent of the effects of aqueous alteration, which occurred after accretion.

Deuterium-rich component acquired by aqueous alteration

Organic material in C1 and C2 chondrites contains a high deuterium enrichment and these meteorites have also experienced aqueous alteration. The preservation of the deuterium enrichment could be due to the lack of thermal metamorphism which would drive off any deuterium-rich water and organic material. Alternatively it is possible that aqueous alteration brought about the deuterium enrichment observed. Possible models which would produce the effects observed are:-

i) The water that caused aqueous alteration could be deuterium-rich (Hutchison *et al.*, 1987). However, as described above water that accreted with the parent body probably had a δD *ca.* -100‰. Alternatively the water that caused aqueous alteration may have been produced by the breakdown of deuterium-rich organic material due to thermal metamorphism. There would need to be a second aqueous phase (either on the parent body or terrestrial weathering), with δD *ca.* 0‰, which then reduced the deuterium concentration of the water in the matrix. It is possible that this could have happened

following the meteorite's fall to Earth since the matrix is more porous than the chondrules, hence able to absorb more atmospheric water. Stepped heating results indicate that this second aqueous alteration phase occurred at lower temperature than the first since the water with δD *ca.* 0‰ was released at a lower temperature.

ii) Deuterium rich organic material was transported by fluids to the sites of aqueous alteration. The mobile water phase could, in principle, have any δD although a normal δD of about 0‰ is most likely. Continued aqueous alteration of the matrix, or terrestrial contamination, could result in a reduction of its average δD.

In both these cases there should be a positive correlation between the deuterium enrichment and the degree of aqueous alteration effects observed in chondrules. Differences between cases (i) and (ii) could be distinguished by determining whether the organic material, if any, was enriched in deuterium. Most hydrogen isotope studies of Semarkona and some other unequilibrated ordinary chondrites have inferred the presence of deuterium-rich organics in these meteorites (see section 1.5.3) which would tend to indicate the second possibility. Bunch and Chang, (1980) suggested that organic compounds in C1 and C2 carbonaceous chondrites may have been synthesised by Fischer-Tropsch-Type (FTT) reactions during aqueous alteration. If deuterium-rich pre-solar organic compounds were already present then these would form more complex molecules similar to the products formed by extened FTT reactions (Anders, 1973).

4.4.4 Evidence for deuterium enrichment caused by aqueous alteration?

As discussed above results from this study should be able to determine whether the deuterium enrichment of chondrules resulted from their accretion or from aqueous alteration. If caused by aqueous alteration then the δD of chondrules will correlate with the degree of alteration. The effects of aqueous alteration are:-

i) destruction of feldspar, hence reduction in TL sensitivity

ii) leaching of calcium and sodium (Pearce, 1975)

iii) addition of iron, from the matrix (Hutchison *et al.*, 1987)

Each of these effects and relationship with δD is discussed in turn.

A graph of δD against TL sensitivity for Semarkona chondrules is shown in fig. 4.22a. It should be pointed out that any trend would tend to be obscured since the TL properties of chondrules are affected by their composition as well as their secondary processing history. Fig.4.22a shows that there is a correlation between TL sensitivity and δD, the best fit line has a correlation co-efficient of only 0.367, which is just significant at the 95% level. However this trend may be obscured by some chondrules which had a naturally low TL sensitivity when incorporated into the Semarkona body but were not affected by aqueous alteration would plot in the lower left of fig. 4.22a, this could be the reason chondrules such as chondrules SC-06 and SC-71 do not lie close to

the best fit line of fig.22a. Also the reduction of TL sensitivity by aqueous alteration assumes that the dominant phosphor is feldspar which may not be the case for many of the chondrules (see section 4.4.1). The notes made as each chondrule was extracted show that the two chondrules which plot in the lower left of fig. 4.22a. had matrix material attached. Although attempts were made to remove matrix material, contamination could have resulted in a low measured δD for these chondrules. The chondrules that may have been contaminated by matrix, as indicated by the notes made during the extraction procedure, (appendix D, table D.1) are shown by filled squares in fig. 4.22a. Fig. 4.22b shows a graph of δD against TL sensitivity where all (five) chondrules that may have been affected by matrix contamination have been removed. The best fit line of fig. 4.22b has a much better correlation coefficient of 0.599 which is significant at the 99.5% level. Thus it does appear that the degree of aqueous alteration is in some way related to δD.

It should be possible to assess the degree of aqueous alteration by looking at major element chemistry since sodium and calcium tend to be more mobile and removed by aqueous alteration relative to aluminium which is non-mobile under aqueous alteration conditions (Pearce, 1975). For the study herein there was no correlation of calcium and sodium content of chondrules with δD. However, it should be noted that the initial composition of chondrules will exhibit a range of sodium and calcium contents. Since aluminium is non-mobile, its presence in excess of that required for feldspar, *i.e.* the corundum (Al_2O_3) concentration in the CIPW norm, can be used as an indication of the amount of aqueous alteration. Fig 4.23 is a plot of the δD of water released by chondrules during the high-temperature step against the corundum in the CIPW norm. Those chondrules with a high corundum content tended to have a high δD, however those chondrules with no corundum in the CIPW norm had a range of δD values which could represent an excess of calcium and sodium in the norm before alteration. The best fit line of fig. 4.23 for all the chondrules is 0.513 which is significant at 95% level.

Perhaps the best indicator of *in situ* aqueous alteration is the degree of transfer of iron from the matrix to the mesostasis of chondrules (Hutchison *et al.*, 1987). The concentration of iron in chondrule mesostasis versus δD of water released during the high-temperature step is shown in fig. 4.24. Apart from chondrule SC-49 (which contained too little water to measure the δD with any confidence, see section 4.3.3) there is a correlation (r = 0.467, significant at 95% level) between iron concentration and δD of the water released. If SC-49 is included then there is no correlation between iron concentration and δD. However any trend is probably obscured by the initial iron concentration of each chondrule when formed. A better indication of degree of aqueous alteration, compensating for initial iron concentration is probably Fe/(Fe+Mg). Fig. 4.25 is a plot of δD against Fe/(Fe+Mg). Grossman *et al.*, (1988) indicate that Fe/(Fe+Mg) usually ranges from 0 to 0.35, hence values higher than this could be an indication of

aqueous alteration. The correlation (r = 0.576, significant at 99% level) between the effects of aqueous alteration and δD of the chondrules suggests that the water that caused the aqueous alteration had a high δD or was a carrier of a deuterium rich component to the sites of aqueous alteration.

Alternatively the correlation in fig. 4.25 could be showing that the deuterium-rich phase is concentrated in the outer portions of chondrules, since the iron to magnesium ratio increases towards the edge of chondrules (Dodd, 1981). However, it is unlikely that this is the case since petrologic and D/H isotope analyses of chondrules were performed on different and large fragments of chondrules.

Another factor that could be an indication of aqueous alteration is the physical properties of the chondrules. Yang and Epstein, (1982) found that the greatest deuterium enrichment in Semarkona was found for the fines, *i.e.* grains which had fallen from the bulk meteorite during storage. It was noted in section 4.3.1 that there was possibly a selection effect in the study herein in that the most friable material may not have been extracted for analysis. As was suggested in section 4.3.1, the graph of δD against chondrule number (fig.4.17) may indicate that the more friable chondrules, possibly those that had been affected by aqueous alteration, had the greatest deuterium enrichments.

4.4.5 Origin of water with low D/H ratio

Some of the chondrules analysed released water above blank levels which was not deuterium enriched. This water had a normal terrestrial D/H ratio and was mostly released below 400°C and so no distinction can be made whether this phase was indigenous to the meteorite or the result of terrestrial contamination. This water with a low, terrestrial, D/H ratio was not involved in aqueous alteration; there was no evidence of the effects of aqueous alteration correlating with the quantity of water released by chondrules during either the low or high temperature step. If the water with low D/H ratio was indigenous to the meteorite then it was acquired after the deuterium-rich component (otherwise it would have been involved with aqueous alteration) and at a lower temperature, as indicated by the lower release temperature upon pyrolysis. As the matrix is more porous than chondrules it would be more easily affected by the second aqueous phase at low temperature resulting in a dilution of the deuterium-rich phase in the matrix.

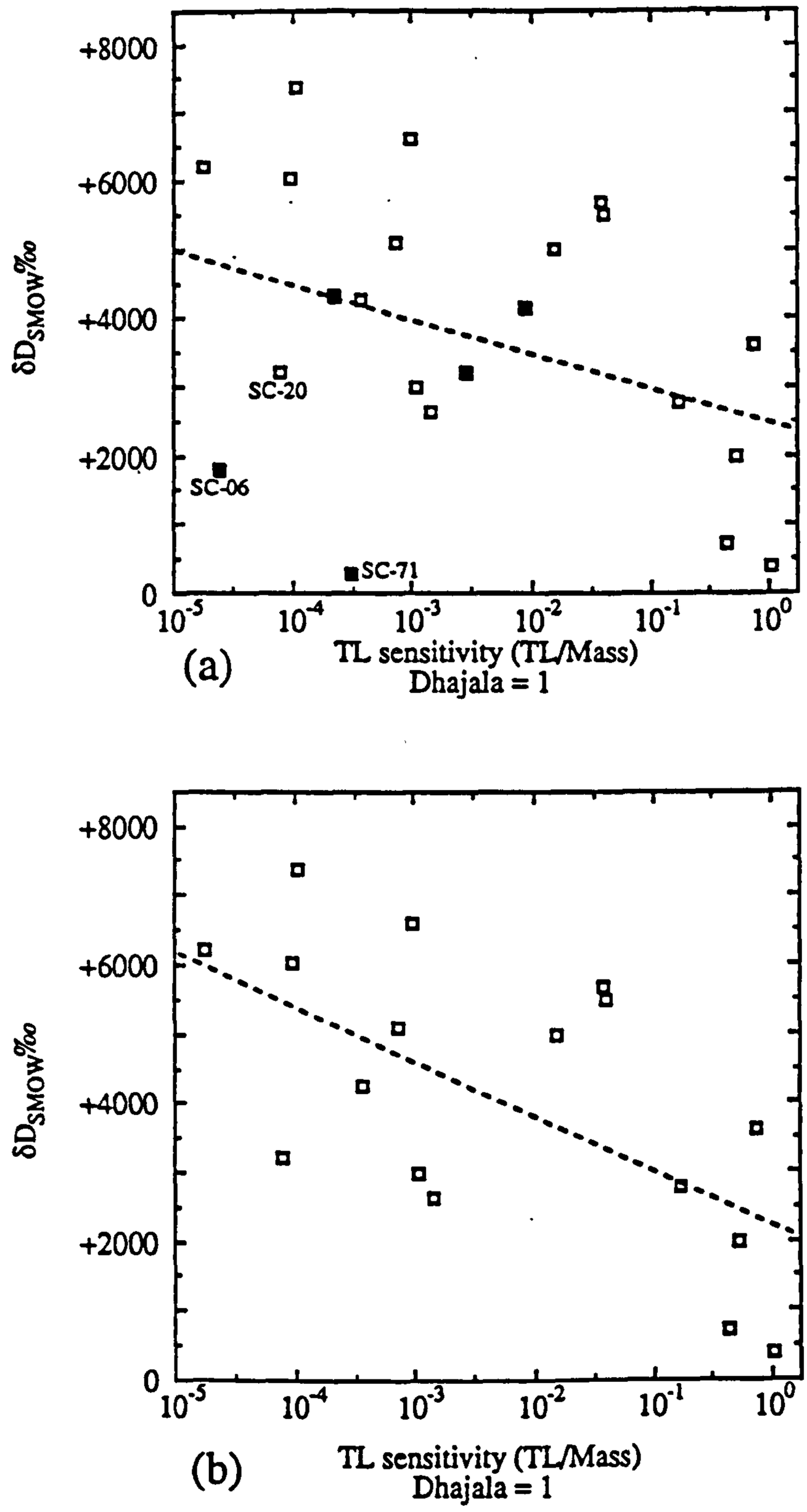

Fig. 4.22 Graphs of δD against TL sensitivity for Semarkona chondrules. a) All chondrules are plotted, those which may be contaminated by matrix are shown as filled squares. The best fit line has equation y = 2510 - 500x, with r = 0.367 which is only just significant at the 95% level. b) Chondrules which may be contaminated by matrix have been removed. The best fit line has equation y = 2180 - 800x, with r = 0.599, significant at the 99.5% level. Both graphs indicate those chondrules that have had their TL sensitivity reduced by aqueous alteration are enriched in deuterium.

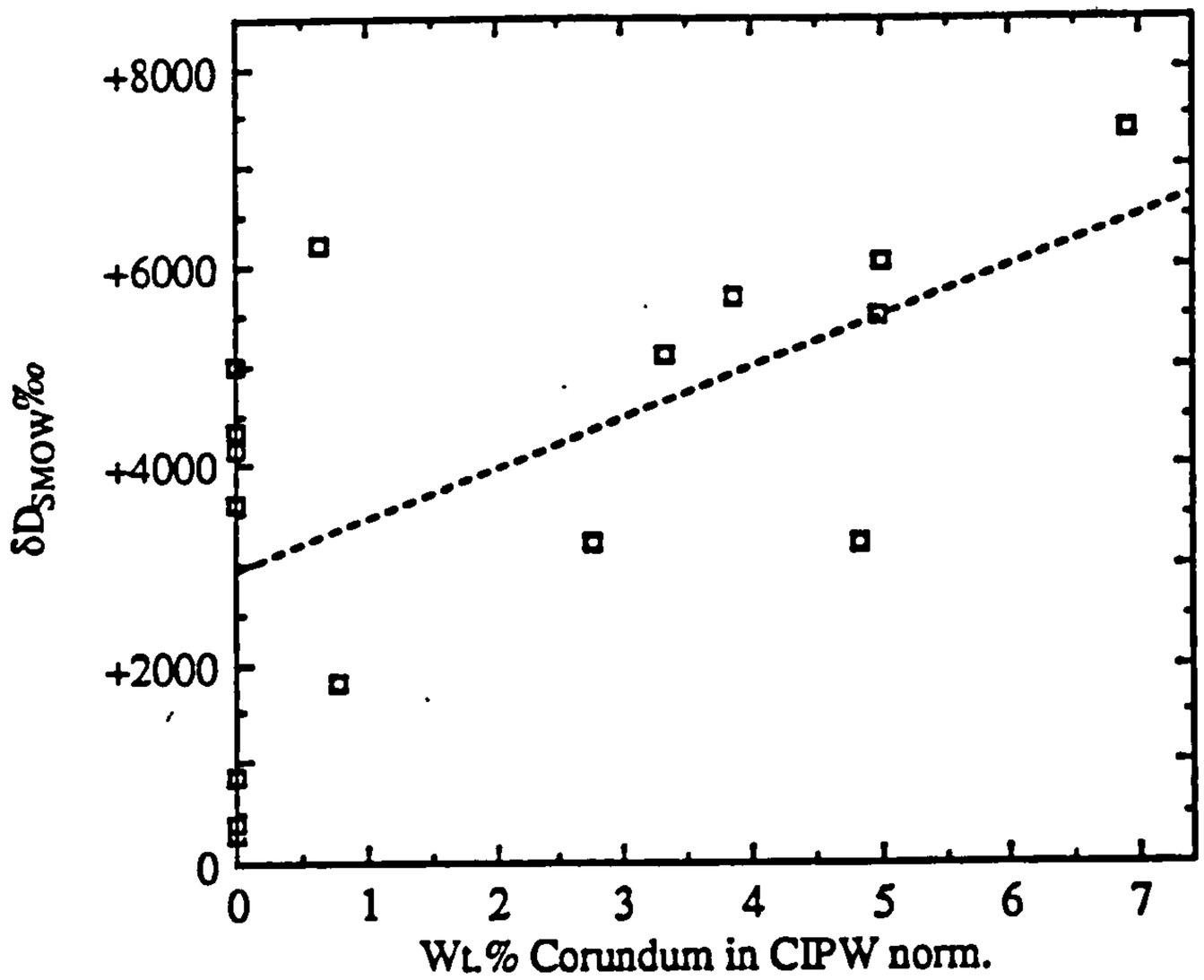

Fig. 4.23 Graph of δD against corundum content in the mesostasis of Semarkona chondrules. The best fit line has equation y = 2940 + 514x, with correlation coefficient r = 0.583, significant at the 95% level.

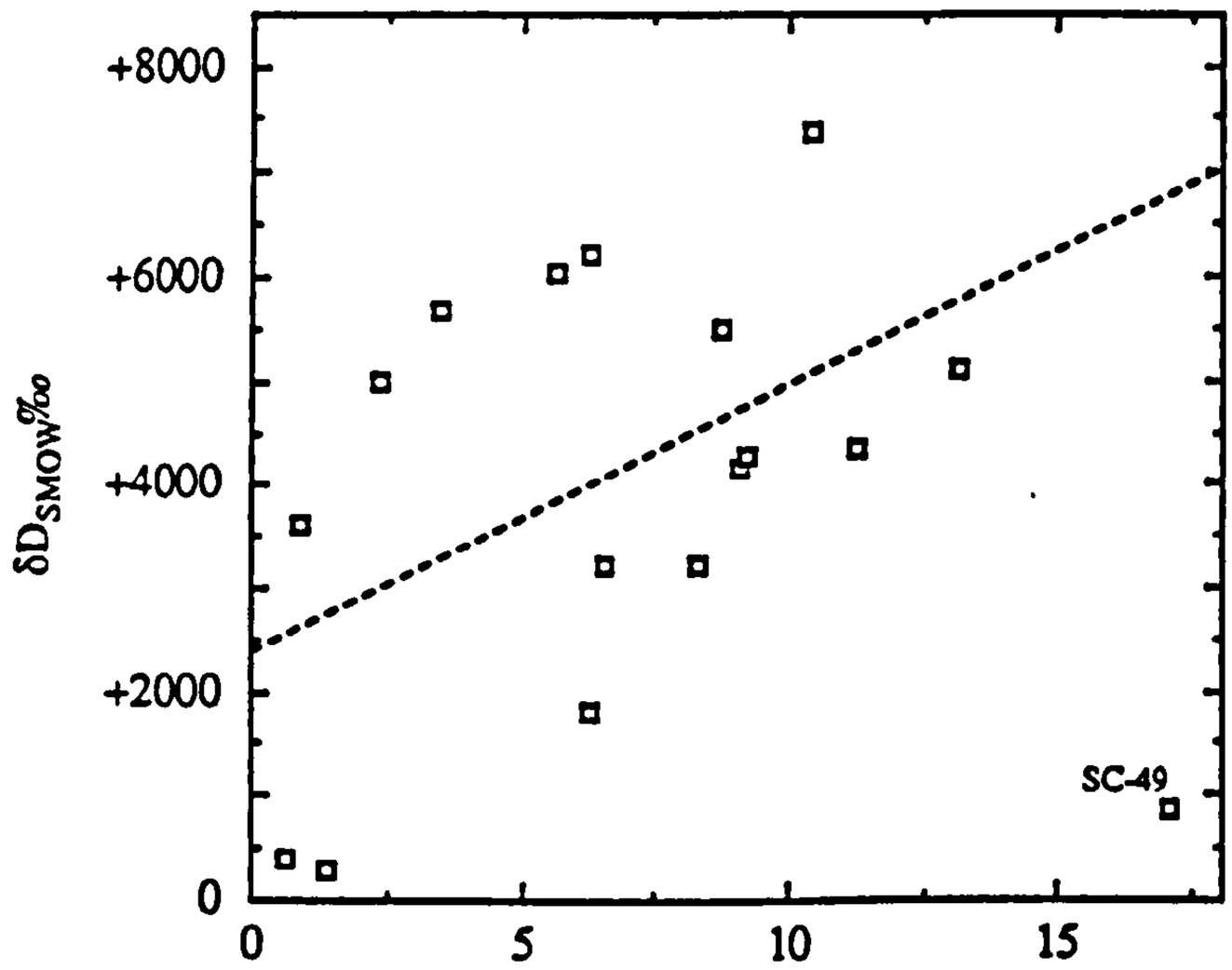

Fig. 4.24 Graph of δD against iron content in the mesostasis of Semarkona chondrules. The best fit line through all points has a correlation coefficient, r = 0.158 which is not significant at 95% level. The best fit line through all points except SC-49 (which had too low a water content to measure the δD) has equation y = 2400 + 252x, with correlation coefficient r = 0.467, significant at the 95% level.

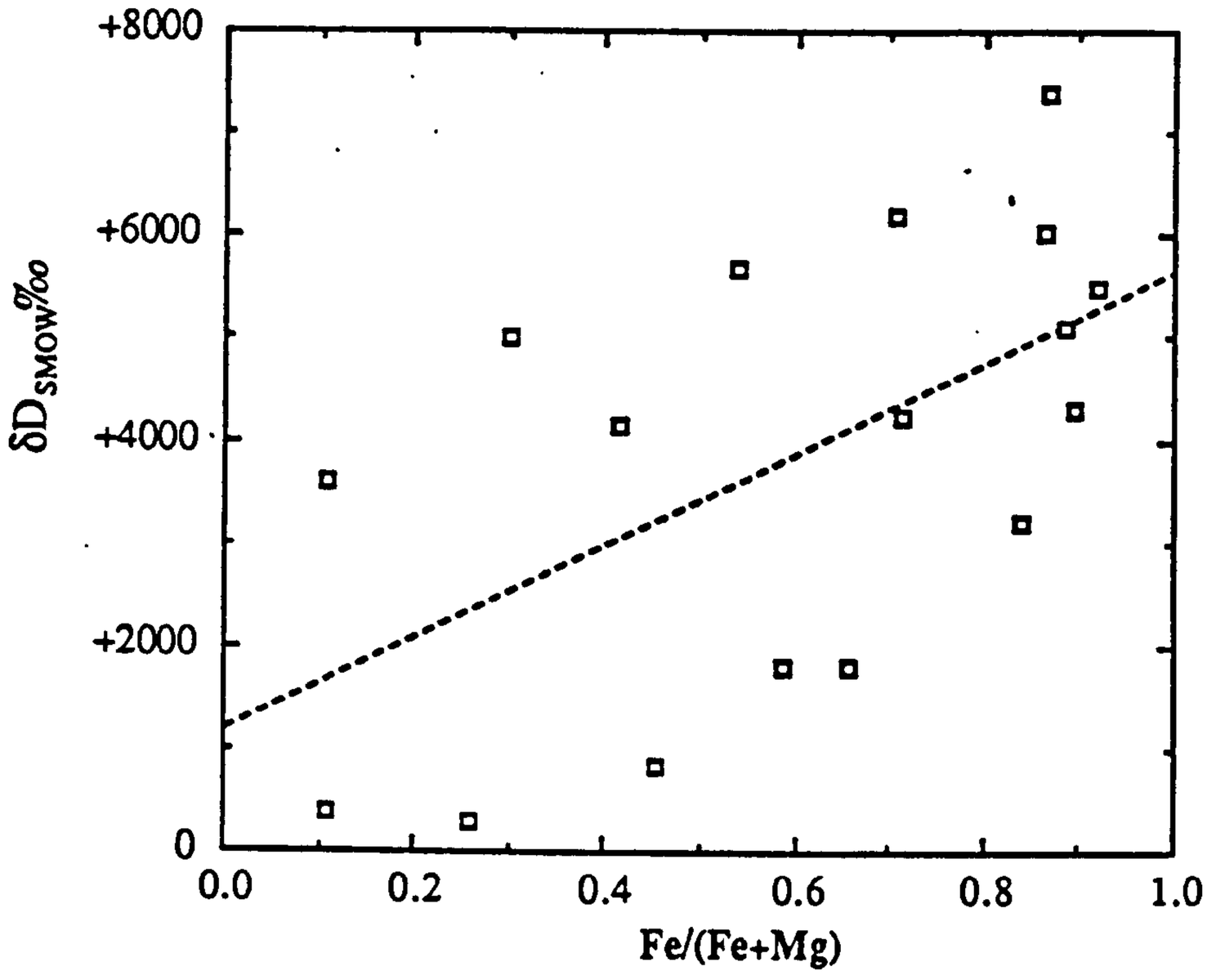

Fig. 4.25 Graph of δD against Fe/(Fe+Mg) ratio in the mesostasis of Semarkona chondrules. The best fit line through all points has equation y = 1190 + 4500x, with correlation coefficient r = 0.576, significant at the 99% level.

4.5 Conclusions and further work

The work described here used three very different analytical techniques (thermoluminescence, D/H isotopes and chemical/petrographic) combined together to enable a detailed study of the Semarkona meteorite. Each analytical technique in isolation was not able to determine the sequence and effects of secondary processing but a combination allows a greater insight than previously obtained.

Chemical and petrographic analysis showed that a few chondrules had experienced the effects of aqueous alteration confirming the results of Hutchison *et al.*, (1987). These effects were not as evident as expected, probably because of different selection effects between the two studies. Chemical analysis also showed the unequilibrated nature of the Semarkona meteorite, as determined by Dodd *et al.* (1967), hence indicating that little thermal metamorphism had occurred since its accretion, temperatures < 400°C.

The TL results confirmed the heterogeneous nature of Semarkona and that any thermal metamorphism that had occurred on the meteorite parent body had been too little to affect feldspar structure, *i.e.* temperature < 450°C. Whether the low TL sensitivity of Semarkona was due to the effects of aqueous alteration, or a lack of thermal metamorphism, could not be determined.

D/H results confirmed the presence of a deuterium-rich component that pyrolysed between 200 - 1100°C with a measured δD of +7500‰. Although this is the highest δD value measured for Semarkona it is not significantly greater than measured δD values obtained previously, and the actual δD value of this component is probably much greater. The deuterium-rich component tends to be concentrated in chondrules, rather than matrix, although not all chondrules contained the deuterium-rich component. This is similar to the results of Robert *et al.* (1979) and Robert *et al.* (1987a) who found that the deuterium-rich component in Chainpur was also concentrated in chondrules, especially chondrule rims, rather than in the matrix. There was no evidence for a deuterium-depleted component in Semarkona, as has been detected in other unequilibrated ordinary chondrites (Robert *et al.*, 1987b), however this could result from the large temperature increments required in this study.

D/H isotope studies on carbonaceous chondrites have concluded that the deuterium-rich phase is an organic material. D/H isotope studies have shown the existence of a deuterium-rich phase in ordinary chondrites and, by analogy to carbonaceous chondrites, inferred that this phase is organic material; although, to date, extra-terrestrial organic material has not been detected in ordinary chondrites. The most plausible method of obtaining such high deuterium enrichment was by the formation of organic molecules by ion-molecule reactions in a large molecular cloud, before incorporation into the solar nebula (Geiss and Reeves, 1981). The temperature increments used in this study for the

D/H analysis were too large to determine the nature of the deuterium-rich phase, however the high pyrolysis temperature of the deuterium-rich phase is consistent with it being an organic material.

The advantage with this study was that the results from each individual technique could be compared with those from other techniques. The chemical and petrographic analysis on the various fragments was used to gain an insight to what was actually analysed by TL or D/H analysis. Chemical and TL analysis indicated that one of the main TL phosphors was indeed feldspar. However, since Semarkona has such a low TL sensitivity, at least one other phosphor was present, although the nature of this phosphor could not be determined.

There was some evidence of a correlation between the degree of aqueous alteration, as determined by chemical analysis, and the deuterium enrichment of individual chondrules. This was most notably in the correlations between δD and Fe/(Fe+Mg) ratio (fig. 4.25) of the chondrules. However this evidence is certainly not conclusive, the correlation between corundum content and δD was only just significant at the 95% level and there was no correlation between calcium or sodium content versus δD. Since the TL sensitivity of chondrules was partly due to the feldspar content then the TL sensitivity could be used as a crude indicator to the degree of aqueous alteration experienced by individual chondrules and indeed, there was a correlation between the TL sensitivity and δD of chondrules.

The deuterium enrichment of chondrules that have experienced aqueous alteration can be accomplished by:-

i) The alteration being achieved by deuterium rich water. The water may have become enriched in deuterium by isotopic exchange with deuterium-rich organics or from the thermal degradation of deuterium-rich organics.

ii) Water transporting deuterium rich organics to the sites of aqueous alteration. Water and deuterium-rich organics being evolved from the region of thermal metamorphism in a layered type parent body.

A study of other primitive ordinary chondrites that have had different degrees of thermal and aqueous processing may help determine the sequence and amount of secondary processes that have affected ordinary chondrites. Also a more detailed investigation of the deuterium-rich component may provide links between ordinary and carbonaceous chondrites. Bunch and Chang (1980) suggested that carbonaceous organics could have been formed by Fischer-Tropsch-Type reactions in the meteorite parent body during aqueous alteration catalysed by phyllosilicate minerals. In which case deuterium-rich organics formed originally in the pre-solar molecular clouds by ion-molecule reactions would have their high D/H ratio diluted. Meteorites such as

Meteorite	Petrologic Type	Wt% Water	Whole-rock δD ‰	Reference
Semarkona	LL 3.0	0.34	+2904	McNaughton *et al.*, (1981)
		0.34	+2350	This work
Krymka	LL 3.0-2	N.D.	+54	McNaughton *et al.*, (1981)
Bishunpur	LL 3.1	0.29	+1101	McNaughton *et al.*, (1981)
		0.81	+286	Robert *et al.*, (1987a)
Chainpur	LL 3.4	0.35	+160	Robert *et al.*, (1979)
		0.26	+58	Robert *et al.*, (1987a)

Table 4.2 Comparison of the δD and water content between unequilibrated ordinary chondrites. The higher petrologic types have a lower concentration of water with lower δD values than Semarkona. Thus the D/H analysis technique does not have the capability to analyse the higher petrologic types.

Semarkona which have suffered more aqueous alteration than type 3.1 to 3.4 ordinary chondrites would have the D/H ratio of the organics reduced by more than the higher petrologic types, however the effects of thermal metamorphism in higher petrologic types may destroy the organics.

Unfortunately one of the major problems with this study has been the limited quality of the D/H data. Comparison between other type 3 ordinary chondrites, table 4.2, shows that Semarkona has the highest water content and largest whole-rock deuterium enrichment. Hence the present D/H technique does not have the capability to analyse other ordinary chondrites in a similar study.

Applications for the flow-thru technique used in this project are very limited. Samples are required which contain *ca.* 0.05 μmol of water with a large range in δD where accuracy in determining δD is not very important. For this reason the technique developed was not used for any other projects. However, this technique has shown that there are applications for a technique which could analyse small amounts of water, *ca.* 0.05 μmol, with a much better accuracy, better than ±100‰. Hence it was decided to continue development of a different technique, described in the next chapter.

Chapter 5
Hydrogen Isotope Analysis Using Static Mass Spectrometry

5.1 Introduction

It was unfortunate that the technique used for the study of Semarkona chondrules (chapter 4) suffered from problems of inaccuracy; two problems were identified, (1) a memory effect and (2) a sample size limitation,the smallest sample that could be analysed was *ca.* 0.1μmol of water. The memory effect, discussed in chapter 3, decreased the precision of the technique, especially for smaller samples, in the latter case isotopic results of poor accuracy were also obtained. The minimum quantity of water that could be analysed, by using the 'flow thru' technique, was about 0.1μmol of water, due to limitations in the sensitivity of the dynamic mass spectrometer. In fact the blank of *ca.* 0.05μmol hydrogen associated with the inlet system enabled slightly smaller samples to be analysed, in effect causing isotopic dilution of the sample. However this resulted in very large errors in δD due to variability in the size and δD of the blank. Coupled with memory effect problems, errors of ±1000‰ were probably appropriate for 0.1μmol samples of water. Clearly there is scope for a technique capable of analysing less than 0.1μmol of water with better accuracy.

An alternative type to the instrumentation used for the work in chapter 4 (and described in chapter 2) is static mass spectrometry; this procedure, considered below, is capable of isotopically analysing <1nmol of some gases. Whilst experiments continued into the cause of the memory effect in the dynamic mass spectrometer systems and attempting to find a solution, it was decided to investigate, in parallel, the possibility of hydrogen isotope analysis by static mass spectrometry.

5.1.1 Static mass spectrometry

During operation of a conventional dynamic mass spectrometer less than 1% of the total gas sample enters the mass spectrometer source. The inlet systems described in chapter 3 attempted to overcome this inefficiency. However a fundamental limitation of dynamic mass spectrometry is that less than 0.1% of the gas which enters the source is ionised, most being removed by the pumping system[1] . An alternative approach is the use of

---

[1] In the 'flow thru' inlet, in which most of the sample entered the source over a period of 4000 seconds, the average m/z 2 ion beam intensity was approximately 0.7×10^{-9}A. Hence only 2.9×10^{-5}mmol of sample was ionised and detected, indicating an ionisation efficiency of 1 molecule in 10 000.

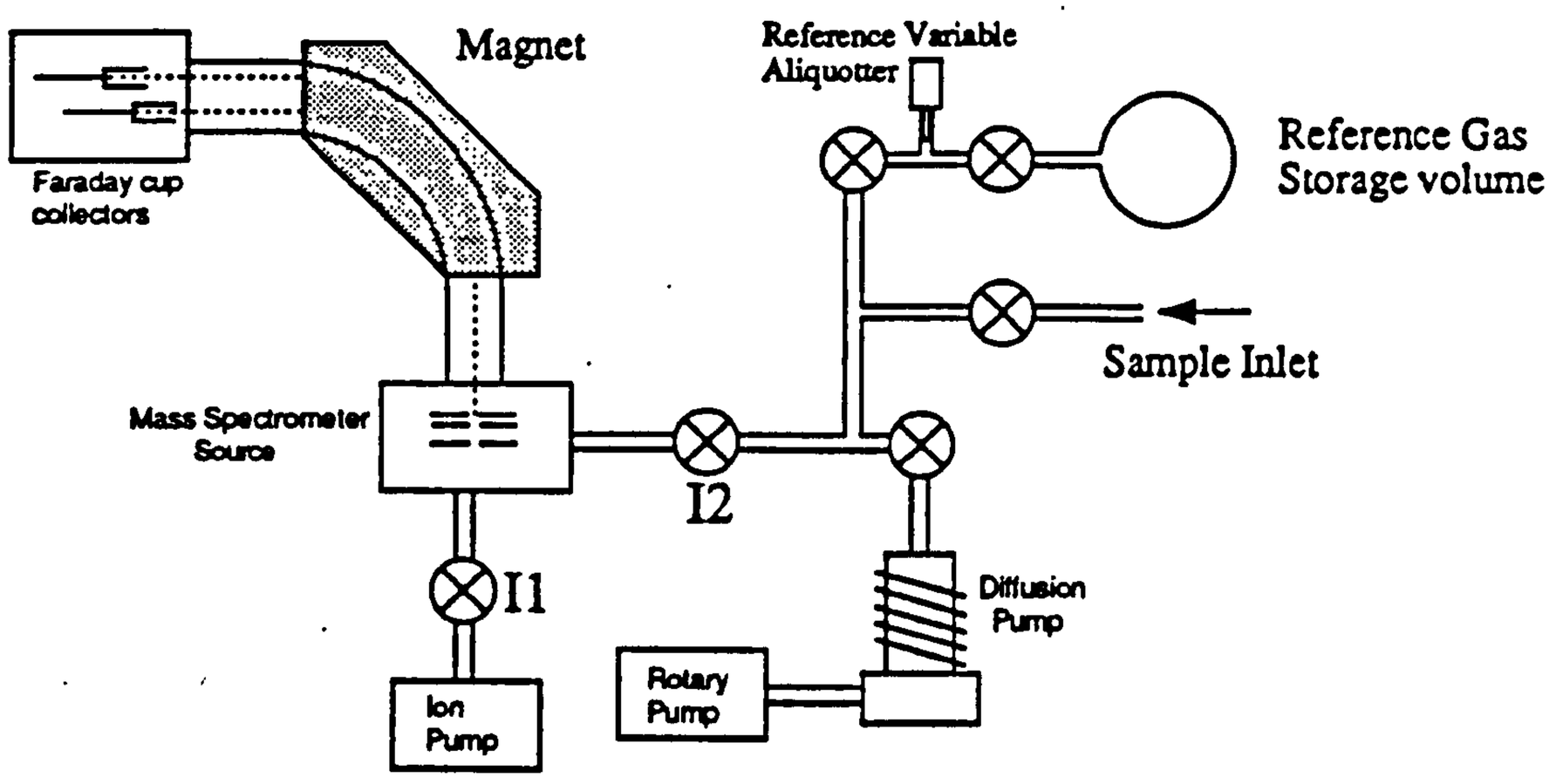

Fig. 5.1 Schematic diagram of a static mass spectrometer. The mass spectrometer is isolated from the pumps before the sample gas is admitted to the source and the ratio of its isotopes measured. The δ value of the sample gas is determined by comparison with the isotopic ratio of the reference gas, measured in a similar fashion once the sample gas has been analysed and evacuated.

static mass spectrometry, developed originally for the isotopic analysis of noble gases (Aldrich and Nier, 1948; Reynolds 1956), in which the instrument is isolated from the vacuum pumps before the sample gas is admitted into the mass spectrometer source. In effect the isolated volume of the mass spectrometer acts as the storage reservoir of the sample gas, fig. 5.1 is a schematic diagram of a static mass spectrometer. Analysis of a sample gas is accomplished by closing the isolation valve I1 and then admitting the sample gas to the mass spectrometer source through valve I2. Valve I2 is then closed and the gas analysed by the mass spectrometer, after which the instrument is evacuated by opening both isolation valves. In order to derive a δ, comparison is made with a reference gas of known isotopic composition analysed in a similar fashion, after evacuation of the sample. A variable volume aliquotter enables the quantities of reference sample gases to be matched. Sensitivity is greatly improved since nearly all the sample gas is admitted into the mass spectrometer and it remains available for the duration of the sample experiment, hence allowing a greater proportion to be ionised. However there are two disadvantages:-

i) Molecular gases (referred to as 'active' to distinguish them from noble gases) sometimes react to form other species or are rapidly dissociated, by the hot filament that produces the ionising electron beam. The half-life of a gas in the mass spectrometer is the time taken for the major ion beam to be reduced to half of its original intensity. If the

half-life is too short then there will be insufficient time to analyse the gas. For noble gases the half-life is many hours (Irako *et al.*, 1975). Static mass spectrometry has been used for carbon isotope analysis, using CO_2 which has a short half-life of about 35s in a source using a hot electron filament (Carr *et al.*, 1986). The exact half-life of a gas varies between different static mass spectrometers, due to different source operating conditions.
ii) Since the reference gas is analysed after the sample gas has been evacuated from the mass spectrometer there is not the ability to perform multiple rapid and repeated comparisons the reference and sample gas. Hence precision in the isotopic measurement may be reduced due to source fluctuations. Precisions of the order of ±1‰ or better for nmol quantities of active gases (Pillinger, 1984), with CD_4 being a particularly suitable species, ±0.25‰ having been achieved (Wright *et al.*, 1983).

The use of static mass spectrometry for the analysis of some active gases has been investigated by Irako *et al.*, (1975) and Gardiner and Pillinger (1979). In these studies hydrogen was found to be unsuitable for use in a static mass spectrometer because of its short half-life of *ca.* 2 seconds, thought to be caused by dissociation of hydrogen molecules to hydrogen atoms, by the hot filament, which are then absorbed by metal surfaces in the instrument, (Irako *et al.*, 1975). The use of a cold cathode, instead of a tungsten filament, to induce ionisation results in a significantly longer life-time for hydrogen in the source, half-life *ca.* 20 minutes (Irako *et al.*, 1975). However there could still problems using static mass spectrometry for hydrogen isotope analysis due to outgassing of hydrogen absorbed on the metal source housing, causing memory effects, and the unknown effects of H_3^+ ions in the high pressure environment of the source, *ca.* $1x10^{-5}$ mbar, (Wright and Pillinger, 1983).

Other hydrogen containing gases that have been investigated for use with static mass spectrometry are methane and n-butane (Irako *et al.*, 1975; Gardiner and Pillinger, 1979; Wright and Pillinger, 1983). Irako *et al.*, (1975) found the half-lives of methane and n-butane to be 20 and 14 minutes respectively (with the cold cathode). Gardiner and Pillinger, (1979) determined the half-life of deuterated methane, CD_4, to be nearly 11 hours under very mild source conditions; *i.e.* an electron emission current of 4μA and low work function filament material, LaB_6. Gardiner *et al.* (1978) explored the use of CD_4 as a potential gas for carbon isotope measurement, the filament current was employed to avoid isotopic fractionation. Fallick *et al.*, (1980) later found that there was no isotopic fractionation during the decay of methane, hence higher emission currents can be used to increase sensitivity.

It was decided to investigate the use of methane as an analysis gas for hydrogen isotope measurement by static mass spectrometry since there are several chemical reaction methods for its production from water (sections 5.4 and 5.5) and it has a reasonably long half-life in a static mass spectrometer. The investigation of the properties of methane in a

static mass spectrometer for isotopic analysis is described in section 5.3. Section 5.4 describes the technique used to convert sample water to methane. A similar study investigating the use of acetylene, produced from calcium carbide was also performed, but acetylene was found to be unsuitable; this is described in Appendix E.

5.2 The static mass spectrometer system

5.2.1 The mass spectrometer

For this study a Micromass 3000 mass spectrometer system was used (MM3000, VG Isotopes Ltd.), which is based on an instrument designed by W.B.Clarke of McMaster University (Clarke *et al.*, 1976). Although the MM3000 was designed specifically for the analysis of $^3He/^4He$ ratios in the static mode of operation, it can also be used for all the other noble gases , up to xenon (m/z = 130 to 136). At first sight this may seem an unusual choice of instrument with which to pursue static mass spectrometry of methane, but it was used because of its availability at the time of the investigation[2] .

The MM3000 analyser, made of stainless steel, consists of a Clarke-type ionisation source , a split flight tube (25 and 30.5cm radii for ^3He and ^4He respectively, the minor beam being deflected by a 90° sector magnetic field of normal entrance and exit angle) and two collectors. The collectors, which are positioned for $^3He/^4He$ analysis, comprise normally of an electron multiplier detector (for ^3He) and a Faraday bucket detector. In this study all ion beam intensity measurements were made on the Faraday detector. The field strength of the electro magnet used for deflection was controlled by varying the electric current through the magnet and measured by a Hall probe fixed on the flight tube. The magnet was supported by a magnet carriage which allowed its position to be adjusted precisely. The MM3000 was used with a resolving power of *ca.* 300; a maximum resolving power of 3000 is possible, but at higher mass resolution (>300) sensitivity is reduced.

A diagram of the analyser and its associated pumping system is shown in fig. 5.2. The analyser was usually pumped by a 25 ls^{-1} ion pump (VG TS2, Varian Associates Ltd.) through valve I1, a CR38 manual bellows valve (VG Hastings). The usual vacuum in the analyser was better than 10^{-9}mbar. The pumping system for the gas inlet was designed to be oil-free, since thermal cracking of pump oil could cause blank problems and also limits the best vacuum obtainable to 10^{-7}mbar. The inlet and backing lines were

---

[2] It is not appropriate to use a nitrogen static mass spectrometer because methane analysis will result in carbonisation of the filament and hence large CO blanks interfering with later nitrogen isotope analyses. Both carbon isotope static mass spectrometers, in our laboratory, are in almost continuous use.

pumped by separate 30 ls^{-1} ion pumps (Starcell, Varian Associates Ltd.). A sorption pump, filled with 5Å molecular sieve (VG Hastings), was used to evacuate the system from atmosphere to a pressure suitable for use of the ion pumps, *i.e.* 10^{-2}mbar. Each of the inlet pumps could be isolated from the inlet by an automatic bellows valve (AV-150M-P, MDC Vacuum Products Corporation) operated by compressed air. Both the inlet and backing ion pumps were protected by Pirani trips to switch them off in the event of vacuum failure. Using this pumping system enabled an ultimate vacuum of $5x10^{-9}$mbar to be obtained in the glass inlet, with a pressure of 10^{-7}mbar in the backing line.

Valve I3 in fig. 5.2 was only ever used to pump the analyser down from atmospheric pressure. In this case the analyser was evacuated by the sorption pump through valve I3 until a pressure of 10^{-2} mbar was obtained, the rest of the sample and reference gas inlet being isolated from the pumps and analyser. All three ion pumps were then used to further evacuate the mass spectrometer whilst it was baked by an oven to 200°C for at least 24 hours.

Several changes were made to the MM3000 so that it could be used with active gases, rather than the noble gases for which the instrument was designed. Usually the instrument is pumped by getters during static analysis in order to remove active gases. Obviously these were surplus to requirement and so were replaced by blank 34mm flanges . The filament that produced the ionising electron beam was originally a tungsten ribbon which gives a very high emission current and improved sensitivity required for helium isotope analysis. Due to difficulties in obtaining a replacement ribbon filament

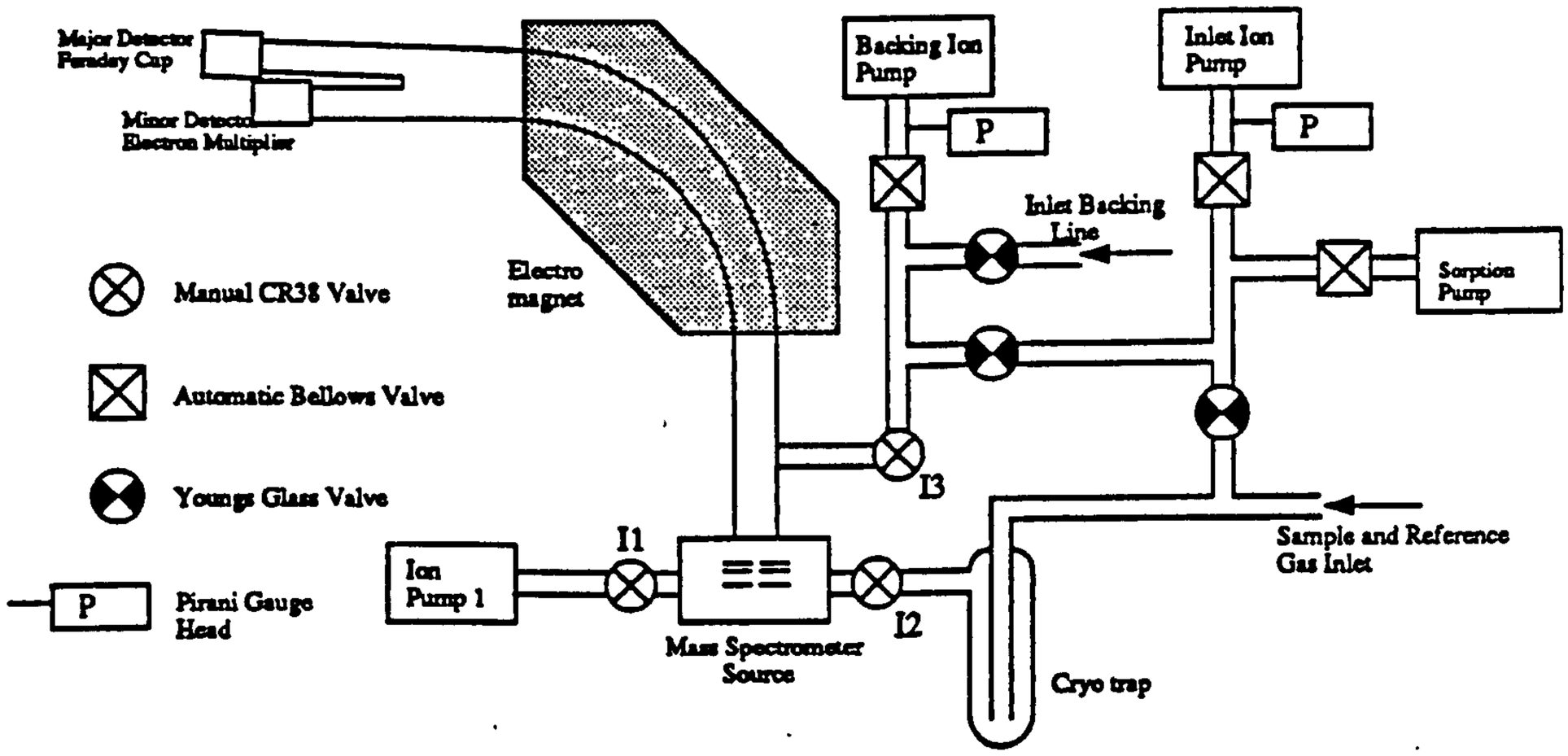

Fig. 5.2 A schematic diagram of the mass spectrometer and inlet pumping system, which was designed to be oil-free. Large amounts of gas were removed by use of the sorption pump,. which reduced the pressure to the operation range of the ion pumps.

this was replaced by 0.125mm diameter tungsten wire (Goodfellow Metals) spot welded to the filament supports. Only the Faraday cup detector was used for analysis, the electron multiplier collector and associated electronics (designed to detect He_3^+ ions) were removed.

A schematic diagram of the electronics systems of the analyser is shown in fig. 5.3. Most of these have a similar function as for the D/H analyser (chapter 2), the major difference being that the source accelerating voltage was constant and the magnet field strength was varied to scan the ion beams over the single Faraday cup collector. As for the D/H mass spectrometer, control of the MM3000 and data acquisition was performed a 6502, 8-bit 1MHz micro-computer (128k BBC micro-computer, Acorn Computers Ltd.), interfaced to the electronic units by a digital input/output adapter (Cubio, Control Universal).

The collection of appropriate ion beam intensity information, magnet scanning and data reduction were performed by the computer, using software written 'in-house' in BASIC. The ion beams of interest were m/z = 16, $^{12}CH_4^+$, and m/z = 17, $^{13}CH_4^+$ and $^{12}CH_3D^+$. As methane gas was admitted to the mass spectrometer the program was started; this initially monitored the m/z 16 ion beam so that the amount of methane admitted to the mass spectrometer could be estimated. After allowing 20 seconds for the methane to enter the mass spectrometer valve I2 (fig. 5.2) was closed manually and the gas allowed to equilibrate for 60 seconds before the analysis would begin. By scanning the magnetic field such that the major, m/z 16, and minor, m/z 17, ion beams passed over the Faraday cup collector the peak positions and widths were determined. From the peak positions the magnetic field strength required for each ion beam to fall on the centre of the Faraday cup collector was calculated. The background signal from the collector for each peak was determined by measuring the signal when the magnetic field was chosen to be 2 peak widths either side of the peak centre (*ca.* ±0.1amu). The ion beam intensity for the major and minor beams were determined by measuring the signal at the peak centre and then subtracting the average of the background measurements made on either side of the peak. This procedure was repeated 12 times, to monitor the decay rates of both ion beams against time; the total time taken for data collection was approximately 10 minutes. The average m/z 16 and 17 ion beam intensities and the m/z 16/17 ratio were calculated, along with 2σ errors. The half-life of each ion beam and initial ion beam intensity when admitted to the mass spectrometer was calculated by fitting a best fit line (using least squares method) to the ion beam intensity relationship with time.

A second program enabled a mass scan of the gas from m/z 12 to 48 which was used initially to check that methane was the only gas entering the mass spectrometer and to determine the effects of the source on the methane cracking pattern. This was rarely

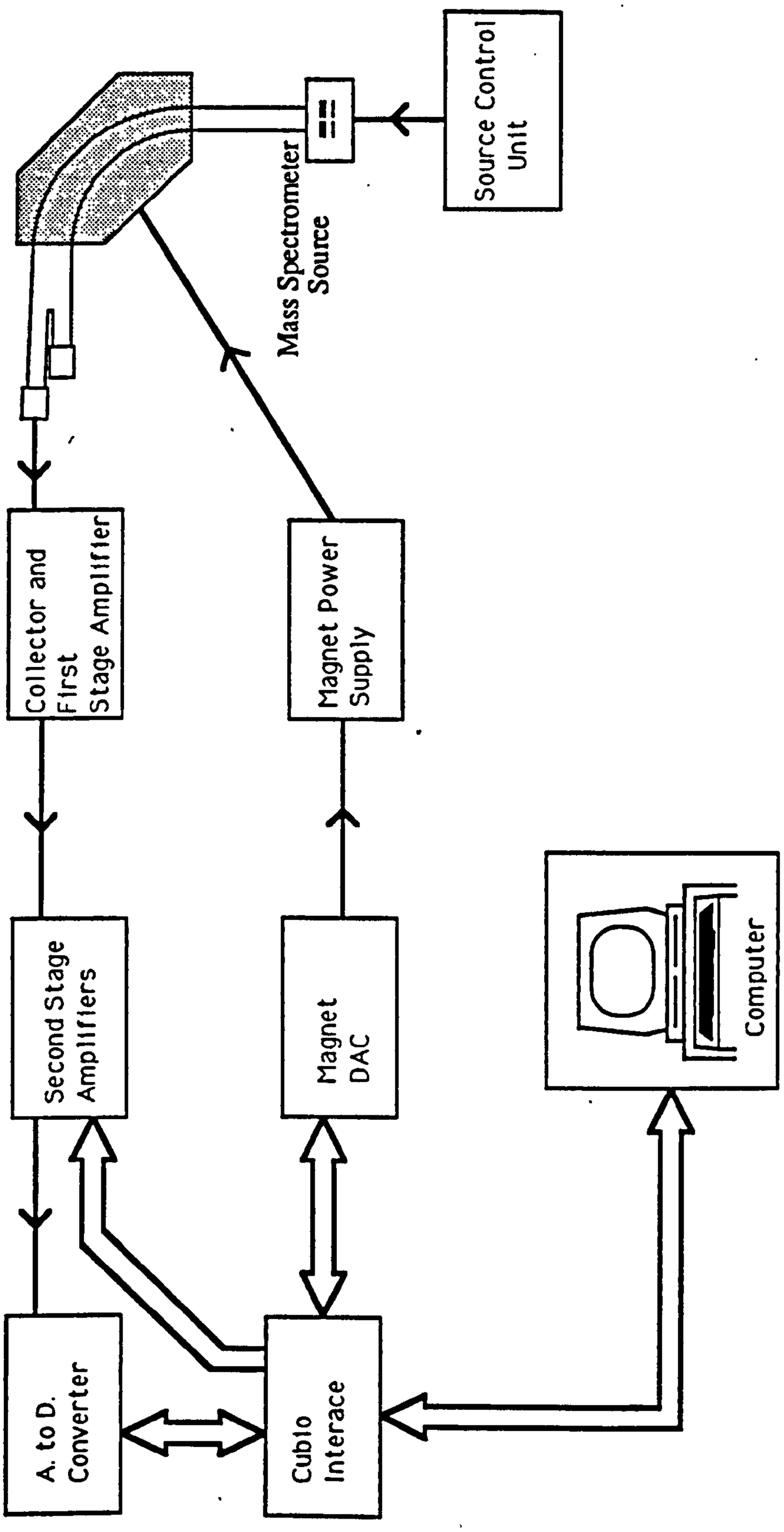

Fig. 5.3 A schematic diagram of the mass spectrometer control and data acquisition electronic units. These are controlled by the computer *via* the Cubio interface. Ion beams were scanned over the Faraday cup detector by varying the magnet field strength.

used during routine analysis because it was found that after scanning high m/z, the magnet was unable to accurately return to the low field strengths used during isotope ratio measurement.

5.2.2 Methane inlet

A schematic diagram of the methane gas inlet system is shown in fig. 5.4. Most of the inlet was constructed from Pyrex glass tube (10mm O.D., 8mm I.D., Cambridge Glass) and greaseless backed valves (PSU/10/RA, J.Young). The backs of the valves were pumped by a separate pumping system from the main inlet (McNaughton et al., 1983), through the backing ion pump.

Methane reference gas was stored in a 2l glass bulb (Cambridge Glass) at a pressure of $2x10^{-2}$mbar; aliquots of the gas could be taken from this by use of the variable volume aliquotter. This device consisted of two needle tip backed valves, R1 and R2 in fig. 5.4, and a backed piston (J.Young), similar to that used by Carr *et al.*, (1986). A total of nine revolutions of the screw top of the piston moved the piston barrel from fully compressed to fully extended. The screw top was marked with 10 equally spaced gradations to enable

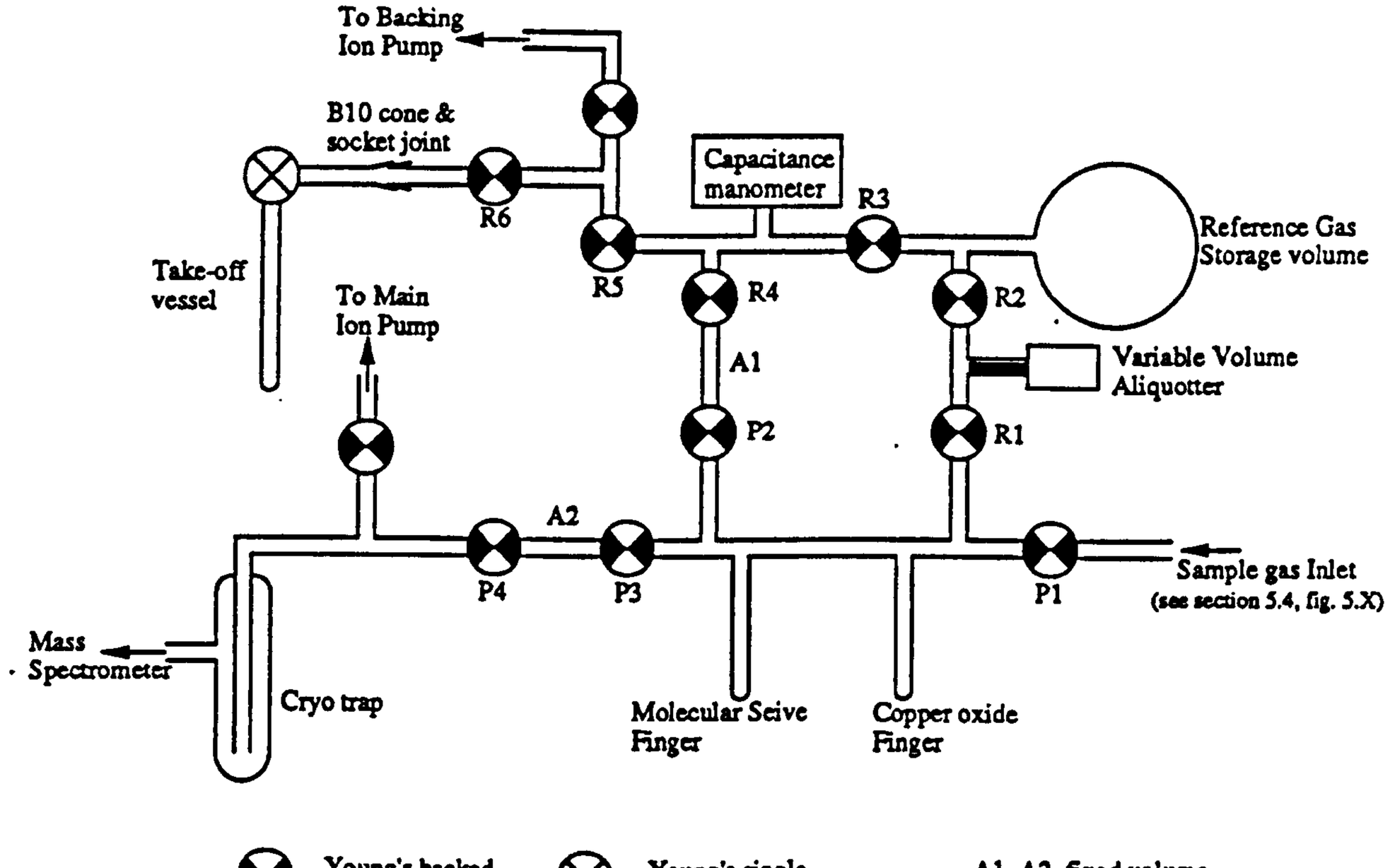

Fig. 5.4 A diagram of the inlet system used to store methane reference gas and purify methane before admission to the static mass spectrometer.

accurate positioning of the piston barrel. Before attaching the variable volume aliquotter to the inlet its volume was determined by weighing when filled with water and subtracting its weight when empty. The range of volume was found to be 0.32cm^3 to 1.32cm^3.

During evaluation of the inlet, a second reference gas of different isotopic composition to that stored in the 2 l bulb could be stored in the section of glass line between valves R3, R4 and R5. The pressure of gas in this section was measured by a capacitance manometer (Chell instruments Ltd.), capable of measuring pressures from 1x10^{-4} to 1 torr. The fixed volume aliquotter A1, which each consisted of two standard backed valves joined together as close as practically possible, had a volume of *ca.* 2.5cm^3. This was used to meter out aliquots of the second reference gas.

The methane reference gas used to evaluate the performance of the mass spectrometer contained 99.5% methane (see section 5.3.1), hence removal of impurities was deemed unnecessary. However an unknown sample may have contaminants associated with it, hence it was necessary to investigate the purification of methane. Purification was achieved by the removal of various impurities by their oxidation and/or cyrogenic separation (Sakai *et al.*, 1976). Methane is non-condensible by liquid nitrogen, so condensible gases, such as carbon dioxide, sulphur dioxide and water, will be removed by a cryo-trap operated at -185°C. It was important that all water was removed by this cryo-trap to prevent isobaric interference between CH_3D^+ and OH^+ during analysis. The purification section was designed to separate non-condensible gases such as hydrogen and carbon monoxide from methane. A molecular sieve finger consisting of a cryo-trap, the inner tube being 10mm O.D., 8mm I.D. filled with 3A molecular sieve (BDH Chemicals Ltd., Poole), was used to cryogenically trap carbon monoxide and methane whilst leaving hydrogen in the gas phase. Opening the purification section to the pumps then rapidly removed most of the hydrogen. The copper oxide finger was then used in the removal of carbon monoxide and any residual hydrogen. The copper oxide finger consisted of a quartz tube (10mm O.D., 8mm I.D.) filled with *ca.* 1g wire form copper II oxide (BDH Chemicals Ltd., Poole) connected to the purification section by a graded quartz-pyrex join (Jencons). It was heated by an non-insulated furnace. The copper oxide removes carbon monoxide and residual hydrogen by oxidising these gases to species which can by cryogenically separated from methane.

$$CuO + CO \rightarrow Cu + CO_2 \qquad 5.1)$$

$$CuO + H_2 \rightarrow Cu + H_2O \qquad 5.2)$$

The efficiency of the purification system was evaluated for carbon monoxide and hydrogen by having the gas of interest in the baratron section. Valves R4, P2, P3 and P4 were opened so that the gas was in contact with the copper oxide finger and the mass spectrometer cryo-trap, other valves being closed. The rates of oxidation of carbon monoxide and hydrogen at different temperatures as measured using the capacitance manometer are shown in figs. 5.5 and 5.6 respectively. It was found that methane did not begin to be oxidised until the temperature of the copper oxide finger was above 550°C. From the results of fig.5.5 and 5.6 it can be seen that both the reactions (5.1 and 5.2 above) are first order, *i.e.* dependent on the pressure of gas in the system. It was decided to operate the copper oxide finger at a constant temperature of 400°C and allow four minutes for the purification of the methane. This temperature was well below that at which methane begins to oxidise and would remove 99.9% of the carbon monoxide and *ca.* 50% of any hydrogen, (note that most hydrogen is removed by use of the molecular sieve trap).

There was no readily available mechanism for the removal of nitrogen impurities. Nitrogen did not condense on the cryo-trap but was condensed on the molecular sieve trap over the same temperature range as methane. Although nitrogen gas can be separated from methane by use of a Zr-Al getter operated at room temperature (Gardiner and Pillinger, 1979). However Gardiner and Pillinger (1979) found that methane was released by the getter at a rate of 3pmol/min which would result in a methane of *ca.* 0.05nmol during analysis of a sample. Another possibility is the removal of nitrogen by a chemical method such as hot lithium (Aldrich and Nier, 1948), although the effect of lithium on nmol amounts of methane is not known. An alternative is the use of gas chromatography to separate nitrogen and methane using helium as a carrier gas (Dumke *et al.*, 1989). None of these purification methods were attempted and instead any nitrogen impurities entered the mass spectrometer along with methane. It was found that the effect of small amounts of nitrogen impurities in the methane gas had no noticeable effect of the isotopic analysis; one of the methane standards used to evaluate the mass spectrometer and inlet, described below, contained 16% nitrogen by volume. If methane is produced from sample water then nitrogen can be readily separated by a cold finger before conversion of the water to methane.

Valve R6 was connected to a B10 cone (Cambridge Glass) which allowed gas to be admitted to the inlet system using a 'take-off' vessel, a single greaseless valve with one end sealed and the other connected to a B10 socket joint (Cambridge Glass), as shown in fig. 5.4.

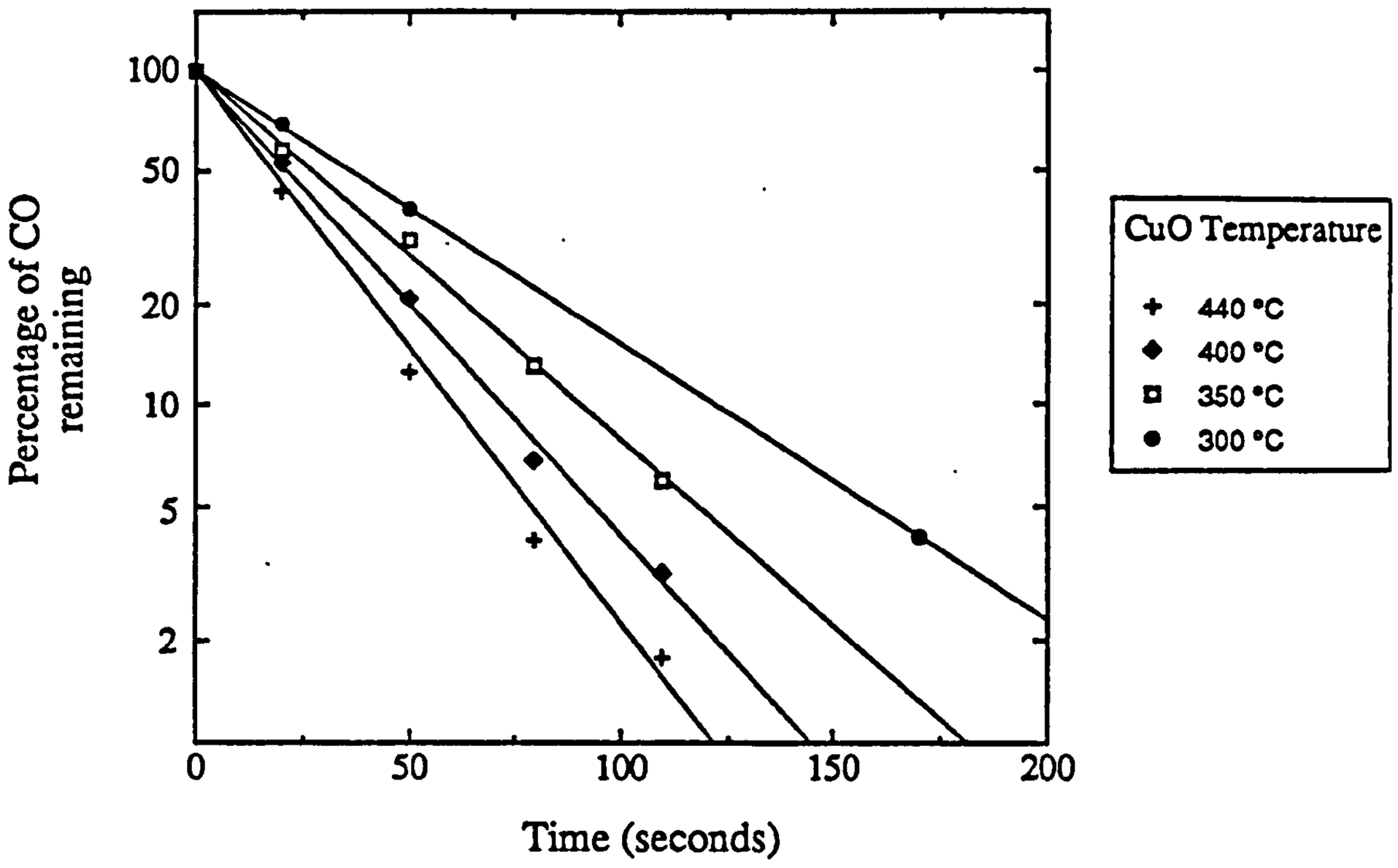

Fig. 5.5 Graph showing the rate of oxidation of carbon monoxide to carbon dioxide by the copper oxide finger at various temperatures.

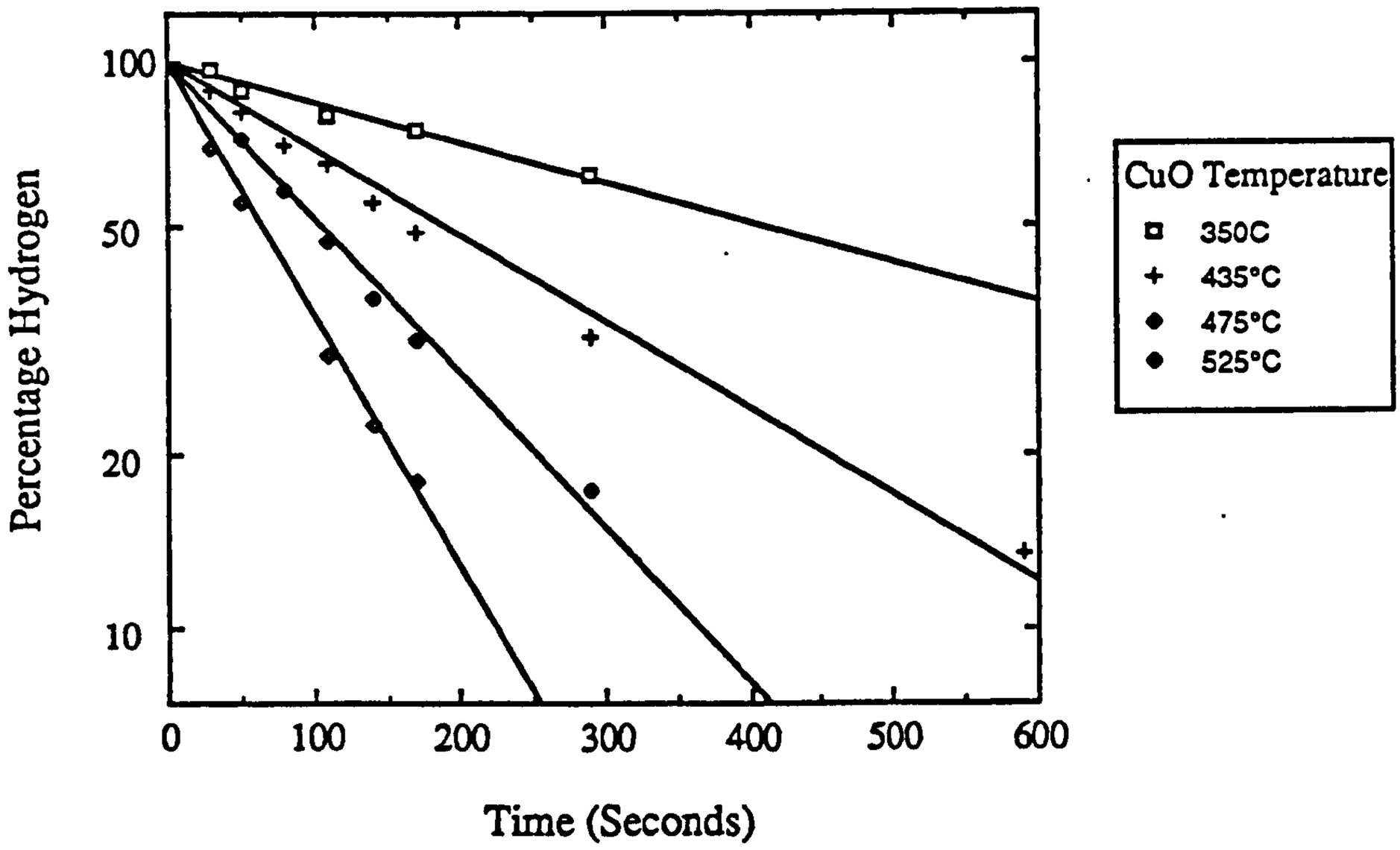

Fig. 5.6 Graph showing the rates of oxidation of hydrogen to water by the copper oxide furnace at various temperatures.

5.3 D/H isotopic analysis of methane

5.3.1 Methane standards

Three methane samples of natural gas were used, obtained from the National Bureau of Standards *via* M.Schoell, and used as standards for this study. Each methane standard was stored in a 50cm^3 canister at a pressure of *ca.* 50bar. The methane content and its hydrogen and carbon isotopic value of each canister is given in table 5.1. The major impurities were carbon dioxide which was cryogenically removed before analysis and nitrogen. Gas from each canister was admitted to a 'take-off' vessel using a separate vacuum system (constructed from similar materials to that of the inlet). This consisted of a manifold of four B10 cones, a 2l expansion bulb (Cambridge Glass) and evacuated by a turbo rotary pump combination. Unused manifold ports were blanked by a sealed B10 socket. The aliquotter consisted of two Nupro bellows valves (North London Valve & Fitting Co.) connected by 2cm of seamless 316 stainless steel tubing (1/4" O.D., 16 gauge), total volume *ca.* 0.35cm^3. This was connected to the vacuum system manifold by a flexible metal section and glass joint (G321-4-GX-2,North London Valves & Fitting Co.) attached to a B10 socket. An aliquot of methane from the gas canister was allowed to expand into the expansion bulb and 'take-off' vessel. The 'take-off' vessel was then closed, containing about 10cm^3 of methane at a pressure of 2mbar, and transferred to the methane inlet as shown in fig 5.4.

Natural Gas Standard	NGS#1	NGS#2	NGS#3
vol.% methane	81.3	52.8	99.5
$\delta^{13}C$ (PDB) ‰	-28.97	-44.58	-72.55
δD (V-SMOW) ‰	-141.8	-175.1	-176.3
Impurities (vol.%)			
ethane	2.79	2.62	0.057
propane	0.376	1.31	0.007
carbon dioxide	1.03	25.5	0.025
nitrogen	14.3	16.5	0.437
argon	0.003	0.024	0.004
helium	0.056	0.042	trace
hydrogen	trace	0.008	trace

Table 5.1 Isotopic and chemical composition of the methane gas samples used to evaluate the inlet system and mass spectrometer. NGS#3 was used as the reference gas since it was virtually pure. The reference material used for carbon isotope analysis is a fossil (Belemnitella americana) from the Peedee formation of South Carolina, abbreviated to PDB. As for SMOW, PDB is no longer available and so most laboratories use secondary standards which have been previously analysed using PDB as a reference.

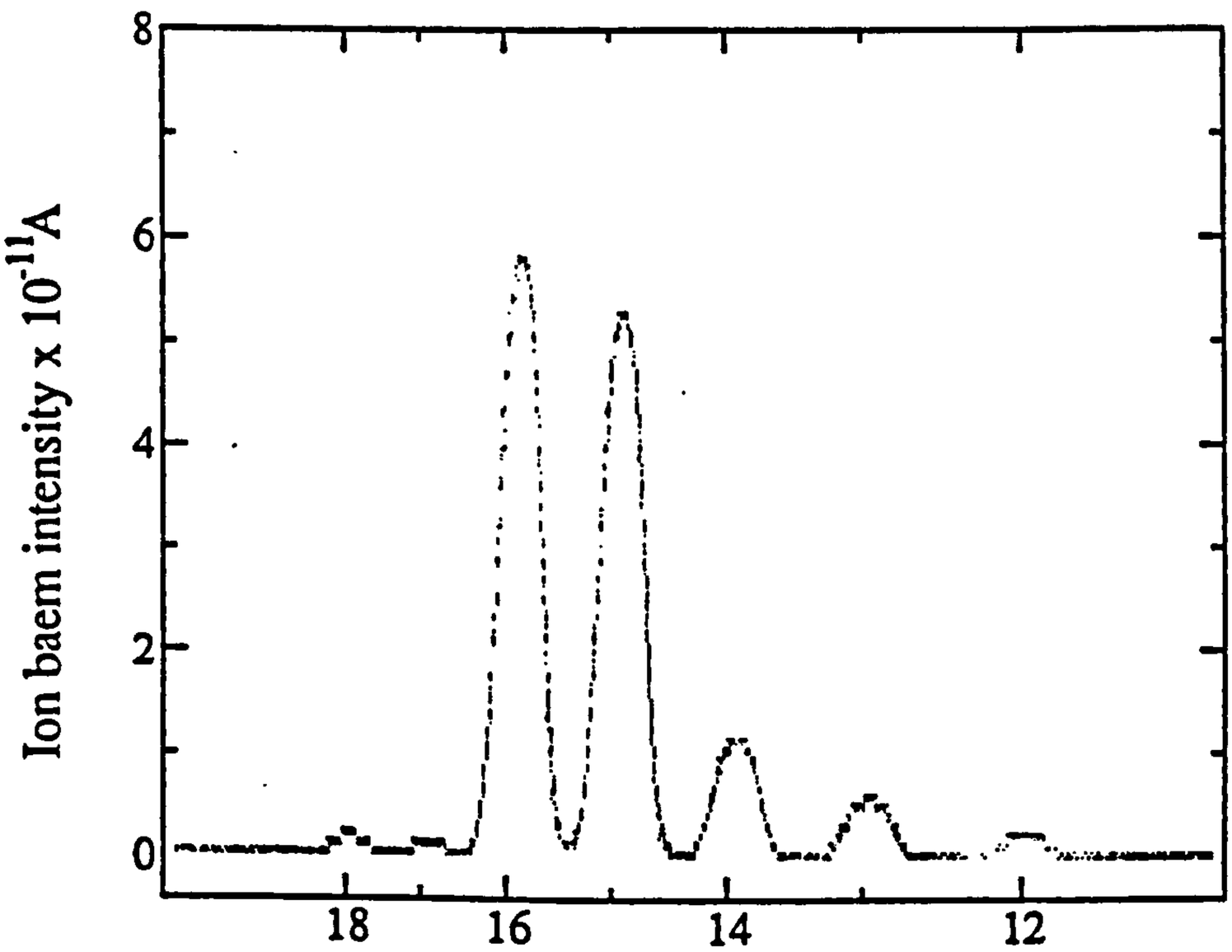

Fig. 5.7 Mass scan of methane using a dynamic mass spectrometer (described in chapter 2). Peaks as well as the m/z 16 peak are present due to the cracking of methane in the source. The presence of water in this analysis is indicated by the presence of the m/z 18 peak.

5.3.2 Source characteristics of methane gas

Some methane (3.4μmol of NGS#3) was analysed using the dynamic mass spectrometer used earlier for hydrogen isotope analysis (described in chapter 2) to obtain an indication of the effect of an ionisation source on methane gas. Fig 5.7 shows the output from the minor amplifier during a mass scan, the accelerating voltage increasing from 200V to 1000V. The main peak, m/z = 16, is mainly due to CH_4^+, the major fragment ion is CH_3^+, with some CH_2^+, H_2^+ and C^+. Provided the fragmentation of methane by the source is first order then the major ion beam will be proportional to the quantity of methane analysed. A mass scan made soon after the methane was admitted to the static mass spectrometer showed similar results to fig. 5.7; however as the m/z 16 ion beam decayed with time it was noted that the m/z 28 and m/z 42 ion beams increased, presumably due to the formation of C_2H_4 and C_3H_6 from the methane fragments. The effect of the fragmentation of isotopically heavy methane on the measured isotopic ratio of methane is considered in section 5.3.4.

An evaluation of the optimum mass spectrometer ion source conditions was made by analysing 11.2ng of methane reference gas (NGS#3). The half-life of methane in the mass spectrometer was found to vary with the trap current as shown in fig. 5.8. The half-life was reduced at higher current, presumably because of thermal cracking by the tungsten filament was at a higher temperature. Even at a low trap current the half-life of methane in this mass spectrometer is short, compared to Gardiner and Pillinger (1979), because of the use of a tungsten filament. The effect of varying the trap current on the measured 16/17 ratio is shown in fig.5.9. Above 5μA there is clearly a dependency of the 16/17 ratio versus trap current. However of interest here is the variation in precision versus trap current; ratios obtained with a higher ionisation current of 50μA had a greater precision of ±0.6‰, compared with the ratios obtained when using a lower ionisation currents; a precision of only ±15‰ was obtained when using an ionisation current of 2μA. Even though methane gas had a longer half life in the source when lower ionisation currents were used the precision was reduced because the ion beam intensity was also reduced, a graph of ion beam intensity against ionisation current is shown in fig.5.10. For this reason an ionisation current of 50μA was chosen for the analysis of methane. Higher ionisation currents were possible but this was not used as this did not increase precision any further and would reduce the life of the tungsten filament. When analysing samples, the quantity of methane admitted into the mass spectrometer was determined from the major, m/z 16, ion beam intensity. Results obtained for the major ion beam intensity against quantity of methane, using a trap current of 50μA, are shown in fig. 5.11 and show that the major ion beam is proportional to the quantity of methane admitted.

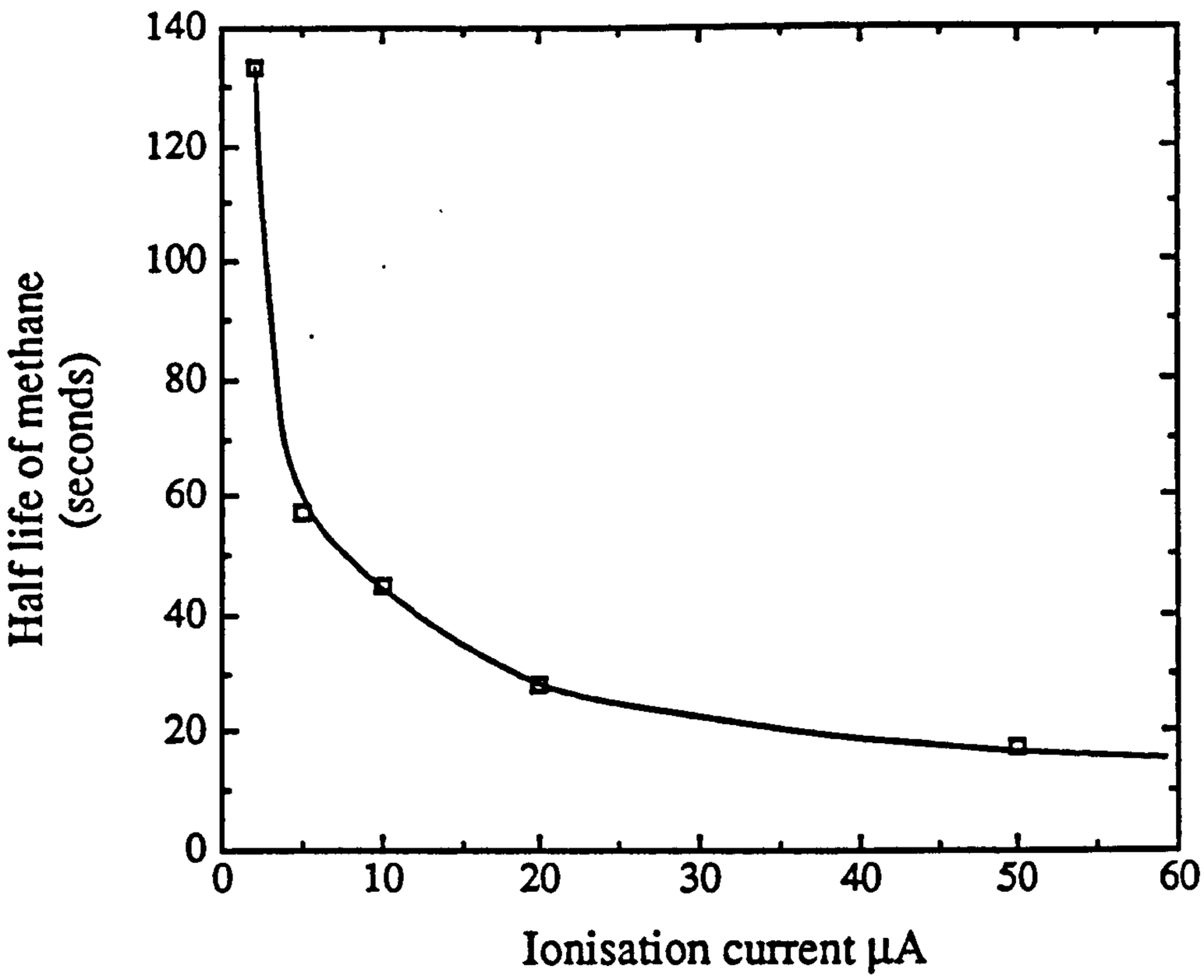

Fig. 5.8 Graph showing the effect of varying trap currents upon the half-life of methane in the mass spectrometer source.

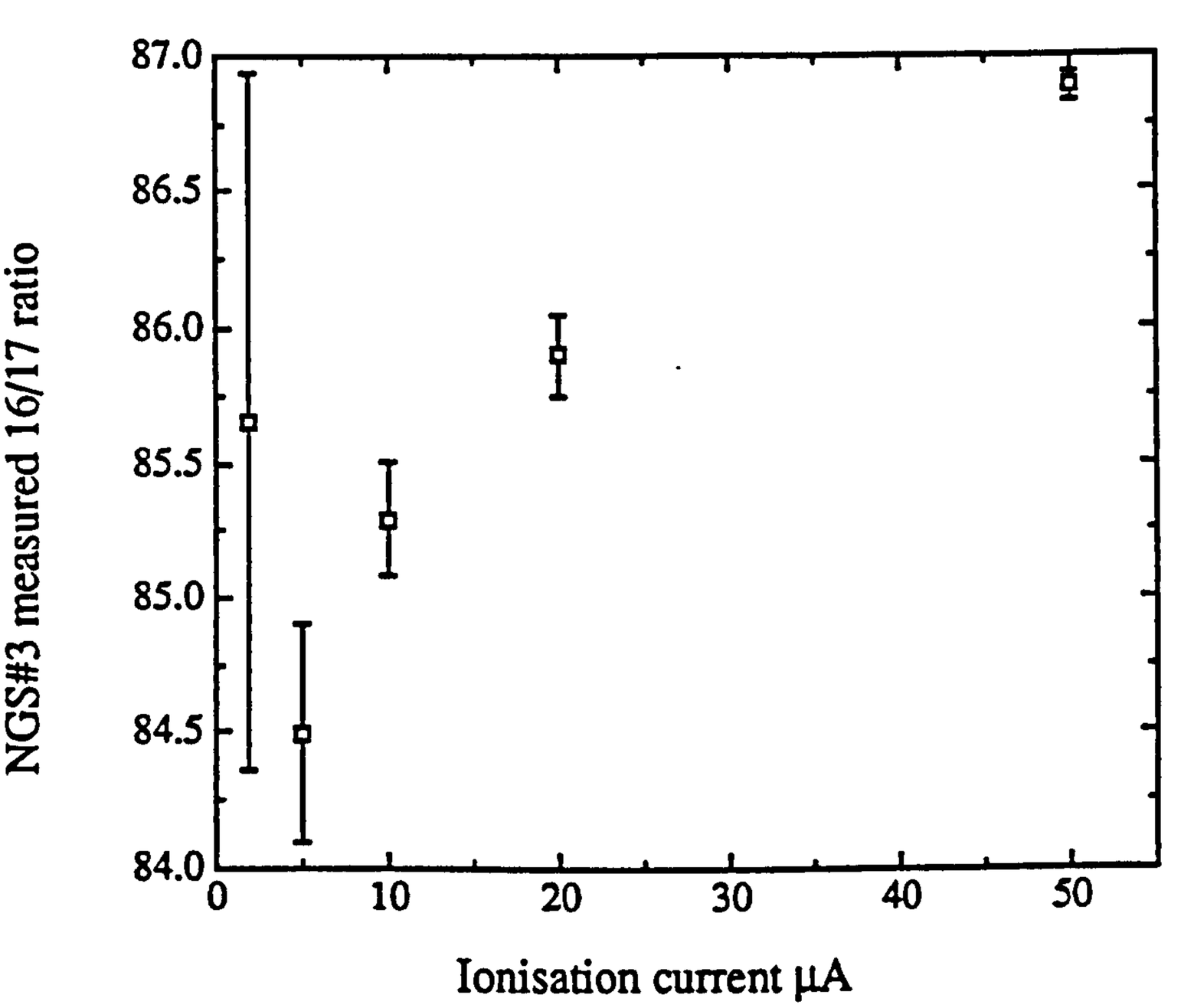

Fig. 5.9 Graph showing the effect of various trap currents on the measured ratio and precision obtained when analysing NGS#3 methane.

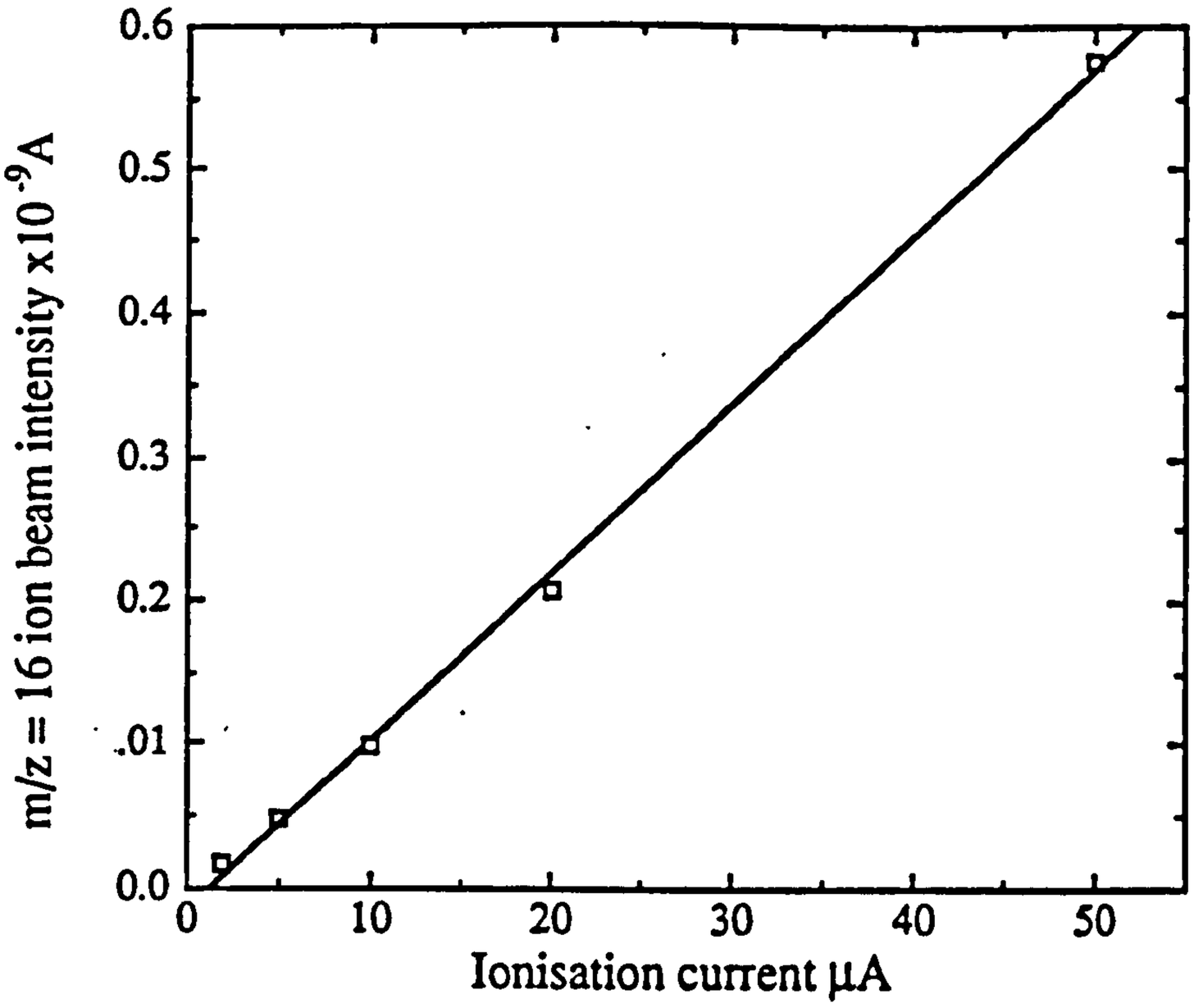

Fig. 5.10 Graph showing the m/z 16 ion beam intensity for 0.5nmol aliquots of methane with various trap currents. Greater precision is obtained with higher trap currents (fig.5.9) due to the higher ion beam intensity.

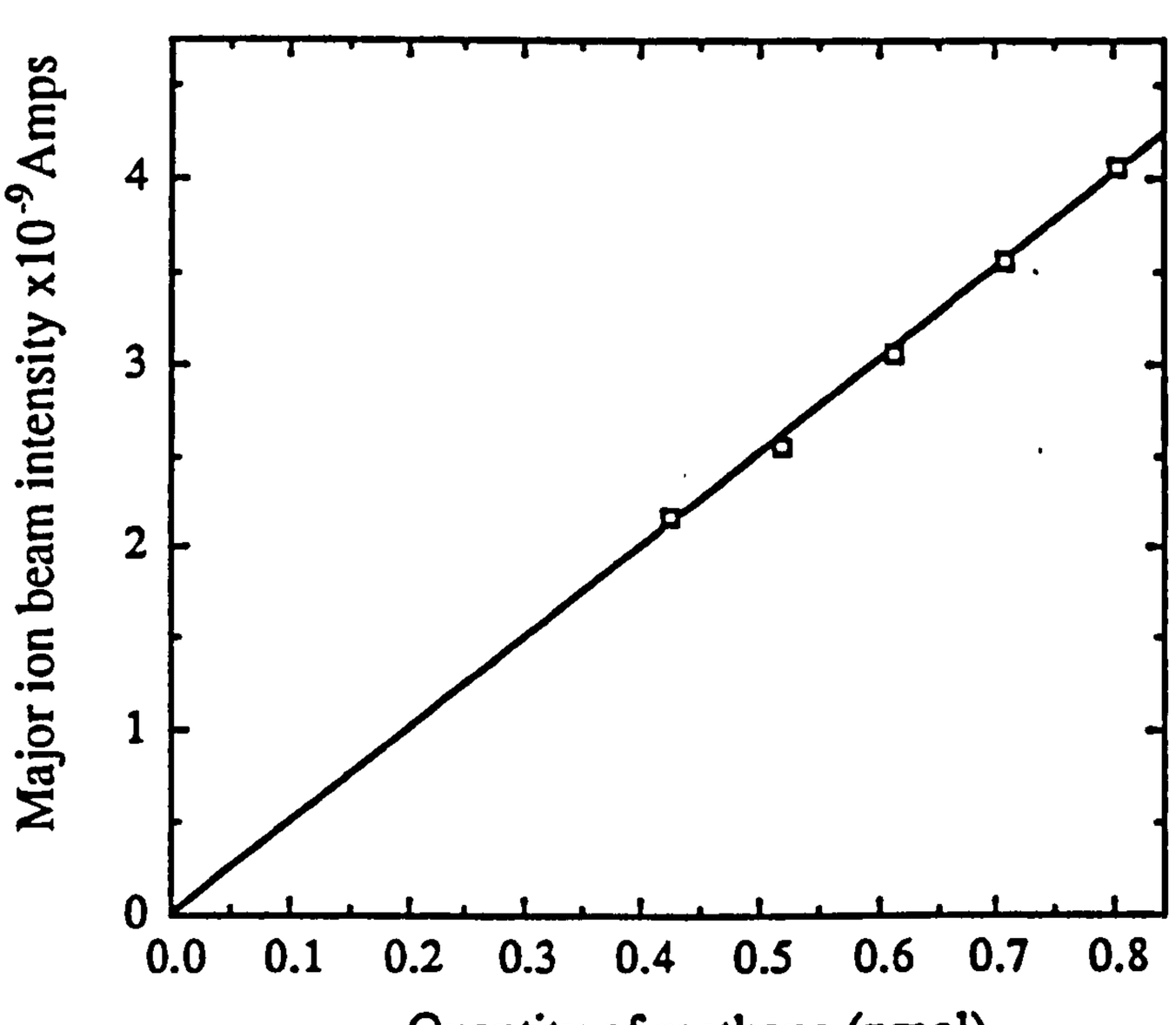

Fig. 5.11 Graph of m/z 16 ion beam intensity against quantity of methane admitted to the mass spectrometer. The best fit line passes through he origin and has slope 5.028nA $nmol^{-1}$ (correlation coefficient r = 0.999). The m/z ion beam intensity was used to measure the amount of sample methane admitted to the mass spectrometer.

To evaluate the precision of the instrument a zero enrichment was performed, using an ionisation current of 50μA, with the reference gas stored in the bulb and a separate NGS#3 aliquot admitted to the capacitance manometer section between valves R3, R4 and R5 of fig.5.4. Approximately 0.5nmol quantities of methane from the capacitance manometer section were admitted to the mass spectrometer and analysed as an unknown sample. This was then compared with an aliquot of methane from the reference section and the $\delta^{17}M$ value calculated. The results of the zero enrichment are shown in table 5.2 and show that the overall precision was *ca.* 0.6‰.

Methane Sample	m/z = 16 intensity ($x10^{-9}A$)	16/17 ratio	2σ error	$\delta^{17}M$ ‰
NGS#3	4.5900	89.301	0.017	
Ref 0.591nmol	4.4642	89.318	0.048	+0.2 ± 0.6
NGS#3	4.4291	89.251	0.047	
Ref 0.573nmol	4.3382	89.299	0.033	+0.5 ± 0.6
NGS#3	4.2787	89.257	0.032	
Ref 0.564nmol	4.2643	89.241	0.036	+0.2 ± 0.5

Table 5.2 Three zero enrichment analyses. The 'sample' gas was not cleaned before admission to the mass spectrometer source. The overall precision of the mass spectrometer is ± 0.6‰.

5.3.3 Determination of δD from $^{17}M/^{16}M$ ratio

Determination of the δD of hydrogen in a methane sample by measuring the 17/16 ratio is complicated by the presence of ^{13}C. The m/z=17 ion beam is due to the presence of both $^{12}CH_3D^+$ and $^{13}CH_4^+$. Hence for a sample, the ratio of m/z 17/16 is given by

$$\frac{^{17}M}{^{16}M} = \frac{^{13}C}{^{12}C} + 4 \times \frac{D}{H} \qquad 5.3)$$

where ^{17}M and ^{16}M are the m/z 16 and 17 ion beam intensities,
$^{13}C/^{12}C$ is the carbon isotope ratio of the methane and
D/H the hydrogen isotope ratio of the methane.

During the analysis of a sample the delta value of the sample, $\delta^{17}M$, is determined by comparing the $^{17}M/^{16}M$ ratio of the sample methane with the reference methane. NGS#3 was chosen as the reference gas for this study when calculating $\delta^{17}M$ because, of the three natural gas samples, it was almost pure methane.

$$\delta^{17}M = \left(\frac{(^{17}M/^{16}M)_{sam}}{(^{17}M/^{16}M)_{ref}} - 1\right) \times 1000 \text{ ‰}$$

$$= ((^{17}M/^{16}M)_{sam} - (^{17}M/^{16}M)_{ref}) \times \frac{1000}{(^{17}M/^{16}M)_{ref}} \text{ ‰} \qquad 5.4)$$

substituting in eq. 5.3) gives

$$\delta^{17}M = \left(4x(D/H)_{sam} + (^{13}C/^{12}C)_{sam} - (^{17}M/^{16}M)_{ref}\right) \times \frac{1000}{(^{17}M/^{16}M)_{ref}}$$

$$= \frac{(4x(\delta D + 1000) \times (D/H)_{SMOW})}{(^{17}M/^{16}M)_{ref}} + \left(\frac{(^{13}C/^{12}C)_{sam}}{(^{17}M/^{16}M)_{ref}} - 1\right) \times 1000 \text{ ‰} \qquad 5.5)$$

For this study NGS#3 was defined as the reference gas, from table 5.2 the calculated $^{17}M/^{16}M$ ratio of the NGS#3 is 0.0109351. Substituting the value for $(^{17}M/^{16}M)_{ref}$ and the D/H ratio for SMOW of 1.5576×10^{-4} in equation 5.5) gives

$$\delta^{17}M = 0.0569762 \times \delta D + (^{13}C/^{12}C)_{sam} \times 91448.6 - 943.024 \qquad 5.6)$$

The $^{13}C/^{12}C$ ratio of the sample can be calculated from its $\delta^{13}C$ to give

$$\delta^{17}M = 0.0569762 \times \delta D + \left(\frac{\delta^{13}C}{1000} + 1\right) \times 1027.63 - 943.024$$

$$= 0.0569762 \times \delta D + \delta^{13}C \times 1.02763 + 84.6028 \qquad 5.7)$$

$$\delta D = \left(\frac{\delta^{17}M - \delta^{13}C \times 1.02763 - 84.6028}{0.0569762}\right) \qquad 5.8)$$

Hence provided the $\delta^{13}C$ (or $^{13}C/^{12}C$ ratio) of the unknown methane is available then the δD can be calculated using eq.5.8 from the measured $\delta^{17}M$. The main source of errors can be demonstrated by rearranging equation 5.5 as shown below

$$\delta D = \frac{\delta^{17}M \times (^{17}M/^{16}M)_{ref}}{4(D/H)_{SMOW}} - \frac{(^{13}C/^{12}C)_{sam} \times 1000}{4(D/H)_{SMOW}} + \frac{(^{17}M/^{16}M)_{ref} \times 1000}{4(D/H)_{SMOW}} - 1000$$

Since the third and fourth terms are constants, any error in the $^{17}M/^{16}M$ ratio of the reference gas results in a systematic error for δD, which will be corrected by analysing samples with known δD. The second term shows that a 1‰ uncertainty in the $^{13}C/^{12}C$ ratio of the unknown methane results in a 17‰ error in δD. However if the $^{13}C/^{12}C$ ratio of the sample methane can be made the same for all samples, as would be the case for methane produced from water by some chemical method, then this would result in a systematic error, which will by corrected by analysing samples of known δD. The first term indicates that a 1‰ error in measured $\delta^{17}M$ will translate to a 17‰ error in δD. The zero enrichment, table 5.2, shows that this instrument was capable of a precision of ±0.6‰ in $\delta^{17}M$, limiting the precision in δD to only ±10‰. However, using a mass spectrometer designed specifically for static analysis of CD_4 gas, Wright and Pillinger (1983) obtained a precision of ±0.25‰ for $\delta^{17}M$, which would give a δD precision of ±4‰. The instrument in question did not have the sophisticated facilities for matching samples and standards available to new generation mass spectrometer (Prosser *et al.*, 1990).

5.3.4 Effect of methane cracking on δD

Thermal processing of methane results in the formation of so-called cracking fragments (i.e. CH_3^+, CH_2^+, CH^+, C^+, and H_2^+). The analysis of methane gas by both dynamic and static mass spectrometry showed that the m/z 15 (CH_3^+) ion beam intensity was approximately 80% of the m/z16 (CH_4^+) ion beam intensity (see fig. 5.7). For the purposes of isotopic measurement it can be assumed that this effect is constant for both sample and reference gasses. However, in concert with the cracking of $^{12}CH_4^+$ there will be a similar effect with $^{13}CH_4^+$ and $^{12}CH_3D^+$ resulting in fragment ions at m/z 16 (i.e. $^{13}CH_3^+$ and some $^{12}CH_2D^+$). The effect of this on $\delta^{17}M$ was calculated for various compositions of sample gas and compared with calculations for which this effect was not

considered, the results are shown in table 5.3. The error in the measured $\delta^{17}M$ caused by cracking against the actual $\delta^{17}M$ value is plotted in fig. 5.12. The results show that for samples with a $\delta^{17}M$ within 100‰ of the reference gas this effect is approximately linear and fairly small; resulting in a 0.1‰ error for every 10‰ difference between the reference and sample gas. Since the precision was limited to ±0.6‰ by the instrument then this effect is negligible for methane samples with a $\delta^{17}M$ less than ±60‰. Hence when using the $\delta^{17}M$ to calculate the δD of a methane sample the cracking effect will only produce detectable errors for samples with δD greater than +1000‰ different to the reference gas.

5.3.5 Results using methane standards

To ensure that isotopic analysis of methane will yield accurate δD values the three methane samples described above were analysed as unknown samples (the analysis of NGS#3 was in effect a zero enrichment). Approximately 20nmol of sample gas was admitted to the baratron section. Aliquots of sample gas, *ca.* 0.5nmol, were admitted to the purification section where the procedure described in section 5.2.2 was used to clean the gas before analysis by the mass spectrometer. After analysis the sample gas was evacuated by the ion pumps for 5 minutes before an aliquot of reference gas was admitted. The δD results obtained on an average of 6 sample/reference comparisons are shown in table 5.3. As can be seen the δD calculated from measuring the m/z 16/17 ratio of methane are, within experimental error, equal to the true δD of the methane standards. This shows that the δD of nmol quantities of methane can be determined to an error of ±20‰ by static mass spectrometry, provided the $^{13}C/^{12}C$ ratio of the methane sample is known.

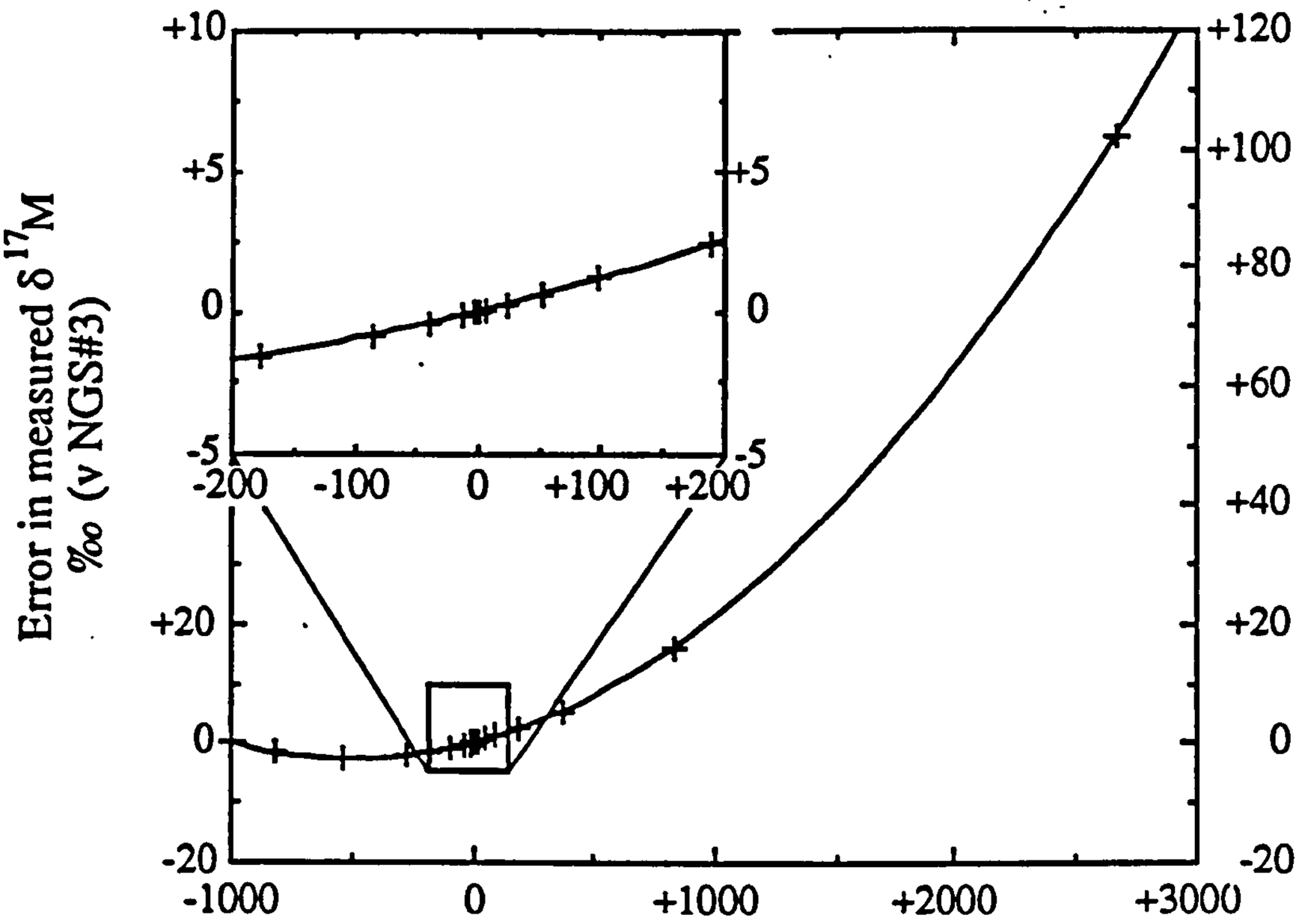

Fig. 5.12 Graph showing the error in $\delta^{17}M$ due to thermal cracking of methane in the source. The curve shown has equation $y = 0.0106\,x + 1.05\times10^{-5}\,x^2$. Near the origin the curve is approximately linear with slope 0.0106, i.e. for every 10‰ difference between sample and reference gas there will be an error in accuracy of 0.106‰,

Sample	δD (v V-SMOW) ‰	$\delta^{17}M$ (v NGS#3) ‰	Measured $\delta^{17}M$ (v NGS#3)	Measured δD (v V-SMOW) ‰
NGS#1	-141.8	+46.7	+46.1 ± 0.8	-153 ± 14
NGS#2	-175.1	+28.0	+28.1 ± 2.1	-188 ± 36
NGS#3	-176.3	0.0	-0.1 ± 1.3	-178 ± 22

Table 5.3 Analysis of 0.5nmol quantities of the three NGS samples by static mass spectrometry. Each result consists of the average of 6 sample/reference comparisons, the sample gas was cleaned before admission to the mass spectrometer source. The δD values of the methane samples were calculated from the measured $\delta^{17}M$ and are equal to the δD of the samples within experimental error. The overall precision of the mass spectrometer and inlet system is ±1.4‰, giving a precision in δD of ±24‰.

5.4 Conversion of water to methane

There are some cases were direct isotopic analysis of methane is desirable (this is discussed in section 5.5.1), however hydrogen is usually released from samples in the form of water. Clearly this water needs to be converted to methane before isotopic analysis by this technique is possible. As an initial investigation to the use of this technique it was decided to use aluminium carbide to convert water to methane, first used for hydrogen isotope analysis by Friedman and Irsa, (1952) and already demonstrated to work at the nmol level by Wright and Pillinger, (1983). The evaluation of the chemical reaction between aluminium carbide and water was investigated using the D/H mass spectrometer and conventional inlet described in chapter 2 and section 3.2. Isotopic analysis on nmol quantities of methane produced was performed by the static mass spectrometer described above.

5.4.1 Aluminium carbide

Aluminium carbide is a yellow-orange microcrystalline solid that reacts with water to form methane (Mellor, 1929; Durrant and Durrant, 1970). At room temperature the reaction is

$$Al_4C_3 + 12H_2O \rightarrow 4Al(OH)_3 + 3CH_4 \qquad 5.9)$$

Since some of the hydrogen in the water is converted to aluminium hydroxide and not methane there is the possibility of fractionation. However aluminium hydroxide decomposes to aluminium oxide and water at 450°C

$$2Al(OH)_3 \rightarrow Al_2O_3 + 3H_2O \qquad 5.10)$$

Hence the reaction of aluminium carbide with water above 450°C is

$$Al_4C_3 + 6H_2O \rightarrow 2Al_2O_3 + 3CH_4 \qquad 5.11)$$

which should in theory convert all the hydrogen in the water to methane.

5.4.2 Preparation of aluminium carbide

A batch of aluminium carbide which had been used in a previous study (Wright and Pillinger, 1983) was available for this study, however it had been found to give a very low yields of methane upon reaction with water. This batch of aluminium carbide had the appearance of a fine grey powder, not orange as expected. Addition of this powder to warm water produced no detectable reaction; instead it separated into two portions, a black powder which floated (possibly graphite or amorphous carbon) and a silver-grey powder which sank (possibly aluminium oxide and hydroxide). Since this commercially obtained batch of aluminium carbide was not suitable it was decided to evaluate the preparation of this material in the laboratory where it could be used relatively quickly after its manufacture.

Commercial aluminium carbide is prepared by heating aluminium powder mixed with an excess of graphite powder to 2200°C, using an electric arc furnace, in a graphite crucible. The reactions of carbon with aluminium or aluminium oxide are

$$4Al + 3C \rightarrow Al_4C_3 \qquad 5.12)$$

$$2Al_2O_3 + 9C \rightarrow Al_4C_3 + 6CO \qquad 5.13)$$

The excess graphite prevents oxidation of the aluminium carbide. Two methods of producing aluminium carbide in the laboratory were devised, described below. Later another commercial batch of aluminium carbide was purchased (Johnson Matthey). This was nominally 98.4% purity, however it had the appearance of a fine dark green powder, presumably the assay tested for impurities and not the quantity of unreacted graphite and aluminium.

There are several steps during the manufacture of aluminium carbide and its reaction with water in which carbon isotopic fractionation may occur. This will occur in any reaction where the products contain carbon in two, or more, different phases.

i) In the reaction of water with aluminium carbide (Eq. 5.11) excess aluminium carbide is used, some will remain unreacted.

ii) During manufacture of aluminium carbide, carbon monoxide is also formed (eq. 5.13). The presence of aluminium oxide cannot be eliminated.

iii) Both preparation methods, described below, resulted in less than 100% yields of aluminium carbide, most the graphite remaining unreacted.

All these reactions were carried out at high temperature, > 600°C, and so isotopic fractionation was small, less than 1‰, confirmed by the results obtained in 5.4.4. However small changes in $\delta^{13}C$ result in large systematic errors in δD (section 5.3.3). Hence if more accurate results are required then the $\delta^{13}C$ of the aluminium carbide will

have to be measured. Clearly any isotopic fractionation problems will be eliminated by using pure ^{12}C during the manufacture of the aluminium carbide. This will also improve accuracy since the m/z 17 ion beam will be free from the $^{13}CH_4^+$ interference.

Preparation method i)

In this method an attempt was made to duplicate the commercial production of aluminium carbide, by heating aluminium powder with excess graphite powder to a temperature of 2200°C. It was produced under vacuum to prevent oxidation of the aluminium carbide . A diagram of the apparatus used is shown in fig. 5.13a. The reaction vessel was constructed in two parts joined by a B19 cone and socket join. The lower part consisted of a B19 socket joined to a Pyrex tube (length 15cm, 22mm O.D., 18mm I.D.; Cambridge Glass), connection to the vacuum line (shown in fig. 5.7) was achieved with a side arm and a B10 socket. The upper part of the reaction vessel consisted of a sealed B19 cone and two tungsten rod feedthroughs (length 20cm, 1.5mm diameter). A heating ribbon filament, 1.5mm wide and 10mm length, was made from tantalum foil (0.025mm thickness, Goodfellow Metals) and spot welded to the tungsten rods. The filament was electrically heated, driven by a transformer (40V, 25A, Morite Windings) and controlled by a variable transformer (2.5A, Zenith). Usually a current of 12Amps through the filament was required to heat the filament to 2200°C, the exact current depended on the filament length and width. The temperature of the filament was measured by an optical pyrometer, accurate to ±50°C.

Aluminium and graphite powder (*ca.* 20mg), mixed to a 1:3 ratio by mass, was loaded into a tantalum bucket made from tantalum foil (0.025mm thickness, Goodfellow metals, approx. dimensions 2 x 2 x 2mm). A tantalum lid was placed over the bucket which was then balanced on top of the ribbon filament; a cross piece on the filament held the bucket in place. The apparatus was carefully assembled as shown in fig. 5.13a and the air slowly evacuated to a pressure of 10^{-5} mbar or better. The temperature was then increased slowly by increasing the electric current through the filament at a rate of about 1Amp per minute. If the filament was heated too rapidly the reactants would leave the tantalum bucket due to the rapid formation of carbon monoxide. Once a temperature of 2200°C was achieved the reaction was allowed to continue for a further five minutes.

Visual observation of the product, with a binocular microscope (Olympus, Tokyo, objective x40), showed it to consist predominantly of graphite powder and *ca.* 10% microcrystalline aluminium carbide which was orange in colour. It was estimated that each batch contained at least 2mg aluminium carbide, which should theoretically be capable of converting 83µmol of water to methane.

This preparation method was capable of producing batches containing a relatively high concentration of aluminium carbide. The small quantities of aluminium carbide

produced was sufficient for reaction with 20μmol quantities of water, however a new batch was required for each aliquot of water analysed on the conventional inlet during evaluation (described below, section 5.4.3). Another problem was that the tantalum ribbon filament would frequently burn-out, requiring its replacement. This was probably due to oxidation of the hot filament by carbon monoxide released during the reaction.

Preparation method ii)

An alternative method was developed in order to produce larger quantities of aluminium carbide, using the apparatus shown in fig. 5.13b. The reaction vessel was simply a 15cm length of quartz tube (12mm O.D., 10mm I.D., Cambridge Glass). This was attached to the vacuum line via a B10 socket joint (Cambridge Glass), a greaseless valve (J.Youngs) and a stainless steel 1/2" Ultra-Torr union (North London Valves & Fittings Co.), as shown in fig 5.13b. Approximately 10g of mixed aluminium and graphite powder, 1:3 ratio by weight, was loaded into the reaction vessel which was then attached to the vacuum line and evacuated. The aluminium/graphite powder was then reacted at a temperature of 1300°C overnight, heated by an insulated furnace, controlled by a variac and transformer.

The product consisted mostly of graphite along with *ca.* 2% aluminium carbide, most of the aluminium powder reacted with the quartz glass. This method was capable of producing larger quantities, *ca.* 200mg, of aluminium carbide, however the purity was lower. A disadvantage with this method was the reaction between the aluminium and the quartz glass, which would often crack resulting in the loss of vacuum (note that a Pirani detector on the vacuum line protected the pumps by automatically switching them off if air entered the system).

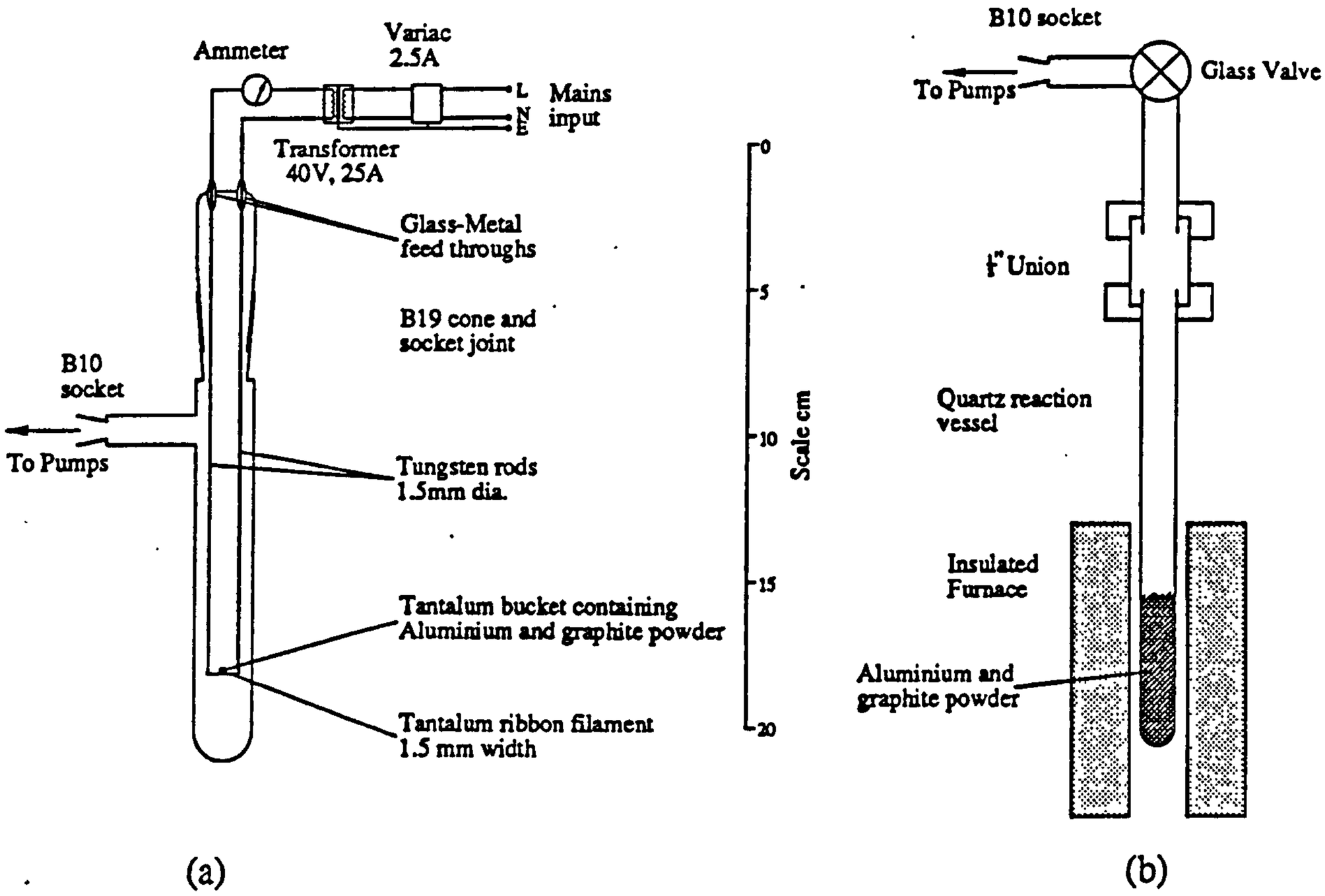

Fig. 5.13 Diagrams showing the methods used to manufacture aluminium carbide. a) 20 mg of graphite/aluminium mixture was heated to 2200°C by a tantalum filament. This produced small amounts of relatively high purity, ~10wt.%, aluminium carbide, *ca.* 2mg. b) 10 g of aluminium/graphite mixture was heated by a electric resistance furnace. This produced *ca.* 200mg of aluminium carbide but the purity was lower, ~2wt.%.

5.4.3 Reaction with water

An evaluation of this technique was made using the D/H mass spectrometer and conventional inlet system (described in chapter 2 and section 3.2). The only modification was the replacement of zinc shot in the reduction furnace with aluminium carbide. The aluminium carbide manufactured by preparation method (i) was usually used, unless stated otherwise. Analysis of the gas produced from the reaction of aluminium carbide and water, consisted of a mass scan from m/z 30 to m/z 12 to detect the presence of air (m/z 28), any unreacted water (m/z 18 and 17) and methane (mainly m/z 16 and 15). Prior to reaction with water the aluminium carbide was heated to 600°C to remove any trapped atmospheric gases and water from aluminium hydroxide. As it was heated there would be a large release of gas between 400°C and 500°C, a mass scan showed that it consisted predominantly of methane, *ca.* 5μmol, presumably by the reaction of water, released from aluminium hydroxide, with aluminium carbide (equation 5.10 & 5.11

above). The water was probably acquired from atmospheric moisture during the transfer of aluminium carbide from the preparation system to the inlet system.

Sample water (de-ionised tap water), usually 11μmol, was injected into the preparation line, purified and transferred to the aluminium carbide furnace using liquid nitrogen, by the same procedure for the conventional inlet (section 3.3.2). Once the water had been transferred the liquid nitrogen was removed and the aluminium carbide heated to 600°C. The water was allowed to react for 15 minutes after which time the gas produced was analysed on the mass spectrometer. It was found that approximately five minutes was sufficient for the conversion of water to methane. With shorter reaction times the sample water was not completely converted to methane, noted by the presence of m/z 18 and m/z 17 peaks, from H_2O^+ and OH^+ respectively, being present during the mass scan of the resultant gas.

A calibration was made for the amount of methane in the inlet section and the m/z = 16 ion beam intensity using standard methane, NGS#3. The septa of the injection port was replaced by a B10 cone to enable connection of a 2l bulb containing the methane standard gas. Aliquots of standard gas were admitted to the inlet section and comparison was made between the pressure measured by the capacitance manometer and the m/z 16 ion beam intensity. The results obtained, shown in table 5.4 and fig. 5.14 show that the m/z 16 ion beam intensity was proportional to the quantity of methane gas in the inlet. In addition the m/z 2 ion beam intensities were also determined, since this results from the thermal cracking of methane in the mass spectrometer source. Knowledge of the 16/2 ratio of methane allows calculation of an additional species at m/z 2, *i.e.* hydrogen which may be produced by the aluminium carbide reaction.

A series of preliminary experiments were performed to determine the optimum temperature for the aluminium carbide-water reaction using 5.5μmol quantities of de-ionised tap water. Below 250°C peaks corresponding to the presence of water (m/z 18 and 17) appeared in the mass scan indicating that some of the water remained unreacted. Between 250°C and 450°C the quantity of methane produced was constant and there was no water evident in the mass scan. Above *ca.* 500°C the yield of methane was approximately double that than when the furnace was operated between 250°C to 450°C. The low yield when the furnace was operated at 250°C to 450°C results from the water forming aluminium hydroxide as well as methane (equation 5.9, above) At higher temperatures, up to 700°C, there was no further increase in the yield of methane. From these results it was decided to operate the furnace at a temperature of 600°C, well above the temperature at which aluminium hydroxide decomposes.

Quantity of CH_4 µmol	Baratron reading V	m/z = 16 ion beam intensity $x10^{-11}$ A	m/z = 2 ion beam intensity $x\ 10^{-12}$A
4.99	2.79	7.96	1.01
2.84	1.586	4.44	0.46
2.66	1.485	4.23	0.41
1.59	0.891	2.47	0.24
1.47	0.822	2.34	0.21
0.89	0.500	1.38	0.11
0.51	0.286	0.770	0.06
0.46	0.259	0.725	0.01
0.30	0.166	0.434	0.02
0.26	0.146	0.401	0.00
0.15	0.082	0.226	0.00
0.09	0.049	0.127	0.00

Table 5.4 m/z 16 and 2 ion beam intensities for various quantities of methane in the dynamic mass spectrometer source.

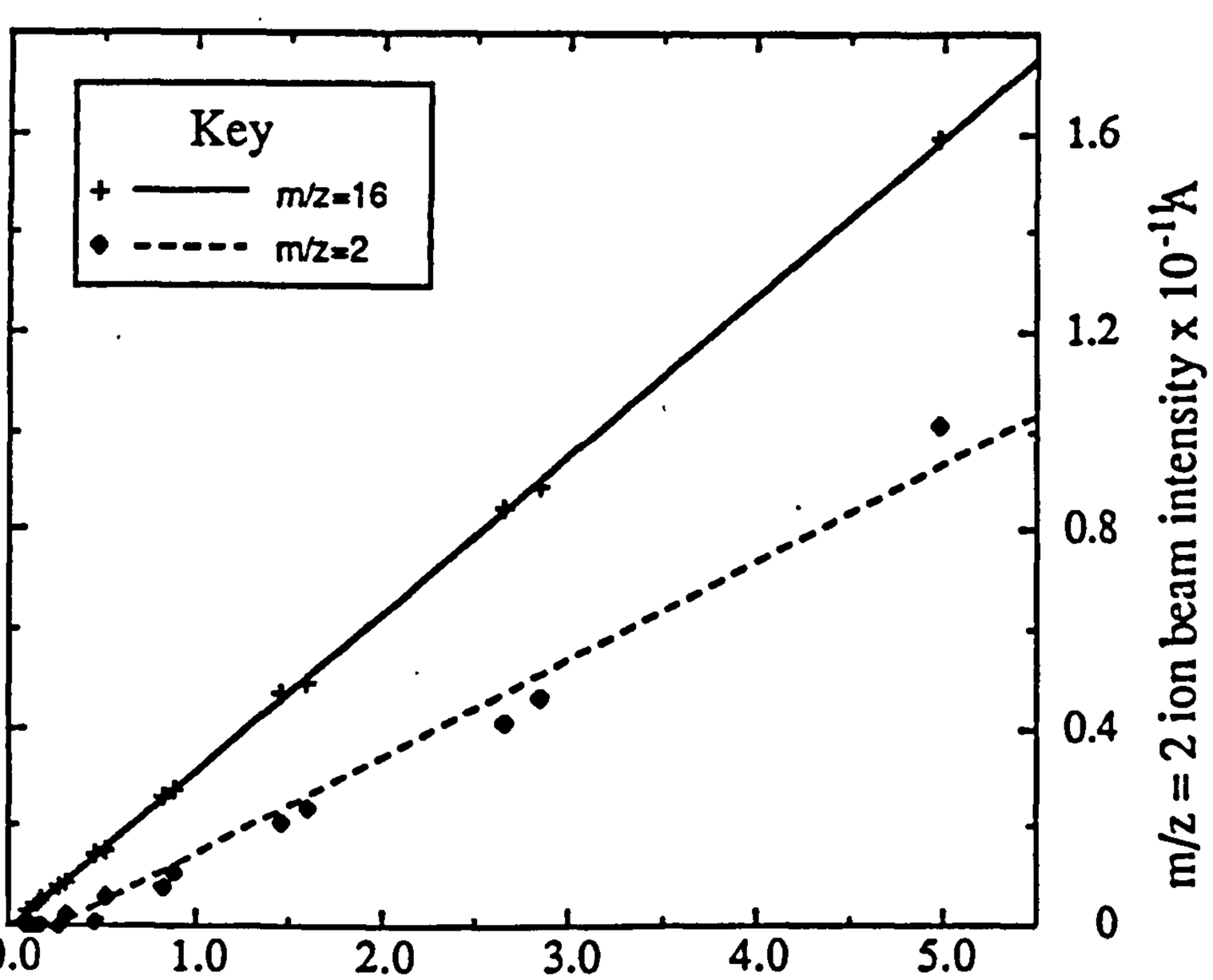

Fig. 5.14 Graph showing the m/z 16 and 2 ion beam intensities for various quantities of methane, used to calibrate the quantity of methane (and hydrogen) produced by the reaction of water with aluminium carbide.

The yield of methane obtained, using the calibration graph of fig. 5.14, was only 80±5% of the theoretical yield. A mass scan from m/z 30 to m/z <2 of the gas produced by aluminium carbide indicated an excess of m/z 2 ion beam intensity when compared to methane standard gas. Thus indicating that hydrogen was also formed as a side reaction of water with either the aluminium carbide or the graphite present as an impurity.

Experiments were performed using *ca.* 400mg quantities of the commercial batch of aluminium carbide to determine whether higher yields of methane could be obtained by varying the conditions of the reaction vessel could result in higher yields of methane. The commercial aluminium carbide was used because it was available in greater quantities, even though the yield of methane produced with 11μmol of water was much lower, 38±3%, than with the laboratory produced aluminium carbide. (The cause of the lower yields of methane obtained with the commercial aluminium carbide was due to the greater quantity of aluminium carbide used; see later). It was found that changing the reaction furnace temperature did not have any effect on the yield of methane.

The effect of analysing different quantities of water are shown in fig.5.15 which shows a plot of fractional yield of methane against quantity of water analysed. The best fit line for the methane has a correlation coefficient of 0.85, which is significant at the 99% level, showing that there is a relationship between yield of methane and sample size. Two possible reasons for the production of hydrogen from water could be i) a side reaction with aluminium carbide as suggested by Friedman and Irsa, (1952) or ii) reduction of water to hydrogen by the graphite powder present in the aluminium carbide (the water-gas reaction).

$$H_2O + C \rightarrow H_2 + CO \qquad 5.14)$$

In order to evaluate the importance of the water-gas reaction, the commercial batch of aluminium carbide was purified, by density separation, to remove the graphite. A solution of bromoform and dichloromethane (BDH Chemicals, Poole), was mixed such that it had a density of 2.30gcm^{-3}. The commercial aluminium carbide was added and centrifuged at 2000 rpm for an hour. The graphite powder which floated, having a density of 2.25 gcm^{-3}, was decanted. The remaining aluminium carbide (and aluminium oxide) was loaded into a glass tube and dried by pumping. The resulting aluminium carbide consisted of an fine orange powder, clearly containing significantly less graphite than the starting material. This aluminium carbide was used in a repeat experiment to determine yields of methane produced from different quantities of water. However the results obtained were no different from the previous results shown in fig. 5.15. Thus it is considered that the production of hydrogen during the conversion of water to methane is not due to the presence of graphite, but is a side reaction of aluminium carbide.

Consideration of the reaction of water with aluminium carbide indicates that the reaction is a two step process. In the first step a water molecule reacts to form a CH_2 group bonded to aluminium carbide; a second water molecule reacts with this CH_2 group to produce methane. However if the intermediate CH_2 group is unstable then this may decompose to form hydrogen before a second water molecule can react to form methane. Hence the proportion of methane produced will depend on the amount of water present after formation of CH_2 groups on the aluminium carbide i.e. it is the water/Al_4C_3 ratio which is important as well as P[H_2O]. This explains the lower yields of methane obtained when using smaller quantities of water. It also indicates that lower yields will be obtained if more aluminium carbide is present, hence the higher yields obtained when using the laboratory produced aluminium carbide. If the formation of methane is a two stage process with an unstable intermediate compound then the dependence of the fractional yield of methane against quantity of water will have the form

$$y = 1 - e^{-kx} \qquad 5.15)$$

where y is the fractional yield of methane,
x the quantity of water and
k is a constant.

Hence a plot of ln(1-yield) against quantity of water will be linear with intercept 0 and slope -k. Fig 5.16 shows such a graph for the results shown in fig.5.15. The best fit line has an intercept of 0, within experimental error (-0.2±0.4), and correlation coefficient 0.83, significant at the 99% level. These results tend to indicate that the hydrogen is formed as a side reaction of water with aluminium carbide and that for nmol samples of water the yield of methane will be even further reduced. Considering the best case when using the laboratory produced aluminium carbide where the yield of methane was 80±5% for 5.56µmol quantities of water, then k=-1.6±0.3 in equation (5.15). This implies that for 0.01µmol of water the yield of methane will be 1.6±0.3%, *i.e.* resulting in the production of .080±0.015 nmol of methane, which is just within the sensitivity range of static mass spectrometry.

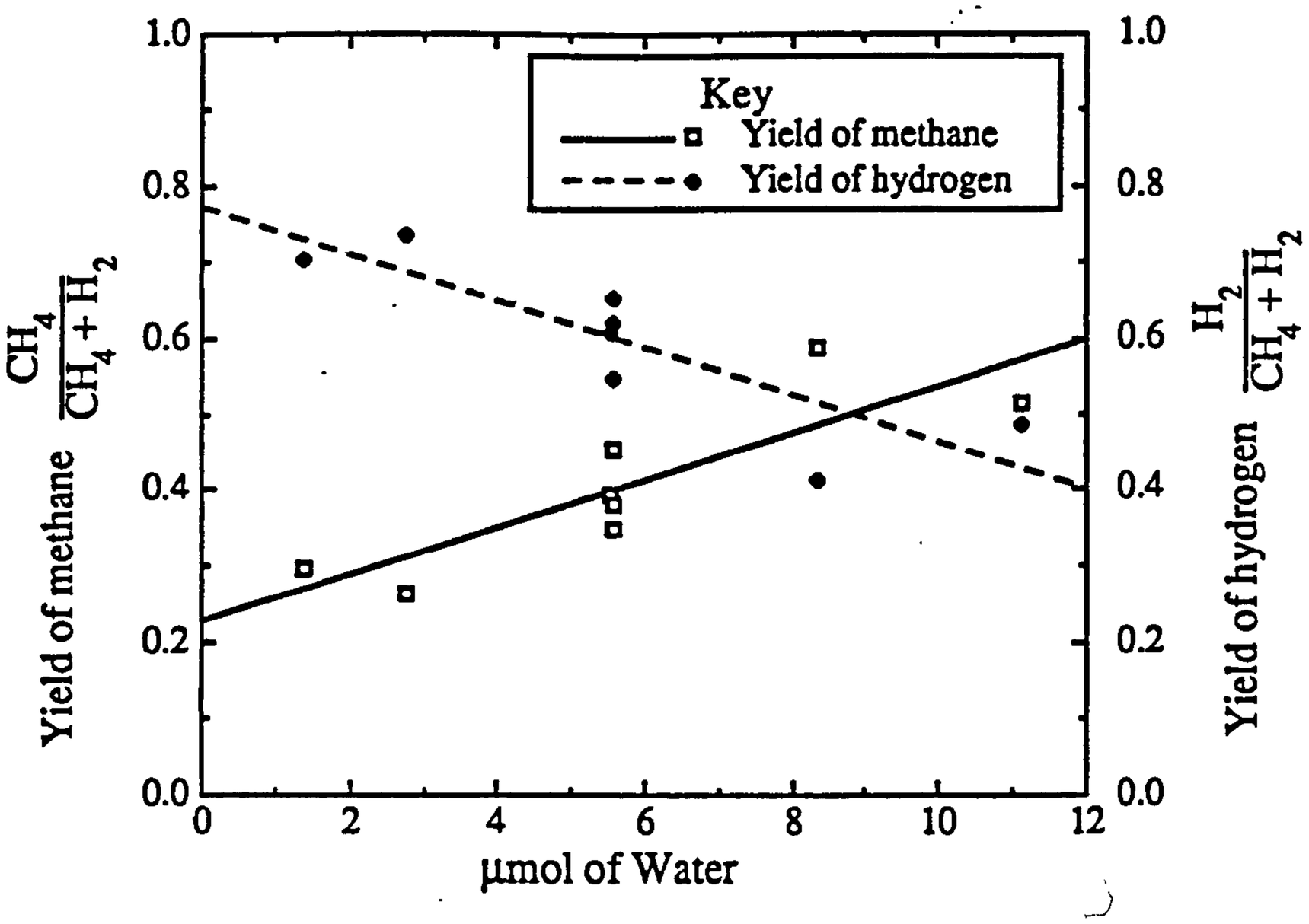

Fig. 5.15 Graph showing the yields of methane and hydrogen (by volume) from the reaction between water and aluminium carbide with different sized water samples. With smaller water samples the proportion of methane to hydrogen decreases.

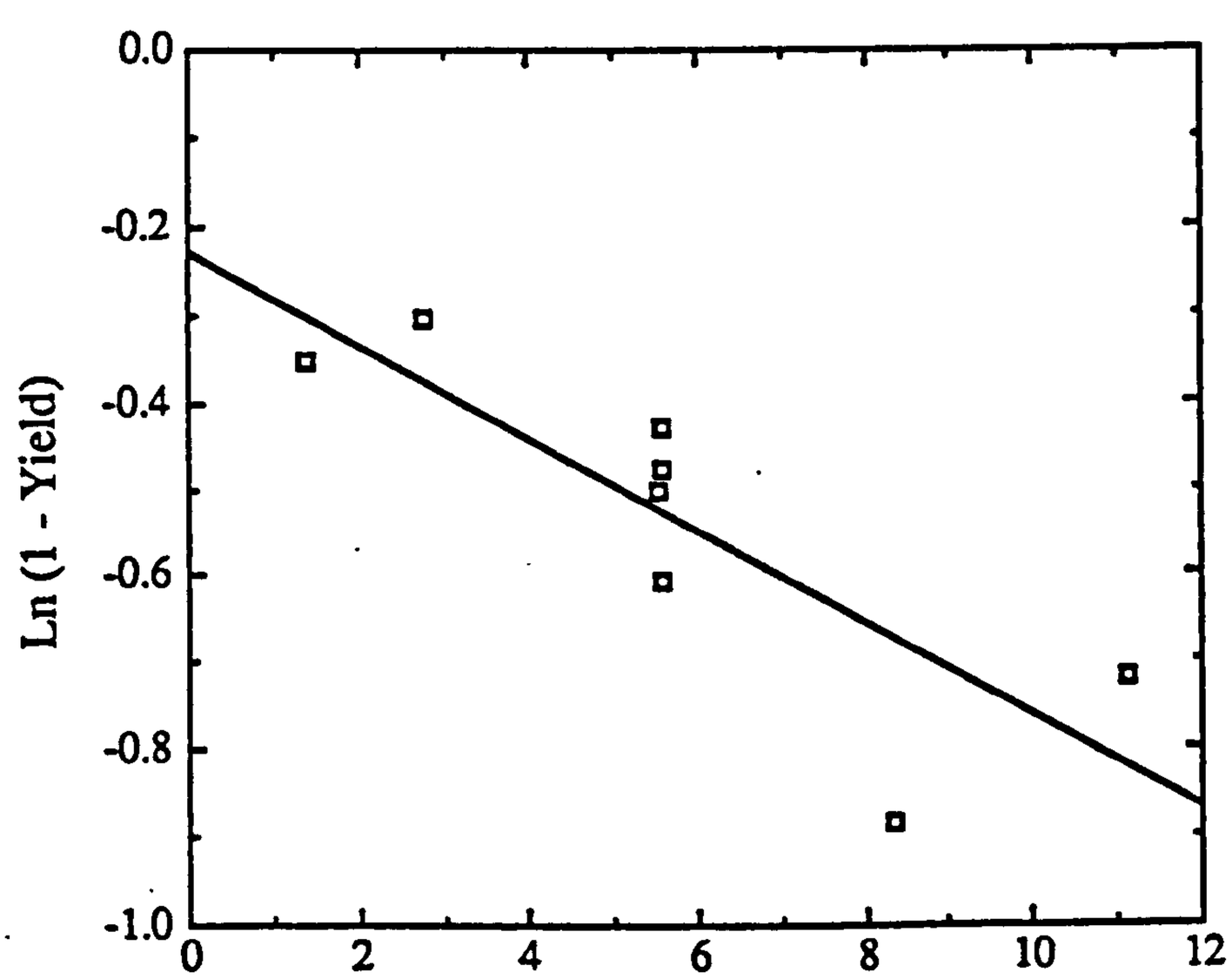

Fig. 5.16 Graph showing the yields of methane between water and aluminium carbide with different sized water samples. The best fit line has a correlation coefficient of 0.83 and within error passes through the origin, indicating the the yields will be further reduced for even smaller samples of water

5.4.4 Hydrogen Isotope determination of water

Despite the low yields of methane obtained it was deemed advantageous to measure the isotopic δD of the methane produced from the reaction of water with aluminium carbide. Due to the low yields, the minimum amount of water that could be analysed was 0.01μmol of water with a precision of ±20‰, which was much better than that obtained using dynamic mass spectrometry; however, of greater importance is the possibility of chemical fractionation of the isotopes. A valve and B10 cone was added to the inlet section of the conventional line to enable a 'take-off' vessel to be attached. A few pellets of molecular sieve were loaded into the 'take-off' vessel which was then attached to the inlet and evacuated. The molecular sieve was gently heated with a hydrogen flame to remove any trapped gases, mainly water. Once methane was produced from samples of standard water (see below), it was transferred to the 'take-off' vessel using liquid nitrogen. The 'take-off' vessel was closed and then transferred to the static mass spectrometer inlet for analysis.

Several water samples were used with δD ranging from -428‰ to *ca.* +10 000‰. Deuterium-rich water samples were used since interference from ^{13}C on the m/z = 17 peak is more significant for deuterium-depleted samples. The deuterium-rich samples had been prepared in 1980 by Dr. R. Hinton (at the University of Cambridge) by mixing weighed amounts of de-ionised water with deuterated water (99.75% isotopic purity, BDH Chemicals Ltd., Poole), to produce a sample with nominal δD of +10 000‰. This was then further diluted to produce 4 water samples with a wide range of δD values. The δD values of the water samples were determined using the conventional D/H inlet and mass spectrometer (using the procedure described in section 3.3.2); the results obtained are shown in table 5.5.

NBS Standards	δD (v V-SMOW) ‰	Mixed Standards	δD (v V-SMOW) ‰
SLAP	-428	nominally	
V-SMOW	0	+10 000‰ (A)	
		1:1, dist:(A)	+4569
		3:1, dist:(A)	+2231
		10:1, dist:(A)	+770
		20:1, dist:(A)	+331

Table 5.5 Measured δD values for isotopically heavy water samples used to evaluate the aluminium carbide reaction.

The aluminium carbide prepared by method (i) was used, a new batch prepared for each water sample of 11μmol. As expected there was a memory effect associated with the glass line (see section 3.3.6). The memory effect was compensated by conditioning the glass line using the following procedure. The zinc furnace was used and the sample water analysed until two consecutive δD determinations gave identical results within experimental error. The zinc furnace was then replaced by a furnace containing aluminium carbide and the methane produced by the following 11 μmol of water was trapped in the 'take-off' vessel and transferred to the inlet of the static mass spectrometer .

An aliquot of methane of approximately 0.5nmol was admitted to the inlet section, any impurities removed and analysed as described in sections 5.2.2 and 5.3.2. The results obtained of the $\delta^{17}M$ for each water sample is shown in table 5.6. The $\delta^{13}C$ of the graphite powder used to produce the aluminium carbide was -25.2‰. Hence the δD of the water samples can be calculated using equation (5.8). The calculated δD values of the methane produced by the samples are also shown in table 5.6. A graph of the δD of the water sample, as measured by conventional mass spectrometry, against δD calculated from $\delta^{17}M$ is shown in fig. 5.17. The best fit line is $y = 0.954x + 2.4$. The slope of the best fit line, 0.954 ± 0.004, is not exactly equal to one, even within statistical error. Fig. 5.18 shows the deviation of the calculated δD from the actual δD of the water sample against δD of the sample. This systematic error in the calculated δD is larger than that expected from the cracking of methane gas in the mass spectrometer source (described in section 5.3.4). It was decided not to use the correction for the cracking of methane but to use the graph shown in fig. 5.18 as a calibration chart, for the following reasons:

i) the exact fraction of methane cracked to CH_3 and possible effect of deuterium on the cracking pattern are not known and

δD of sample water (v V-SMOW) ‰	Measured $\delta^{17}M$ (v NGS#3) ‰	Calculated δD (v V-SMOW) ‰
-428	+34.2 ± 1.0	-430 ± 17
0	+60.4 ± 1.4	+30 ± 24
+331	+76.8 ± 0.3	+318 ± 5
+770	+100.4 ± 0.6	+731 ± 10
+2231	+180.5 ± 0.7	+2138 ± 12
+4569	+306.9 ± 1.6	+4356 ± 28

Table 5.6 Results of the isotopic analysis of methane produced by the reaction of sample waters with aluminium carbide. The δD of the hydrogen in the original water samples was then calculated from the measured $\delta^{17}M$.

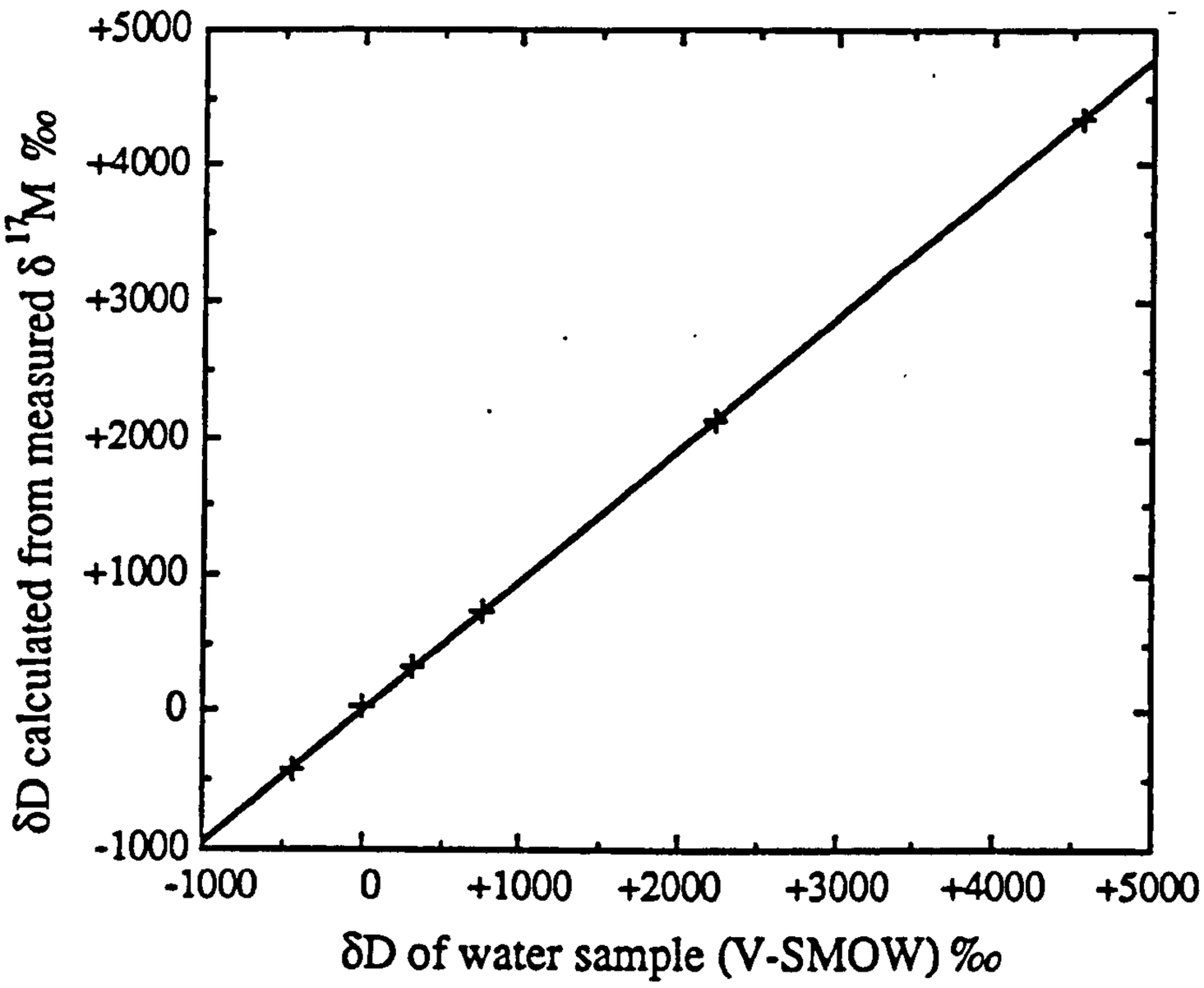

Fig. 5.17 Graph of the δD of various water samples against the δD calculated from analysis of 0.5nmol aliquots of methane produced from the reaction of the water with aluminium carbide. The best fit line has equation $y = 0.954x + 2.4$ (with correlation coefficient, $r = 1.000$).

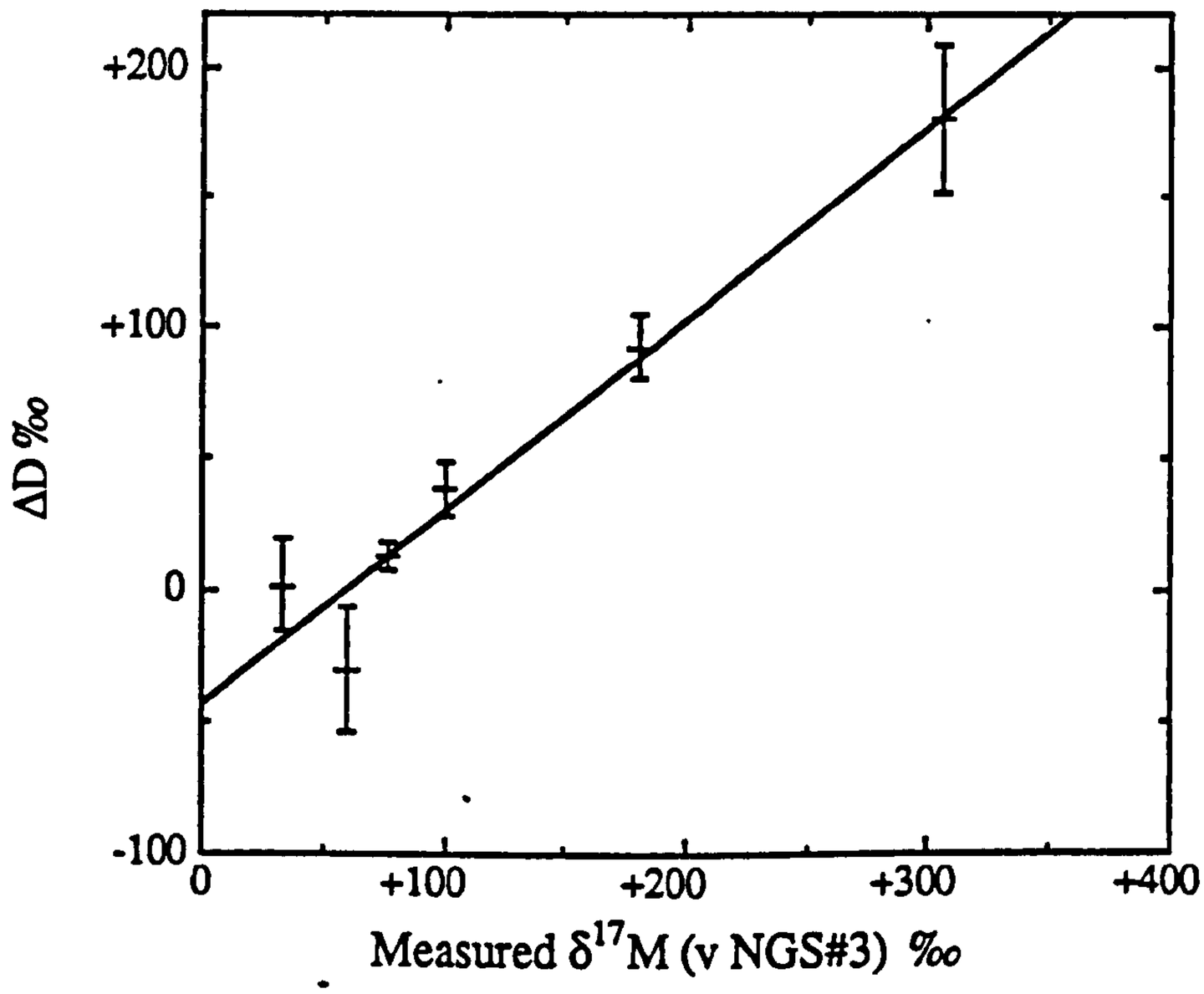

Fig. 5.18 Graph showing the difference between the actual δD and calculated δD for the water samples. The error in calculated δD becomes larger for higher $\delta^{17}M$ values of the methane analysed. This is partly due to the thermal cracking of methane in the source.

ii) there may be other instrumental systematic fractionation effects associated with deuterium-enriched samples.
The adoption of a calibration chart obtained by experiment compensated for both these instrumental effects.

The results obtained from the water standards indicate that the amount of isotopic fractionation resulting from the low yields of methane obtained from aluminium carbide was not detectable within experimental error. The yield of methane was only *ca.* 80±5% of the expected yield.

5.5 Summary

The aim of this study was to determine the potential use of static mass spectrometry to analyse nmol quantities of hydrogen, in the form of methane. Previous studies (Irako *et al.*, 1975; Gardiner and Pillinger, 1979) have shown that hydrogen is not suitable for isotopic analysis by mass spectrometry due to its very short half life in the source; however methane has a much longer half-life and so should be more appropriate.

A MM3000 static mass spectrometer was used to investigate the possibility of the isotopic analysis of methane. It was found that the greatest precision in measuring the m/z=17/16 ratio was obtained when using a relatively high ionisation current of 50μA. Under these source conditions the methane had a half life of *ca.* 17 minutes in the source and a precision in δD of ±0.6‰ was obtained on 0.6nmol quantities of methane.

An inlet system was developed to remove impurities from methane samples before admission to the static mass spectrometer. Condensible gases such as carbon dioxide, sulphur dioxide and water were removed by a cryo-trap operated at -185°C. Most carbon monoxide (99.9%) and 50% of the hydrogen was removed by passing the gas over copper oxide at a temperature of 400°C in conjunction with the cryo-trap. Most of the hydrogen was removed by condensing the methane onto 3A molecular sieve using liquid nitrogen and then evacuating the hydrogen which was non-condensible. It was not possible to remove nitrogen impurities by the inlet. However in a system where sample water is converted to methane, the nitrogen could be readily removed before the water was converted to methane.

The inlet system was evaluated by analysis of methane natural gas standards The precision in $\delta^{17}M$ of the inlet and mass spectrometer was 1‰ for 0.5 nmol quantities of methane. The δD value of the methane was calculated from the measured $\delta^{17}M$ of the sample gas and the known $\delta^{13}C$ of both the sample and reference gas. It was determined that the presence of ^{13}C in the methane would result in a 17‰ error in δD for each 1‰ error in $\delta^{17}M$. Another possible source of error considered was that due to methane

cracking in the mass spectrometer source. Calculation indicated that this would result in a small systematic error of 1‰ in the measured $\delta^{17}M$ for every 100‰ difference between the $\delta^{17}M$ of the sample and reference gas and so in most cases is negligible. The δD values of the natural gas standards were calculated from the measured $\delta^{17}M$ values and compared to the known δD values of the standards. Results showed that this technique was capable of analysing the δD of 0.5nmol quantities of methane to a precision of ±17‰.

A preliminary investigation was performed to evaluate the use of aluminium carbide to convert sample water to methane for isotopic analysis by this technique. However hydrogen was also produced in a side reaction between the water and aluminium carbide. The yield of methane was larger when converting larger amounts of water or using smaller quantities of aluminium carbide. Due to the lower yields obtained when using smaller quantities of water the minimum amount of water that would give enough methane for isotope analysis is 0.01μmol. Analysis of 0.5nmol aliquots of methane produced from 5.56μmol water samples with δD ranging from -428 to + 4350‰ showed that the low yields of methane did not result in any significant fractionation in the hydrogen isotopes of the methane produced.

Chapter 6
Conclusions

6.1 Summary

At the onset of this work it was recognised that hydrogen isotopes in various extra-terrestrial materials can be diagnostic of processes and events that formed them. Most hydrogen and deuterium was produced in the initial processes of the universe and subsequent events serve only to remove these isotopes from the system. Deuterium is consumed at a faster rate than hydrogen during stellar nucleosynthesis hence, unlike other elements stellar processing reduces rather than increases its abundance relative to hydrogen. Changes in deuterium/hydrogen isotope ratios are mainly the result of physical and chemical isotopic fractionation. However, as the mass ratio between the two hydrogen isotopes is very large, compared to the isotopes of other elements, large isotopic fractionation can be induced by physical and chemical fractionation processes. As a result hydrogen isotope analysis can provide different information from the study of other element isotope ratios.

A dynamic mass spectrometer system was constructed to analyse hydrogen isotopes of extra-terrestrial samples. Conventional dynamic mass spectrometers are capable of analysing D/H ratios with high precision on reasonably small samples, (typically ±2‰ on 0.05mmol of hydrogen). However, it was realized that the sample size requirement was too large for the analysis of extra-terrestrial material and a much more sensitive instrument required. Conventional D/H mass spectrometers and inlet systems are usually designed to give maximum accuracy but in achieving this very little of the sample gas is actually analysed; the rest provides a high stabilising pressure in the inlet or is bled to waste. It was considered that this high wastage could be considerably reduced by appropriate design of an inlet system. The D/H mass spectrometer was designed to allow development and evaluation of various inlet systems. Table 6.1 compares the sensitivity and accuracy of the various inlet systems developed.

One inlet was similar to conventional inlets and used to evaluate the mass spectrometer and identify potential problems with smaller samples. Care was taken to make this inlet as small as practically possible to increase the sensitivity of the mass spectrometer. This inlet and mass spectrometer system enabled the analysis of 10μmol of hydrogen with a precision of ±2‰. The blank from this system was found to be negligible, *ca.* 0.2μmol hydrogen. However, a much more serious problem was found to be a memory effect, where the sample was contaminated by the previous sample

analysed. A series of experiments was performed on the conventional inlet to determine the cause of the memory effect and, if possible, eliminate it. These experiments indicated that the memory effect was due to water adhering to the glass walls (or possibly the teflon valves) in the inlet system. Sample water would isotopically exchange with the adhering water before it was reduced to hydrogen. Although the memory effect could not be eliminated a correction could be applied to compensate for it. For samples containing at least 10μmol of water and a δD value within ±200‰ of the previous sample then the error in accuracy was less than 10‰.

The conventional inlet was useful in determining the cause of the memory effect and analysing the enriched water samples prepared by Dr. R. Hinton (see section 5.4.4). This inlet is routinely used for bulk hydrogen isotope analysis of terrestrial rocks (Maynard *et al.*, 1990) and some meteorite samples (Grady *et al.* in prep.). However, the relatively large sample size requirement prevents this technique being used for the analysis of many extra terrestrial samples.

Two inlet systems were developed to improve the sensitivity of the dynamic mass spectrometer. Both attempted to increase sensitivity by increasing the percentage of hydrogen sample gas that entered the mass spectrometer source. In the 'pusher' technique sample was transferred to a capillary zinc furnace for reduction to hydrogen, where-upon aliquots, *ca.* 10% of the sample, were then pushed by a flow of helium into the mass spectrometer for isotopic analysis. Samples containing 0.3μmol hydrogen could be analysed with a precision of ±15‰. There were problems with the zinc furnace being able to reduce a maximum of 17μmol of water before it became exhausted and this technique still did not possess the sensitivity required.

The 'flow thru' technique increased sensitivity by manipulating water as the sample gas. Sample was transferred to a capillary from where a small leak flowed towards the change-over valve of the mass spectrometer. The sample water was reduced to hydrogen as it passed over the zinc furnace placed immediately in front of the change-over valve. This inlet system had the greatest sensitivity, capable of analysing 0.1μmol of hydrogen. However the precision was poor due to the blank of 0.055±0.017μmol hydrogen and the memory effect. Most of the blank contribution originated from hydrogen being evolved from the zinc furnace and was equivalent to analysing a sample containing between 0.025 and 0.05μmol hydrogen; the blank introduced during sample loading was smaller, 0.02±0.01μmol hydrogen. The overall precision due to the blank and memory effect was *ca.* ±1000‰ for samples containing 0.1μmol hydrogen.

The high sensitivity of the 'flow thru' technique enabled it to be used as part of a study of secondary alteration in Semarkona, an unequilibrated ordinary chondrite (type LL3.0). The high sensitivity was required since the samples consisted of fragments of individual chondrules most containing less than 0.05μmol water. The hydrogen isotope

results combined with the other techniques, thermoluminescence and petrography, confirmed the degree of unequilibration of this meteorite and suggested that chondrules which had experienced aqueous alteration were enriched in deuterium.

A more detailed study of Semarkona and other equilibrated ordinary chondrites is needed to enable the nature of the deuterium carrier and the relationship between petrologic sub-type and secondary processes to be determined. However the 'flow thru' technique was at the limit of its sensitivity, the other meteorites of interest had lower δD values and contained less water than Semarkona. Most of the relevant meteorites are available in only small amounts.

For these reasons it was decided to continue development of a small sample D/H mass spectrometer. The dynamic mass spectrometer only just had the required sensitivity when most of the hydrogen sample gas was admitted to the source. Instead of concentrating on the inlet system a different approach was adopted, the use of static mass spectrometry. The use of methane as a static mass spectrometer gas was evaluated, and it was shown that the δD could be measured to an accuracy of ±20‰ on 0.5nmol quantities of methane. An initial investigation of the use of aluminium carbide to convert sample water to methane was performed. Despite the low yields of methane, due to the formation of hydrogen as a by-product, there was no detectable hydrogen isotope fractionation. The effect of low yields limits the smallest sample size that could be analysed to ca. 0.01μmol of water, which would be sufficient for continuing the investigation of secondary processes in unequilibrated ordinary chondrites.

Mass Spectrometer Technique	Sample size (nmol) H_2	Accuracy δD ‰ (2σ)	Comments
Conventional Inlet	10 000	4	
Pusher Inlet	300	15	Short lifetime of zinc furnace
Flow Thru	100	1000	Used for Semarkona project
Static m.s. (H_2O)	10	17	low yield of methane to water conversion
Static m.s. (CH_4)	1	17	Analysis of methane gas.

Table 6.1. A comparison of the sensitivity and accuracy of the various inlet systems developed. The most sensitive was the static mass spectrometer with an accuracy comparable to conventional dynamic mass spectrometry.

6.2 Further work

Most of the work described in this thesis has been concerned with the development of D/H mass spectrometers capable of analysing small samples of hydrogen. Clearly the static mass spectrometer technique has the most potential. However two problems remain before the full capability of this technique can be realised, apart from the current lack of a dedicated static mass spectrometer: i) the memory effect must be overcome and ii) the low yields of methane obtained by the reaction of water and aluminium carbide artificially limit the ultimate sensitivity.

The memory effect will reduce the accuracy and limit the sample size whatever mass spectrometer technique is used to analyse the hydrogen from water, since it is due to the exchange of water in the inlet. Experiments are needed to investigate the use of materials, apart from glass, in the construction of the inlet. Teflon is one possibility, since it is chemically inert, however there may be problems with gas trapped in small cracks. If no other material is suitable then the design of an inlet capable of being heated to high temperature, ~400°C, may reduce the memory effect. To completely eliminate the memory effect it may be necessary to extract water from samples and convert it to hydrogen or methane (depending on mass spectrometer technique) in separate individual closed ampoules.

Some applications for a static mass spectrometer capable of analysing nmol quantities of methane are described in section 6.3. The main problem for any direct analysis of methane would be the removal of large quantities of nitrogen probably requiring the development of a gas chromatography system. Obtaining water from samples by combustion or pyrolysis of samples will enable the easy removal of nitrogen form the sample water by cryogenic separation. This would then require a method of converting water to methane. The low yields of methane obtained by the aluminium carbide reaction limits the technique to the analysis of 0.01 µmol of water. Since yields are not constant it may be necessary to measure the amount of hydrogen produced, by capacitance manometer, in order to determine the original sample size. If a closed ampoule technique is employed to prevent memory effects then the addition of copper oxide to the aluminium carbide may give higher yields since hydrogen produced will be oxidised back to water. Methane was found to be stable over copper oxide at temperatures below 550°C.

Other chemical conversion methods may produce much higher yields of methane, these include the reaction of hydrogen with graphite to produce methane using a nickel catalyst (Mellor, 1929), or reaction of water with grignard type reagents (Greenwood and Earnshaw, 1984). The reaction of water with graphite is

$$2H_2 + C \leftrightarrow CH_4 \qquad 5.16)$$

Hydrogen can be readily produced by reaction of the sample water with zinc. By condensing methane onto a molecular sieve as it is produced high yields may be obtained. Grignard reagents are organometallic compounds, (strictly speaking only organomagnesium compounds) with chemical formula, RMX, where R is an organic group, such as CH_3, M is a metal and X is a halide. Hydrolysis with water produces the organic group

$$H_2O + 2RMX \rightarrow 2RH + MO + XH \qquad 5.17)$$

This reaction was used by Orchin *et al.*, (1949) using methyl magnesium iodide for D/H isotopic analysis, but low yields of methane were obtained. A derivative of the grignard reagents are dimethyl compounds which react (explosively) with water to form methane.

$$H_2O + RMR \rightarrow MO + 2RH \qquad 5.18)$$

Clearly this is a single step reaction and the only products are the metal oxide and methane; hence there is no possibility of hydrogen isotope fractionation due to the formation of hydrogen halides, as in reaction (5.17). Use of dimethyl zinc may be favourable since this is less reactive than dimethyl magnesium and is a liquid. As a bonus this may remove water adsorbed on the glass walls of the reaction vessel and so eliminate any memory effect. Consideration of the handling of these reagents is required since they also have the potential of removing the operator.

6.3 Applications

At present this static mass spectrometer technique is capable of isotopic analysis of nmol amounts of hydrogen in methane, but if the hydrogen is in the form of water then at least 10nmol of water is required. The isotopic analysis of methane itself has several applications, a few concerning the study of meteorites.

One possibility is the determination of the origin of methane in lunar soils. Early analysis of lunar soils (Ponnamperuma *et al.*, 1970; Abell *et al.*, 1970) indicated the presence of indigenous hydrocarbons, mainly methane. The methane is thought to be produced by interaction of solar wind carbon and hydrogen in the lunar soil, hence the D/H of lunar hydrogen and hydrogen in the methane should be deuterium free. Measurements of the δD of hydrogen released by lunar fines have been complicated by

the exchange between hydrogen and water in the lunar rocks during extraction, the lowest δD measured for the hydrogen is -873‰ (Epstein and Taylor, 1970). Analysis of the methane in lunar fines may confirm the solar wind hypothesis and place a maximum D/H ratio of the solar wind.

A similar study of methane in gas rich meteorites along with carbon isotope analysis may determine the irradiation source and place constraints on formation models of these meteorites (reviewed in Caffee *et al.*, 1988). If the source of the radiation is of solar wind origin then methane produced would be deuterium depleted, carbon isotopes of the methane may even provide information about changes in the solar wind isotopic composition. Alternatively the irradiation could be from galactic cosmic rays resulting in spallation and deuterium enrichments.

Most uses for the isotopic analysis of methane concern environmental and climatic effects. Methane is an efficient green house gas and measurements of its abundance in air from trapped ice core samples indicate that it has been increasing since the industrial revolution (Craig *et al.*, 1988), however it is not produced in large abundances directly by industrial processes. It has also been varying over much longer time scales due to climatic cycles (Chappellaz *et al.*, 1990). Carbon isotope analysis of sources of methane of various origins have been used to indicate the relative magnitude of each source. Hydrogen isotope analysis of methane may be of further use in such studies. Methane abundance of *ca.*1ppm in air has required 20l of air for carbon isotope studies and hydrogen isotope studies have not been practical. Use of static mass spectrometry systems would require *ca.* 5cm^3 for both carbon and hydrogen isotope analysis.

Clearly if the chemistry involved in the conversion of water to methane was developed then there are many more potential uses, apart from the obvious use of such an instrument for continuing the secondary alteration study described in chapter 4. The separation of nitrogen from methane in the projects described above could be achieved by oxidation of methane, followed by cryogenic separation of the nitrogen before conversion of the water back to methane. The following section briefly describes some possible uses, terrestrial and extra-terrestrial, for a static D/H mass spectrometer capable of analysing nmol quantities of water

a) Carbonaceous chondrites: D/H isotope analysis of acid resistant residues of carbonaceous chondrites have shown that the organic matter in these meteorites is enriched in deuterium. In these studies samples are limited and D/H analysis is performed in a few temperature increments (for example Kerridge, 1982; Robert and Epstein, 1982; Fallick *et al.*, 1983; Yang and Epstein, 1984). One problem associated with the analysis of chemically processed residues is the possibility of hydrogen isotope exchange between the organic residue and the acids used during the extraction (Robert *et al.*, 1987c). Although this can be avoided by the analysis of whole-rock samples, these

are complicated by the presence of water in these meteorites evolved at the same temperature at which the organic material yields its gas. A more sensitive D/H technique will enable smaller temperature increments to be utilised and so may enable the differentiation of water and even different organic components to be made. Comparisons with ordinary chondrites may provide links between these two groups of meteorites. Of particular interest may be a detailed study of Renazzo (type CR2) which contains a postulated deuterium-rich phase, δD *ca.* +18000‰, that combusts over a narrow temperature range (Wright and Pillinger, 1983). Such a high deuterium enrichment may be representative of organic molecules formed almost entirely by ion-molecule reactions in the interstellar medium.

b) Organic molecules: Gas chromatography (GC) and combined gas chromatography-mass spectrometry (GC-MS) has been used to separate individual organic molecules or classes of molecule from meteoritic residues (Kvenvolden *et al.*, 1970; Cronin *et al.*, 1988). The collection of individual organic compounds and then, hydrogen isotope analysis, along with carbon and nitrogen isotopic analyses, may help place constraints on the formation models of these molecules.

c) Martian Meteorites: Most martian meteorites, the SNC's, weigh less than 1kg and so it is important that hydrogen isotope studies of these meteorites destroy the minimum amount of sample. The only successful D/H ratios obtained for two SNC's has required the destruction of several grams of sample (Kerridge, 1988). Recently the existence of organic compounds in the Shergottite, EETA 79001, has been detected by the carbon release profile during stepped combustion (Wright *et al.*, 1989). Although the carbon isotopic composition is similar to terrestrial contamination, the amount of organic material well above normal blank levels suggesting that the organics were indigenous to the sample. D/H isotope analysis of this material might determine the origin of these organics, since if they are of martian origin then they may be enriched in deuterium.

d) Pre-solar grains: Grains of diamond and silicon carbide have been extracted from carbonaceous chondrites by treatment of the meteorite with various acids. These grains have been identified as of pre-solar origin from their anomalous isotopic compositions. Some hydrogen isotope analyses have been performed using an ion probe, however the results have been inconclusive, possibly due to contamination of the pre-solar grains by hydrogen exchange on the surface of these grains during acid treatment. Conventional hydrogen mass spectrometer analysis is not possible due to the small amounts of material. Static D/H mass spectrometry should have the sensitivity to analyse these samples, it may be possible to resolve the indigenous hydrogen from surface contamination by stepped combustion.

e) Diamonds: Hydrogen is usually the main impurity in terrestrial diamonds (Melton and Giardini, 1974) having a concentration of at least 1000 atomic ppm in some

diamonds (Runciman and Carter, 1971). From the study of nitrogen isotopes (the second most abundant impurity) in conjunction with carbon isotopes, Boyd (1988) showed that diamonds formed in the mantle may have experienced several growth events. A similar investigation with hydrogen isotopes may provide more information.

Undoubtedly there are many more projects for which a static hydrogen mass spectrometer will be useful. It will reduce the amount of sample destroyed and allow more information to be obtained from samples than currently possibly with dynamic mass spectrometry.

Appendices

Appendix A: Circuit diagrams of mass spectrometer electronic units

(a)

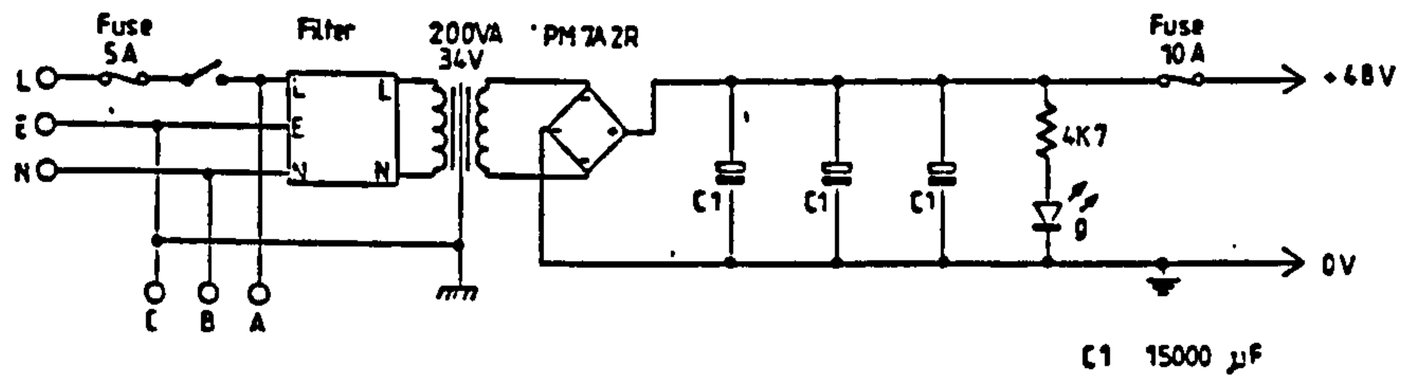

(b)

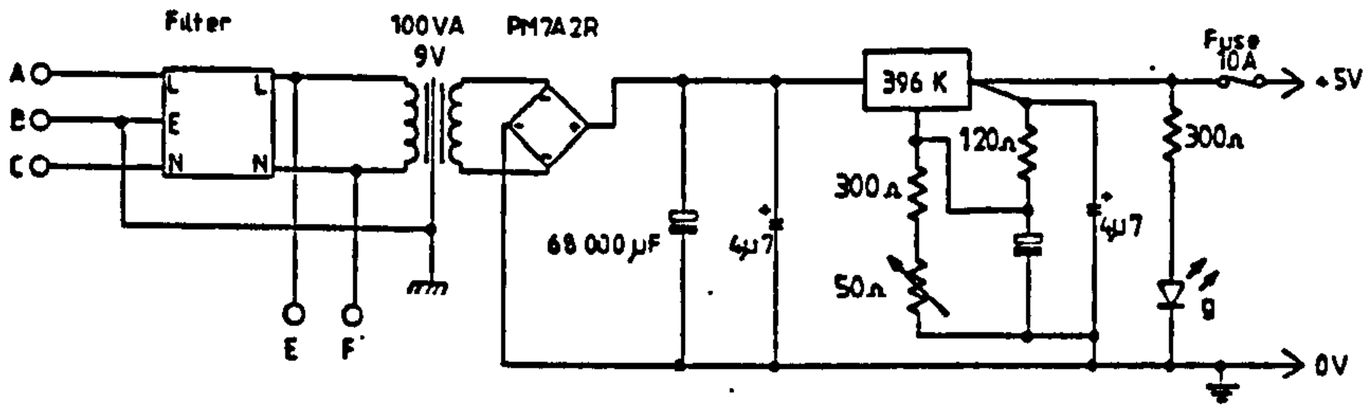

(c)

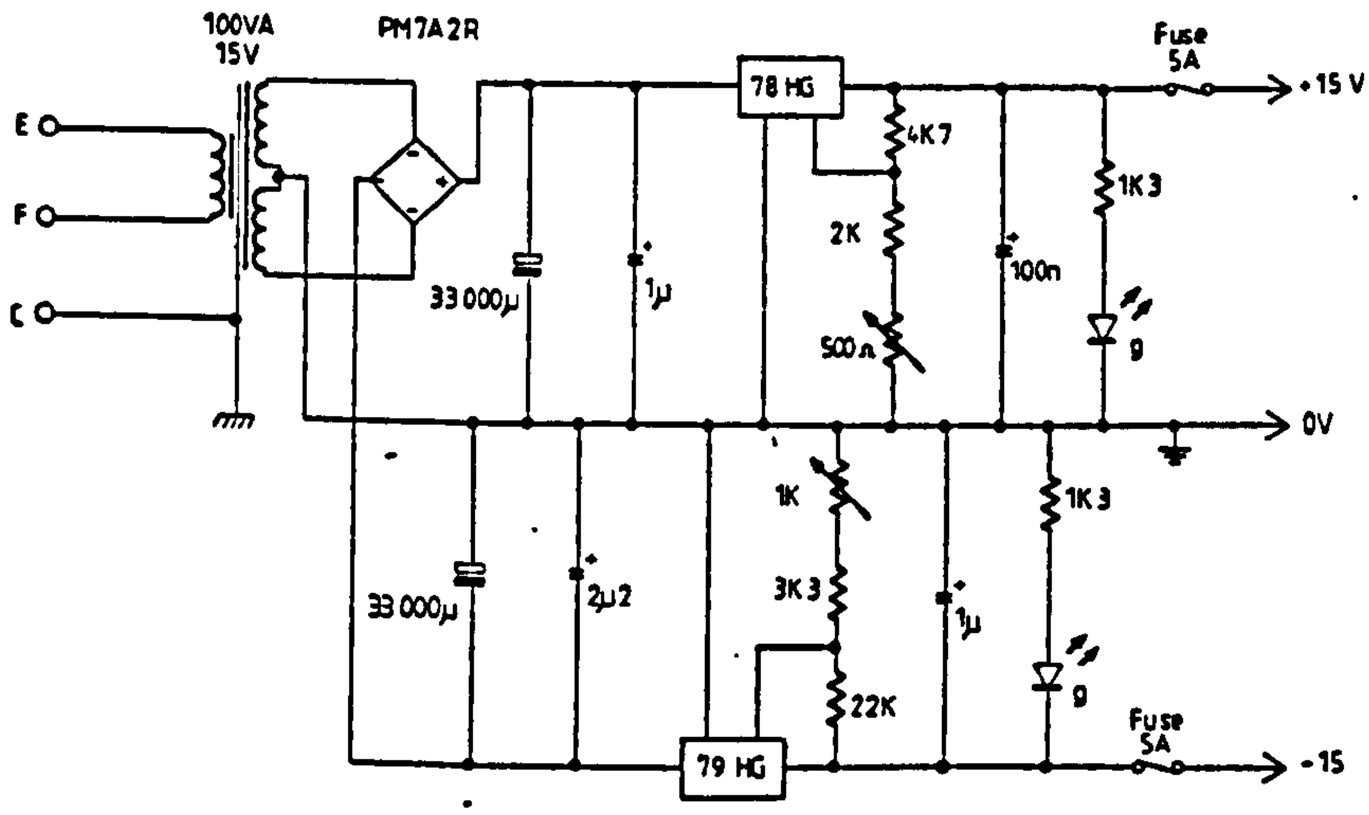

Fig. A.1 Power supply unit for the other electronic units. a) +48V power supply, max current 6A, used by solenoid valves for the inlet and the change-over valve b) +5V power supply, max current 10A. c) ±15V power supply unit, max current 2A.

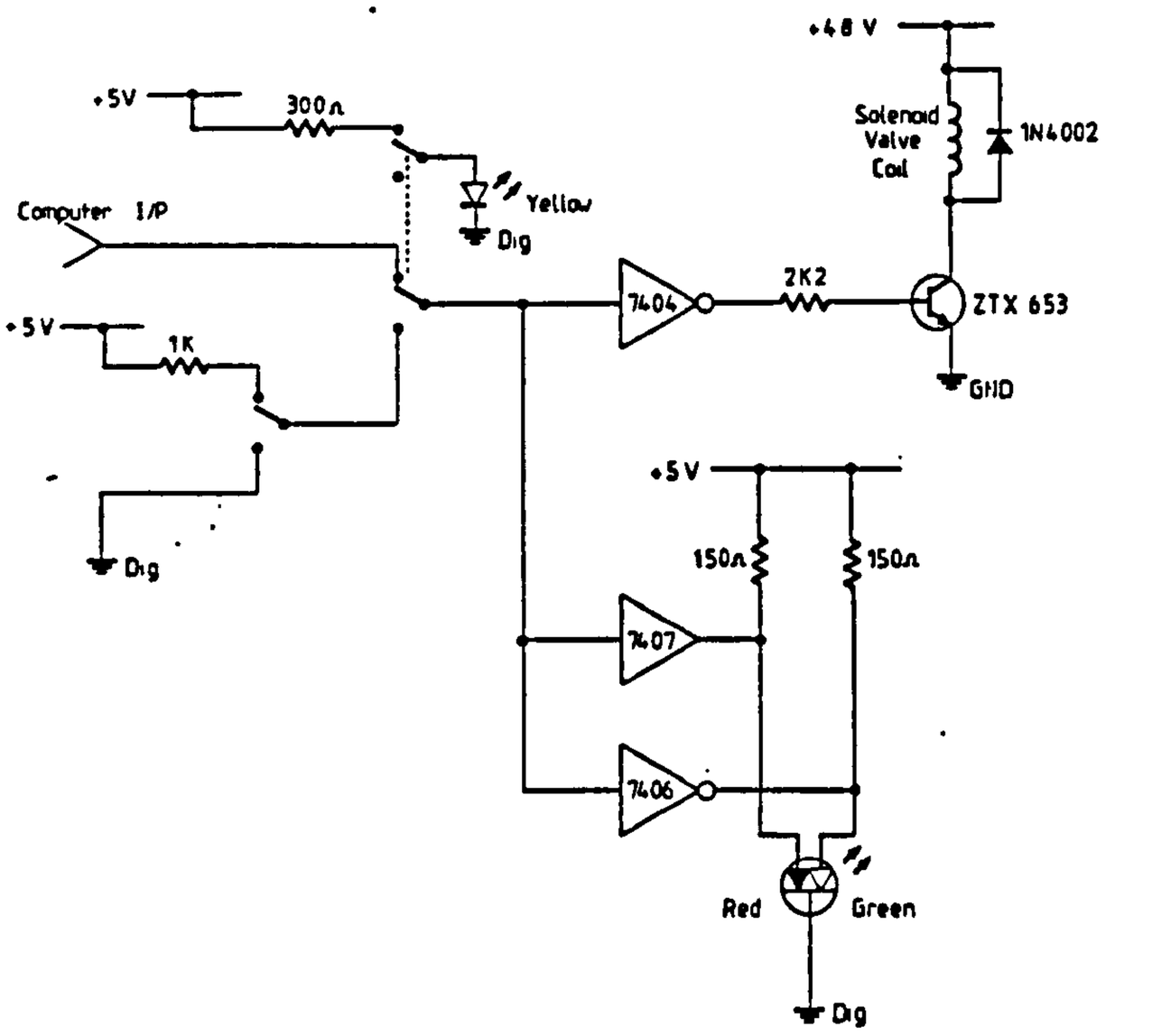

Fig. A.2 Diagram of the control electronics for each solenoid valve. The valve control unit, capable of controlling power to twelve separate solenoid valves consisted of 12 such sub-units.

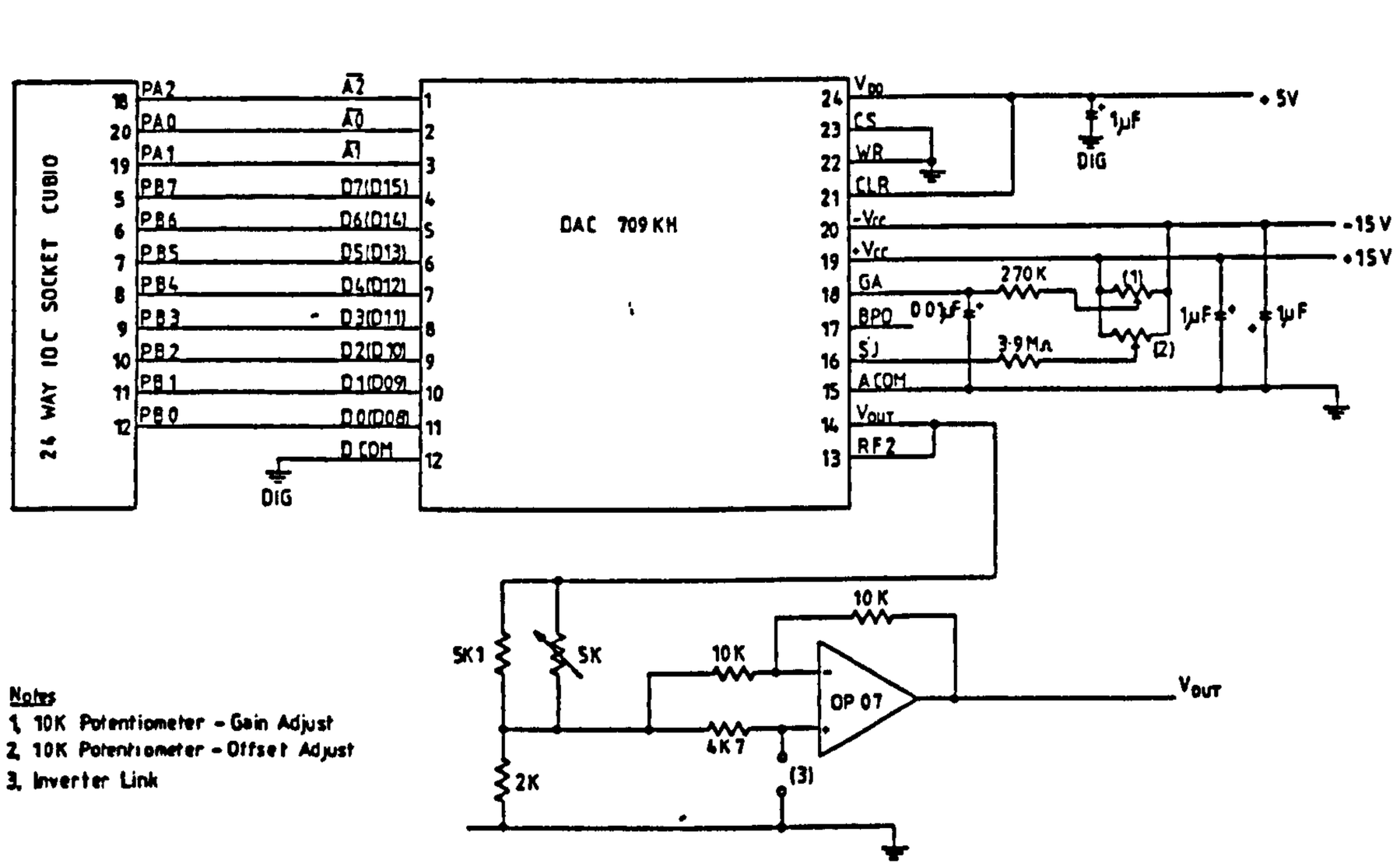

Fig. A.3 Digital to analogue converter (DAC 709KH, Burr Brown). A 16 bit signal input as two bytes was converted to an analogue output signal 0 to +10V. This was then reduced to a 0 to +5V signal for the programmable source control unit (880 Unit, VG Isogas, now Isotech).

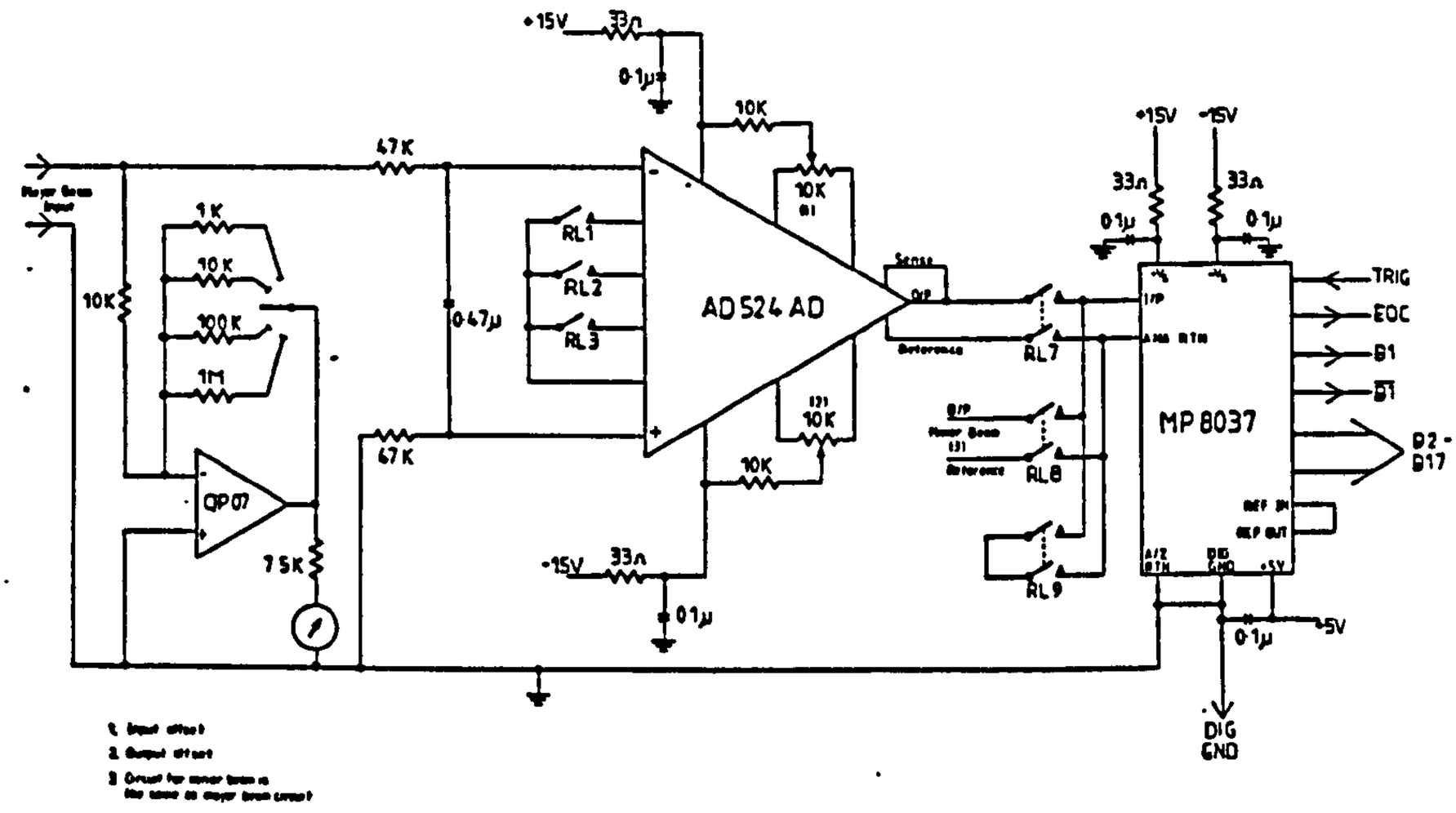

Fig. A.4 Second stage amplifiers. The beam signal from the first stage amplifier is further amplified by the second stage amplifier, AD 524 AD (Radio Spares). The minor beam is amplified by a similar second stage amplifier. The output signal is then converted to a 16 bit digital signal, with sign by the analogue to digital converter (MP 8037, Analogic Ltd.) and then read by the computer. Control of the relays was achieved by the computer *via* the digital input/output adapter

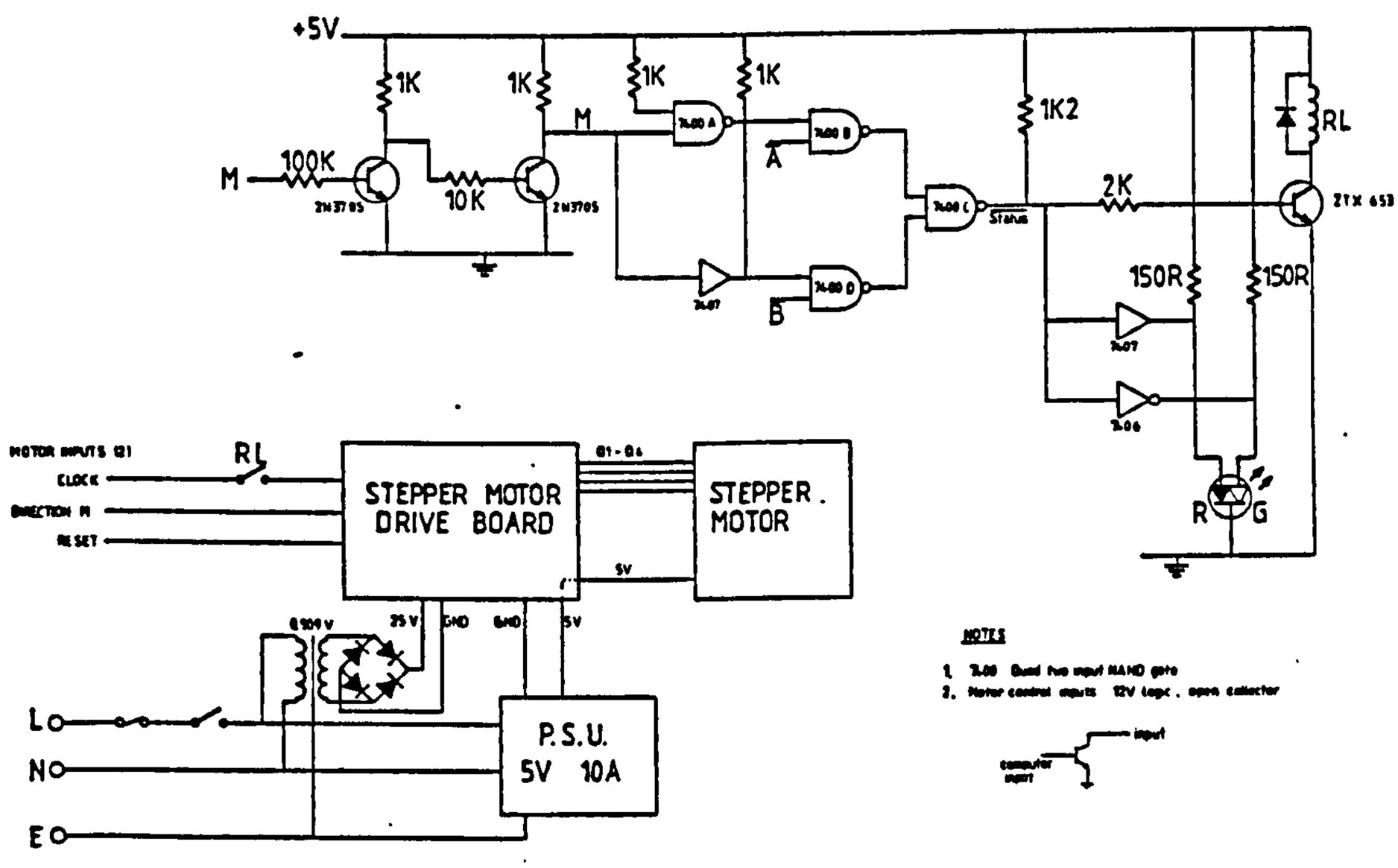

Fig. A.5 Stepper motor power supply unit and control electronics. When either inputs A or B are grounded control of the stepper motor will be suspended, by operation of the relay, if the computer attempts to over extend or compress the belows. The direction of the stepper motor is given by control line M.

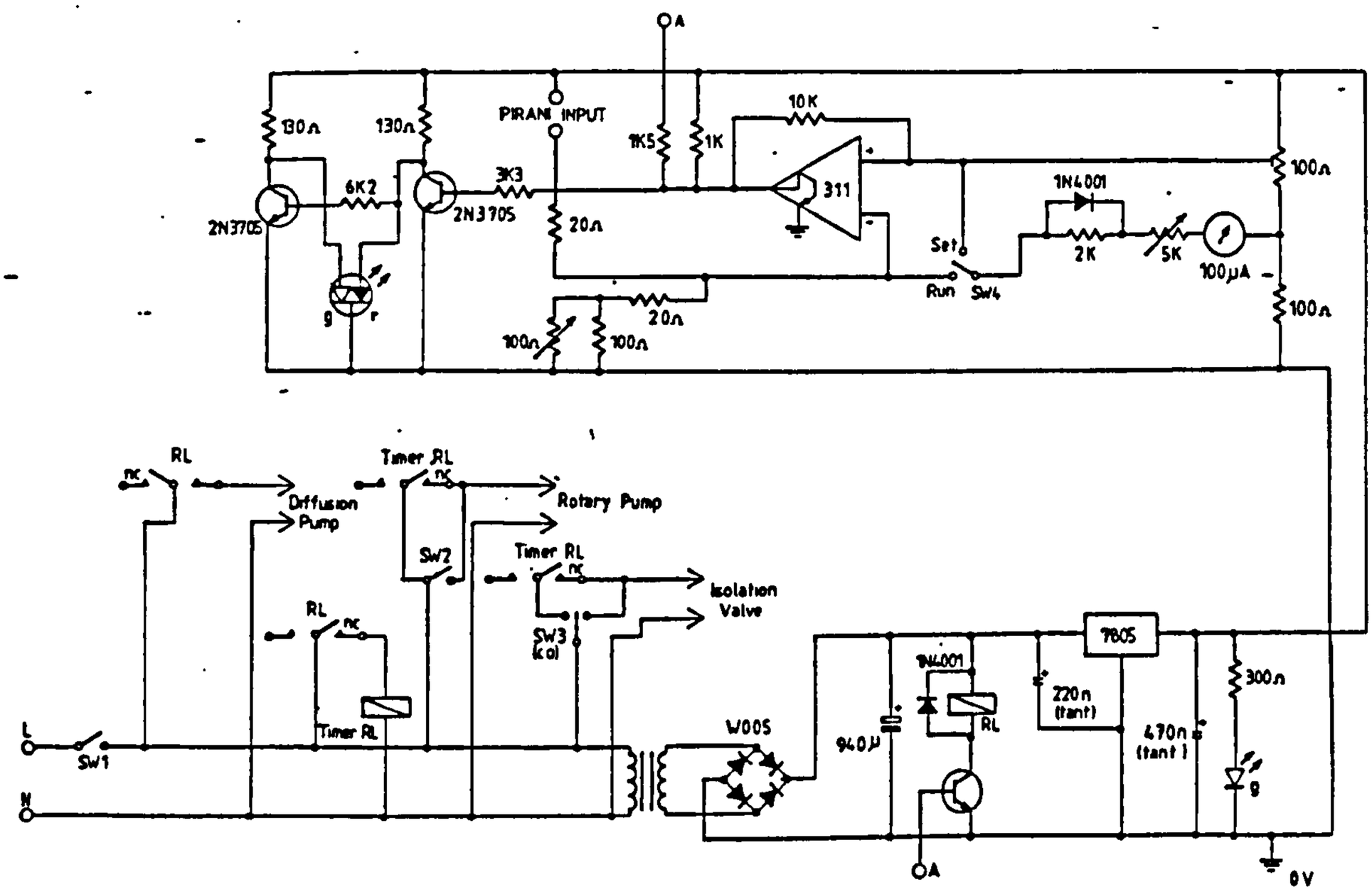

Fig. A.6 Piranni controller for protection of the rotary and diffusion pumps. In the event of vacuum failure the relay is de-energised and power to the diffusion pump immediately stopped. The rotary will continue to pump for a further 10 minutes while the diffusion pump cools. The trip can by by-passed by use of override switches, SW2 and SW3.

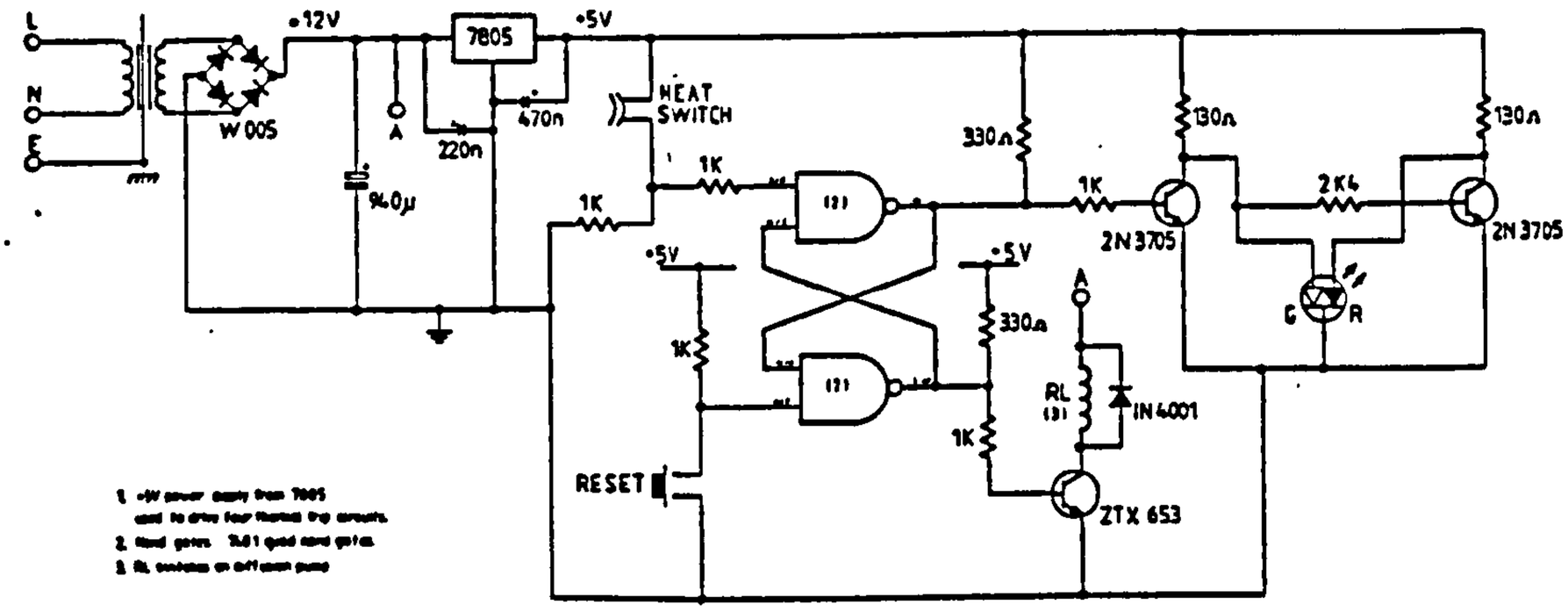

Fig. A.7 Thermal trip for protection of the diffusion pumps. The heat switch mounted on the side of the diffusion pump detects the loss of cooling water resulting in cutting the power supply to the diffusion pumps. Once tripped the pumps will remain off, even when cool, until reset.

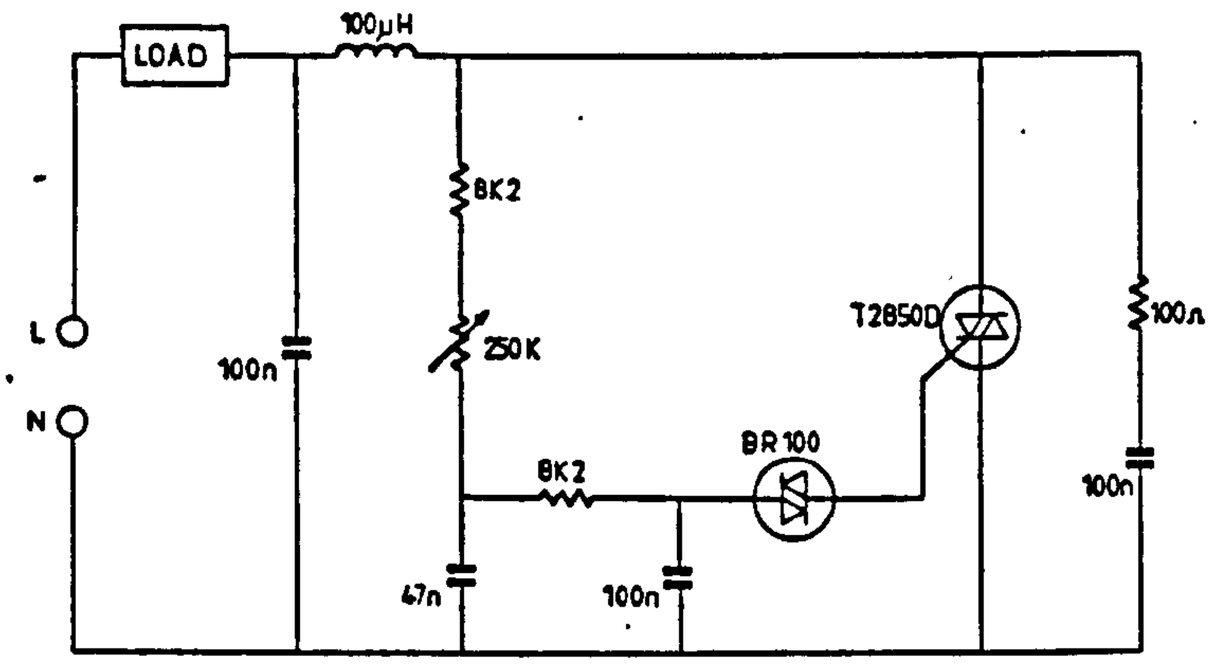

Fig. A.8 Heater tape controller, power to the heater tape controlled by the 250K potentiometer. Each unit contained 4 identical, but separate, heater tape controllers all powered through the single transformer.

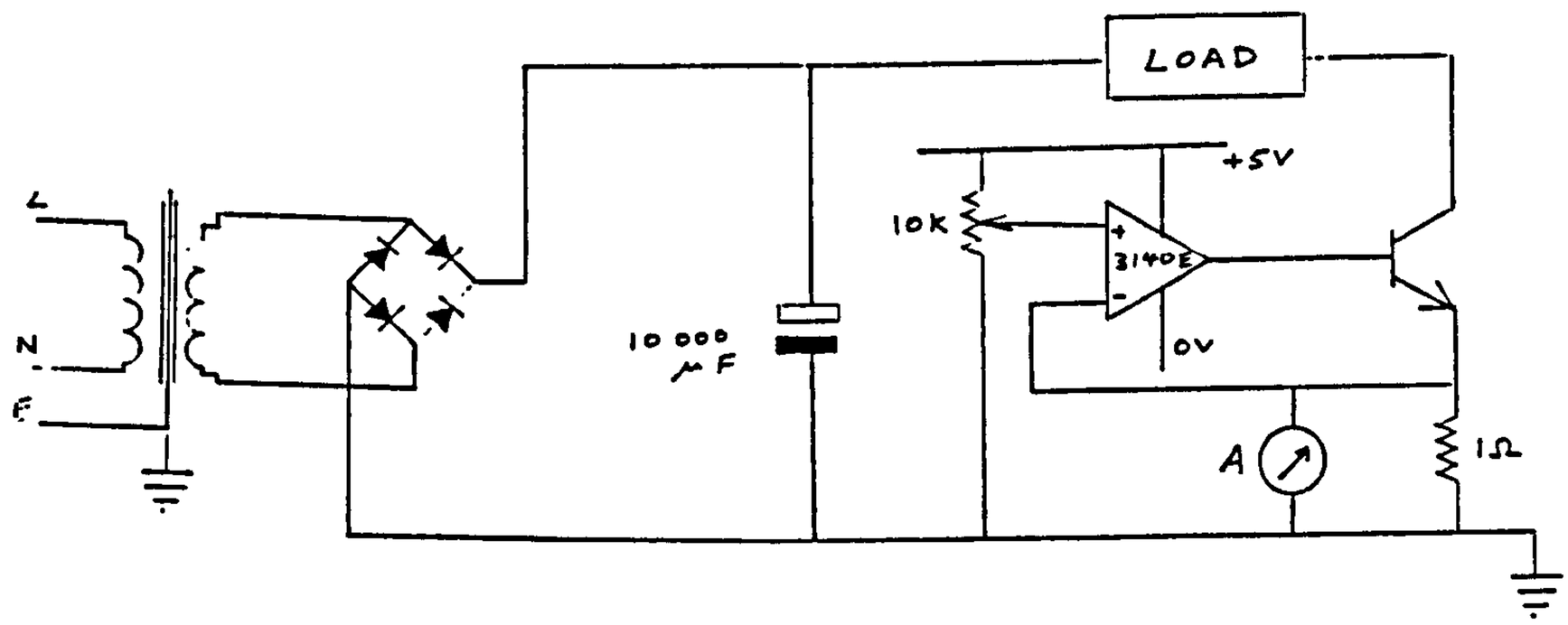

Fig. A.9 Circuit diagram of the cryotrap controller, the current was controlled by adjusting the 10K potentiometer. The cryotrap unit consisted of 4 identical, but separate, controllers.

Appendix B: Company addresses

Acorn Computers Ltd., Fullbourne Road, Cherry Hinton, Cambridge.

Analog Devices, Central Avenue, East Molesley, Surrey.

Analogic Ltd., 68 High Street, Weybridge, Surrey, KT13 8BN.

Bambi Air Compressors Ltd., 10 Eyre Street, Springhill, Birmingham, B18 7AA.

BDH Chemicals Ltd., Broom Road, Poole, Dorset, BH12 4NN.

BDH Ltd., Fourways, Carlyon Industrial Estate, Atherstone, Warwickshire, CV9 1JG.

British Nuclear Fuels Ltd., Risley, Warrington, WA3 6AS.

Burr Brown, International Airport Industrial Park, PO Box 11400, Tuscon, Arizona 85734, U.S.A.

Cambridge Glass Blowing, Brookfield Industrial Estate, Twenty Pence Road, Cottenham, CB4 4PS.

Cambridge Instruments, Unit 11b, Melbourne Science Park, Moat Lane, Melbourne, Royston.

Camlab Ltd., Nuffield Road, Cambridge, CB4 1TH.

Chell Instruments Ltd., Tudor House, Grammar school Road, North Walsham, Norfolk, NR28 9JH.

Comark Electronics Ltd., Russington, Littlehampton, West Sussex, BN16 3QZ.

Control Universal Ltd., 137 Ditton Walk, Cambridge, CB5 8QF.

Edwards High Vacuum, Manor Royal, Crawley, West Sussex, RH10 2LW.

Electrothermal Engineering Ltd., order through Jencons (Scientific) Ltd.

Genevac Ltd., Alpha Works, Whitehouse road, Ipswich, 1PI 5LU.

Goodfellow Metals Ltd., Cambridge Science Park, Cambridge, CB4 4DJ.

Harrington Brothers Ltd., Wier Road, Balham, London.

Jencons (Scientific) Ltd., Cherry Court Way Industrial Estate, Stanbridge Road, Leighton Buzzard, Bedford, LU7 8UA.

Johnson Matthey PLC., Orchard Road, Royston, Hertfordshire, SG8 5H4.

J.Young (Scientific Glassware) Ltd., 11 Colville Road, London, W£ 8BS.

McLennon Servo Supplies Ltd., York Town Industrial Estate, Doman Road, Camberley, Surrey.

MDC Vacuum Products Corporation, 23842 Cabot Boulevard, Hayward California, U.S.A.

Monsanto Company, St.Louis, Missouri 63167, U.S.A.

Morite Windings Co., 11 Clifton Road, Industrial Estate, Cherry Hinton Road, Cambridge.

National Bureau of Standards, Office of Standard Reference Materials, Gaithersburg, MD20899, U.S.A.

North London Valve & Fitting Co., 34 Capitol Way, Capitol Industrial Park, London, NW9 0ED.

Olympus (Tokyo), order through Olympus (Optical Co. UK Ltd.), 2-8 Honduras Street, London, EC1Y OTX.

Phase Separations Ltd., Deeside Industrial Estate, Queensferry, CH5 2LR.

RS Components, PO Box 99, Corby, Northants, NN17 9RS.

Sartorius GMBH, Göttingen, Germany.

Scientific Glass Engineering (UK) Ltd., Potters Lane, Kiln Farm, Milton Keynes, MK11 3LA.

Standard Bellows Company, 375 Turnpike Road, Windsor Locks, CT 06096, U.S.A.

Vacuum Generators Ltd. (Hastings), Menzies Road, Hastings, Sussex, TN34 1QY.

Varian associates Ltd., 28 Manor Road, GB-Walton-on-Thames, Surrey.

VG Isogas, changed to VG Isotech.

VG Micromass, changed to VG Isotech.

VG Isotech, Aston Way, Middlewich, Cheshire, CW10 0HT.

VG Isotopes Ltd., Ion Path, Road Three, Winsford, Cheshire, CW7 3BX.

Zenith Electrical Co.Ltd., Wavendon, Milton Keynes,MK17 8AT.

Zoedale, 58 Hurst Grove, Bedford, MK40 4DR.

Appendix C: Derivation of blank and memory effect correction.

When two sources of hydrogen are mixed the D/H ratio of the resulting sample will be a weighted average D/H ratio of each individual sample. Considering the case of sample gas contaminated by a blank then

$$(D/H)_m[H]_m = (D/H)_s[H]_s + (D/H)_b[H]_b \qquad C.1)$$

where (D/H) is the atomic deuterium to hydrogen ratio, [H] is the quantity of hydrogen and the subscripts m,s and b, refer to the measured sample, actual sample and blank respectively. Also, since hydrogen is not lost or gained,

$$[H]_m = [H]_s + [H]_b \qquad C.2)$$

The D/H ratio of each gas,x, can be given in terms of the delta notation (section 1.2.1),

$$(D/H)_x = \left(\frac{\delta D_x}{1000} + 1\right) x\ (D/H)_{ref} \qquad C.3)$$

where (D/H)ref is the atomic D/H ratio of the reference gas. Substituting eq.(C.3) into eq.(C.1) gives

$$\left(\frac{\delta D_m}{1000} + 1\right) x\ (D/H)_{ref}\,[H]_m =$$
$$\left(\frac{\delta D_s}{1000} + 1\right) x\ (D/H)_{ref}[H]_s + \left(\frac{\delta D_b}{1000} + 1\right) x\ (D/H)_{ref}[H]_b$$

Therefore

$$(\delta D_m + 1000)[H]_m = (\delta D_s + 1000)[H]_s + (\delta D_b + 1000)[H]_b$$

From 3.2 gives

$$\delta D_m[H]_m = \delta D_s[H]_s + \delta D_b[H]_b \qquad C.4)$$

Showing that the delta notation can be used in place of the ratio for a mass balance equation. Rearranging equation (C.4) and substituting in equation (C.2) gives the blank correction equation 3.13 in section 3.5.3:

$$\delta D_s = \frac{[H]_m \, \delta D_m}{[H]_m - [H]_b} - \frac{[H]_b \, \delta D_b}{[H]_m - [H]_b}$$

For the memory effect shown in fig 3.9, a mass balance equation gives

$$\delta D_m = \frac{[H]_s \, \delta D_s}{[H]_s + [H]_{me}} + \frac{[H]_{me} \, \delta D_p}{[H]_s + [H]_{me}}$$

Where the subscripts m,s and me refer to the measured value, actual sample and memory effect respectively. In the memory effect experiments for the flow-thru inlet, described in section 3.5.3, consecutive analyses of a sample were performed after the inlet had been conditioned with V-SMOW ($\delta D = 0‰$). For the moment, ignoring the isotope dilution effect then when analysing a sample with $\delta D = \delta D_s$ then the measured value δD_{m1} for the first analysis is:

$$\delta D_{m1} = \frac{[H]_s \, \delta D_s}{[H]_s + [H]_{me}} + \frac{[H]_{me} \, \delta D_p}{[H]_s + [H]_{me}}$$

$$= \frac{[H]_s \, \delta D_s}{[H]_s + [H]_{me}}$$

and for the second analysis is:

$$\delta D_{m2} = \frac{[H]_s \, \delta D_s}{[H]_s + [H]_{me}} + \frac{[H]_{me} \, \delta D_{m1}}{[H]_s + [H]_{me}}) \qquad \text{C.5)}$$

$$\text{Let } B = \frac{[H]_{me}}{[H]_s + [H]_{me}} \qquad \text{C.6)}$$

Therefore

$$\delta D_{m2} = \frac{[H]_s \, \delta D_s}{[H]_s + [H]_{me}} + \delta D_{m1} \, B$$

$$= \frac{[H]_s \, \delta D_s}{[H]_s + [H]_{me}} + \frac{[H]_s \, \delta D_s}{[H]_s + [H]_{me}} B = \frac{[H]_s \, \delta D_s}{[H]_s + [H]_{me}} (1 + B)$$

In general for the x^{th} analysis,

$$\delta D_{mn} = \frac{[H]_s \, \delta D_s}{[H]_s + [H]_{me}} (1 + B + B^2 + ... + B^{(x-1)}) \qquad C.7)$$

But from equation (C.6) $[H]_s = [H]_{me}\left(\frac{1-B}{B}\right)$ which on substituting into equation (C.7) gives

$$\delta D_{mn} = \delta D_s (1-B) (1 + B + B^2 + ... + B^{(x-1)})$$

$$= \delta D_s(1 + B^x) \qquad C.8)$$

In equation (C.8), at large x δD_{mx} approaches δD_s. However in the flow-thru inlet it was found that a different value was obtained due to the isotope dilution effect. This is corrected by replacing δD_s by a correction term, A. Hence

$$\delta D_{mn} = A(1 + B^x) \qquad C.9)$$

where $A = \frac{R}{\delta D_s}$, R is the ratio of the measured δD of the sample (after many consecutive analyses) to the actual δD of the sample.

Appendix D: Data tables for chapter 4

Table D.1 Notes made of chondrule and matrix fragments during extraction procedure. The analytical techniques used on each chondrules are also indicated.

Sample No.	Mass (mg)	Description	Analysis type		
			Pet.	TL	Isotopic
SC01	6.0502	Barred Olivine? Incomplete glassy surface sulphides *ca.* 2mm dia.	Y	Y	Y
SC02	n.m.	Half chondrule, some sulphide on surface, also small clumps of matrix	Y	Y	Y
SC03	Lost	Egg shaped, sulphide rich, bronze colour. Lost while weighing	-	-	-
SM04	0.3068	Regular dark clump of matrix *ca.* 2x1mm	-	Y	Y
SC05	Lost	Fragment of chondrule, olivine rich, no rust - disintegrated during extraction			
SC06	n.m.	Chondrule, came from matrix, may be small bit of matrix attached *ca.* 1mm	Y	Y	Y
SM07	Lost	Matrix from which SC06 extracted, unfortunately lost			
SC08	n.m.	Part of chondrule, some sulphide on surface, might be altered.	Y	Y	-
SC09	n.m.	Small half of chondrule embedded inside crystalline fragment	Y	Y	Y
SM10	Lost	Matrix with light material - lost	-	-	-
SC11	n.m.	Fragment (~25%) of dark chondrule, interior dark, some rust, interior glassy.	Y	Y	-
SM12	0.1548	Matrix with chondrule mold, fine jet black			
SM13	0.8954	Matrix with chondrule mold, matrix is unclean *ca.* 1.5mm	-	Y	-
SC14	n.m.	$\sim\frac{2}{3}$ part chondrule from matrix SM13. Blisters in places, inside quite coarse and fairly dark., may have been altered.	Y	Y	-
SC15	n.m.	Chondrule, rough black surface. Fine internal structure.	Y	Y	Y
SM16	2.2742	Matrix from which SC15 extracted, not completely clean, a lot of white crystals, olivine?	-	Y	Y
SC17	n.m.	Chondrule, radiating pyroxene? half chondrule.	Y	Y	Y
SM18	1.0805	70% pure matrix	-	Y	Y
SC19	0.0796	Half chondrule, pure glass, some fibrous matrix contamination, looks like fusion crust	Y	Y	Y
SC20	n.m.	Large chondrule, *ca.* 2mm dia. Rough black surface, flat on one side	Y	Y	Y
SM21	n.m.	Matrix adjacent to SC20	-	-	-
SC22	0.2158	60% chondrule, greenish	Y	Y	-
SC23	n.m.	Two chondrules touching. Larger chondrule black surface, coarse crystalline interior	Y	Y	-
SC24	Lost	Smaller chondrule from SC23 - Lost			
SM25	0.4100	90% pure matrix, fragmented during extraction	-	Y	-
SC26	0.2430	Probably a chondrule, dark crystalline, could be a clast	Y	Y	-
SM27	0.6904	Matrix, mineral grains and bits of chondrule from a chondrule surface	-	-	-
SC28	n.m.	Granular crystalline chondrule, probably sulphide, suspect matrix and mesostasis hydrothermally altered.	Y	Y	Y
SC29	n.m.	White chondrule, very fibrous	Y	Y	-
SM30	n.m.	Very rusty matrix, black with red, looks like a bunch of grapes	-	-	-
SM31	n.m.	Dark matrix material with light coloured crystals on one side	-	Y	-
SC32	Lost	Half chondrule, mainly green colour, a corner looks rusty. Lost	-	-	-
SC33	n.m.	Piece of chondrule showing radiating pyroxene interior, white zoned 'chill margin' and irregular fine grained mass adhering to outside.	Y	Y	-
SC34	n.m.	Similar to SC33 except chondrule very finely crystalline	-	Y	Y
SC35	0.0964	Very small fragment from a chondrule with crystalline glassy interior	Y	-	-
SC36	n.m.	Large fragment, about half, crystalline interior, rough exterior texture	Y	Y	Y
SC37	n.m.	Single fractured crystal, about a quarter of original crystal, yellowish colour, probably heavily altered	Y	-	-
SM38	0.1271	Matrix, jet black, fine grained	-	Y	-
SC39	n.m.	75% whole chondrule, with fine grain interior structure, probably radiating pyroxene, managed to extract only 50% of chondrule	Y	Y	-
SM40	0.5875	Matrix attached to SC39, matrix not very clean	-	Y	Y
SC40	1.1556	Rim of chondrule extracted from SM40	Y	Y	Y
SC41	0.6599	25% of a chondrule, hemispherical crystalline interior, could be another part of SC39	Y	-	-
SC42	1.1517	Half chondrule, uniform dark green glassy interior, matrix attached to exterior	Y	Y	Y
SM43	0.3916	Fragment of fine grained black matrix.	-	Y	-
SC44	n.m.	Third fragment of a chondrule, grain structure with white 'chill margin'	Y	Y	Y
SC45	1.0414	Piece of SC44? Same interior, white zone and sawn face	Y	Y	-
SC46	0.9117	Piece of SC44 or SC45? Fibrous black interior, white zone and sawn face	Y	Y	Y
SC47	0.9404	Small half of a chondrule, coarse crystalline interior with black crust	Y	Y	Y
SC48	Lost	Small half chondrule, black finely crystalline interior - Lost	-	-	-
SC49	0.2076	Small black chondrule, perfect sphere	Y	-	Y
SC50	0.1492	Small black, smooth, nearly complete sphere, piece missing which could be impact crater	Y	Y	-
SC51	0.5526	Clean transperent spherical chondrule *ca.* 1mm dia.	Y	Y	-
SC52	3.7543	Half chondrule, hemishperical, *ca.* 2mm dia. Coarse crystalline interior	Y	Y	-
SC53	n.m.	Chondrule embedded in matrix has concentric zones. Very fine crystalline interior, most matrix removed	Y	Y	-
SC54	5.3171	Large piece of chondrule <25%. Black rough surface, green fibrous very fine interior. Could be piece of SC53	Y	Y	Y
SC55	0.9103	Black spherical complete chondrule. No matrix attached	Y	Y	-
SC56	0.5355	Shiny black sphere, with a bit of rust (metallic?), magnetic. Was not able to split, metal chondrule	-	-	-
SC57	n.m.	Black spherical, quite large, dark dull black surface	-	-	-
SC58	1.2688	Appears to be interior of a chondrule, *ca.* 10% chondrule, very rusty	Y	Y	Y

SC59	a.m.	Half chondrule fine grain rusty interior	Y	Y	.
SC60	0.4966	White chondrule 80-90% complete, finely crystalline interior	Y	Y	.
SM61	0.4580	Rusty matrix, chondrule mould in middle, white zone around chondrule mould	.	Y	.
SM62	Lost	Rust matrix, similar to SM61 - Lost	.	.	.
SC63	a.m.	Black spherical chondrule, complete sphere, surface gloss black	.	.	.
SC64	0.1378	Small black chondrule, rough black exterior	Y	.	.
SC65	2.8815	Small fragment, ca. 10%, of a large chondrule. Rough black exterior, Interior crystalline, radiating pyroxene	Y	Y	Y
SC66	1.0455	Medium sized chondrule, egg shaped, rough black exterior	Y	Y	.
SC67	1.4745	Third of chondrule, rough black crystalline exterior with rusty crystalline interior. Some matrix attached	Y	Y	.
SC68	1.1367	Third of a chondrule fragment. Exterior thin black shell. Interior fine crystalline	Y	Y	.
SC69	2.2455	Small fragment of a chondrule, thick coat crystalline black exterior. Interior crystalline, rust coloured, very fine grained	Y	Y	.
SC70	0.7107	Small black nearly complete chondrule	Y	Y	Y
SC71	0.2452	Very small complete black chondrule. Some matrix still attached	Y	Y	Y
SC72	3.6315	Small fragment of a large chondrule. Coarse crystalline interior	Y	Y	Y

Table D.2 Average chemical composition of the mesostasis of each Semarkona chondrule.

Sample	Wt. % Oxide												
	SiO	TiO	Al_2O_3	FeO	MnO	MgO	CaO	Na_2O	K_2O	Cr_2O	Ni	S	Sum
SC-01	64.90	0.45	9.98	9.25	0.38	3.73	6.98	1.52	0.58	0.38	0.0	0.28	98.42
SC-02	69.02	0.47	12.87	6.57	0.38	4.60	2.92	1.22	0.66	0.26	0.0	0.30	99.29
SC-06	72.77	0.51	11.28	6.31	0.34	3.29	4.11	1.41	0.66	0.40	0.0	0.57	101.65
SC-11	68.56	0.37	6.94	9.36	0.47	4.38	7.58	0.65	0.5	0.87	0.0	0.042	100.06
SC-14	70.44	0.40	8.63	5.41	0.51	4.99	6.08	0.71	0.59	0.55	0.0	0.53	98.83
SC-17	52.30	0.43	22.01	0.94	0.28	7.72	15.17	1.09	0.07	0.44	0.0	0.16	100.64
SC-19	60.45	0.77	16.30	0.66	0.15	5.42	14.30	0.46	0.01	0.56	0.0	0.00	99.13
SC-20	73.30	0.45	11.24	8.31	0.27	1.61	1.98	2.45	0.80	0.07	0.0	0.31	100.81
SC-22	72.74	0.47	12.86	5.08	0.28	1.90	1.73	1.71	0.80	0.08	0.0	0.00	97.66
SC-23	63.36	0.55	14.47	6.98	0.66	5.99	7.66	1.65	0.44	0.13	0.0	0.00	101.88
SC-26	68.35	0.47	15.20	5.97	0.28	1.54	2.89	2.29	0.71	0.05	0.0	0.00	97.75
SC-28	67.08	0.50	13.00	11.26	0.51	1.30	3.49	4.02	0.71	0.05	0.0	0.60	102.56
SC-29	68.06	0.46	10.39	6.53	0.57	3.16	7.44	3.08	0.47	0.45	0.0	0.12	100.73
SC-33	63.20	0.09	3.27	13.30	0.57	17.50	1.06	0.26	0.27	0.55	0.0	0.00	100.10
SC-36	67.76	0.51	14.50	8.78	0.37	0.78	3.18	1.81	0.69	0.12	0.0	0.00	98.44
SC-39	63.28	0.43	19.10	5.36	0.23	1.01	4.26	7.25	0.06	0.03	0.0	0.00	101.05
SC-40	55.58	0.37	12.44	9.10	0.63	12.71	4.28	3.96	0.08	0.27	0.0	0.00	99.54
SC-41	68.67	0.50	14.39	6.44	0.40	2.47	4.69	1.59	0.61	0.21	0.0	0.00	99.90
SC-42	77.15	0.40	7.65	6.27	0.25	2.63	1.80	1.77	0.77	0.04	0.0	0.00	98.71
SC-47	52.85	0.00	19.51	2.347	0.47	5.56	11.86	2.77	0.13	0.59	0.00	0.00	96.01
SC-49	53.81	0.14	2.88	17.05	0.80	20.44	2.14	0.45	0.12	0.77	0.00	0.79	99.43
SC-51	45.36	0.97	19.20	0.13	0.08	21.38	13.39	0.31	0.00	0.12	0.00	0.00	100.96
SC-52	69.22	0.00	14.22	10.65	0.44	1.45	3.67	0.84	0.68	0.04	0.00	0.00	101.20
SC-53	72.00	0.42	11.12	11.26	0.26	0.61	2.66	1.26	0.79	0.02	0.00	0.36	100.77
SC-54	67.55	0.39	10.53	13.16	0.33	1.72	3.14	0.59	0.49	0.09	0.00	0.08	98.05
SC-55	64.38	0.00	18.94	3.38	0.90	1.64	6.21	1.24	0.53	0.00	0.00	0.00	97.28
SC-59	53.92	0.48	18.57	0.66	0.00	10.53	14.68	0.00	0.00	0.32	0.00	0.00	99.13
SC-60	71.56	0.00	12.32	5.41	0.24	6.54	3.02	0.71	0.72	0.40	0.00	0.00	100.94
SC-64	57.10	0.39	17.95	4.18	0.91	3.68	7.55	1.73	0.00	0.31	0.00	0.00	93.75
SC-65	65.90	0.43	15.41	10.41	0.21	1.58	1.48	3.09	0.66	0.08	0.00	0.00	99.27
SC-66	66.00	0.62	16.70	5.52	0.41	2.85	4.97	1.66	0.64	0.05	0.00	0.00	99.40
SC-67	67.56	0.13	6.96	5.20	0.24	18.00	1.05	2.64	0.24	0.39	0.00	0.00	102.45
SC-67(Smc)	37.53	0.00	1.39	35.00	0.20	10.23	1.02	2.59	0.14	0.29	0.00	1.807	90.20
SC-68	72.80	0.00	20.50	0.86	0.00	0.00	0.69	11.42	0.46	0.00	0.00	0.00	106.73
SC-69	49.70	0.00	17.10	8.51	0.30	13.80	10.40	0.30	0.01	0.36	0.00	0.00	100.89
SC-70	63.22	0.00	18.36	3.51	0.73	3.00	4.77	3.29	0.40	0.31	0.00	0.00	97.59
SC-71	59.62	0.00	21.30	1.39	0.85	3.97	10.81	3.37	0.28	0.23	0.00	0.00	101.82
SC-72	64.08	0.00	18.72	5.68	0.26	0.91	5.46	1.94	0.56	0.05	0.00	0.00	97.71

Table D.3 Water content and hydrogen isotope composition of the Semarkona fragments.

Sample	Mass	Low Temperature <200°C			High Temperature 200°C - 1100°C		
No.	(mg)	H_2O µmol	Wt.% H_2O	δD ‰	H_2O µmol	Wt.% H_2O	δD ‰
SC01	1.3731	0.017	0.022	-600±200	0.017	0.022	+4250±1200
SC02	1.0690	0.017	0.028	+3200±652	0.072	0.122	+1800±600
SC06	1.0118	0.017	0.030	+1120±500	0.139	0.247	+1800±600
SC09	0.0789	0.017	0.038	-780±200	0.017	0.380	+740±800
SC15	0.8274	0.017	0.036	+750±350	0.017	0.036	+2650±1200
SC17	0.0869	0.061	1.266	+480±300	0.050	1.036	+3600±900
SC19	0.0426	0.017	0.704	+650±300	0.017	0.704	+380±400
SC20	1.5291	0.017	0.020	-400±300	0.017	0.020	+3200±1400
SC28	0.3522	0.017	0.085	+150±300	0.028	0.142	+4320±1000
SC34	0.1739	0.033	0.345	+900±400	0.017	0.173	+2800±1600
SC36	0.4828	0.017	0.062	+550±400	0.017	0.062	+5500±1000
SC40	0.3570	0.050	0.252	+480±300	0.072	0.364	+4150±800
SC42	0.4902	0.017	0.061	+100±300	0.017	0.061	+6200±1300
SC44	0.9118	0.017	0.033	+950±400	0.017	0.033	+3000±600
SC46	0.5300	0.056	0.189		0.061	0.208	+2000±1300
SC47	0.3367	0.017	0.089	+1300±400	0.017	0.089	+5000±900
SC49	0.0591	0.017	0.508	+550±300	0.017	0.508	+850±400
SC54	1.9223	0.056	0.052	-620±200	0.078	0.073	+5100±1100
SC58	0.3143	0.017	0.095	+3300±700	0.017	0.096	+6620±1500
SC65	0.9666	0.056	0.103	+2650±600	0.056	0.104	+7380±1200
SC70	0.2698	0.083	0.558	+1850±450	0.083	0.556	+5680±1300
SC71	0.0952	0.017	0.315	-300±250	0.017	0.315	+280±300
SC72	1.2479	0.022	0.032	+1700±500	0.117	0.168	+6050±1000
SM04	0.0900	0.017	0.333	0±300	0.017	0.333	+1300±1300
SM16	0.6208	0.033	0.097	+1100±400	0.017	0.048	+3000±900
SM18	0.4488	0.156	0.624	+750±350	0.189	0.758	+2250±600
SM40	0.2082	0.122	1.057	+1450±400	0.294	2.546	+3000±800

Table D.4 Thermoluminescence results for the Semarkona chondrules

Sample	Mass (mg)	Log (TL/Mass) Dhajala = 1	Peak Width FWHM °C	Tmax ℃
SC-01	1.1799	-3.43		132
SC-02	0.4239	-2.54	50	130
SC-06	0.3349	-4.62		
SC-09	0.0758	-0.36	88	163
SC-11	0.0689	-3.26		
SC-15	0.4204	-2.83		
SC-17	0.0802	-0.14	92	142
SC-19	0.0214	0.01		163
SC-20	2.9497	-4.11		179
SC-22	0.0386	-0.15		186
SC-23	0.2495	-1.82		
SC-26	0.0789	-3.37		
SC-28	0.1091	-3.66		
SC-29	0.4598	-2.65		
SC-33	0.0872	-1.46	160	175
SC-34	0.0915	-0.76	84	103
SC-36	0.2255	-1.38	45	112
SC-39	0.6734	-1.63	92	186
SC-40	0.3243	-2.06	125	179
SC-42	0.3922	-4.75		
SC-44	0.4372	-2.97	150	170
SC-45	0.4332	-1.91	125	155
SC-46	0.4332	-0.27	198	200
SC-47	0.3762	-1.81	165	185
SC-50	0.0392	-0.20	113	145
SC-51	0.2511	-2.00	145	155
SC-52	1.2000	-5.60		
SC-53	2.6495	-3.27	90	156
SC-54	1.9788	-3.14	100	158
SC-55	0.4719	-2.73	103	146
SC-58	0.7787	-3.00	120	149
SC-59	0.9495	-3.45	150	181
SC-60	0.0913	-2.33	55	120
SC-65	1.1200	-3.98		
SC-66	0.4440	-4.87		
SC-67	0.6087	-2.50	120	158
SC-68	0.3253	-1.73	135	203
SC-69	1.3108	-3.52	110	140
SC-70	0.2956	-1.41	142	187
SC-71	0.0914	-3.50		
SC-72	1.6411	-4.01		150

Table D.5 Results obtained for the CIPW norm calculation of the mesostasis composition of the Semarkona chondrules.

Sample	CIPW norm components wt.%								
	Q	Or	Ab	An	Di	C	Hy	Ol	Il
SC-01	29.030	3.45	12.90	18.65	13.48	0.00	19.41	0.00	0.86
SC-02	40.84	3.88	10.32	14.47	0.00	4.85	23.45	0.00	0.89
SC-06	43.15	3.88	11.93	20.41	0.00	0.77	19.57	0.00	0.96
SC-11	37:14	2.94	5.51	15.54	19.37	0.00	18.60	0.00	0.70
SC-14	41.39	3.52	6.01	18.60	9.49	0.00	18.00	0.00	0.75
SC-17	5.37	.40	9.22	54.96	15.95	0.00	13.30	0.00	0.82
SC-19	25.09	.08	3.88	42.38	22.27	0.00	3.37	0.00	1.46
SC-20	42.52	4.73	20.72	9.80	0.00	2.76	19.03	0.00	0.86
SC-22	49.02	4.75	14.50	8.58	0.00	6.02	13.82	0.00	0.89
SC-23	22.33	2.58	13.95	30.81	5.93	0.00	25.13	0.00	1.04
SC-26	38.94	4.23	19.38	14.34	0.00	5.40	14.52	0.00	0.89
SC-28	22.52	4.22	33.99	15.33	1.75	0.00	23.12	0.00	0.96
SC-29	27.22	2.76	26.09	13.13	19.99	0.00	10.11	0.00	0.87
SC-33	20.76	1.60	2.20	5.26	0.00	0.62	68.92	0.00	0.17
SC-36	39.33	4.10	15.33	15.76	0.00	4.99	17.90	0.00	0.97
SC-39	6.23	0.37	61.37	19.38	1.53	0.00	11.29	0.00	0.83
SC-40	0.00	0.50	33.54	15.91	4.31	0.00	37.25	6.96	0.70
SC-41	38.02	3.60	13.43	23.27	0.00	2.59	17.89	0.00	0.94
SC-42	51.03	4.53	14.94	8.92	0.00	0.65	17.86	0.00	0.75
SC-47	4.33	0.75	23.41	40.44	14.80	0.00	11.66	0.00	0.00
SC-49	1.93	0.72	3.83	5.47	4.21	0.00	81.43	0.00	0.26
SC-51	0.00	0.00	2.62	51.00	10.03	0.00	2.91	32.00	0.45
SC-52	42.46	4.02	7.07	18.21	0.00	5.44	23.98	0.00	0.00
SC-53	45.73	4.66	10.64	13.22	0.00	3.35	21.98	0.00	0.81
SC-54	41.98	2.88	4.98	15.58	0.00	3.33	28.41	0.00	0.74
SC-55	35.84	3.13	10.45	30.78	0.00	5.05	11.95	0.00	0.00
SC-59	11.38	0.00	0.00	50.66	17.23	0.00	18.63	0.00	0.92
SC-60	43.74	4.27	6.03	14.96	0.00	4.88	26.67	0.00	0.00
SC-64	21.43	0.00	14.60	37.46	0.00	1.39	17.88	0.00	0.74
SC-65	21.34	3.90	26.10	7.35	0.00	6.92	22.73	0.00	0.82
SC-66	34.54	3.75	14.05	24.63	0.00	4.26	16.95	0.00	1.19
SC-67	17.76	1.45	22.30	5.21	0.00	0.45	54.61	0.00	0.25
SC-67(Smc)	0.00	0.81	6.40	0.00	4.33	0.00	27.59	45.37	0.00
SC-68	2.45	2.72	96.61	3.33	0.07	0.00	1.55	0.00	0.00
SC-69	0.00	0.06	2.54	45.29	5.10	0.00	44.66	2.48	0.00
SC-70	24.34	2.33	27.81	23.67	0.00	3.85	15.27	0.00	0.00
SC-71	10.46	1.65	28.52	42.17	9.24	0.00	9.57	0.00	0.00
SC-72	32.64	3.32	16.40	27.09	0.00	5.00	13.17	0.00	0.00

Appendix E: Use of acetylene for static mass spectrometry

This section briefly describes an investigation into the use of acetylene for static mass spectrometry. Production of acetylene from water is achieved by reaction with calcium carbide, which can be readily obtained commercially. Unlike aluminium carbide, the reaction of water with commercial calcium carbide is known to work; use of light provided by the combustion of acetylene produced by this reaction, is frequently used for cave exploration (speleology). At room temperature the reaction of calcium carbide and water is:

$$CaC_2 + 2H_2O \rightarrow Ca(OH)_2 + C_2H_2$$

Since some of the hydrogen in the water is converted to calcium hydroxide and not acetylene there is the possibility of fractionation. However calcium hydroxide decomposes to calcium oxide and water at 580°C

$$Ca(OH)_2 \rightarrow CaO + H_2O$$

Hence the reaction of calcium carbide with water above 580°C is

$$CaC_2 + H_2O \rightarrow CaO + C_2H_2 \qquad \text{E.1)}$$

From equation (E.1) it can be seen that only one molecule of water is required to produce each molecule of acetylene, which suggests that there may not be a side reaction forming hydrogen, as in the case of aluminium carbide. Calculation of the hydrogen isotope composition of the acetylene would be similar to that for methane (section 5.5.3).

Experiments were carried out to ascertain the yield of acetylene by the reaction of water with calcium carbide at various furnace temperatures. The experimental procedure was the same as that used for aluminium carbide experiments, section 5.4.3, apart from the use of calcium carbide instead of aluminium carbide. The results obtained are shown in fig. E.1. It was found that above 200°C the yield of acetylene increased, presumably due to the decomposition of some calcium hydroxide. However, above 325°C the yield of acetylene decreased and ethene was produced instead.

Despite the low yields of acetylene an attempt was made to analyses the hydrogen isotopic composition using static mass spectrometry. Acetylene was found to have an

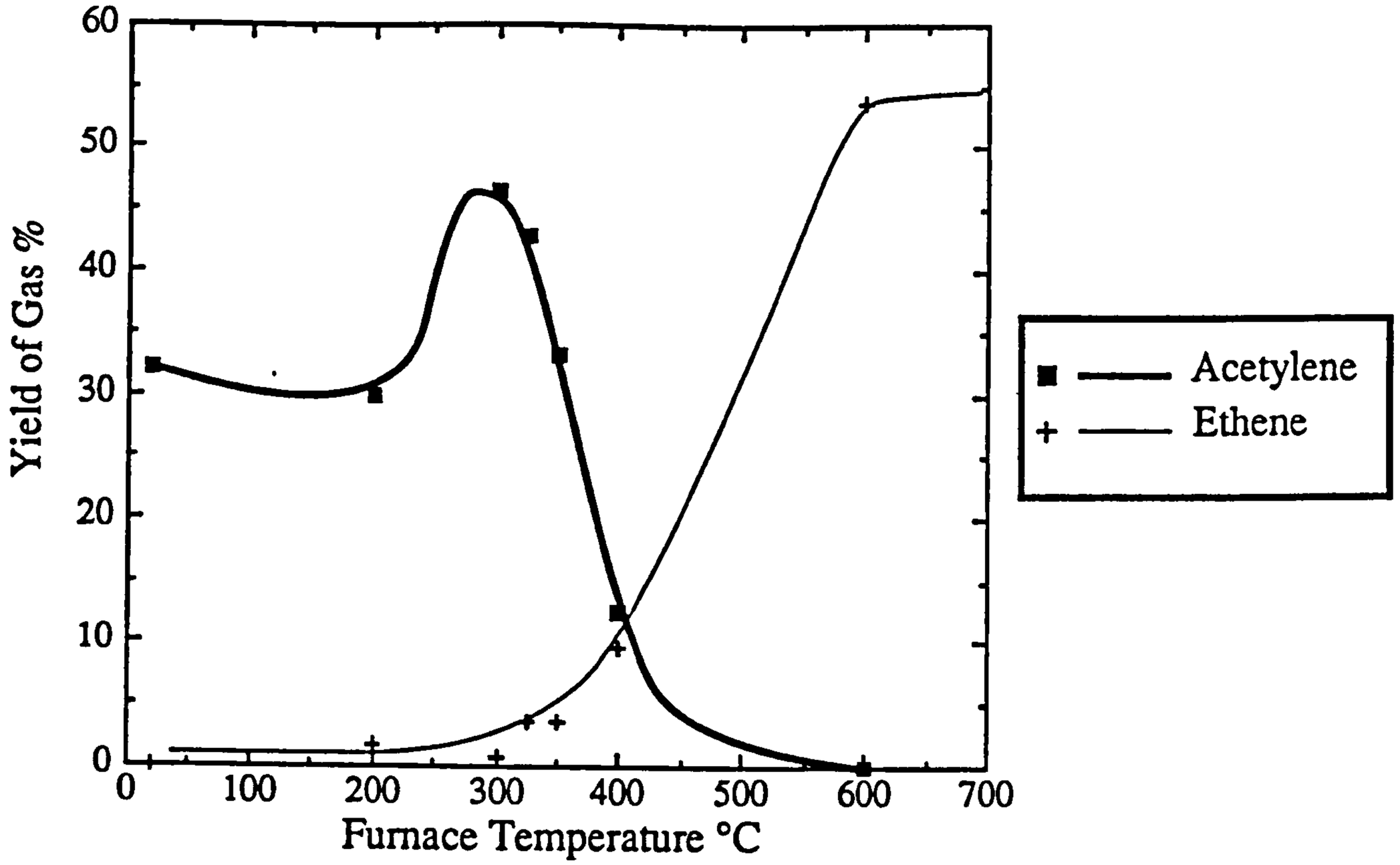

Fig E.1 Yield of acetylene and ethene by the reaction of water with aluminium carbide at various temperatures.

advantage in that it condensed at a temperature between -150°C and -160°C making it transferable by liquid nitrogen. The ethene was non condensible at liquid nitrogen temperatures. However the acetylene was found to have a half-life of less than 5 seconds in the mass spectrometer source. When performing a mass scan a large peak was observed at m/z 28, presumably due to the formation of ethene. Ethene was considered unsuitable as a static mass spectrometer gas due to isobaric interference from nitrogen. Ethene could not be cryogenically separated from nitrogen and a small amount of nitrogen would result in large errors in the δD calculation. Hence, further investigation of the use of acetylene for static mass spectrometry was abandoned.

References

Abell P.I., Draffan G.H., Eglington G., Hayes J.M., Maxwell J.R. and Pillinger C.T. (1970) Organic analysis of the returned lunar sample. *Science*, **167**, 757-759.

Affiattalab F. and Wasson J.T. (1980) Composition of the metal phases in ordinary chondrites: Implications regarding classification and metamorphism. *Geochim.Cosmochim.Acta*, **44**, 431-436.

Ahrens L.H., Von Michaelis H., Erlank A.J. and Willis J.P. (1968) Fractionation of some abundant lithophile element ratios in chondrites. In: *Meteorite research*, Ed. Millman P.M., D. Reidel, Dordrecht, 166-173.

Aitken M.J., Fleming S.J., Reid J. and Tite M.S. (1968) In: Thermoluminescence of geological materials., Ed. McDougall D.J., Academic, London, 133-142.

Aldrich L.T. and Nier A.O. (1948) Argon 40 in potassium minerals. *Phys.Rev.*, **74**, 876-877.

Alexander C.M.O'D., Arden J.W., McGarvie D., Schelhaas N., Ott U., Wright I.P. and Pillinger C.T. (1988) Stable isotopes in the ordinary chondrites: characterisation of isotopically anomalous phases. *LPSC*, **XIX**, 5-6.

Alexander C.M.O'D., Arden J.W. and Pillinger C.T. (1989a) Carbonaceous components in ordinary chondrites: implications for metamorphism vs heterogeneous accretion. *LPSC*, **XX**, 7-8.

Alexander C.M.O'D., Hutchison R. and Barber D.J. (1989b) Origin of chondrule rims and interchondrule matrices in unequilibrated ordinary chondrites. *Earth Planet.Sci.Lett.*, **95**, 187-207.

Alfin-Slater R.B., Rock S.M. and Swislocki M. (1950) Determination of isotope ratios of known deuterium-hydrogen samples using a mass spectrometer. *Anal.Chem*, **22**, 421-423.

Anders E. (1964) Origin, age and composition of meteorites. *Space Sci.Rev.*, **3**, 583-714.

Anders E. (1973) Organic compounds in meteorites. *Science*, **182**, 781-790.

Anders E. (1986) What can meteorites tell us about comets? *The comet nucleus sample return mission proc. workshop*, Canterbury,U.K. 15-17 July, ESA SP-249 (Dec 1986).

Anders E. and Ebihura M. (1982) Solar-system abundances of the elements. *Geochim.Cosmochim.Acta*, **46**, 2363-2380.

Anders E. and Owen T. (1977) Mars and Earth: Origin and abundance of volatiles. *Science*, **198**, 453-465.

Anders E. and Zadnik M.G. (1985) Unequilibrated ordinary chondrites : A tentative sub-classification based on volatile element concentration. *Geochim.Cosmochim.Acta.*, 49, 1281-1291.

Anders E., Lewis R.S., Ming T. and Zinner E. (1989) Interstellar grains in meteorites: diamond and silicon carbide. In: *Interstellar dust*, Eds. Allamadola L.J. and Tielens A.G.G. Publ: Kluwer Academic Publ. Co., Dordrecht, 389-402.

Ash R.D. (1990) Interstellar dust from primitive meteorites: A carbon and nitrogen isotope study. Unpublished PhD Thesis, Open University.

Aston F.W. (1919) A positive ray spectrograph. *Phil.Mag.*, 38, 707-714.

Becker R.H. and Epstein S. (1982) Carbon, nitrogen and hydrogen isotopes in solvent extractable organic matter from carbonaceous chondrites. *Geochim.Cosmochim Acta*, 46, 97-103.

Bertaux J. and Clarke J.T. (1989) Deuterium content of the Venus atmosphere. *Nature*, 338, 567-568.

Bertout C. (1984) T Tauri stars: an overview. *Rep.Prog.Phys.*, 47, 111-174.

Bigeleisen J. Perlman M.L. and Prosser H.C. (1952) Conversion of hydrogenic materials to hydrogen for isotopic analysis. *Anal.Chem.*, 24, 1356-1357.

Black D.C. (1973) Deuterium in the early solar system. *Icarus*, 19, 154-159.

Boato G. (1954) The isotopic composition of hydrogen and carbon in the carbonaceous chondrites. *Geochim.Cosmochim.Acta*, 6, 209-220.

Bond G.C. (1987) Heterogeneous catalysis: Principles and applications. Oxford science publications: *Clarendon Press, Oxford*, 15-16.

Boyd S.R. (1988) A study of carbon and nitrogen isotopes from the Earth's mantle. Unpublished PhD Thesis. Open University.

Boyd S.R., Wright I.P., Franchi I. and Pillinger C.T. (1988) Preparation of sub-nanomole quantities of nitrogen gas for stable isotopic analysis. *J.Phys. E: Sci.Instrum.*, 21, 876-885.

Bradley J.P., Sandford S.A. and Walker R.M. (1988) Interplanetary dust particles. In: *Meteorites and the early solar system* (Eds) Kerridge J.F. and Matthews M.S., publ:University of Arizona Press, Tuscon, 861-895.

Bridger N.I., Craig R.D. and Sercombe J.S.F. (1974) New mass spectrometer for isotopic analysis of small samples. *Adv.Mass Spectrom.*, 6, 365-375.

Briggs M.H. (1963) Evidence for an extraterrestrial origin for some organic constituents of meteorites. *Nature*, 197, 1290.

Bunch T.E. and Chang S. (1980) Carbonaceous chondrites II. Carbonaceous chondrite phyllosilicates and light element geochemistry as indicators of parent body processes and surface conditions. *Geochim.Cosmochim.Acta*, 44, 1543-1577.

Bunch T.E. and Rajan R.S. (1988) Meteorite regolithic breccias. In: *Meteorites and the early solar system*, (Eds) Kerridge J.F. and Matthews M.S., publ:University of Arizona Press, Tuscon, 144-164.

Burgess R. (1987) An investigation of sulphur in carbonaceous and enstatite chondrites by stepped combustion. Unpublished PhD Thesis. Open University.

Caffee M.W., Goswami J.N., Hohenberg C.M., Marti K. and Reedy R.C. (1988) Irradiation records in meteorites. In: *Meteoritics and the early solar system*, Eds. Kerridge J.F. and Mathews M.S., University of Arizona Press, Tuscon 205-245.

Cameron A.G.W. (1966) The accumulation of chondritic material. *Earth Planet.Sci.Lett.*, 1, 93-96.

Carr M.H. (1987) Water on Mars. *Nature*, 326: 30-35.

Carr R.H., Wright I.P., Joines A.W. and Pillinger C.T. (1986) Measurement of carbon stable isotopes at the nanomole level: a static mass spectrometer and sample preparation technique. *J.Phys.E:Sci.Instrum.*, 19, 798-808.

Cassen P. and Boss A.P. (1988) Protostellar collapse, dust grains and solar-system formation. In: *Meteoritics and the early solar system*, Eds. Kerridge J.F. and Mathews M.S., University of Arizona Press, Tuscon, 304-328.

Chappellaz J., Barnola J.M., Raynaud D., Korotkevich Y.S. and Lorius C. (1990) Ice core record of atmospheric methane over the past 160,000 years. *Nature*, 345, 127-131.

Clarke W.B., Jenkins W.J. and Top Z. (1976) Determination of tritium by mass spectrometric measurements of ^{3}He. *Int.J.Appl.Rad.Isotope*, 27, 515-522.

Clayton D.D. (1988) Stellar nucleosynthesis and chemical evolution of the solar neighbourhood. In: *Meteorites and the early solar system*, Eds. Kerridge J.F and Mattews M.S, published University of Arizona Press, Tuscon, 1021-1062.

Clayton R.N. (1981) Isotopic variation in primitive meteorites. *Phil.Trans.Roy.Soc.*, A303, 339-349.

Clayton R.N. and Mayeda T.K. (1984) The oxygen record in Murchison and other carbonaceous chondrites. *Earth Planet.Sci.Lett.*, 67, 151-161.

Close F. (1983) The cosmic onion. Published: Heinemann London,159-162.

Coleman M.L., Shepherd T.J., Durham J.J., Rouse J.E. and Moore G.R. (1982) Reduction of water with zinc for hydrogen isotope analysis. *Anal.Chem.*, 54, 993-995.

Colgate S.A. (1974) The formation of deuterium and the light elements by spallation in supernova shocks. *Astrophys.J.*, 187, 321-332.

References

Coustenis A., Bézard B. and Gautier D. (1989) Titan's atmosphere from Voyager infrared observations. *Icarus*, **82**, 67-80.

Cox K.G., Bell J.D. and Pankhurst R.J. (1979) The interpretation of igneous rocks. published George Allen & Unwin (Publishers) Ltd., London, 407-414.

Craig H. (1961) Standard for reporting concentrations of deuterium and oxygen-18 in natural waters. *Science*, **133**, 1833-1834.

Craig H. (1964) Petrological and compositional relationships in meteorites. In: *Isotope and cosmic chemistry*, Eds. Craig H., Miller S.L. and Wasserburg G.J., published North Holland, Amsterdam, 401-451.

Craig H., Chou C.C., Welhan J.A., Stevens C.M. and Engelkemeir A. (1988) The isotopic composition of methane in polar ice cores. *Science*, **242**, 1535-1539.

Cronin J.R. and Pizzarello S. (1986) Amino acids of the Murchison meteorite. III Seven carbon acyclic primary a amino alkanoic acids. *Geochim.Cosmochim.Acta.*, **50**, 2419-2427.

Cronin J.R., Pizzarello S. and Cruikshank D.P. (1988) Organic matter in carbonaceous chondrites, planetary satellites, asteroids and comets. In: *Meteoritics and the early solar system*, Eds. Kerridge J.F. and Mathews M.S., published University of Arizona Press, 819-857.

DeBurgh C., Lutz B.L., Owen T. and Chauville J. (1988) Monodeuterated methane in the outer solar system. III Its abundance on Titan. *Astrophys.J.*, **329**, 951-955.

DeHart J.M., Lofgren G.E. and Sears D.W.G. (1987) Electron-microprobe and cathodoluminescence study of glasses in type 3 ordinary chondrites: Relevance to metamorphism and aqueous alteration. *LPSC*, **XVIII**, 225-226.

Dodd R.T. (1965) Preferred orientation of chondrules. *Icarus*, **4**, 308-316.

Dodd R.T. (1969) Metamorphism of the ordinary chondrites: A review. *Geochim.Cosmochim.Acta.*, **33**, 161-203.

Dodd R.T. (1981) Meteorites: A Petrologic-Chemical Synthesis. published: Cambridge University Press, London.

Dodd R.T. and Van Schmus W.R. (1965) Significance of unequilibrated ordinary chondrites. *J.Geophys.Res.*, **70** 3801-3811.

Dodd R.T., Grover J.E. and Brown G.E. (1975) Pyroxenes in the Shaw (L-7) chondrite. *Geochim.Cosmochim.Acta*, **39**, 1585-1694.

Dodd R.T., Van Schmus W.R. and Koffman D.M. (1967) A survey of the unequilibrated ordinary chondrites. *Geochim.Cosmochim.Acta*, **31**, 921-951.

Donahue T.M., Hoffman J.H., Hodges R.R. and Watson A.J. (1982) Venus was wet: a measurement of deuterium to hydrogen. *Science*, **216**, 630-633.

Dreibus G. and Wänke H. (1981) On the origin of the excess volatile trace elements in the dark portion of gas-rich chondrites. *Meteoritics*, **15**, 284-285.

Drossart P., Encrenaz T., Kunde V. and Hanel R. (1982) An estimate of the PH_3,CH_3D and GeH_4 abundances on Jupiter from the voyager IRIS data at 4.5μm *Icarus*, **49**, 416-426.

DuFrense E.R. and Anders E. (1962) On the chemical evolution of the carbonaceous chondrites. *Geochim.CosmochimActa.*, **26**, 1085-1114.

Dumke I.,Faber E. and Poggenburg J. (1989) Determination of stable carbon and hydrogen isotopes of light hydrocarbons *Anal.Chem.*, **61**, 2149-2154.

Eberhardt P., Dolder U., Schulte W., Kranhowsky D., Lammerzahl P. Hoffman J.H., Hodges R.R., Berthelier J.J. and Illiano J.M. (1986) The D/H ratio in water from Halley. *Proc. 20th ESALAB on the exploration of Halley's comet*, published: Heidelberg, ESA SP-259.

Edwards G. (1955) Isotopic composition of meteoritic hydrogen. *Nature*, **176**, 109-111.

Epstein R.I., Lattimer J.M. and Schramm D.N. (1976) The origin of deuterium. *Nature*, **263**, 198-202.

Epstein S. and Taylor H.P. (1970) $^{18}O/^{16}O$, $^{30}Si/^{28}Si$, D/H and $^{13}C/^{12}C$ studies of lunar rocks and minerals. *Science*, **167**, 533-535.

Epstein S. and Taylor H.P. (1972) O^{18}/O^{16}, Si^{30}/Si^{28}, C^{13}/C^{12} and D/H studies of Apollo 14 and 15 Samples. *Proc. 3rd Lunar Sci. Conf.*, 1429-1454.

Epstein S. and Taylor H.P. (1973) The isotopic composition and concentration of water, hydrogen and carbon in some Apollo 15 and 16 soils and in the Apollo 17 orange soils. *Proc.4th Lunar Sci.Conf.*, **2**, 1559-1575.

Epstein S., Krishnamurthy R.V., Cronin J.R., Pizzarello S. and Yuen G.U. (1987) Unusual stable isotopes in amino acid and carboxylic acid extracts from the Murchison meteorite. *Nature*, **326**, 477-479.

Fallick A.E., Gardiner L.R., Jull A.J.T. and Pillinger C.T. (1980) Instrument effects in the application of static mass spectrometry to high sensitivity carbon isotope measurements. *Adv.Mass Spectrom.*, **8A**, 309-317.

Fallick A.E., Hinton R.W., McNaughton N.J. and Pillinger C.T. (1983) D/H ratios in meteorites: some results and implications. *Annales Geophysicae*, **1**, 129-134.

Farkas A. and Farkas L. (1934) Experiments on heavy hydrogen Part I *Proc.Roy.Soc.Lond.*, **A144**, 467-480.

Fisher I.P. and Brown W.F. (1971) The analysis of deuterium content of hydrogen at and below natural abundance levels. *Int.J.Mass Spectrom.Ion Phys.*, **7**, 273-279.

Florkowski T. (1985) Sample preparation for hydrogen isotope analysis by mass spectrometry. *Int.J.Appl.Radiat.Isot.*, **36**, 991-992.

Friedman I. (1953) Deuterium content of natural waters and other substances. *Geochim.Cosmochim.Acta*, **4**, 89-103.

Friedman L. and Irsa A.P. (1952) Determination of deuterium in water. *Anal.Chem*, **24**, 876-878.

Gamow G. (1948) The evolution of the universe. *Nature*, **162**, 680.

Gardiner L.R., Jull A.J.T. and Pillinger C.T. (1978) Progress towards a direct measurement of $^{13}C/^{12}C$ ratios for hydrolysable carbon in lunar soils by static mass spectrometry. *Proc. Lunar Planet. Sci. Conf.*, **9**, 2167-2193.

Gardiner L.R. and Pillinger C.T. (1979) Static mass spectrometry for the determination of active gases. *Anal.Chem.*, **51**, 1230-1236.

Gautier D. and Owen T. (1983) Cosmological implications of helium and deuterium abundances on Jupiter and Saturn. *Nature*, 302, 215-218.

Geiss J., Buehler F., Cerutti H., Eberhardt P. and Meister J. (1971) The solar wind composition experiment. *NASA SP-272*, 221-226.

Geiss J., Eberhardt P., Bühler F. and Meister J. (1970) Apollo 11 and 12 solar wind composition experiments: fluxes of He and Ne isotopes. *J.Geophys.Res.(Space Phys.)*, **75**, 5972-5959.

Geiss J. and Reeves H. (1972) Cosmic and solar system abundances of deuterium and helium-3. *Atron. Astrophys*, **18**, 126-132.

Geiss J. and Reeves H. (1981) Deuterium in the solar system. *Atron. Astrophys*, **93**, 189-199.

Gooding J.L. (1984) Aqueous alteration on meteorite parent bodies: Possible role of "unfrozen" water and the Antarctic meteorite analogy. *Meteoritics*, **19**, 228-229.

Gonfiantini R. (1978) Standards for stable isotope measurements in natural compounds. *Nature*, **271**, 534-536.

Grady M.M., Swart P.K. and Pillinger C.T. (1982) The variable carbon isotopic composition of type 3 ordinary chondrites. *Proc.Lunar Planet.Sci.Conf*, **XIII**, J.Geophys.Res.Suppl., 87, A289-A269.

Graff J. and Rittenberg D. (1952) Microdetermination of deuterium in organic compounds. *Anal.Chem.*, **24**, 878-881.

Graham A.L., Bevan A.W.R. and Hutchison R. (1985) *Catalogue of meteorite*, fourth edition, British Museum (Natural History).

Greenberg J.M. (1982) What are comets made of? A model based on interstellar dust. In: *Comets*, ed. Wilkening L.L., Univ.Arizona Press, 131-163.

Greenwood N.N. and Earnshaw A. (1984) Chemistry of the elements. Pergammon press 146-153 & 1416-1418.

Grimm R.E. and McSween H.Y. (1989) Water and the thermal evolution of carbonaceous chondrite parent bodies. *Icarus*, 82, 244-280.

Grimm R.E. (1985) Penecontemporaneous metamorphism, fragmentation and reassembly of ordinary chondrite parent bodies. *J.Geophys.Res.B*, 90, 2022-2028.

Grossman J.N, Rubin A.E., Nagahara H. and King A.E. (1988) Properties of chondrules. In: *Meteorites and the early solar system*, Eds. Kerridge J.F. and Matthews M.S., University of Arizona Press, Tuscon, 619-659.

Grossman J.N. (1988) Formation of chondrules. In: *Meteorites and the early solar system*, Eds. Kerridge J.F. and Matthews M.S., University of Arizona Press, Tuscon, 680-696.

Guimon R.K., Keck B.D., Weeks K.S., DeHart J. and Sears D.W.G (1985) Chemical and physical studies of type 3 chondrites - IV: Annealing studies of a type 3.4 ordinary chondrite and the metamorphic history of meteorites. *Geochim.Cosmochim.Acta*, 49, 1515-1524.

Guimon R.K., Lofgren G.E. and Sears D.W.G.S. (1987) Chemical and physical studies of type 3 chondrites IX: Thermoluminescence and hydrothermal annealing experiments and their relationship to metamorphism and aqueous alteration in type <3.3 ordinary chondrites. *Geochim.Cosmochim.Acta*, 52, 119-127.

Hageman R. and Lohez P. (1978) Twin mass spectrometers for simultaneous isotopic analysis of hydrogen and oxygen in water. *Adv.Mass Spectrom.*, 7A, 504-508.

Halas S. and Krouse H.R. (1983) Isotopic analysis of nanomole gas samples by means of dynamic flow mass spectrometry. *Rev.Sci.Instrum.*, 54(4), 437-443.

Halliday D. and Miller A.G. (1977) Precise measurement of the total body water using trace quantities of deuterium oxide. *Biomed.Mas Spectrom.*, 4, 82-87.

Halsted R.E and Nier A.O. (1950) Gas flow through the mass spectrometer viscous leak. *Rev.Sci.Instrum.*, 21, 1019-1021.

Hartley P.E. (1980) Mass spectrometric determination of deuterium in water at natural levels. *Anal.Chem.*, 52, 2232-2234.

Hayashi C. (1966) Evolution of protostars. In: *Ann.Rev.Astron.Astrophys.*, Eds. Burbidge G., Layzer D. and Phillips J., Annual Reviews Inc., Palo Alto, Calif., Vol 4, 171-192.

Hayatsu R. and Anders E. (1981) Organic compounds in meteorites and their origins. *Topics in current chemistry*, Springer-Verlag, Berlin, 99, 1-37.

Hayatsu R., Mutsuok S., Scott R.G. Studier M. and Anders E. (1977) Origin of organic matter in the early solar system VII. The organic polymer in carbonaceous chondrites. *Geochim.Cosmochim.Acta*, 41, 1325-1339.

Hayatsu R., Winans R.E., Scott R.G., McBeth R.L., Moore C.P. and Studier M.H. (1980) Phenolic ethers in the organic polymer of the Murchison meteorite. *Science*, 207, 1202-1204.

Hayes J.M. (1967) Organic constituents in meteorites - a review. *Geochim.Cosmochim.Acta*, 31, 1395-1440.

Herbig.H. (1978) Some aspects of early stellar evolution that may be relevant to the origin of the solar system. In: *The Origin of the solar system*, Ed. Dermott S.F., Wiley and Sons, New York, 219-235.

Heyse J.W. (1978) The metamorphic history of LL-group chondrites. *Earth Planet.Sci.Lett.*, 40, 365-381.

Hinton R., Long J.V.P., Fallick A.E and Pillinger C.T. (1983) Ion probe measurements of D/H ratios in meteorites. *LPSC*, XIV, 313-314.

Horita J. (1988) Hydrogen isotope analysis of natural waters using an H_2 - water equilibration method: a special application to brines. *Chem Geol.(Isotope Geoscience)*, 72, 89-94.

Hoefs J. (1987) Stable isotope geochemistry (third edition). Publ: Springer-Verlag, Berlin.

Hoyle F. and Clayton D.D. (1974) Nucleosynthesis in white-dwarf atmospheres. *Astrophys.J.*, 191, 705-710.

Hubbard W.B. and MacFarlane J.J. (1980) Theoretical predictions of deuterium abundances in the Jovian planets. *Icarus*, 44, 676-682.

Huss C.R., Keil K. and Taylor G.J. (1978) Composition and recrystallization of the matrix of unequilibrated (type 3) ordinary chondrites. *Meteoritics*, 13, 495-497.

Huss C.R., Keil K. and Taylor G.J. (1981) The matrices of unequilibrated ordinary chondrites: implication for the origin and history of chondrules. *Geochim.Cosmochim.Acta*, 45, 33-51.

Hutchison (1983) The search for our beginning, British Museum (Natural history), Oxford University Press.

Hutchison R., Alexander C.M.O. and Barber D.J. (1987) The Semarkona meteorite: First recorded occurrence of smectite in an ordinary chondrite and its implications. *Geochim.Cosmochim.Acta*, 51, 1875-1882.

Irako M., Oguri T. and Kanomato I. (1975) The static operation mass spectrometer. *Jpn.J.Appl.Phys.*, 14(4), 533-545.

Jean-Baptiste P., Andrie C. and Lelu M. (1988) Mesure du couple tritium/hélium océanique par spectrometrie de masse. In: *Radionuclides: a tool for oceanography.* Eds. Guarry J.C., Guegueniat P. and Pentreath R.J, Elsevier, 45-54.

Kaiser T., Kelly W.R. and Wasserberg G.J. (1980) Isotopically anomalous silver in the Santa Clara and Piñon iron meteorites. *Geophys.Res.Lett.*, 7, 271-274.

Kamen M.D. (1948) In: *Radioactive tracers in biology*, New york Academic press, New York.

Keck B.D., Guimon R.K. and Sears D.W.G.S. (1986) Chemical and physical studies of type 3 ordinary chondrites VII. Annealing studies of the Dhajala H3.8 chondrite and the thermal history of chondrites and chondrules. *Earth Planet.Sci.Lett.*, 77: 419-427.

Kelly W.R. and Wasserburg G.J. (1978) Evidence for the existence of ^{107}Pd in the early solar system. *Geophys.Res.Lett.*, 5, 1079-1082.

Kendall C. and Coplen T.B. (1985) Multisample conversion of water to hydrogen by zinc for stable isotope determination. *Anal.Chem.*, 57: 1437-1440.

Kerridge J.F. (1982) Isotopic composition of C, H, N in carbonaceous chondrite polymer using stepwise combustion. *Lunar Planet.Sci*, XIII, 381-382.

Kerridge J.F. (1988) Deuterium in Shergotty and Lafayette (and on Mars?). *LPSC*, XIX, 599-600.

Kerridge J.F. and Bunch T.E. (1979) Aqueous alteration on asteroids: Evidence from carbonaceous meteorites. In: *Asteroids*, ed. Geherels T., University Arizona Press, Tuscon, 745-764.

Kolodny Y., Kerridge J.F. and Kaplan I.R. (1980) Deuterium in carbonaceous chondrites. *Earth Planet.Sci>lett.*, 46, 149-158.

Kubaschewski O., Evans E.U. and Alcock C.B. (1967) Metallurgical Thermochemistry, Publ: Pergammon, London.

Kvenvolden K., Lawless J., Pering K., Pterson E., Flores J., Ponnamperuma C., Kaplan I.R. and Moore C. (1970) Evidence for extraterrestrial amino-acids and hydrocarbons in the Murchison meteorite. *Nature*, 228, 923-926.

Lange J.W., Lambert P. and Ahrens T.J. (1985) Shock effects on hydrous minerals and implications for carbonaceous chondrites. *Geochim.Cosmochim.Acta*, 49, 1715-1726.

Langevin Y., Kissel J., Bertaux J.L. (1987) Impact ionization mass spectrometry of cometary grains on board Giotto VEGA 1 and VEGA 2 space crafts: preliminary statistical analysis of spectra in compressed modes *LPSC*, XVIII, 533-534.

Larimer J.W. and Anders E. (1967) Chemical fractions in meteorites. II Abundance patterns and their interpretation. *Geochim.Cosmochim.Acta*, 31, 1239-1270.

Lattimer J.M and Yahil A. (1989) Analysis of the neutrino events from supernova 1987A. *Astrophys.J.*, 340, 426-434.

References

Lee T., Papanastassiou D.A. and Wasserburg G.J. (1976) Demonstration of ^{26}Mg excess in Allende and evidence of ^{26}Al. *Geophys.Res.Lett.*, **3**, 109-112.

Lepp S., Delgarno A., Van Dishoeck E.F. and Black J.H. (1987) Large molecules in diffuse interstellar clouds. *Astrophys.J.*, **329**, 418-424.

Levy E.H. (1988) Energetics of chondrule formation. In: *Meteorites and the early solar system.* Eds. Kerridge J.F. and Matthews M.S., University of Arizona Press, Tuscon, 697-711.

Loriot G. and Movan T. (1975) Reliability of a capacitance manometer in the range $2x10^{-4}$ - $5x10^{-6}$ torr. *Rev.Sci.Instr.*, **46**, 140-142.

Lyon G.L. and Cox M.A. (1980) The reduction of water to hydrogen for D/H ratio analysis, using zinc in a matrix of sand. *INS-R-254. Institute of Nuclear Sciences. DSIR. New Zealand.*, Internal report.

MacDougall J.D., Lugmair, G.W. and Kerridge J.F. (1984) Early solar system aqueous activity: Sr isotope evidence from the Orgueil CI meteorite. *Nature*, **307**, 249-251.

Majzoub M. and Nief G. (1968) A mass spectrometer for the isotopic oxygen analysis of water. *Adv.Mass Spectrom.*, **4**: 511-519.

Marquardt (1963) An algorithm for least squares estimation of nonlinear parameters. *J.Soc.Ind.Appl.Maths.*, **11**, 431-441.

Matsunami S. (1984) The chemical compositions and textures of matrices and chondrule rims of eight unequilibrated ordinary chondrites. *Proc.Lunar Planet.Sci.Conf; J.Geophys.Res., Suppl.*, **87**, A297-A302.

Maynard J., Prichard H.M. and Pillinger C.T. (1990) Some stable isotopic constraints on base-metal sulphide genesis in the Shetland ophiolite. *Mineral Deposits Study Group (Christmas meeting)*, **21**.

McElroy M.B. and Hunten D,M. (1969) The ratio of deuterium to hydrogen in the Venus atmosphere. *J.Atmos.Sci.*, **28**, 879-884.

McKeegan K.D., Swan P., Walker R.M., Wopenka B. and Zinner E. (1987) Hydrogen isotopic variations in interplanetary dust particles. *LPSC*, **XVIII**, 627-628.

McKeegan K.D., Walker R.M. and Zinner E. (1985) Ion microprobe isotopic measurements of individual interplanetary dust particles. *Geochim.Cosmochim.Acta*, **49**, 1971-1987.

McKinney C.R., McCrea J.M., Epstein S. Allen H.A. and Urey H.C. (1950) Improvements in mass spectrometers for the measurement of small differences in isotopic abundance ratios. *Rev.Sci.Instr.*, **21**, 724-730.

McNaughton N.J., Borthwick J., Fallick A.E. and Pillinger C.T. (1981) Deuterium/hydrogen ratios in unequilibrated ordinary chondrites. *Nature*, **294**, 639-641.

McNaughton N.J., Borthwick J., Fallick A.E. and Pillinger C.T. (1982a) Deuterium enrichments in primitive meteorites. *Lunar Planet.Sci.*, **XIII**, 501-502.

McNaughton N.J., Fallick A.E. and Pillinger C.T. (1982b) Deuterium enrichments in type 3 ordinary chondrites. *J.Geophys.Res.*, **87**, A297-A302.

McNaughton N.J.,Abell P.I., Wright I.P., Fallick A.E. and Pillinger C.T. (1983) Preparation of nanogram quantities of deuteromethane for stable carbon isotope analysis. *J.Phys.E.Sci.Instrum.*, **16**, 505-511.

McSween H.Y. (1984) SNC meteorites: Are they Martian rocks? *Geology*, **12**, 3-6.

McSween H.Y., Sears D.W.G. and Dodd R.T. (1988) Thermal metamorphism. In: *Meteoritics and the early solar system.* Eds. Kerridge J.F. and Mathews M.S., University of Arizona Press, Tuscon, 102-113.

Medlin W.L. (1968) In: Thermoluminescence of geological materials., Ed. McDougall D.J., Academic, London, 193-223.

Mellor J.W. (1929) A comprehensive treatise on inorganic and theoretical chemistry. **Vol V**, Longmans, 870-871.

Melton C.E. and Giardini A.A. (1974) The composition of gas released from natural diamonds from Africa and Brazil. *Amer.Min.*, **59**, 775-782.

Merlivat L., Nief G. and Roth E. (1972) Deuterium content of lunar material. *Proc. 3rd Lunar Sci. Conf.*, **2**, 1473-1477.

Merrill G.P. (1921) On metamorphism in meteorites *Geol.Soc.Amer.Bull.*, **32**, 395-416.

Meyer P.,Ramaty R. and Weber W.R. (1974) Cosmic rays - astronomy with energetic particles. *Phys.Today*, **27**, 23.

Millar T.J., Bennett A. and Herbst E. (1989) Deuterium in dense interstellar clouds. *Astrophys.J.*, **340**, 906-920.

Miller S.L. (1953) A production of amino acids under possible primitive Earth conditions. *Science*, **117**, 528-529.

Miller S.L. and Urey H.C. (1959) Organic compound synthesis on the primitive Earth. *Science*, **130**, 245-251.

Mills A.A., Sears D.W. and Hearsey R. (1977) Apparatus for the measurement of thermoluminescence. *J.Phys (E):Sci.Instrum.*, **10**, 51-56.

Miyamoto M., Fujii N. and Takeda H. (1981) Ordinary chondrite parent body: An internal heating model. *Lunar Planet.Sci.Conf*, **12**, 1145-1152.

Mullie F. and Reisse J. (1987) Organic matter in carbonaceous chondrites. In: *Topics in Current Chemistry* , Springer-Verlag, Berlin, vol 139, 85-117.

Murphey B.F. (1947) The high temperature variation of the thermal diffusion factors for binary mixtures of H,D and He. *Phys.Rev.*, **72**, 834-837.

Nagahara H. (1984) Matrices of type 3 ordinary chondrites - primitive nebular records. *Geochim.Cosmochim.Acta*, **48**, 2581-2595.

Nier A.O., Ney E.P. and Inghram M.G. (1947) A null method for the composition of two ion currents in a mass spectrometer. *Rev.Sci.Instrum.*, **18**, 294-297.

Nier A.O.C. (1947) A mass spectrometer for isotope and gas analysis. *Rev.Sci.Instr.*, **18**, 398-411.

Orchin M., Wender I. and Friedel R.A. (1949) Determination of deuterium in water. *Anal.Chem.*, **21**, 1072-7013.

Owen T., Biemann K., Rushneck D.R., Biller J.E. Howarth D.W. and Lafluer A.L. (1977) The composition of the atmosphere at the surface of Mars. *J.Geophys.Res.(Space Sci.)*, **82**, 4635-4639.

Owen T., Lutz B.L. and DeBergh C. (1986) Deuterium in the outer solar system: Evidence for two distinct reservoirs. *Nature*, **320**, 244-246.

Owen T., Maillard J.P., DeBergh C. and Lutz B.L. (1988) Deuterium on Mars: The abundance of HDO and the value of D/H. *Science*, **240**, 1767-1770.

Pearce J.A. (1975) Basalt geochemistry used to investigate past tectonic environments on Cyprus. *Tecnophys.*, **25**, 41-67.

Pellas P. and Storzer D. (1979) Differences in the early cooling histories of the chondritic asteroids. *Meteoritics*, **14**, 513-515.

Pillinger C.T. (1979) Solar wind exposure effects in the lunar soil. *Rep. Prog. Phys.*, **42**, 897-961.

Pillinger C.T. (1984) Light element stable isotopes in meteoritics - from grams to pico grams. *Geochim.Cosmochim.Acta*, **48**, 2739-2766.

Ponnamperuma C., Kvenvolden K., Chang S., Johnson R., Pollock G., Philpott D., Kaplan I., Smith J., Schopf J.W., Gehrke C., Hodgson G., Breger I.A., Halpern B., Duffield A., Krauskopf K., Barghoorn E., Holland H. and Keil K. (1970) Search for organic compounds in the lunar dust from the sea of tranquility. *Science*, **167**, 760-762.

Prosser S.J., Wright I.P. and Pillinger C.T. (1990) A preliminary investigation into the isotope measurement of carbon at the picomole level using static vacuum mass spectrometry. *Chem.Geol.*, **83**, 71-88.

Reeves H. and Bottinga Y. (1972) The D/H ratio in Jupiter's atmosphere. *Nature*, **238**, 326-327.

Reynolds R.H. (1956) High sensitivity mass spectrometer for noble gas analysis. *Rev.Sci.Instr.*, **27**, 928-934.

Richet P., Bottinga Y. and Javoy M. (1977) A review of hydrogen, carbon, nitrogen, oxygen, sulphur and chlorine stable isotope fractionation among gaseous molecules. *Ann.Rev.Earth Sci.*, 5, 65-110.

Rietmeijer F.J.M. (1985) A model for diagenesis in proto-planetary bodies. *Nature*, 313, 293-294.

Robert F. and Epstein S. (1982) The concentration and isotopic composition of hydrogen , carbon and nitrogen in carbonaceous meteorites. *Geochim.Cosmochim.Acta*, 46, 81-95.

Robert F., Halbout J., Javoy M. (1987c) Hydrogen isotopic contamination during HF-HCl dissolution and H_2O_2 oxidation of bulk carbonaceous chondrites. *Meteoritics*, 22, 491-493.

Robert F., JavoyM., Halbout J., Dinon B. and Merlivat L. (1987a) Hydrogen isotope abundances in the solar system. Part I: Unequilibrated chondrites. *Geochim.Cosmochim.Acta*, 51, 1787-1805.

Robert F., Javoy M., Halbout J., Dinon B. and Merlivat L. (1987b) Hydrogen isotope abundances in the solar system. Part II: Meteorites with terrestrial-like D/H ratio. *Geochim.Cosmochim.Acta*, 51, 1807-1822.

Robert F., Merlivat L. and Javoy M. (1978) Water and deuterium content in the Chainpur and Orgueil meteorites. *Meteoritics*, 13, 613-615.

Robert F., Merlivat L. and Javoy M. (1979) Deuterium concentration in the early solar system: Hydrogen and oxygen isotope study. *Nature*, 282, 785-789.

Rolfs C., Trautrether H.P. and Rodney W.S. (1987) Current status of nuclear astrophysics. *Rep. Prog. Phys.*, 50, 233-325.

Runciman W.A. and Carter T. (1971) High resolution infrared spectra of diamond. *Solid State Comm.*, 9, 315-317.

Ruzicka (1982) Flow-injection methods: a new tool for instrument analysis. *Phil.Trans.R.Soc.Lond.*, A305, 645-656.

Sagan C. and Khare B.N. (1979) Tholins: organic chemistry of interstellar grains and gas. *Nature*, 277, 102-107.

Sakai H., Smith J.W., Kaplan I.R., and Petrowski C. (1976) Micro-determination of C, N, S, H, He, metallic Fe, $\delta^{13}C$, $\delta^{15}N$ and $\delta^{34}S$ in geologic samples. *Geochem.J.*, 10, 85-96.

Schoeller D.A., Peterson D.W. and Hayes J.M. (1983) Double-comparison method for mass spectrometric determination of hydrogen isotopic abundances. *Anal.Chem.*, 55, 827-832.

Scott E.R.D. and Rajon R.S. (1981) Metallic minerals, thermal histories, and parent bodies of some xenolithic, ordinary chondrites. *Geochim.Cosmochim.Acta*, 45, 53-67.

Scott E.R.D. and Taylor G.J. (1985) Petrology of types 4-6 carbonaceous chondrites. *Proc.Lunar Planet.Sci.Conf.* 15: C699-C709.

References

Scott E.R.D., Barber D.J., Alexander C.M., Hutchison R. and Peck J.A. (1988) Primitive material surviving in chondrites: Matrix. In: *Meteorites and the early solar system.* Eds. Kerridge J.F. and Matthews M.S., University of Arizona Press, Tuscon, 718-745.

Sears D.W., Grossman J.N, Melcher C.L. Ross L.M. and Mills A.A. (1980) Measuring metamorphic history of unequilibrated ordinary chondrites. *Nature*, **287**, 791-795.

Sears D.W., Kallemeyn G.W. and Wasson J.T. (1982a) The compositional classification of chondrites: II The enstatite chondrite groups. *Geochim.Cosmochim.Acta.*, **46**, 597-608.

Sears D.W.G and Dodd R.T. (1988) Overview and classification of meteorites. In: *Meteoritics and the early solar system.* Eds. Kerridge J.F. and Mathews M.S., University of Arizona, Tuscon, 3-31.

Sears D.W.G and Hasan F.A. (1987) The type three ordinary chondrites: A review. *Suv.Geophys.*, **9**, 43-97.

Sears D.W.G. and Weeks K.S. (1983) Chemical and physical studies of type 3 chondrites, II Thermoluminesence of sixteen type 3 ordinary chondrites and relationships with oxygen isotopes. *Proc.14th Lunar Sci.Conf. Part I. Geophys.R.Suppl.*, **88**, B301-B311.

Sears D.W.G., Grossman N.J. and Melcher C.L. (1982b) Chemical and physical studies of type 3 chondrites - I: Metamorphism related studies of Antarctic and other type 3 ordinary chondrites. *Geochim.Cosmochim.Acta*, **46**, 2471-2481.

Sears D.W.G., Sparks M.H. and Rubin A.E. (1984) Chemical and physical studies of type 3 chondrites III: Chondrules from the Dhajala H3.8 chondrite. *Geochim.Cosmochim.Acta*, 48, 1189-1200.

Smith D., Adams N.G. and Alge E. (1982) Some H/D exchange reactions involved in the deuteration of interstellar molecules. *Astrophys.J.*, 263, 123-129.

Smith J.W. and Rigby D. (1981) Comment on D/H ratios in chondritic matter. *Earth Planet.Sci.Lett.*, **54**, 64-66.

Smith WM.H., Schempp W.V., Simon J. and Baines K.H. (1989) D/H for Uranus and Neptune. *Astrphys.J.*, 336, 962-966.

Smyth H.D. (1931) Products and processes of ionization by low speed electrons. *Rev.Mod.Phys*, 3, 347-391.

Sonett C.P. (1979). On the origin of chondrules *Geophys.Res.Lett*, **6**: 677-680.

Sonett C.P., Colburn D.S., Schwartz K. and Kiel K. (1970) The melting of asteroidal-sized bodies by unipolar dynamo induction from a primordial T Tauri sun. *Astrophys.Space Sci.*, 7, 446-488.

Sonett C.P. and Reynolds R.T. (1979) Primordial heating of asteroid parent bodies. In: *Asteroids.* Ed. T.Gehrels, University of Arizona Press Tuscon, 822-848.

Sorby H.C. (1877) On the structure and origin of meteorites. *Nature*, **15**, 495-498.

Sudzuki N. (1987) A water conversion method for D/H ratio analyses and its accuracy. *Geochem.J.*, **21**, 29-33.

Tanweer A., Hut G. and Burgman J.O. (1988) Optimal conditions for the reduction of water to hydrogen by zinc for mass spectrometric analysis of the deuterium content. *Chem.Geol.(Isotope Geoscience)*, **73**, 199-203.

Taylor G.J., Okada A., Scott E.R.D., Rubin A.E., Huss G.R. and Keil K. (1981) The occurrence and implications of carbide-magnetite assemblages in unequilibrated ordinary chondrites. *Lunar Planet Sci.*, **XII**, 1076-1078.

Thomas B.W. (1950) Determination of heavy water by mass spectrometer. *Anal.Chem.*, **22**, 1476-1478.

Tilton G.R. (1988) Solar-system age. In: *Meteoritics and the early solar system.* Eds. Kerridge J.F. and Mathews M.S., University of Arizona Press, Tuscon, 259-275.

Todd B.J. (1955) Outgassing of glass. *J.Appl.Phys.*, **26**, 1238-1243.

Tomeoka K. and Buseck P.R. (1985) Hydrated interplanetary dust particles linked with carbonaceous chondrites? *Nature*, **314**, 338-340.

Trafton L. and Ramsey D.A. (1980) The D/H ratio in the atmosphere of Uranus: detection of the $R_5(1)$ line of HD. *Icarus*, **41**, 423-429.

Trauger J.T., Roesler F.L., Carlton N.P. and Traub W.A (1973) Observations of HD on Jupiter and the D/H ratio. *Astrophys.J.Lett.*, **184**, L137-L141.

Trimble V (1975) The origin and abundances of chemical elements. *Rev.Mod.Phys.*, **47**, 877-976.

Urey H.C. (1948) Oxygen isotopes in nature and in the laboratory. *Science*, **108**, 489-496.

Urey H.C. and Craig H (1953) The composition of stone meteorites and origin of meteorites. *Geochim.Cosmochim.Acta*, **4**, 36-82.

VanSchmus W.R. and Wood J.A (1967) A chemical-petrologic classification for the chondritic meteorites. *Geochim.Cosmochim.Acta*, **31**, 747-765.

Wagonner R.V (1973) Big-Bang nucleosynthesis revisited. *Astrophys.J.*, **179**, 343-360.

Watson A.J., Donahue T.M. and Walker J.C.G. (1981) The dynamics of a rapidly escaping atmosphere: applications to the evolution of Earth and Venus. *Icarus*, **48**, 150-166.

Watson W.D. (1976) Interstellar molecule reactions. *Rev.Mod.Phys.*, **48**, 513-552.

Wdowiak T.J., Flickinger G.C. and Cronin J.R. (1988) Insoluble organic material of the Orgueil carbonaceous chondrite and the unidentified infrared bands. *Astrophys.J.*, **328**, L75-L79.

Weinberg S. (1977) The first three minutes., Andre Deutch, London.

Wetherill G.W. and Chapman C.R. (1988) Asteroids and meteorites. In: *Meteorites and the early solar system.* Eds. Kerridge J.F. and Matthews M.S., University of Arizona Press, Tuscon, 35-67.

Whipple. (1966) Chondrules: suggestions concerning their origins. *Science*, **153**, 54-56.

Whipple F.L. (1987) A review of cometary sciences. *Phil.Trans.R.Soc.Lond.*, **A323**, 339-347.

Wong W.W., Caberra M.P. and Klein P.D. (1984) Evaluation of a dual mass spectrometer system for rapid simultaneous determination of hydrogen-2/hydrogen-1 and oxygen-18/oxygen-16 ratios in aqueous samples. *Anal.Chem.*, **56**, 1852-1858.

Wood J.A. (1967) Chondrites: Their metallic minerals, thermal histories, and parent bodies. *Icarus*, **6**, 1-49.

Wood J.A. (1979) Review of the metallographic cooling rates and a new model for the planetesimals in which they formed In: *Asteroids*, ed. Gehrels T., University of Arizona Press, Tuscon, 849-891.

Wood J.A. (1983) Formation of chondrules and CAIs from interstellar grains accreting to the solar nebula *Mem.Natl.Polar Res. Special Issue*, **30**, 84-92.

Wood J.A. (1984) On the formation of meteoritic chondrules by aerodynamic drag heating in the solar nebula. *Earth Planet.Sci.Lett.*, **70**, 11 - 26.

Wright I.P. and Pillinger C.T. (1983) Deuterium enrichments in Renazzo revealed by static mass spectrometry. *Meteoritics*, **18**, 425-426.

Wright I.P., Grady M.M. and Pillinger C.T. (1989) Organic materials in a martian meteorite. *Nature*, **340**, 220-222.

Wright I.P., McNaughton N.J., Fallick A.E., Gardiner L.R. and Pillinger C.T. (1983) A high senstivity - high precision stable carbon mass spectrometer. *J.Phys (E)*, **16**, 497-504.

Yang J. and Epstein S. (1982) On the origin and composition of hydrogen and carbon in meteorites. *Meteoritics*, **17**, 301.

Yang J. and Epstein S. (1983) Interstellar organic matter in meteorites. *Geochim.Cosmochim.Acta*, **47**, 2199-2216.

Yang J. and Epstein S. (1984) Relic interstellar grains in Murchison meteorite. *Nature*, **311**, 544-547.

York D.G. and Rogerson J.B. (1976) The abundance of deuterium relative to hydrogen in interstellar space. *Astrophys.J.*, **203**, 378-385.

Zinner E. (1988) Interstellar cloud material in meteorites. In: *Meteoritics and the early solar system.* Eds. Kerridge J.F. and Mathews M.S., University of Arizona, Tuscon, 956-983.

References

Zinner E., McKeegan K.D. and Walker R.M. (1983) Laboratory measurements of D/H ratios in interplanetary dust. *Nature*, 305, 119-121.

Zolensky M. and McSween J.R. (1988) Aqueous alteration. In: *Meteoritics and the early solar system.* Eds Kerridge J.F. and Mathews M.S., University of Arizona Press, Tuscon, 114-143.